Virtual Reaction Chambers as a tool for Polymerase Chain Reaction and Protein Thermal Shift Assays

Dissertation
zur Erlangung des Grades
des Doktors der Ingenieurswissenschaften
der Naturwissenschaftlichen-Technischen Fakultät II
-Physik und Mechatronik-
der Universität des Saarlandes

von

Christian Daniel Ahrberg

Saarbrücken
2016

Tag des Kolloquiums: 20 Mai 2016

Vorsitzender:
Univ.-Prof. Dr.-Ing. M. Vielhaber

Gutachter:
Hon.-Prof. Dr. A. Manz
Univ.-Prof. Dr.-Ing. St. Seelecke

Akad. Mitarbeiter:
Dr. A. Leschhorn

Bitte unterschrieben als Einzelblatt einreichen
und in die Arbeit eingebunden, ebenfalls unterschrieben.

Eidesstattliche Versicherung

Hiermit versichere ich an Eides statt, dass ich die vorliegende Arbeit selbstständig und ohne Benutzung anderer als der angegebenen Hilfsmittel angefertigt habe. Die aus anderen Quellen oder indirekt übernommenen Daten und Konzepte sind unter Angabe der Quelle gekennzeichnet. Die Arbeit wurde bisher weder im In- noch im Ausland in gleicher oder ähnlicher Form in einem Verfahren zur Erlangung eines akademischen Grades vorgelegt.

Ort, Datum

_____

Unterschrift

_____

Abstract

In the frame of this thesis Virtual reaction chambers (VRCs) were analysed as a tool for polymerase chain reaction and protein analysis. VRCs are digital microfluidic reactors, consisting of a aqueous sample volume (100nL - 300 nL) encapsulated by an oil droplet ($\sim 1\mu$L).

Firstly a portable system for the temperature manipulation and fluorescence measurement of VRCs was constructed for this thesis. Subsequently the device was used to perform polymerase chain reactions (PCR) from DNA as well as reverse transcription PCR from RNA. Furthermore two methods of multiplexed PCR were developed, one of which specifically exploits the advantages of VRCs. Thus it can be concluded that virtual reaction chambers are a suitable tool for polymerase chain reaction of DNA and RNA especially for point-of-care applications. Furthermore a mathematical model based on chain growth was constructed to describe the PCR, with particular focus on the extension step.

Additionally the heating device and fluorescence measurement were used to measure the thermal stability of proteins. Here advantage was taken of the fact that VRCs are easily superheatable. Thus proteins still stable at temperatures above $100°C$ can be measured using this system. This and the low sample consumption makes VRCs an ideal tool for screening purposes in protein analysis.

F

Zusammenfassung

Im Rahmen dieser These wurden Virtual Reaction Chambers (VRCs) als Werkzeug für die Polymerase Kettenreaktion (PCR) und die Analyse von Proteinen getestet. VRCs sind digitale, mikrofluidische Reaktionsvolumen die aus einem wässrigen Probevolumen (100 - 300nL) eingeschlossen von einem Öltropfen ($\sim 1\mu$L) bestehen.

In einem ersten Schritt wurde ein tragbares System für die Temperaturmanipulation sowie Flureszensmessung von VRCs konstruiert. Im Folgenden wurde mit dem Gerät die Polymerase Kettenreaktion von DNA, sowie reverse transkriptions PCR von RNA durchgeführt. Im Weiteren wurden zwei Methoden zur multiplex PCR entwickelt, von denen eine die Vorteile von Virtual Reaction Chambers nutzt. Aus den Ergebnissen kann gefolgert werden, dass VRCs ein geeignetes Werkzeug für die PCR von DNA und RNA sind, im Besonderen für Point-of-Care Anwendungen. Außerdem wurde ein mathematisches Modell zur Beschreibung der Reaktion geschrieben. Das Modell basiert auf Chain-Growth Prozessen und ist im Besonderen auf den Elongination-Schritt der Reaktion fokussiert.

In einem zweiten Teil wurde das entwickelte Gerät benutzt, um die Temperatur-Stabilität von Proteinen zu messen. Hier wurde ausgenutzt, dass VRCs eine einfache Möglichkeit zum Superheating von Flüssigkeiten bieten. Dadurch konnten Proteine gemessen werden, welche auch noch bei $100°C$ stabil sind. Dies und der niedrige Probenverbrauch machen aus VRCs ein geeignetes Werkzeug zur Analyse von Proteinen, insbesondere im Rahmen von Screening-Versuchen.

G

H

Acknowledgement

For support and scientific discussions during my time working on this thesis, I would like to thank Andreas Manz, as well as my former group leader Pavel Neuzil. Also I would like to thank Robert Bojan Ilic, for the work and assistance on the Lab on a chip paper.

Furthermore I am grateful to Yoojung Lee and Jaewon Hwang who, during their internship at KIST Europe, helped performing experiments related to the modelling paper as well as conducted experiments regarding sample preparation. Ahyeon Gyeon assisted in culturing GFP-transfected bacteria and extracting the protein, which I want to thank her for.

Lastly I would like to thank all members of KIST Europe and the Universität des Saarlandes, who provided valuable input to this work through discussions.

Contents

Chapter 1

Introduction

1.1 Microfluidics - Lab on a Chip and Virtual Reaction Chambers

Through the advances in transistors and processors technology methods of fabrication of complex three-dimensional silicon structures became available to a broad spectrum of researchers. A group at the Stanford Electronic Laboratories used these techniques to miniaturize a gas chromatographic column [1]. Ten years later a high pressure liquid chromatography was conducted on a silicon chip [2] which today is widely regarded as the birth of microfluidics . But why did researchers strive to miniaturize equipments and processes? On one side microfluidics allows to substantially decrease the size of equipments giving the possibility to construct portable devices. Furthermore reagent and sample consumption can be reduced and micro-machining provides ways of reducing equipment costs through cost economies. On the other side the scale dependences of heat and mass transfer allows for better control over these processes resulting in improved performance. Through this reactions can be carried out faster, more efficiently and more controlled. Many applications in microfluidics are conducted in continuous flow mode with only one phase. While this allows for simple chip layout designs and handling it also has some disadvantages. When using pressure driven flow a parabolic flow profile develops leading to a residence time distribution in the chip. The direct contact of the liquid phase with the walls of the chip causes adsorption of analytes on the surfaces and can cause cross contamination when reusing chips. To address these issues scientist began using so called segmented flow either in the form of plugs separated in a second phase [3] or in the form of droplets encapsulated through the second phase [4]. Both approaches reduce the residence time distribution to a mono-dispersed distribution. In plug-flow mode the phase containing the analyte still has contact to the reactor walls allowing wall adsorption and cross contamination. In contrast the analyte phase is completely encapsulated through the second

phase on droplet-mode preventing the problems mentioned before.

In parallel to the development of segmented flow microfluidics digital microfluidics was developed. In digital microfluidics aqeous droplets are manipulated on an open, hydrophobic surface. The droplets can be moved, mixed, merged with other droplets or split thought the application of electric fields [5] or surface acoustic waves in later applications [6]. For these applications droplets are often of a micro- to nanoliter volume and can be placed by a micropipette. Droplets are sometimes covered through a glass slide or second phase to stop evaporation of the droplets. In contrast to segmented flow in microfluidics using digital platforms does not require redesign of the chip when the protocol is changed. On the downside a bigger range of droplet volumes (microliter to picoliter) can be accessed through channel based systems. Furthermore channel based flow can generate droplets in the kilohertz range and handle them while digital microfluidics is often limited to a low number of droplets.

Some processes only require few droplets and no spatial manipulation of those. In these cases the design can be further simplified. Encapsulating single, aqueous sample droplets with volumes in the low microliter range with slightly bigger oil droplets one creates a so called virtual reaction chamber (VRC) [7]. As in digital microfluidics the droplets are placed on a hydrophobic surface. VRCs offer a simple way of exploiting the advantages of microfluidics and droplets while circumventing many of the practical problems in microfluidics.

1.1.1 Superheating in Virtual Reaction Chambers

Classical nucleation theory states that a liquid needs to be heated up to its boiling temperature but for it to start boiling a seed in the form of a nucleation site or mechanical disturbance is also required [8]. In the absence of a seed it is possible to heat the liquid past its boiling point without it starting to boil. This process is called superheating or sometimes also boiling retardation. As scratches in the walls of containers and dust particles serve as nucleation seed superheating can only rarely be observed on a bulk scale[1]. Droplets encapsulated in a second phase in microfluidic channels or on an open surface like VRCs usually have no or little contact to a solid surface. Thus they are not effected by defects in solid surfaces which can act as nucleation sites for boiling or crystallization. Hence these droplets can easily be superheated without increasing the pressure of the system like required for bulk systems. Through the use of pure reagents, free of particles that

[1] Water explosions can rarely occur in microwave ovens. These incidents of superheating require the use of very pure water and clean containers as demonstrated by the popular science TV-show Mythbusters

could serve as nucleation site, superheating in VRCs has been demonstrated up to $240°C$ and supercooling down to $-12°C$ [9].

1.2 PCR

"...I very quickly brought the Honda to a stop near the roads edge, but sticking out into the potential logging trucks. With me, my girlfriend still asleep, and my new invention in peril, I contemplated what would happen if they had been extended a long way. Their extension products would be primed by the other oligos and these would also now be extended.

I would have doubled the signal, and I could do that over and over, and I could add a tremendous excess of my own deoxynucleoside triphosphates as they are cheap, soluble in water and legal in California.

I'd better get out of the road. ..."

These are the words with which Kary Mullis describes how he invented the polymerase chain reaction (PCR) in the spring of 1983 while driving to his weekend cabin on a Friday night. In 1993 he would receive the Nobel Price in Chemistry for his invention.

The invention of PCR enabled the amplification of deoxyribonucleic acid (DNA) across several orders of magnitude. In the original invention by Mullis a template composed of double stranded DNA (dsDNA) is added to an aqueous buffer containing sodium chloride ($NaCl$), magnesium chloride ($MgCl_2$) and tris(hydroxymethyl)aminomethanechloride ($Tris - Cl$). Furthermore the four deoxynucleoside triphosphates (nucleotides), deoxyadenosine (A), thymidine (T), deoxycytidine (C) and deoxyguanosine (G), are added to the reaction buffer. The last components of the buffer are two oligonucleotide primers which are able to hybridise to different strands of the template. The mixture is heated to 95°C at which the dsDNA template is denatured into two single strands of DNA (ssDNA). Next the temperature is lowered to 56°C. At this lower temperature the oligonucleotide primers hybridise to their respective template strand. Through the addition of Escherichia coli DNA polymerase I the hybridised fragments are extended starting at the primer location towards the 3‘-end of the template. After this step one has made two dsDNA fragments for every dsDNA fragment present in the initial sample. Through repeating these steps of denaturation, primer hybridization and extension (called cycle) over and over again a fragment defined by the 5‘-ends of the two primers can be amplified exponentially across several orders of magnitude. The system is very specific due to its nature [10].

An important observation is that the original template will produce a new ssDNA of indefinite length [11] limited only by the length of the template. This ssDNA of indefinite length will only produce ssDNA of length defined by the two primers in subsequent cycles. Therefore the amount of products of indefinite length increases linearly with cycle number while the amount of product with a defined length increases exponentially.

A couple of years later the original method of PCR was improved by replacing the polymerase from *Escherichia coli* with a polymerase extracted from *Thermus aquaticus* (Taq) [12]. As the name suggests Thermus aquaticus is a species of bacteria that can tolerate high temperatures and can often be found in hot springs or geysers. The main advantage of Taq polymerase is that it does not deactivate during the denaturation step at 95°C unlike the polymerase from *Escherichia coli*. Thus the Taq polymerase does not require subsequent addition at every extension step, removing a labour intensive and error prone step in the protocol. The temperature chosen for hybridization and extension steps also has to be raised to meet the activity maximum of the enzyme. With the change in polymerase hybridization steps could now be carried out between 40°C and 60°C while the extension step is carried out between 60°C and 72°C. Through this yield as well as specificity and length of amplifiable products could be improved. Furthermore the specificity was greatly improved because at the elevated hybridization and extension temperatures poorly matched primer-template hybrids would dissociate and only highly matched substrates remained for amplification.

1.2.1 Quantitative PCR / Real-Time PCR

Although PCR became a popular method for biologists and molecular biologists there were still drawbacks to the method shortly after its invention. Once thermal cycling was complete samples had to be analysed by methods like gel or electrophoresis for example. While these tasks were not only labour intensive and a bottleneck for high throughput applications they also inherited the risk of workspace contamination through removing the PCR products from their reaction tubes. To improve efficiency of post PCR analysis people began experimenting with fluorescent markers during PCR.
One of the first examples can be found in the work of Chehab and Kan [13] who modified the primers used for PCR with a fluorescent dye on the 5'-end. This eliminated the requirement for labeling the samples for later analysis. Furthermore their advancement increased specificity of the detection and enabled the detection of single nucleotide polymorphisms (SNPs) as long as these were spanned by the primer. A couple of years later oligonucleotide probes which were non extendable at the 3'-end and labelled with a fuorophor at the 5'-end were introduced for the use in PCR [14]. These

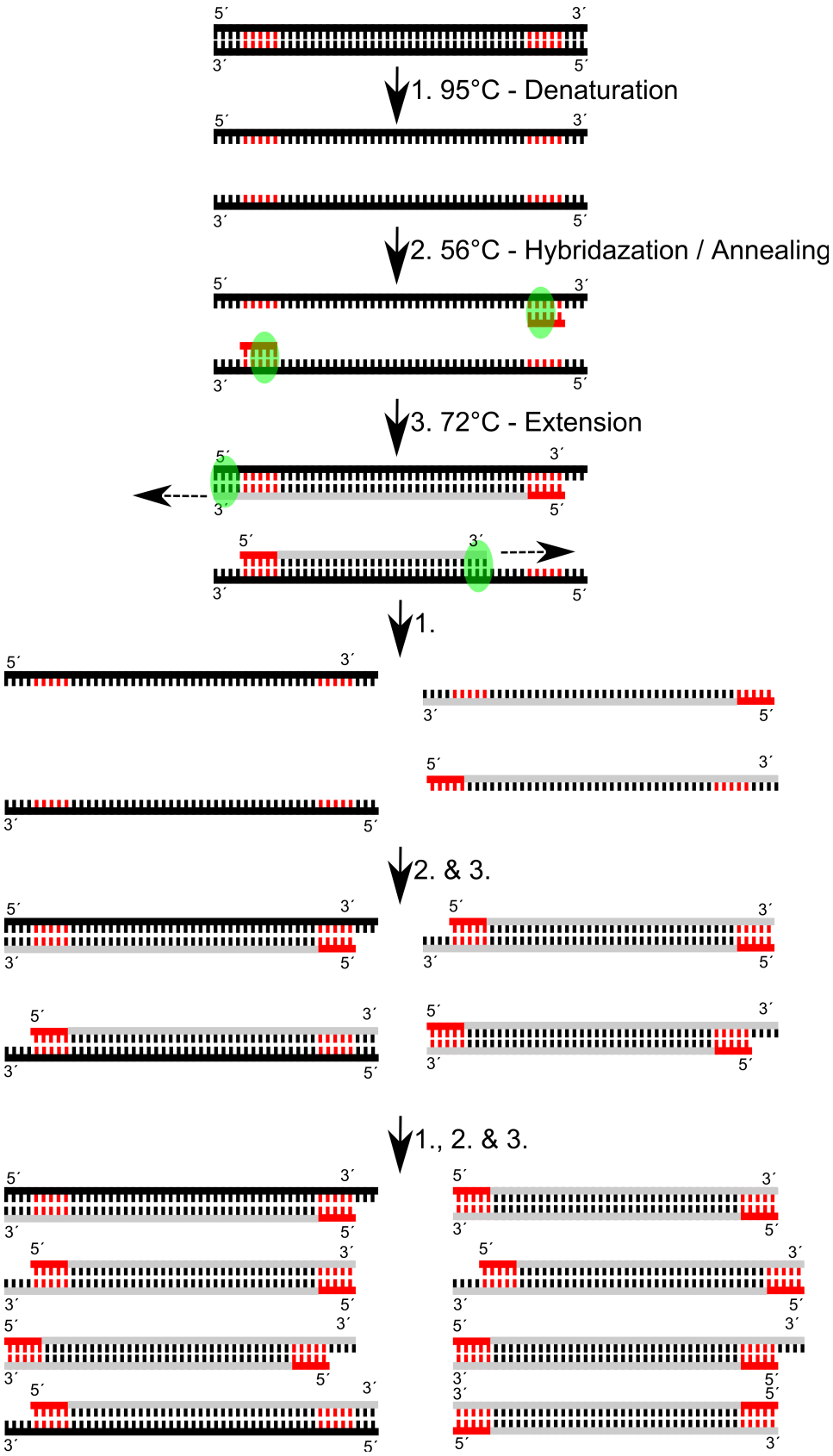

Figure 1.1: Diagram illustrating how PCR is conducted commonly today (Right).In this diagram the original template dsDNA is depicted in black, primers binding in the annealing step are shown in red. Extension is carried out through the polymerase attaching (green). The diagram also shows a likely distribution of product length during the first 3 cycles performed.

probes were complementary for a sequence in-between the two primers used for PCR. The method made use of the exonuclease activity of the Taq-polymerase which degraded the probe into smaller fragments when the polymerase encountered a hybridised probe during extension. After thermal cycling intact probes could be differentiated from degraded probes through simple separation methods like electrophoresis for example without the requirement of labeling the sample.

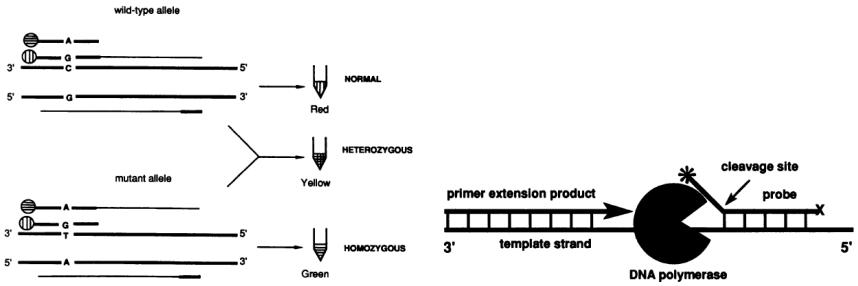

Figure 1.2: Diagram showing how to differentiate between single nucleotide polymorphisms using labeled primers *Chehab F.F. et al.* ***Proceedings of the National Academy of Sciences****, vol. 86 (9178 - 9182), 1989* (Left). Figure illustrating the functioning of a labelled probe *Holland P.M. et al.* ***Proceedings of the National Academy of Sciences****, vol. 88 (7276 - 7280), 1991* (Right).

At the same time the company Hoffmann La Roche bought the rights to PCR from Cetus corporation and a group of scientist around Russel Higuchi started research into PCR. They experimented with adding ethidium bromide (EtBr) into the PCR mixture [15]. EtBr is a fluorescent dye that selectively binds to dsDNA in a reversible manner, called intercalating. The dye only expresses fluorescence when bound to dsDNA. Quickly they realised that the addition of EtBr allowed them to measure the concentration of dsDNA during thermal cycling in real time through simple fluorescent measurements [16]. Hence they called their method real-time PCR, today often referred to as quantitative PCR (qPCR) [2]. A 96-well thermal cycler was equipped with a UV-light-source for excitation as well as a CCD-camera including optical filters. They measured fluorescence intensity in every cycle in the middle of the extension step. As a result they were the first to obtain the sigmoidal amplification curves typical for real-time PCR shown in figure 1.3. The sigmoidal shape of the curve arises due to the fluorescent signal being much lower than the background noise for the initial cycles. Once the signal is strong enough to overcome background noise one can observe an

[2]Sometimes rtPCR or RT-PCR is used instead of qPCR, for this thesis only qPCR is used while rtPCR is reserved reverse transcription PCR as commonly done in literature

exponential increase until depletion of reagents leads to a plateauing of the reaction.

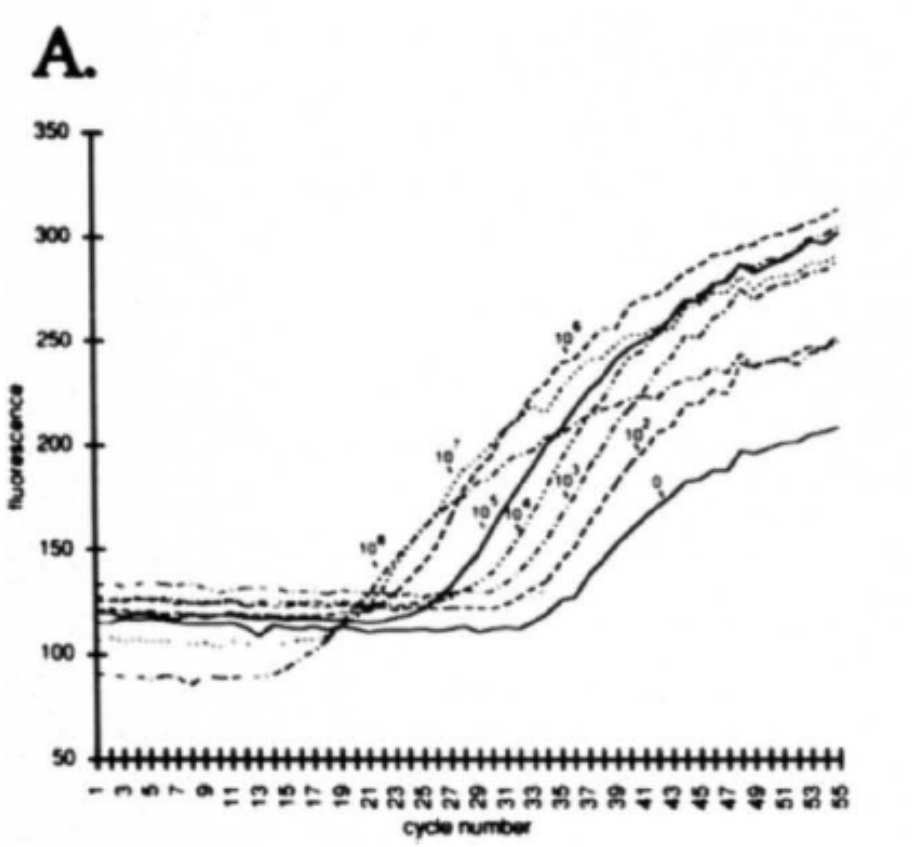

Figure 1.3: Raw fluorescence measured by Higuchi et al. for eight PCR samples containing ethidium bromide and different concentrations of template *Higuchi R. et al.* ***Nature Biotechnology****, vol. 11 (1026 - 1030), 1993*

Since ethidium bromide is considered as carcinogenic and hindering the PCR[17] it is often replaced through the intercalating dyes SYBR-Green I and Eva-Green in modern systems. To increase specificity a probe based system similar to the probes suggested by Holland et al. was developed for use in qPCR. The approach uses hybridization probes with a dual label. On one end of the probe a fluorescent reporter is placed whose fluorescence is quenched through a second fluorescent dye on the other end of the probe [18]. The quenching process takes place through fluorescence resonance energy transfer (FRET). When the polymerase cleaves the hybridized probe during extension the reporter is separated from the quencher. This interrupts the FRET transfer and an increase in fluorescence can be observed.

The approach is often referred to as TaqMan[3] chemistry.

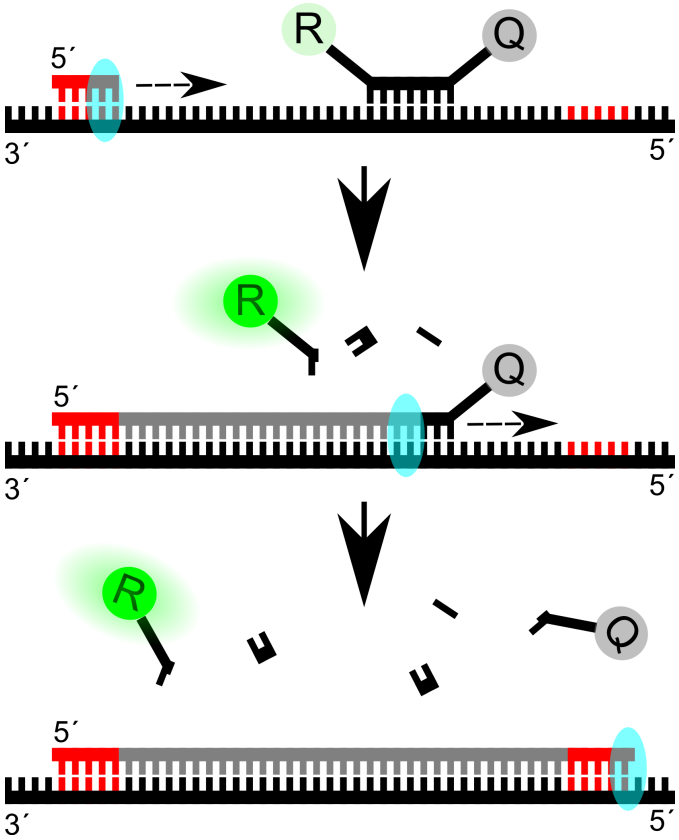

Figure 1.4: Diagram showing how TaqMan chemistry works. In a first step the TaqMan probe and primers hybridise to the template. Through the spatial proximity the reporter (R) is quenched by the quencher (Q). Once the polymerase (blue) encounters the probe during extension it cleaves the reporter from the quencher. Through this the fluorescence from the quencher becomes detectable.

The method is called quantitative PCR because the real time fluorescence data gathered during the experiment can be used to quantify the concentration of template. In general there are two strategies for quantification: absolute quantification and relative quantification. While absolute quantification requires a calibration curve to relate the PCR signal to the initial concentration of template, relative quantification measures the ratio of one template to another one during amplification.

[3]The name TaqMan originates from Taq-polymerase and the popular video game Pac-Man, which reminds of the polymerase degrading the probe.

Relative Quantification

In relative quantification the ratio of the target concentration compared to a internal control is determined. The control often is an added reference gene or a housekeeping gene and can be co-amplified in a multiplex assay in the same reaction tube or amplified in a separate reaction tube. For the calculation of the ratio of the two genes there are several methods based on crossing points (CP) or threshold cycles (C_t). The methods can be classified in two main classes with and without efficiency correction.

One of the most popular methods is the $\Delta\Delta C_T$ method suggested through Kenneth Livak and Thomas Schmittgen [19] [4]. The method is based on the equation shown in equation 1.1.

$$X_n = X_0(1 + E_X)^n \tag{1.1}$$

In the above equation X_n is the number of dsDNA molecules after n cycles, X_0 is the initial number of molecules, E_X is the efficiency of target amplification and n is the number of PCR cycles conducted. The cycle at which the amount of target reaches a certain threshold (K_X) is denominated by the threshold cycle C_{TX}:

$$X_T = X_0(1 + E_X)^{C_{TX}} = K_X \tag{1.2}$$

The same definition can be made for a reference (R), which is an internal control gene:

$$R_T = R_0(1 + E_R)^{C_{TR}} = K_R \tag{1.3}$$

Assuming the same amplification efficiency for target and control ($E_X = E_R = E$) and dividing equation 1.2 by equation 1.3 one obtains:

$$\frac{X_0}{R_0}(1 + E)^{C_{TX} - C_{TR}} = \frac{K_X}{K_R} = K \tag{1.4}$$

where K is the ratio of K_X to K_R. Introducing the normalized amount of target X_N as X_0/R_0 and ΔC_T as the difference in threshold cycle for target and reference ($C_{TX} - C_{TR}$) one obtains after rearrangement:

$$X_N = K(1 + E)^{-\Delta C_T} \tag{1.5}$$

In a last step the normalized amount of target for any sample (q) (X_{Nq}) is divided by the normalized target amount of the calibrator (cb) (X_{Ncb}):

[4] The method was originally proposed in the Applied Biosystems User Bulletin No. 2 (P/N 4303859). The paper was published later on to present the derivation of the method for general literature.

$$\frac{X_{Nq}}{X_{Ncb}} = \frac{K(1+E)^{-\Delta C_{Tq}}}{K(1+E)^{-\Delta C_{Tcb}}} \tag{1.6}$$

Assuming the efficiency to be equal to unity ($E = 1$) and introducing $-\Delta\Delta C_T = \Delta C_{Tcb} - \Delta C_{Tq}$ one obtains:

$$\frac{X_{Nq}}{X_{Ncb}} = 2^{-\Delta\Delta C_T} \tag{1.7}$$

Not making the assumption of the efficiency being equal to unity and assuming different efficiencies for target and calibrator one arrives at a model accounting for different efficiencies [20]:

$$\frac{X_{Nq}}{X_{Ncb}} = \frac{E_q^{\Delta C_{Tq}}}{E_{cb}^{\Delta C_{Tcb}}} \tag{1.8}$$

Absolute Quantification

While relative quantification determines the change in steady-state concentration of a gene to a reference, absolute quantification methods attempt to determine the initial number of copies of the gene present in the reaction mix. One of the earliest methods of absolute quantification was suggested through Rudolf Wiesner et al. [21]. They took a sample after the each consecutive cycle of the reaction starting with cycle 16, in earlier cycles the concentration of DNA was to low to be determined. Once they determined the concentration of DNA in the samples they plotted the logarithm of the concentration against the cycle number. Linear regression using equation 1.9 allowed them to determine the initial concentration of DNA (N_0), the y-axis intercept, and the efficiency (E_x) the gradient of the curve.

$$log(N_n) = log(E_x n) + log(N_0) \tag{1.9}$$

where n is the cycle number and N_n the DNA concentration after the n-th cycle. Since this method is very labour intensive by requiring collection of consecutive samples after every PCR cycle different methods were developed, taking advantage of real-time PCR capabilities.

In 1998 Tom Morrison et al. [22] used SYBR Green I in combination with real-time PCR to determine the initial concentration of a template.They ran a dilution series of the template with known concentration and extracted the threshold cycles of this dilution series. Like Wiesner they plotted the extracted threshold cycles against the logarithm of the initial template concentration. Afterwards a simple linear regression could be done, giving a relation to determine the initial DNA concentration of an unknown sample.

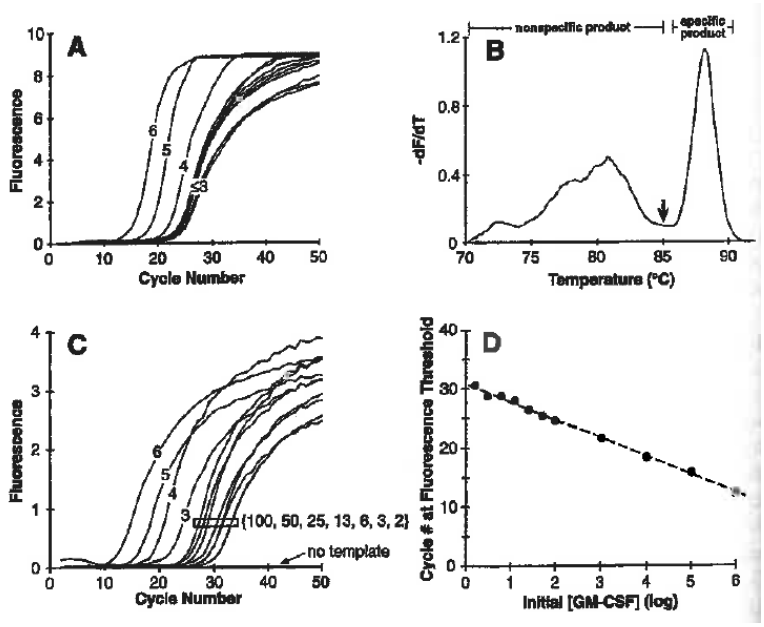

Figure 1.5: Original figure illustrating the method of absolute quantification of GM-CSF suggested by Morrison et al. Real-time fluorescence signal from a serial dilution containing 10^6,10^5,10^4,10^3,10^2,50,25,12,6.3,3.1,1.6 or 0 templates (A). Typical derivative melting curve for an experiment containing 100 starting copies of the template (B). Real-time fluorescence signal from a serial dilution containing 10^6,10^5,10^4,10^3,10^2,50,25,12,6.3,3.1,1.6 or 0 templates, specificity enhanced through the addition of Taq-Antibody (C). Fractional cycle number of threshold cycles against log of initial template concentration, and linear fit through data (D). All figures from *Morrison T. et al.* ***BioTechniques****, vol. 24 (954 - 962), 1998*

Following this method provides a less labour intensive mean of absolute quantification. The required standard curve can be recorded in the same thermal cycler run as is used for unknown sample. Furthermore the method has the advantage of not requiring any assumptions on the efficiency of the reaction. Due to these advantages this approach is commonly used today and integrated into many commercial PCR softwares used for absolute quantification.

1.2.2 Melting Curve Analysis

Before the introduction of fluorescent markers, allowing the real-time observation of PCR, amplification and analysis required sequential operations. Usually amplification was done automatically on a thermal cycler. Products were then manually transferred to an analysis step like agarose or polyacry-

lamide electrophoresis for example. Ririe et al. [23] realised that when they observed the fluorescence of SYBR Green I continuously throughout a temperature cycle the denaturation of the template can be observed as a rapid loss of fluorescence. The temperature at which this occurs, called the melting temperature (T_M), is characteristic for the template. The length, GC-content and sequence of the product influence the melting temperature. Ririe et al. exploited this by running a linear temperature gradient from the extension to denaturation temperature after amplification while continuously recording fluorescence. Afterwards they removed background fluorescence and the temperature effect of fluorescence from the data and plotted the first negative derivative with respect to temperature against temperature. Through this trick melting peaks can be obtained from melting curves. Similar methods are used in melting curve analysis in spectroscopy, hence the method is called melting curve analysis (MCA). The method is able to differentiate products with a difference in T_M of less than $2°C$. Enabling automated analysis of products, without the risk of contamination by manual manipulation, is the main advantage of the method. Furthermore MCA allows the differentiation of products with the same length but different sequence or GC-content which would not be possible by gel electrophoresis.

By the means of equipments specialised on MCA giving temperature resolution down to $0.002°C$ and providing 50 fluorescent measurements for every $1°C$ during ramping high resolution melting curve analysis (HRMCA) can be performed [24]. In this method of operating MCA melting curves are recorded with a gradient of $0.1°C/s$ in the presence of an intercalating dye like LCgreen. Unlike in normal MCA the fluorescence signal is first normalized and optionally temperature shifted. Afterwards the normalised curves are subtracted from a reference curve. This gives a horizontal line for the reference curve and different paths corresponding to different genotypes. Even single nucleotide polymorphisms can be detected using HRMCA.

1.2.3 Reverse Transcription PCR

In 1956 Francis Crick formulated his ideas on Protein Synthesis [25] which are known today as the central dogma of molecular biology. Later-on he refined the idea in a second paper in Nature [26]. The dogma describes the relations between DNA, RNA (Ribonucleic acid) and proteins. Crick describes the key content of the dogma with the following words [25]: "Once information has got into a protein it can't get out again". to illustrate the content of the dogma it might be simpler to visualize it in a diagram 1.7. The solid lines in the diagram represent transfers that occur in most cells, while the dashed lines illustrate processes that only occur under special circumstances.
In the meantime Howard Temine at the University of Wisconsin had dis-

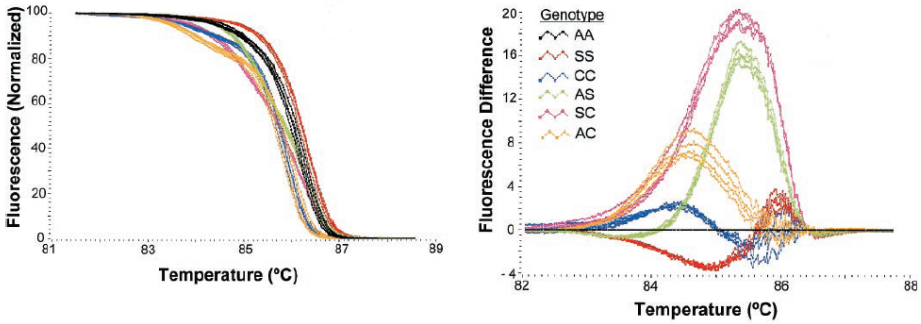

Figure 1.6: Graph showing normalised and temperature shifted fluorescence (to overlay them with the AA wild type between 5 and 10 fluorescence units) as function of temperature for different genotypes containing single nucleotide polymorphisms (left). Fuorescence difference curves obtained through the subtraction of the wild type curve (AA) from each curve (right). Due to the temperature shifting of the initial curve the temperature axis does not correspond to actual temperature but rather reflects temperature difference compared to superimposed parts of the curve. Figure from *Wittwer CT. et al.* ***Clinical Chemistry****, vol. 49 (853 - 860), 2003*

covered the reverse transcriptase enzyme which would allow the synthesis of complementary DNA to an RNA molecule [27]. Thus it should be possible to start with a RNA molecule, synthesise a DNA template from it using reverse transcriptase and then amplify it using PCR. In fact even before the discovery of PCR through Mullis scientists at Havard synthesis DNA from RNA followed by an extension from DNA polymerase resulting in double stranded DNA [28]. Thus it is not surprising that soon after the introduction of PCR the synthesis of the first strand of dsDNA was followed by thermal cycling to amplify the signal. Because this method relies on an initial reverse transcription step before PCR this mode of operating PCR is called reverse transcription PCR (rtPCR) [5].

1.2.4 Multiplexed PCR

In many applications, especially in diagnostics, it is desirable to detect more than one target sequence. In order of achieving this there are two main options, one can either run reactions in parallel with different sets of primers or employ the primer sets for different targets in the same reaction. In the first case one speaks of simplex PCR while the second is often referred to as multiplex PCR.

[5]Sometimes the abbreviation rtPCR is used for real time PCR, in this work it is exclusively used for reverse transcription PCR

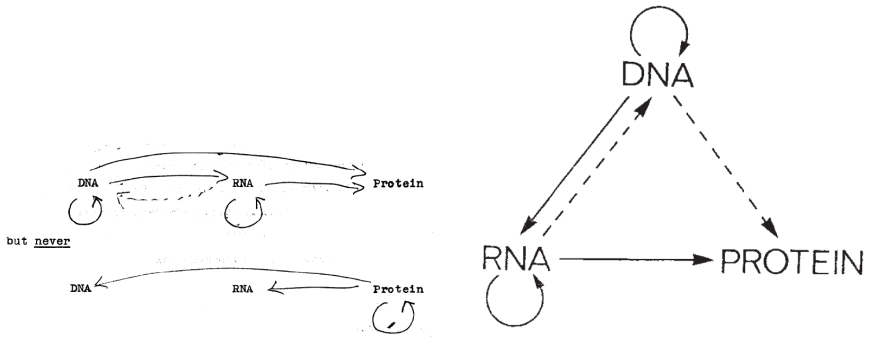

Figure 1.7: Diagrams illustrating the central dogma of molecular biology as proposed by Crick in his original paper *Crick F.* ***Symp. Soc. Exp. Biol.****, XII (139 - 163), 1956* (left) and revised paper *Crick F.,* ***Nature****, vol. 227 (561 - 563), 1970* (right). In both diagrams solid arrows represent processes happening in most cells while dashed arrows indicate process that may occur under special circumstances.

Commonly fluorescent probes with different emission wavelength for each amplicon are used [13]. These are detected using optical filters specific to the probes used (refereed to as fluorescent channels). Depending on the kind of probe used fluorescence detection can be done in real-time (for TaqMan probes for example) or through analysis after amplification (when using labelled primers). Initially only one target could be detected per fluorescent channel but Rajagopal et al. [29] developed a method using linear combinations of the different coloured TaqMan probes for different targets. In theory the number of targets being detectable through this system becomes unlimited. In practice this is limited through overlap, crosstalk and false positives of the probes however.

Alternatively products can be differentiated after amplification using capillary electrophoresis[30] or gel electrophoresis [31] for example. Since these mobility based separation methods will not work for products of the same length melting curve analysis can also be used [32].

1.2.5 Modelling of PCR

To enhance understanding of the reaction and to optimize reaction conditions models have been developed describing the polymerase chain reaction. Two simple models have already been introduced when describing quantification, namely the $\Delta\Delta C_T$ method. When assuming unity for the efficiency one arrives at the following equation as already shown previously:

$$X_n = X_0 2^n \tag{1.10}$$

where X_n is the number of molecules after the n-th cycle, X_0 is the initial number of molecules, and n is the number of cycles. As shown previously one can extend this model through the introduction of an efficiency not equal to unity:

$$X_n = X_0(1+E)^n \tag{1.11}$$

where E is the efficiency of the reaction. Both of these models make strong assumptions on the efficiency and indeed experiments have shown that efficiency is rarely equal to unity and often is strongly dependent on the cycle number. For this reason more elaborate models have been constructed. Gevertz et al. [33] made a model describing all three steps of the reaction (denaturation, annealing and extension) using either equilibrium or kinetic equations. Through this they have been able to find an efficiency for every step in every cycle and obtain better predictions of experimental outcomes. Other models focus on single steps of the reaction like the melting of dsDNA during denaturation [34] or the origin of unspecific products during annealing when dealing with complex templates [35]. Yet other models describe the proofreading function of DNA polymerase during extension on a molecular level [36].

1.3 Thermal Cylcers

Thermal cyclers for PCR have to be able to control the temperature of a liquid sample in such a manner that temperatures for denaturation, annealing and extension are met. Typically the samples have volumes of 5 to $100\mu L$ and require 20 to 50 cycles of amplification. A successful reaction necessarily requires a homogeneous temperature distribution inside the sample. Furthermore evaporation of the sample has to be prevented during thermal cycling. Real-time detection for qPCR needs systems for exciting the fluorophor during the course of the amplification process as well as means of measuring the fluorescent signal. In order to perform MCA and HRMCA the device has to be able to produce a time dependent temperature gradient with a slope of around $0.1°C/s$ while measuring fluorescence. Again a homogeneous temperature distribution inside the sample is crucial especially for HRMCA.

Thermal cycler can be divided into two main classes, time-domain (stationary PCR) and space-domain (flow-trough) machines [37]. While in time-domain PCR samples remain fixed in their position and temperature is changed through a heater and either active or passive cooling, a time-space

conversation is done in space-domain PCR. Here samples are moved through zones having the corresponding temperature. Space domain often has the advantage of featuring significantly higher heating and cooling rates since they have lower thermal masses compared to time-domain machines. On the down side space-domain machines are often less flexible regarding step times and temperatures and are more complex in their construction.

Through the vast number of applications of PCR in research and diagnostics a need for portable devices for use outside laboratories in remote locations is present. The world health organisation (WHO) has created a list of criteria a point-of care device should full fill to be suitable for in field use known as the **ASSURED** criteria [38]:

- **A**ffordable
- **S**ensitive
- **S**pecific
- **U**ser-friendly
- **R**apid and Robust
- **E**quipment free
- **D**elivered

In the original definition of the ASSURED criteria the WHO defined sensitive as avoiding false negative results and likewise specific as avoiding false positive results. User-friendly was specified as simple to perform and using non-invasive techniques. Delivered meant accessibility to the end-user.

1.3.1 Commercial Devices

A variety of companies offers thermal cyclers and real-time thermal cyclers on the market. Most of these commercial machines are made for high throughput applications in laboratories and use time-domain technology. Sample volumes used in most commercial devices lie in the range of 5 to $50\mu L$. Three commercial devices will be introduced in the following as an examples for the number of devices available on the market.

The most typical example for a high-throughput laboratory machine here is the AppliedBiosystems 7500 Fast Real-Time PCR machine. It consists out of a Peltier-based 96-well block, suitable for plates used in these applications. Through the high thermal mass of the heating block and well-plate heating and cooling rates are only $5.5°C/s$ in fast mode and a mere $1.6°C/s$ in standard operation mode. For real-time detection the system employs a Tungsten-Lamp for excitation combined with excitation and emission filters

Figure 1.8: Two commercial thermal cyclers, namely: (a) ABI 7500 Fast (b) Roche Light Cycler capillary based

for five different dyes. Emission light is captured using a charged-coupled device camera (CCD camera)[39].

While plates have the advantage of being handleable through lab robots and thus allowing automation of processes in labs Roche has chosen a different way when designing their LightCycler Capillary based system. Here samples are stored in glass capillaries with volumes of $20\mu L$ or alternatively $100\mu L$. The system can cycle 96 of these capillaries at the same time in the old version, or 32 capillaries in the new system. The main disadvantage of capillaries is that they can not be handled automatically and are thus not suitable for high-throughput applications. They can, however, be heated and cooled using air allowing significantly faster heating and cooling rates of up to $20°C/s$. The LightCycler is equipped with light emitting diodes (LED) for excitation and has the corresponding excitation and emission filters equipped. The system is either available with three or alternatively six fluorescence channels[40].

The real-time thermal cyclers from Roche and AppliedBiosystems are both significantly heavier than $20kg$ and meant to be used in a laboratory as a bench-top device. In 2014 PrimerDesign introduced the Genesig q16 weighing only $2kg$ and occupying only $120cm^2$ for use outside traditional laboratories by medical doctors or veterinarians for example. As it is designed to be used outside of laboratories it is not set up for high-throughput measurements usually done in labs, instead it can only handle 16 samples in parallel each having a volume of $20\mu L$. Heating and cooling are done using a Peltier-element allowing rates of $3°C/s$ for heating and $2°C/s$ for cooling. For fluorescence detection a complementary metal-oxide-semiconductor

(CMOS) detector is used while a LED is used for excitation [41]. Through these simplified optics the Genesig q16 can only detect one dye unlike the systems offered for use in conventional labs.

The systems offered commercially are often designed for laboratory use and well suited for automation of processes and high-throughout applications. On the downside these machines are relatively expensive and bulky, thus not suitable for in-field use. Furthermore most commercial thermal cyclers require sample volumes higher than $5\mu L$. Additionally the use of thermal blocks and Peltier elements for heating and cooling causes high thermal masses of the systems and thus often long ramping times between the individual steps.

1.3.2 Academic Devices

A wide variety of thermal cyclers has been suggested through the academic community. Unlike commercial cyclers which are mainly time domain and often realise heating with blocks powered through Peltiers academic devices use time as well as space domain. Furthermore a bigger variety in heating and cooling as well as detection methods can be seen here. In the following a couple of examples are given for systems using space-domain as well as systems time-domain.

Space-domain Devices

Space-domain thermal cyclers often use the advantages microfluidics has to offer in terms of controllable and fast thermal transfer. By passing the sample through zones of alternating temperature avoids temperature cycling of the entire device making the process faster and energy efficient. Many design either continuously flow a sample through different heat zones along a channel or they employ plugs or droplets.

One of the first space-domain thermal cyclers was presented in 1998 by Kopp et al. [42]. The device used a serpentine, microfluidic channel passing through three different temperature zones for denaturation, annealing and extension (fig. 1.9(a)). The design featured a channel with a length of $2.2m$ resulting in 20 cycles. The time spend in each cycle was determined through the flow rate. The length of channel in each temperature zone determined the time for each step. Through variations in flow rate the twenty cycles could be performed in times ranging between 90 seconds and 19 minutes. The use of microfluidics and the small channel dimensions ($40\mu m$ x $90\mu m$) allowed for heating and cooling times of about $100ms$ equating to rates of about $200°C/s$. In this case detection of the samples was done of chip by collecting sample at the outlet and afterwards performing gel electrophoresis.

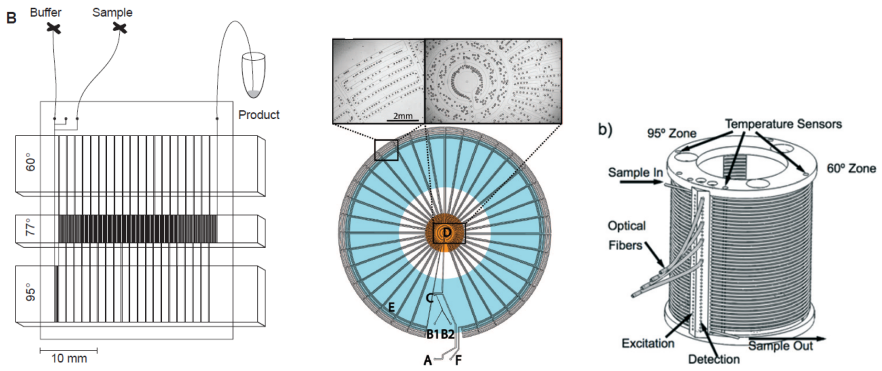

Figure 1.9: Continuous flow through PCR chip layout featuring a serpentine channel going though three temperature zones for denaturation, annealing and extension *Kopp M.U. et al.* ***Science****,vol. 280 (1046 - 1048), 1998* (left). Radial chip design employing droplets and two temperature zones for amplification. The red circle in the middle of the design marks the position of the one copper heating element used. Droplets were generated using a T-junction droplet generator marked with C in the schematic *Schaerli Y. et al.,* ***Anal. Chem.****, vol. 81 (302 - 306), 2009* (middle). Drawing of a thermal cycler consisting out of tubing wrapped around a cylinder compromising two different temperature zones. The design also includes optical fibres for measuring the fluorescence intensity of the sample at the end of every cycle *Hatch A.C. et al.,* ***Lab Chip****, vol. 14 (562 - 568), 2014* (right).

Starting from this initial flow through device many variants were developed. A radial design using droplets is one of the more worthy of note here [43]. The design includes a channel passing repeatedly through the centre followed by the periphery of the design (fig. 1.9(b)). A single heating element in the middle of the design defines the denaturation zone while the extension and annealing zone were created through a thermal gradient towards the periphery established through a Peltier. Droplets containing the template were created using a T-junction droplet generator on the chip. The use of droplets has several advantages for this application. Firstly droplets reduce the risk of cross contamination and cross talk caused by adsorption of template molecules to the wall of the channel. Additionally droplets allow the analysis of genomic libraries, man-made libraries and complementary DNA (cDNA) libraries. Lastly digital PCR can be performed by only encapsulating a single template molecule in each droplet. This has particular advantages when dealing with rare DNA strands in a complex mixture of DNAs. Again products were analysed by collecting sample at the outlet of the chip followed by different analysis methods of chip.

Another popular radial design compromises a capillary or tubing wrapped

around a cylinder having different heating zones. An example for this was published by Hatch et al. [44] made out of $10m$ tubing with an internal diameter of $0.5mm$ twisted around an aluminium cylinder that had two temperature zones (fig. 1.9(c)). One of the temperature zones was used for denaturation the other one for annealing and extension. Unlike the previous examples shown the cycle number could be varied by changing the number of turns of the tubing around the cylinder. Samples were either introduced as plugs or as droplets with the fluorinated oil FC-40 as the continuous phase. In this design for a thermal cycler real-time fluorescence detection was done after every cycle through optical fibbers aligned with the tubing after every cycle. A LED was used for excitation while a multi anode photomultiplier tube was used for measuring the emission light.

A remarkable space-domain thermal cycler is constructed from two water baths, one boiling at $95.5°C$ [6] the other one between $25°C$ and $74°C$ depending on the experiment [45]. A $5\mu L$ sample in a glass capillary was moved repeatedly from one water bath to the other one using a stepper motor. Real time fluorescence detection was done using fibre optics in the colder of two water baths. Since the aim of the experiments was to achieve an as short as possible time per cycle the sample was either moved after a set time to the next bath, or alternatively once a thermocouple attached next to the capillary obtained a pre-set temperature. Through this set-up a 35 cycle PCR could be performed in under 15 seconds.

Time-domain Devices

The number of cycles and length of the different steps in time-domain cyclers can often be controlled by software or other easy to modify means making them easier to adapt to different PCR protocols. Through this advantage time-domain machines are not only popular for commercial devices but are also chosen for a variety of developmental devices.

A zwitter device between time and space domain was proposed in form of a portable cycler powered through a candle [46]. The device consisted out of $15ml$ water bath which was heated to the boiling point using a candle (fig. 1.10(a)). Glass capillaries were held into this water bath in such a manner that the bottom part would be submerged and the top part would be exposed to ambient conditions. Through the temperature gradient inside of the capillary internal convection occurred cycling the sample between denaturation temperature at the bottom of the capillary and annealing and extension temperatures at the top of the capillary. The device should be considered as a zwitter between space and time domain because the sample

[6] Experiments were conducted in Salt Lake City, Utah, where water boils at $95.5°C$ due to the altitude.

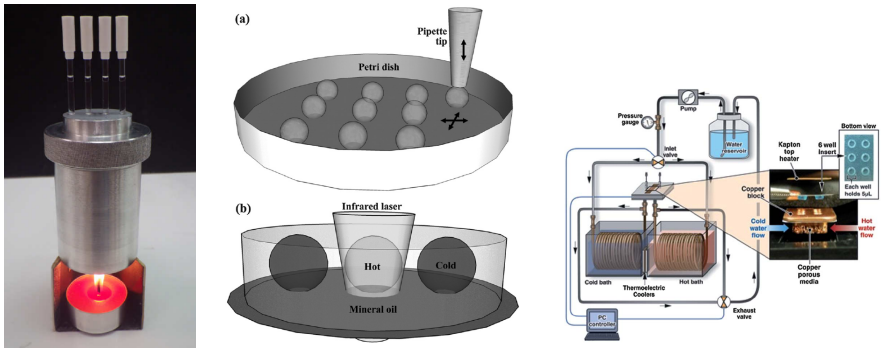

Figure 1.10: PCR with phase change as intrinsic thermal control. The heat source for this device heating a small water bath ($15ml$) till boiling providing the denaturation temperature. Through internal convection the sample moves to colder parts for annealing and extension *Hsieh Y. et al.* ***Appl. Phys. Lett.****,vol. 102 (173701.1 - 173701.3), 2013* (left). Device employing a printed droplet array covered with mineral oil, Heating is done with a modulated infra red laser focused on individual droplets *Kim H. et al.,* ***Lab Chip****, vol. 9 (1230 - 1235), 2009* (middle). Device employing a porous heat exchanger underneath the reaction chamber. To change the temperature of the reaction chamber preheated water was flown through the heat exchanger from a reservoir. *Wheeler E.K. et al.,* ***Analyst****, vol. 136 (3707 - 3712), 2011* (right).

is not actively shuttled between the temperature zones and the reaction conditions are defined through time and temperatures not by device geometry. In this device detection of products was done after the completed reaction by gel electrophoresis.

Kim et al. employed an array of printed droplets containing the sample with volumes in the sub-microliter range [47]. The droplets were placed on a polystyrene surface and covered with mineral oil making them similar to virtual reaction chambers. Heating was done using a modulated infra-red laser focused on individual droplets (fig. 1.10(b)). Through modifications in the duty cycle of the laser temperature could be raised. Heat dissipated through the surrounding mineral oil was used for passive cooling. An LED and CCD was used for excitation and detection providing means for real-time detection. This approach allows for different step times as well as cycling numbers for each individual droplet mearly by software modification.

To achieve fast heating and cooling rates Wheeler et al. utilized a porous heat exchanger underneath of a $5\mu L$ reaction chamber [48]. To change the temperature preheated water was flown through the heat exchanger (fig.

1.10(c)). This also allowed for active cooling resulting in equal heating and cooling rates of $45°C/s$. An electric heating element was also included to allow for higher heating rates when required. In the published version product analysis was done through gel electrophoresis but optics for real-time detection are planned for future versions of the device.

A further popular method of realizing a time-domain amplification is using isothermal amplification. In isothermal amplification the entire PCR is conducted at one temperature, however the reaction follows a different pathway to reactions conducted at two or three different temperatures. A recent device for example uses a slip chip to perform digital, isothermal amplification [49]. Here the reaction mixture was compartmentalised through the slip chip and consequently isothermal amplification was carried out. Here the process of the reaction was exclusively determined by the reaction time since there is no cycling. After amplification fluorescence of the individual compartments was measured using an optical filter set and a smartphone camera. Isothermal PCR shows a bigger robustness against disturbances influencing the reaction efficiency compared to real-time PCR. On the downside the dynamic range is significantly lower and reaction times are longer.

Due to a high thermal conductivity and well known fabrication methods, even for sub-micrometer features, silicon is a popular choice for PCR devices. One of the first thermal cyclers made from silicon consisted out of a chamber etched into a silicon wafer with a volume of $10\mu L$ capped by glass [50]. Heating and cooling was achieved using a computer controlled Peltier underneath the silicon chip. Despite the optical transparent cover of the chip real-time detection was not performed, instead products were analysed through gel-electrophoresis after amplification. A more recent, portable device makes use of silicon heating blocks combined with platinum heaters [51]. Standard plastic $20\mu L$ vials are used as reaction vessels. LEDs with two different wavelength and corresponding filters are used for the real-time detection of 6-carboxyfluorescein (FAM) and 6-carboxy-4',5'-dichloro-2',7'-dimethoxyfluoresceine (JOE) dyes.

1.4 Protein Analysis

Although protein denaturation was known since 1910 the process was not understood well and mostly a mystery to scientists. Years later scientist realised that protein denaturation is a structural change in the protein and began suggesting the first models for protein folding. One of the first models was the cyclol model by Dorothy Wrinch [52]. Although the model had to be amended later on some of the assumptions still proved to be correct like the prediction that one of the main driving forces for protein folding

are hydrophobic interactions. Today protein structure is determined using a variety of different techniques like X-ray crystallography, nuclear magnetic resonance spectroscopy or cryo-electron microscopy.

For researchers not only the conformation of the protein is of interested but also the kinetics and mechanisms of the folding and unfolding process [53]. To study these kinetics and to probe the thermal stability of proteins calorimetric measurements, like differential scanning calorimetry and isothermal titration calorimetry, are widely used [54]. Fluorescence microscopy can also be used as a highly sensitive method through the exploitation of intrinsic fluorescence, fluorescence markers or dyes. Extrinsic dyes that interact noncovalantly with the protein, for example, are of high interest. One example of this is 1-anilinonaphtalene-8-sulfonate (ANS) which is strongly fluorescent in apolar solvents but loses almost all of its fluorescence in aqueous environments. This property allows observation of protein denaturation by fluorescence microscopy as during denaturation the hydrophobic sites formerly inside the protein become exposed. ANS can interact with these sites and an increase in fluorescence is observed [55]. Thus an indirect measurement of protein stability is done. This method is often referred to as fluorescence thermal shift assay since denaturation of the protein is often done by the application of a temperature gradient. Another use of these technique lies in the identification of protein ligand interactions for example to screen for potential therapeutic substances.

Bibliography

[1] S.C. Terry, J.H. Jerman, and J.B. Angell. A gas chromatographic air analyzer fabricated on a silicon wafer. *Electron Devices, IEEE Transactions on*, 26(12):1880–1886, Dec 1979.

[2] A. Manz, Y. Miyahara, J. Miura, Y. Watanabe, H. Miyagi, and K. Sato. Design of an open-tubular column liquid chromatograph using silicon chip technology. *Sensors and Actuators B: Chemical*, 1(1-6):249 – 255, 1990.

[3] J. R. Burns and C. Ramshaw. The intensification of rapid reactions in multiphase systems using slug flow in capillaries. *Lab Chip*, 1:10–15, 2001.

[4] T. Thorsen, R.W. Roberts, F.H. Arnold, and S.R. Quake. Dynamic Pattern Formation in a Vesicle-Generating Microfluidic Device. *Phys. Rev. Lett.*, 86:4163–4166, Apr 2001.

[5] M. Washizu. Electrostatic actuation of liquid droplets for micro-reactor applications. *Industry Applications, IEEE Transactions on*, 34(4):732–737, Jul 1998.

[6] Z. Guttenberg, H. Muller, H. Habermuller, A. Geisbauer, J. Pipper, J. Felbel, M. Kielpinski, J. Scriba, and A. Wixforth. Planar chip device for PCR and hybridization with surface acoustic wave pump. *Lab Chip*, 5:308–317, 2005.

[7] P.l Neuzil, J. Pipper, and T.M. Hsieh. Disposable real-time microPCR device: lab-on-a-chip at a low cost. *Mol. BioSyst.*, 2:292–298, 2006.

[8] D. Zahn. How Does Water Boil? *Phys. Rev. Lett.*, 93:227801, Nov 2004.

[9] P. Neuzil, W. Sun, T. Karasek, and A. Manz. Nanoliter-sized overheated reactor. *Applied Physics Letters*, 106(2), 2015.

[10] K. Mullis, F. Faloona, S. Scharf, R. Saiki, G. Horn, and H. Erlich. Specific enzymatic amplification of DNA in vitro: The polymerase chain reaction. *Cold Spring Harbor Symposia on Quantitative Biology*, 51(1): 263–273, 1986.

[11] K.B. Mullis and Faloona F.A. *Specific synthesis of DNA in vitro via a polymerase-catalyzed chain reaction*, volume 155 of *Methods in Enzymology*. Academic Press, 1987.

[12] R.K. Saiki, D.H. Gelfand, S. Stoffel, S.J. Scharf, R. Higuchi, G.T. Horn, K.B. Mullis, and H.A. Erlich. Primer-directed enzymatic amplification

of DNA with a thermostable DNA polymerase. *Science*, 239(4839): 487–491, 1988.

[13] F. F. Chehab and Y. W. Kan. Detection of specific DNA sequences by fluorescence amplification: a color complementation assay. *Proceedings of the National Academy of Sciences*, 86(23):9178–9182, 1989.

[14] P.M. Holland, R.D. Abramson, R. Watson, and D.H. Gelfand. Detection of specific polymerase chain reaction product by utilizing the 5'—-3' exonuclease activity of Thermus aquaticus DNA polymerase. *Proceedings of the National Academy of Sciences*, 88(16):7276–7280, 1991.

[15] R.l Higuchi, G. Dollinger, P. S. Walsh, and R. Griffith. Simultaneous Amplification and Detection of Specific DNA Sequences. *Nat Biotech*, 10(4):413–417, 1992.

[16] R. Higuchi, C. Fockler, G. Dollinger, and R. Watson. Kinetic PCR Analysis: Real-time Monitoring of DNA Amplification Reactions. *Nat Biotech*, 11(9):1026–1030, 1993.

[17] W.H. Elliott. The effects of antimicrobial agents on deoxyribonucleic acid polymerase. *Biochemical Journal*, 86(3):562–567, 1963. ISSN 0264-6021.

[18] C.A. Heid, J. Stevens, K.J. Livak, and P.M. Williams. Real time quantitative PCR. *Genome Research*, 6(10):986–994, 1996.

[19] K.J. Livak and T.D. Schmittgen. Analysis of Relative Gene Expression Data Using Real-Time Quantitative PCR and the $2 - \Delta\Delta C_T$ Method. *Methods*, 25(4):402 – 408, 2001. ISSN 1046-2023.

[20] M.W. Pfaffl. A new mathematical model for relative quantification in real-time RT-PCR. *Nucleic Acids Research*, 29(9):e45, 2001.

[21] R.J. Wiesner, J.C. Ruegg, and I. Morano. Counting target molecules by exponential polymerase chain reaction: Copy number of mitochondrial DNA in rat tissues. *Biochemical and Biophysical Research Communications*, 183(2):553 – 559, 1992.

[22] T.B. Morrison, J. Janis, and C.T. Wittwer. Quantification of Low-Copy Transcripts by Continuous SYBR Green I Monitoring during Amplification. *BioTechniques*, 24(6):954 – 962, 1998.

[23] K.M. Ririe, R.P. Rasmussen, and C.T. Wittwer. Product Differentiation by Analysis of DNA Melting Curves during the Polymerase Chain Reaction. *Analytical Biochemistry*, 245(2):154 – 160, 1997.

[24] C.T. Wittwer, G.H. Reed, C.N. Gundry, J.G. Vandersteen, and R.J. Pryor. High-Resolution Genotyping by Amplicon Melting Analysis Using LCGreen. *Clinical Chemistry*, 49(6):853–860, 2003.

[25] F. Crick. Ideas on Protein Synthesis. *Symp. Soc. Exp. Biol.*, 12:139–163, 1956.

[26] F. Crick. Central Dogma of Molecular Biology. *Nature*, 227(5258): 561–563, 1970.

[27] H.M. Temin. The effects of actinomycin D on growth of Rous sarcoma virus in vitro. *Virology*, 20(4):577 – 582, 1963.

[28] A. Efstratiadis, F.C. Kafatos, A.M. Maxam, and T. Maniatis. Enzymatic in vitro synthesis of globin genes. *Cell*, 7(2):279 – 288, 1976.

[29] A. Rajagopal, A. Scherer, A. Homyk, and E. Kartalov. Supercolor Coding Methods for Large-Scale Multiplexing of Biochemical Assays. *Analytical Chemistry*, 85(16):7629–7636, 2013.

[30] E.T. Lagally, C.A. Emrich, and R.A. Mathies. Fully integrated PCR-capillary electrophoresis microsystem for DNA analysis. *Lab Chip*, 1: 102–107, 2001.

[31] S.K. Poddar. Influenza virus types and subtypes detection by single step single tube multiplex reverse transcription-polymerase chain reaction (RT-PCR) and agarose gel electrophoresis. *Journal of Virological Methods*, 99(1-2):63 – 70, 2002.

[32] M. Hernandez, D. Rodriguez-Lazaro, T. Esteve, S. Prat, and M. Pla. Development of melting temperature-based SYBR Green I polymerase chain reaction methods for multiplex genetically modified organism detection. *Analytical Biochemistry*, 323(2):164–170, 2003.

[33] J.L. Gevertz, S.M. Dunn, and C.M. Roth. Mathematical model of real-time PCR kinetics. *Biotechnology and Bioengineering*, 92(3):346–355, 2005.

[34] O. Dahlen and T.S. van Erp. Mesoscopic modeling of DNA denaturation rates: Sequence dependence and experimental comparison. *The Journal of Chemical Physics*, 142(23), 2015.

[35] E. Rubin and A.A. Levy. A Mathematical Model and a Computerized Simulation of PCR Using Complex Templates. *Nucleic Acids Research*, 24(18):3538–3545, 1996.

[36] J. Abbotts and L.A. Loeb. DNA polymerase α and models for proofreading. *Nucleic Acids Research*, 13(1):261–274, 1985.

[37] C. Zhang, J. Xu, W. Ma, and W. Zheng. PCR microfluidic devices for DNA amplification. *Biotechnology Advances*, 24(3):243 – 284, 2006.

[38] H. Kettler and S. Hawkes. *Mapping the landscape of diagnostics for sexually transmitted infections*. WHO/TDR, 2004.

[39] AppliedBiosystems. ABI7500 Fast product specifications. `https://products.appliedbiosystems.com/ab/en/US/adirect/ab?cmd=catNavigate2&catID=603784&tab=TechSpec`, 2015. Online; accessed 15 September 2015.

[40] Roche Life Sciences. LightCycler 2.0 Product specifications. `https://lifescience.roche.com/shop/en/global/products/lightcycler14301-20-instrument`, 2015. Online; accessed 15 September 2015.

[41] PrimerDesign. Genesig q16 Product specifications. `http://www.primerdesign.co.uk/products/9696`, 2015. Online; accessed 15 September 2015.

[42] M.U. Kopp, A.J. DeMello, and A. Manz. Chemical Amplification: Continuous-Flow PCR on a Chip. *Science*, 280(5366):1046–1048, 1998.

[43] Y. Schaerli, R.C. Wootton, T. Robinson, V. Stein, C. Dunsby, M.A.A. Neil, P.M.W. French, A.J. deMello, C. Abell, and F. Hollfelder. Continuous-Flow Polymerase Chain Reaction of Single-Copy DNA in Microfluidic Microdroplets. *Analytical Chemistry*, 81(1):302–306, 2009.

[44] A.C. Hatch, T. Ray, K. Lintecum, and C. Youngbull. Continuous flow real-time PCR device using multi-channel fluorescence excitation and detection. *Lab Chip*, 14:562–568, 2014.

[45] J.S. Farrar and C.T. Wittwer. Extreme PCR: Efficient and Specific DNA Amplification in 15-60 Seconds. *Clinical Chemistry*, 61(1):145–153, 2015.

[46] Y-F. Hsieh, E. Yonezawa, L-S. Kuo, S-H. Yeh, P-J. Chen, and P-H. Chen. Polymerase chain reaction with phase change as intrinsic thermal control. *Applied Physics Letters*, 102(17), 2013.

[47] H. Kim, S. Vishniakou, and G.W. Faris. Petri dish PCR: laser-heated reactions in nanoliter droplet arrays. *Lab Chip*, 9:1230–1235, 2009.

[48] E. K. Wheeler, C. A. Hara, J. Frank, J. Deotte, S. B. Hall, W. Benett, C. Spadaccini, and N. R. Beer. Under-three minute PCR: Probing the limits of fast amplification. *Analyst*, 136:3707–3712, 2011.

[49] D.A. Selck, M.A. Karymov, B. Sun, and R.F. Ismagilov. Increased Robustness of Single-Molecule Counting with Microfluidics, Digital Isothermal Amplification, and a Mobile Phone versus Real-Time Kinetic Measurements. *Analytical Chemistry*, 85(22):11129–11136, 2013.

[50] P. Wilding, M.A. Shoffner, and L.J. Kricka. PCR in a silicon microstructure. *Clinical Chemistry*, 40(9):1815–8, 1994.

[51] J.A. Higgins, S. Nasarabadi, J.S. Karns, D.R. Shelton, M. Cooper, A. Gbakima, and R.P. Koopman. A handheld real time thermal cycler for bacterial pathogen detection . *Biosensors and Bioelectronics*, 18(9): 1115 – 1123, 2003.

[52] D.M. Wrinch. The Pattern of Proteins. *Nature*, 137:411 – 412, 1936.

[53] C.M. Dobson. Protein folding and misfolding. *Nature*, 426:884 – 890, 2003.

[54] N.C. Garbett and J.B. Chaires. Thermodynamic studies for drug design and screening. *Expert Opinion on Drug Discovery*, 7(4):299–314, 2012.

[55] A. Hawe, M. Sutter, and W. Jiskoot. Extrinsic fluorescent dyes as tools for protein characterization. *Pharmaceutical Research*, 25(7): 1487–1499, 2008.

Chapter 2

Aim and Structure of the Thesis

Motivation

As state by the title the most important aim of the thesis is to evaluate the feasibility of virtual reaction chambers as a tool for the analysis of DNA and proteins. In the context of this thesis the analysis of DNA shall be limited to the polymerase chain reaction, or reverse transcription PCR when starting from RNA, respectively. The property of proteins that is researched in this thesis is their thermal stability.
To evaluate the usefulness of VRCs for these purposes a system for the analysis and thermal manipulation of VRCs has to be devised first. To make it feasible for real world PCR applications, possibilities for multiplexing in VRCs are explored.
Furthermore, in case of VRCs beeing feasible for the mentioned applications, it is desirable to take advantage of the benefits of microfluidics and construct a portable, point-of-care-device for in field diagnostics.

Structure of the Thesis

After the introduction the thesis is structured in eight chapters. In a first chapter a portable PCR device is introduced. The results of this chapter have been published in a paper in Lab on a Chip. In the subsequent chapter reverse transcription PCR is demonstrated on the portable PCR device from the first chapter. The next two chapters deal with multiplexed PCR, firstly using two different dye chemistries, and secondly by utilizing the advantages of VRCs. Both contributions have been published as papers in Scientific Reports. Concluding the work on PCR is a chapter dealing with the development of a mathematical model describing the reaction.
Lastly a chapter deals with the applications of VRCs in applications for pro-

tein analysis making use of the superheating capacity. Finally the thesis is concluded with an conclusion on the work conducted for this thesis and an outlook towards possible future work. At the end short definitions of some key words as well as the published papers of this thesis in their original formatting can be found in the appendix.

Chapter 3

Handheld PCR device

3.1 Motivation and relation to the thesis

In order to perform polymerase chain reaction inside of virtual reaction chambers a method had to be found to manipulate the temperature of the VRC. Ideally the device is able to heat and cool the sample rapidly while maintaining a homogeneous temperature distribution inside the sample. Furthermore real-time detection requires fluorescence measurements of the sample thus optical access to the sample should not be hindered by the temperature control device. In this chapter a silicon based heating chip is developed and tested fulfilling the mentioned criteria. The chip is subsequently used in the following work as a means of manipulating the temperature of VRCs.

As virtual reaction chambers provide a relatively simple, equipment inextensive access to microfluidics, not requiring syringe pumps for example, and the developed chip only measures 15 x 15 mm it was decided to implement the chip in a portable PCR device. Hence the development of a handheld, real-time PCR device capable of the parralel performance of four polymerase chain reactions is described in the following. The system is based on virtual reaction chambers and the developed heating chip.

3.2 State of the art

Virtual reaction chambers have already been utilized in the past for PCR. To fulfil this task methods of temperature control had to be devised. A micromachined silicon chips was used for this purpose in a couple of examples. The chip consisted out a doughnut shaped silicon structure suspended on a cantilever. In the centre of the doughnut either another doughnut or silicon disk was placed (Fig. 3.1). A gold resistive heater as well as temperature sensor were attached to the back side of the inner doughnut or disc, respec-

tively. On top of the silicon heating chip a thin, hydrophobically covered glass slide was placed. This configuration has the advantage of providing fast heat transfer though the silicon chip as well as a clean surface by the disposable glass slide. A first example of the system in use was demonstrated in 2006 [1] with relatively large sample volumes of $1\mu L$. Shortly afterwards the same system was used to demonstrate the fastest PCR at the time in under six minutes [2]. To accelerate the PCR the sample volume was reduced to $100nL$ while keeping the same silicon chip for heating. This way heating rates of $175°C/s$ could be achieved while a cooling rate of $125°C/s$ was obtained by passive cooling.

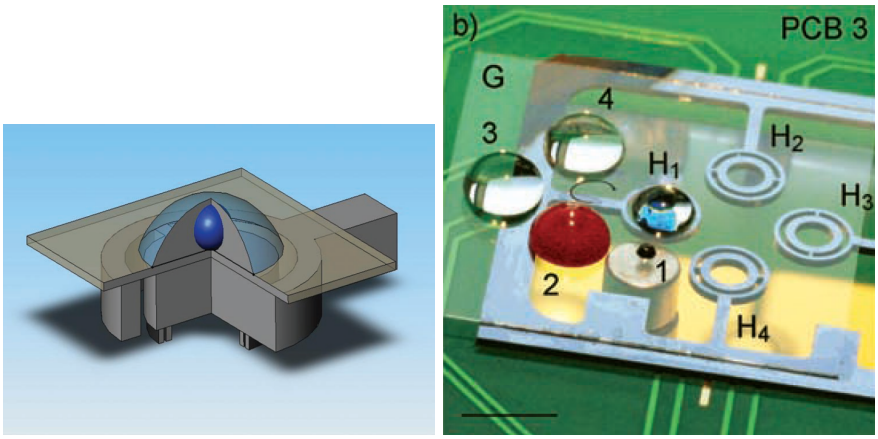

Figure 3.1: Schematic showing the VRC on the silicon heating chip. In this case cross-section shows the outer doughnut structure and the inner silicon disc used in this case. The gold resistive heater and sensor can be seen on the bottom of the inner disc. *P. Neuzil et al.* ***Nucleic Acids Research****, vol. 34 (e77), 2006* (Left). Picture showing the clockwork-PCR device. The four droplets on the left of the picture are for sample preparation, while the sample is moved with the droplet located at H1 through the different temperature zones provided by the silicon heater (H1 - H4). Below the chip the permanent magnet moving the sample can be seen (marked with 1) *J. Pipper et al.* ***Angewandte Chemie****, vol. 120 (3964 - 3968), 2008* (right)

The chip had dimensions of 24.2 x 24.2 mm and was used later on in combination with a motorized stage, permanent magnet and magnetic beads for sample preparation. One example here is the detection of bird flu RNA from a saliva sample [3]. Throat swab samples were placed on the glass slide and the virus RNA extracted using magnetic beads. Once the RNA was extracted and washed it was moved into a droplet containing PCR master mix and reverse transcriptase. The temperature of this droplet was then manipulated using the silicon chip to initiate reverse transcription followed by PCR. A similar method was introduced later, also using magnetic par-

ticles to extract in this instance DNA from GFP-transfected bacteria (See figure 3.1(b))[4]. Again the beads with the bound DNA were merged with a VRC on top of a silicon heater. In this instance, however, thermal cycling was not achieved by changing the temperature of the heater. Instead the beads and VRC were moved between 4 different silicon heaters at the temperatures required for PCR.

In this chapter the existing system of silicon heating chip, hydrophobic glass slide and virtual reaction chamber is further developed. Firstly the dimensions of the chip are reduced to 15 x 15 mm with the ability to analyse four samples in parallel. Secondly the chip is integrated in a portable real-time PCR system. While in previous applications of the system fluorescence measurements were made using a microscope parts for florescence detection had to be miniaturized and made compatible with the heating chip. As the inner doughnut or disc respectively present in earlier versions of the chip blocked the optical path the design had to be modified to obtain optical access to the chip.

3.3 Paper: Handheld real-time PCR device

As published in: *Christian D. Ahrberg, Bojan Robert Ilic, Andreas Manz and Pavel Neuzil, Handheld real-time PCR device,* ***Lab on a Chip*** *(2016)*

Here we report one of the smallest real-time polymerase chain reaction (PCR) systems to date with an approximate size of 100 mm x 60 mm x 33 mm. The system is an autonomous unit requiring an external 12 V power supply. Four simultaneous reactions are performed in the form of virtual reaction chambers (VRCs) where a ≈200 nL sample is covered with mineral oil and placed on a glass cover slip. Fast, 40 cycle amplification of an amplicon from the H7N9 gene was used to demonstrate the PCR performance. The standard curve slope was -3.02 ± 0.16 cycles at threshold per decade (mean ± standard deviation) corresponding to an amplification efficiency of 0.91 ± 0.05 per cycle (mean ± standard deviation). The PCR device was capable of detecting a single deoxyribonucleic acid (DNA) copy. These results further suggest that our handheld PCR device may have broad, technologically-relevant applications extending to rapid detection of infectious diseases in small clinics.

The invention of polymerase chain reaction (PCR) 32 years ago is considered to be one of the greatest inventions of the last century [5]. Over the years, many variants of the original system have been developed. One of the most important advancements is the real-time PCR analysis system [6]. The approach enables real-time PCR amplification, monitoring, and quantification of the number of deoxyribonucleic acid (DNA) copies in the sample under consideration. This method is commonly referred to as quantitative PCR (qPCR) [6]. The main advantage of real-time PCR is the elimination of any post-processing, such as electrophoresis or hybridization to detect the PCR product.

The PCR reaction is performed by thermal cycling in the presence of specific oligonucleotides, the enzyme polymerase, free nucleic acids and bivalent salts such as $MgSO_4$ or $MgCl_2$. This cocktail is commonly referred to as the PCR master mix. The detection of PCR product amplification is conducted by monitoring the fluorescence amplitude during the PCR. In the presence of an intercalating dye, such as SYBR Green I, the fluorescence amplitude is proportional to the concentration of the DNA amplicon, the product of the PCR. In order to verify amplification specificity, upon PCR completion, employment of an intercalating dye enables performing melting curve analysis (MCA). Another improvement of the PCR is the addition of the reverse transcriptase enzyme to the PCR cocktail, forming reverse

transcription PCR (RT-PCR).
PCR has become the method of choice for the detection of DNA and RT-PCR to detect RNA. These two reactions have revolutionized genetics. Furthermore, PCR has many diverse applications in infectious disease diagnostics for detection of viruses or bacteria[7], in forensic science [8] [9] paternity tests [10], security applications [11] and myriad other commercial applications [12]. Commercial systems are typically rather large tabletop tools used for high throughput mass screenings and are impractical for use in point-of-care applications (POC), where the most important system parameters are portability and power consumption. The quest for a miniaturized PCR version suitable for POC diagnostics was initiated at Lawrence Livermore Laboratories [13] [14] more than two decades ago. Agrawal et al. have developed a pocket-sized conventional PCR system[15] that requires extensive sample post-processing to identify the presence of an amplicon. In contrast, real-time PCR eliminates the need for sample processing once PCR is completed.
Real-time PCR systems consist of a heater, temperature sensor, and fluorescence excitation and detection unit. Temperature cycling is performed by heating and cooling of samples. Within the PCR process, the cooling rate is one of the primary limiting factors. Bulky commercial systems have large heat capacities, hence heat removal is challenging, and is typically accomplished by using a thermoelectric cooler (TEC), commonly known as the Peltier element. Since these bulky systems consume a considerable amount of power, they are generally unsuitable for field testing POC applications.
Small PCR instruments are often based on microfluidic devices, so-called lab-on-a-chip devices [16]. These systems comprise two major groups, spatial-domain and time-domain PCRs. On the one hand, time-domain PCRs have a single heater with samples placed in direct contact. Here, temperature cycling is carried out by changing the heater element temperature. On the opposite end of the spectrum, the spatial-domain PCR has several heaters, each held at a different temperature. In this scenario, temperature cycling is accomplished by moving samples between heaters.
A typical representative of a spatial-domain system is the continuous PCR-on-a-chip[17]. Within this system, the sample flow in the microfluidic chip is positioned over the heaters, each kept at a different temperature. The sample flows through tubes, thereby achieving thermal cycling. Here, PCR duration is only limited by the flow rate and the heat transfer between the sample and the side walls, for both heating and cooling. The two major drawbacks of a flow-through PCR are system complexity and a high likelihood of sample-to-sample cross-contamination.
An alternative version was introduced a few years ago where the sample was in the form of a virtual reaction chamber (VRC)[1][18] [19]. The VRC self-assembly system consists of a water droplet covered with mineral oil, preventing water evaporation from the sample. In this scenario, the water

droplet contained the PCR master mix with a pre-determined number of DNA copies. Here, the VRC with DNA was separated from the micromachined silicon heaters by a disposable, hydrophobically-coated microscope cover slip. To eliminate sample-to-sample contamination, the glass cover slip was a disposable part of the system, and therefore each cover slip was a single use component. The sample contained magnetic particles which facilitated sample motion between heaters [3]. A pocket-size real-time PCR system capable of processing a single sample was introduced a few years later[20]. The system had an integrated miniaturized optical detection unit, LCD display and control electronics. One of the key features was the implementation of lock-in amplification for optical signal processing[3]. The lock-in amplification feature allowed for ambient system operation without light protection, thereby rendering the system robust and user-friendly. One of the system drawbacks was processing a single sample at a time and furthermore, the device was bulky.
A practical system to conduct PCR for POC applications requires simultaneous processing of 4 or more samples. Diagnoses of clinical samples should be concurrently conducted with positive and negative control samples, thereby eliminating false negative or positive events.
In our work, we introduce a new portable PCR system (Fig. 3.2) capable of concurrently analyzing four $\approx$ 200nL volume samples. The system speed is determined by the heating and cooling rates. The heating rate collectively arises from the VRC thermal capacitance (H) and the dissipated Joule heat. The rate of passive cooling applied within our system is given by the thermal time constant (τ) of the system, which is given by H/G, where G is the thermal conductance. Since the specific heat of water is exceptionally large, the thermal properties of our system are strongly dependent on the sample water volume. Consequently, a smaller sample size results in a faster system[2].

System samples consist of a negative control, also called no template control (NTC), a positive control, and two samples of interest. The four sample system architecture represents the minimal number of samples required for practical applications. Our system conducts 40 PCR cycles in less than $\approx$ 35 min, while simultaneously processing the results. Furthermore, our portable real-time PCR is capable of detecting a single DNA copy.
The PCR performance was evaluated by detecting a complementary DNA from the avian influenza virus (H7N9) as well as two human transcripts, hypoxanthine phosphoribosyltransferase (HPRT) and glyceraldehyde-3-phosphate dehydrogenase (GAPDH). To the best of our knowledge, our system platform represents the smallest realtime PCR system.
Our PCR instrument has two key features:

1. The four samples are in the VRC form and are placed on a disposable glass cover slip over micromachined silicon heaters. Upon PCR com-

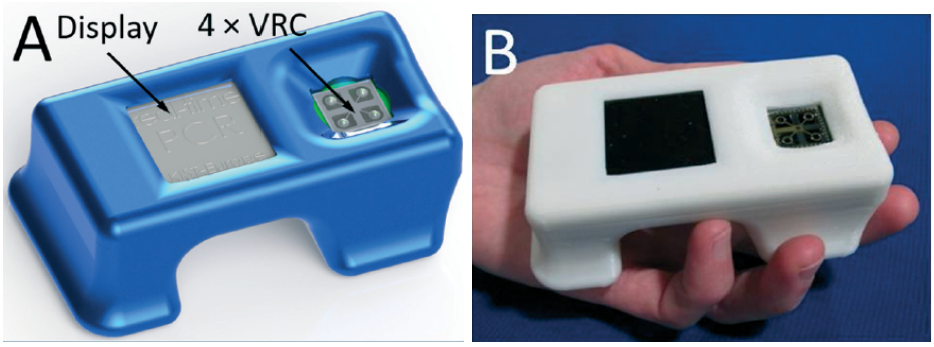

Figure 3.2: (A) CAD design drawing of the handheld PCR. The illustration shows a display with a compartment accommodating 4 samples in the VRC form. (B) Fabricated and assembled complete real-time PCR device packaged within a 3D printed casing.

pletion, the single-use, disposable glass element is removed and a new glass cover slip is placed on top of the silicon heater.

2. The fluorescence excitation/detection system is based on a lock-in amplifier, thereby rendering the system immune to ambient light. The PCR instrument is equipped with a graphical 84 x 48 pixel liquid crystal display (LCD) with a diagonal size of ≈ 38.1 mm to show the reaction progress and final results. The captured data is stored in an internal memory and can be uploaded for external processing via a universal serial bus (USB). The system is powered by an external 12 V battery.

System setup

Our current system has two new key features: an integrated optical head and simplified control electronics.

1. Integrated optical head

A fluorescence detection system for a single spot requires a light source, three filters (excitation, dichroic mirror and emission) and a detector. We redesigned the original head [21] [22] with 5 filters for the four units (see Fig. 3.3). Each measurement spot is illuminated with a light emitting diode (LED) with a principal emission wavelength of 470 nm and a luminous intensity in the range of 7.2 cd to 12 cd. Light passes through an excitation band pass filter with a center wavelength of ≈ 470 nm and a band pass of ≈ 40 nm, blocking light from the LED with wavelengths longer than ≈ 490 nm. Light is then reflected off of a long pass dichroic mirror with a cut-off wavelength of ≈ 495 nm, and focused by a lens with a focal length of ≈ 3.1

mm, a numerical aperture of ≈ 0.68 and an antireflective coating in the range of ≈ 350 nm to ≈ 700 nm. The emitted fluorescence (F) is collimated by the same lens, passing through the dichroic mirror. The residual blue light is suppressed by a long pass emission filter with a cut-off wavelength of ≈ 510 nm, and fluorescence is captured by the conventional silicon photodiode with a radiant sensitive area of ≈ 7.5 mm. The cross section schematic of the handheld PCR system illustrating the optical path is shown in Fig. S1(Supplemental material in section 11.2.1). The resulting photocurrent is converted into voltage using an ultra-low bias current operational amplifier with dielectrically-isolated field effect transistor inputs (diFET) as a transconductance amplifier. In this configuration, the four sample systems share optical filters. Four LEDs are mounted in two pairs. Within each pair, the LEDs were parallel, thus requiring only two excitation and two dichroic filters for all 4 LEDs. Finally, there is only a single emission filter for all photodiodes. A potential expansion to eight systems would require additional LEDs and photodiodes with amplifiers.

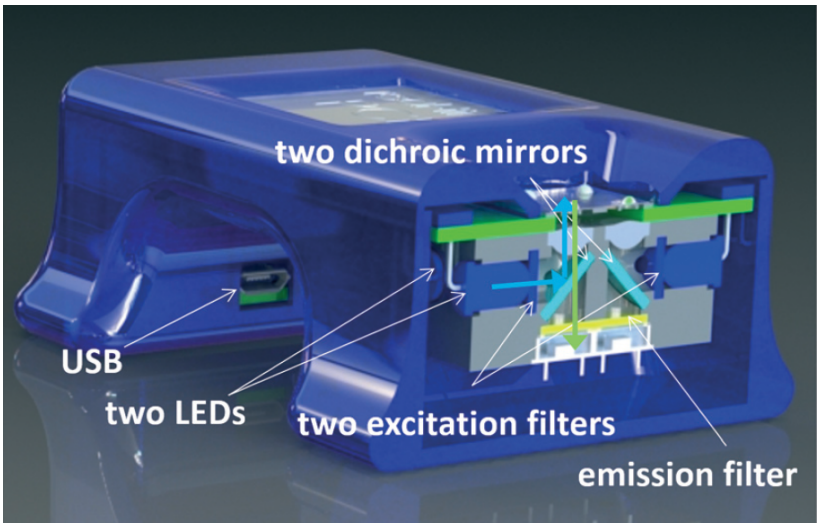

Figure 3.3: Schematic illustration of the integrated optical head. Blue arrows show the optical path from one LED with filters to the VRC. The green arrow shows the optical path of excited fluorescence to the photodiode. Light emitted from a blue LED passes through the blue filter in order to remove the green portion of emitted light, then reflects off of the dichroic mirror through a donut-shaped heater and is focused on the sample by an aspherical lens. Excited fluorescence is collimated by the same lens, passing through the dichroic mirror with the blue portion filtered out by a green filter. Residual green light interacts with a photodiode and induces a photocurrent, which is further processed.

2. Control electronics

A previously published system[20] had one lock-in amplifier for a single fluorescence detection system and a second one for temperature measurement. This scenario was very inefficient since fluorescence was monitored for ≈ 2 s during each PCR cycle. The second lock-in amplifier for temperature measurement was used during the entire PCR operation. Our current system employs a single lock-in amplifier to monitor the sample temperature and capture fluorescence from all four spots. The system heaters were connected in a serial-parallel combination, wherein the system controlled the average temperature of all four heaters. We used a similar AC biased Wheatstone bridge to convert the resistance of the resistance temperature detector (RTD) into a DC voltage as previously described[20].
The control electronics for the optical system was a simplified version of our previous work[20]. Here, each PCR system (spot) had its own LED, collimating lens and a photodiode with a respective transconductance amplifier while the optical filters are shared. We activated one LED at a time, thereby feeding the signal to a single, corresponding transconductance amplifier. Outputs of the four amplifiers were connected together and processed as one signal. The complete schematic of the PCR system is shown in Fig. S2 (Supplemental material in section 11.2.1). The incident photocurrents from the photodiodes were converted into voltage using four dedicated operational amplifiers. The amplifier outputs were connected together and a single composite signal was further processed. The cross talk between four measured spots was minimized since one LED was activated at a time; therefore the resulting total amplitude of the processed photocurrent originated from a single dedicated PCR reaction. All important devices are listed in Table S1 (Supplemental material in section 11.2.1).

Experimental

A typical real-time PCR protocol with an intercalating dye such as SYBR-Green I initiates with a hot start to activate the polymerase. PCR cycles consist of denaturation, annealing and extension steps. The fluorescence amplitude is measured at the end of the extension step for a period of ≈ 2 s. We controlled the heater temperature using the proportional integrative-derivative (PID) closed feedback loop method. The amount of heat delivered through dissipated Joule heating was controlled using a pulse-width modulation (PWM) technique. The last ≈ 2 s of the amplification cycle were used for fluorescence monitoring (see Fig. 3.4). In this step, following temperature stabilization, we monitored the duty cycle of the PWM and calculated its average. During the last ≈ 2 s, the feedback loop was disconnected, the temperature was not monitored and the average value of the PWM was

employed. During the system development phase, we monitored the heater temperature and found that the method described above gives us a temperature variation of less than $\pm 0.5^{\circ}C$ over a $\approx$ 2 s time interval. The sample temperature follows the heater temperature with a $\approx$ 1.5 s delay[23], therefore a $\pm 0.5^{\circ}C$ temperature variation at the heater does not affect the PCR performance. The measured temperature profile from $\approx$ 6 PCR steps is shown within the system liquid crystal display (LCD) in Fig. 3.5 A.

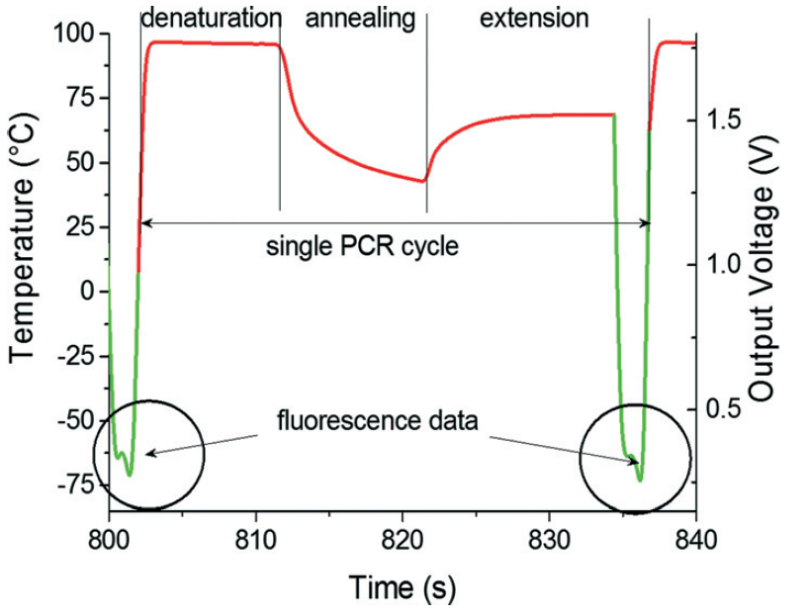

Figure 3.4: PCR thermal profile of a single amplification step. The heater temperature (red part) is linearly proportional to the built-in lock-in amplification output, which was captured with an oscilloscope. While performing denaturation at $\approx 93^{\circ}C$, annealing at $\approx 56^{\circ}C$ and most of the extension step at $\approx 72^{\circ}C$, the built-in lock-in amplifier is utilized to measure the average temperature of all four heaters. In the last two seconds of the extension step, the lock-in amplifier is used to sequentially process the fluorescence signal (green part) from the 4 measurement spots (circled area). These data are stored in their original format in analog-to-digital converter units (ADC units) within the memory of a microcontroller. Once fluorescence is measured, the heater is powered by the average value of pulse width modulation obtained during the extension phase.

During the last two seconds of the extension step, the fluorescence measurement system was activated. Sequentially, each LED was individually powered for $\approx$ 0.5 s and the emitted fluorescence was captured by the respective photodiode and lock-in amplifier. At the completion of an amplifica-

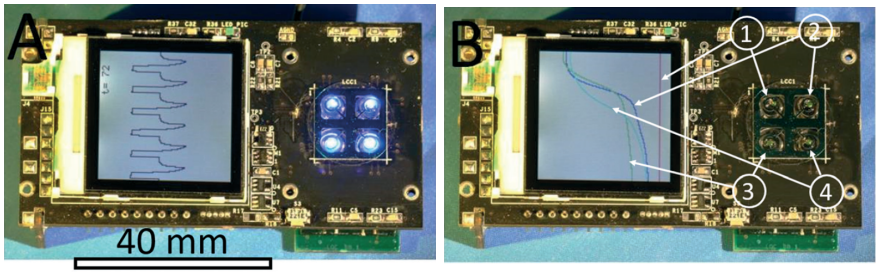

Figure 3.5: (A) An assembled PCR system with four VRCs, each consisting of a $\approx 0.5\mu L$ sized sample covered with $\approx 1.5\mu L$ of M5904 mineral oil, showing the PCR temperature profile (protocol) within the LCD display. The device size is 82 mm x 45 mm x 20 mm (length, width and height). Scale bar is 40 mm. The protocol started by a hot start to activate the polymerase enzyme for ≈ 10 min at $\approx 95°C$, followed by 40 cycles of PCR amplification. Each amplification cycle consisted of 3 steps. First, denaturation for ≈ 10 s at $\approx 95°C$, then annealing for ≈ 10 s at $\approx 50°C$ and the last step was extension for ≈ 15 s at $\approx 68°C$ (instead of typical $\approx 72°C$), during which fluorescence was measured. The LCD display shows 6 cycles. At the completion of each PCR amplification cycle, fluorescence amplitude at each spot was calculated and amplification curves were plotted in (B). We placed NTC at position 1, a low concentration of complementary DNA (cDNA) from H7N9 HA gene at position 3, a medium concentration at position 2 and the highest concentration (positive control) at position 4. The results show that the PCR reaction was successfully accomplished without PCR amplification of the NTC sample. Furthermore, the results prove that the samples were not cross contaminated, thereby eliminating false positive outcomes. Positive control results at position 4 indicate the absence of false negative results, thereby showing a successful PCR amplification process.

tion cycle, the system was switched back into the temperature measurement mode, initiating the start of a new cycle. The PCR amplification curves were plotted for each spot and the captured amplitude of fluorescence was displayed on the LCD display. The typical PCR amplification curve is shown in Fig. 3.5B. Directly following the PCR process, melting curve analysis (MCA) was performed. Since temperature measurement during the MCA is time consuming, we performed this step without a feedback loop. In the course of the PCR, we monitored and recorded the PWM duty cycle of three fixed temperature points: denaturation, annealing and extension temperatures. These three points were used to calculate the required duty cycle for temperature scans ranging from $\approx 68°C$ to $\approx 94°C$ without a closed feedback loop. The system was stabilized at $\approx 68°C$. The temperature of each heater was then gradually increased to $\approx 95°C$ while the fluorescence in each

of the four spots was sequentially measured. The measurement of each spot required a duration of ≈ 0.5 s, hence ≈ 2 s was required to measure all 4 VRCs. This measurement setup allowed for fluorescence measurement from each spot with an offset of $\approx 0.25°C$ between adjacent VRCs. Once the MCA was completed, we stabilized the sample at the assumed temperature of $\approx 95°C$ and then measured the actual temperature. Directly following this, the system's central processing unit (CPU) performed two corrections. First, the MCA was recalculated based on the actual final temperature. Second, the correction accounts for the temperature offset between individual VRCs. Consequently, the MCAs for each spot were recalculated accordingly. Finally, a negative derivative value of fluorescence with respect to temperature ($-dF/dT$) was calculated.

The device performance was evaluated using synthetic complementary DNA (cDNA) for the hemagglutinin of the H7N9 avian influenza virus. Forward and reverse primers were chosen as suggested earlier [24]: forward primer: TACAGGGAAGAGGCAATGCA, reverse primer: AACATGATGCCCCCGAAGCTA, giving a total amplicon length of 104 base pairs with a melting temperature of $\approx 81.1°C$, as measured using a commercial real time PCR system.

The PCR master mix was prepared by mixing $\approx 2\mu L$ of FastStart DNA Master SYBR Green I, $\approx 2\mu L$ of $MgCl_2$ solution, $\approx 2\mu L$ of sample HA ($5 * 10^{-5} ng\mu L^{-1}$), $\approx 0.3\mu L$ of $\approx 400 mgmL^{-1}$ BSA solution and primers in a final concentration of $\approx 1.8 * 10^{-6} molL^{-1}$. We added deionized (DI) water with a resistivity higher than 18 MΩ cm at $25°C$ to create the final volume of $\approx 20\mu L$. The NTC sample had $\approx 2\mu L$ HA gene volume replaced with DI water.

First, we performed basic real-time PCR with different contents of cDNA per μL as shown in Table 3.1 with NTC at position 1 and different contents at positions 2 to 4. The amplification curves are shown in Fig. 3.6A. Once the PCR process was completed, we also conducted a MCA (not shown here). The MCA shape is not suitable for performing highresolution analysis[25]; nevertheless, it does show that a specific DNA was amplified with the melting temperature of $83.36 \pm 0.63°C$ (mean ± standard deviation), in close proximity to the measured value of $T_M \approx 81.1°C$. The marginal difference in the T_M values is due to the uncertainty of calibration precision of the commercial PCR system used as a benchmark tool. The T_M resolution is sufficient to verify specific DNA amplification; however, it may not be suitable for performing high-resolution melting curve analysis[26].

We then performed a series of four identical measurements using an HA content of $\approx 5 * 10^{-5} ng$ in a μL of cDNA (see data in Table 3.2 and a graphical representation in Fig. 3.6B). Different PCR locations resulted in performance variation, consequently producing mean C_T values in the range of ≈ 8 to ≈ 9.6 with a standard deviation ranging between ≈ 0.8 and ≈ 1.5. The difference in C_T values at positions 2 to 4 might be caused by

Position	**Mean C_T**	**Standard Deviation**	**Concentration HA ($ng\mu L^{-1}$)**
1	-	-	-
2	28.7	1.5	$\approx 5.0 * 10^{-8}$
3	27.0	1.0	$\approx 7.5 * 10^{-8}$
4	20.0	1.0	$\approx 5.0 * 10^{-6}$

Table 3.1: Typical results with NTC (position one) serving as negative control and three different sample concentrations at positions 2 to 4. The sample at position 4 serves as positive control

imperfections due to manual VRC placement. The VRC at position 1 appears to have a lower heat transfer rate than VRCs at other positions. We attribute the variation to a slower transition from amplification to saturation of the DNA amplification curve (Fig. 3.6B). We further presume that heater defects at position 1 could give rise to a temperature that is different in comparison with the other three positions, consequently leading to a differing PCR efficiency. Additionally, this discrepancy could be attributed to the stress induced during chip-to-PCB soldering, giving rise to bending of the chip. The silicon chip deformations could cause both variations in the intermediate oil layer thickness and a differing heat rate.
Finally, we obtained standard PCR curves. The samples were prepared by the following procedure. We mixed a sample with cDNA corresponding to 12 500 copies per $200nL$ volume. This sample was diluted 10x, yielding 1250 copies per $200nL$ volume; the next dilution yielded 125 copies per $200nL$ volume. The last two dilutions had a statistical number of 12.5 copies per $200nL$ and 1.25 copy per $200nL$ volume, respectively. The PCR results as well as the normalized data are shown in Fig. 3.6C and D, demonstrating that our portable real-time PCR is able to detect a single DNA copy with an excellent efficiency of 0.91 ± 0.05 per cycle (mean $\pm$ standard deviation), which is well within the required range of PCR efficiency between 0.8 and 1.0.

Discussion

The PCR protocol consisted of a $\approx$ 10 min hot start at $\approx 95°C$, followed by 40 cycles of $\approx$ 10 s at $\approx 95°C$, $\approx$ 10 s at $\approx 50°C$ and $\approx$ 15 s at $\approx 68°C$. Once the PCR amplification was completed, we conducted an MCA with a scan rate of $\approx 0.2°Cs^{-1}$. This protocol required a total time for amplification of less than 35 minutes with an additional $\approx$ 150 s for the MCA. The ultimate speed of the PCR was not the primary target of this work. Nevertheless, the time required for DNA amplification can be shortened by using different types of hot starts, Taqman chemistry (or both)[27] or even not using the hot start at all [28].

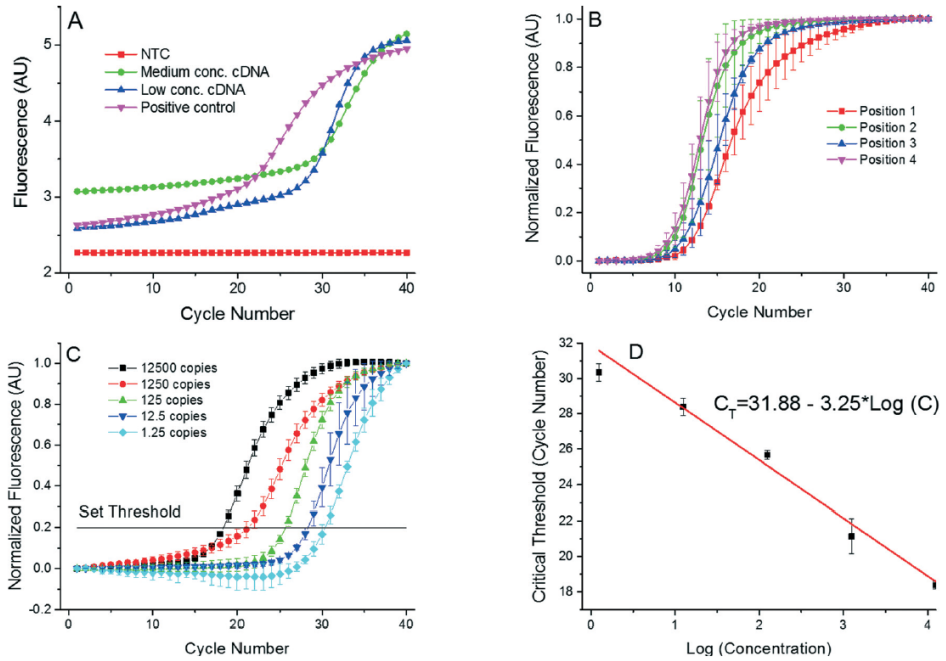

Figure 3.6: (A) Single PCR run as it appears in the PCR display. These PCR amplification curves show results from the 4 positions of the PCR device. We used complementary DNA (cDNA) from the H7N9 HA gene for testing purposes. AU stands for arbitrary units. Once the PCR was completed, the MCAs were performed with a melting temperature value of $83.36 \pm 0.63°C$ (mean $\pm$ standard deviation). Measurement uncertainties emanate from the manual placement of the droplet. Slight droplet misalignments at the heater cause temperature variations between various experimental runs, thereby affecting the overall PCR efficiency. Also, due to these temperature variations, we readily observe a slight shift in the measured melting temperature. (B) Measurements performed at the 4 positions with identical concentration of all samples performed three times to suppress random error. The corresponding extracted critical thresholds (C_T) are shown in Table 3.2. A greater value of CT at position 4 suggests a lower amplification efficiency at that position. This may be caused by a temperature variation due to a non-optimized bonding process of the silicon chip to the PCB. (C) PCR results from position 1 with the calculated number of cDNA copies in the sample from ≈ 12500 down to ≈ 1.25. These numbers are calculated by a 10x dilution starting from ≈ 12500. Since only whole numbers of cDNA copies per sample exist, fractional values imply the statistically most probable value. Each experiment was performed three times. (D) Extracted standard real-time PCR curve from results in Fig. 3.6C showing the C_T value as a function of LOG (cDNA concentration). The slope of -3.02 ± 0.16 cycles at threshold per decade (mean $\pm$ standard deviation) corresponds to the PCR efficiency of 0.91 ± 0.05 per cycle (mean $\pm$ standard deviation).

Position	**Mean C_T**	**Standard Deviation**	**Concentration HA ($ng\mu L^{-1}$)**
1	9.6	1.5	$\approx 5.0 * 10^{-5}$
2	9.0	1.2	$\approx 5.0 * 10^{-5}$
3	9.5	0.6	$\approx 5.0 * 10^{-5}$
4	8.0	0.8	$\approx 5.0 * 10^{-5}$

Table 3.2: Results of critical threshold from 4 measurements at each PCR location with identical concentration of the HA gene. The graphical output is shown in Fig. 3.6B. The discrepancy between results from individual samples was probably caused by sample misalignment with respect to the heater as they were placed manually

Here we used the same heater as in our previous work. The dissipated Joule heat P depends on the square of voltage V: $P = V2/R$, where R is the heater resistance. The Joule heat dissipation and the consequent heating rate were enhanced with either an increased voltage bias or by lowering the heater resistance. In a previous work [23], we increased the bias voltage up to 20 V using an external power supply. Here, the heater is powered using a 12 V external power supply in either an AC/DC converter or a battery type configuration. A change in this voltage would require additional space for a step up voltage converter. The additional feature would further require either a redesign of the heater on a micromachine, requiring a new mask for the metal lithography level, or the use of a thicker metal layer with a lower sheet resistance. Both cases would require the fabrication of new PCR chip architectures[29]. The current PCR chip layout is shown in Fig. S3 (Supplemental material in section 11.2.1) and the chip fabrication process in section 5 (Supplemental material in section 11.2.1).
In principle, the fundamental limitation in the speed of the device is determined by the heat transfer between the heater and the sample, which is ≈ 1.5 s for each temperature step. Nevertheless, the device can still run as fast as its predecessor achieving ≈ 9.5 s per PCR cycle, still being considered as one of the fastest real-time PCRs demonstrated at that point in time [27]. Furthermore, we enhance the system robustness by not incorporating moving parts. The system light source consists of 4 LEDs with an estimated lifetime of more than 50 000 hours. A single 40 cycle PCR run requires each LED to operate for less than 1 min. The most vulnerable part is the micromachined silicon chip mounted directly on the main PCB. We envision a new version of our system, currently under development, with the brittle silicon chip mounted on a dedicated PCB. Therefore, if the fragile part is damaged, a replacement silicon chip can be easily exchanged. In order to limit interference between PWM pulses and temperature sensing signals, the layout of the micromachined silicon chip will incorporate electrical shielding between

integrated heaters and sensors. In this scenario, the chip size will increase to $\approx$ 18 mm x 18 mm. Also, this configuration provides additional space in order to further modify the optical housing and facilitate the removal of the PCB from the optical path. The current version of the system exhibited a large self-induced fluorescence due to the PCB being illuminated by the blue LEDs. Finally, we plan to reduce the complexity of the optical housing by reducing the number of parts. This would also allow us to replace the silicon chip once variations in PCR efficiency are discovered.
Furthermore, in future experiments, we plan to use either microscope glass cover slips with upfront lyophilized PCR or a single step RT-PCR master mix. In this configuration, the pipetted $\approx 200nL$ volume sample will be entirely composed of DNA (RNA).

Conclusions

We designed and tested one of the smallest real-time PCR devices. It has a length of $\approx$100 mm, a width of $\approx$60 mm and a height of $\approx$33 mm and weighs only $\approx$ 90 g. The device measured 4 PCRs simultaneously in less than $\approx$ 35 min, including MCA. The sample was processed in the form of a virtual reaction chamber (VRC) where $200nL$ of a sample was placed on a disposable glass cover slip covered with mineral oil to prevent water evaporation from the sample. The sample only interacts with the glass cover slip to eliminate possibilities of sample-to-sample cross-contamination; the glass element was a single-use, disposable system component. Our negative control tests further demonstrate the lack of cross contamination between samples. The system depicted in Fig. 3.5 was successfully utilized for at least 100 distinct PCR runs. We have demonstrated its performance by amplifying the cDNA of an HA gene of the H7N9 avian influenza virus and displayed the results on an integrated LCD display. We demonstrated the capability of simultaneously running 4 samples at a time with good reproducibility. The PCR efficiency was demonstrated by obtaining a PCR standard curve in the range of 12500 to 1.25 copies with an achieved slope of -3.02 ± 0.16 cycles at threshold per decade (mean $\pm$ standard deviation). The value corresponds to a PCR efficiency of 0.91 ± 0.05 per cycle (mean $\pm$ standard deviation). The system was also capable of detecting a single DNA copy within the sample.
The captured data was subsequently transferred to a personal computer (PC) via a USB interface for further processing. This tiny real-time PCR device is a promising diagnostic system for remote clinics as well as a tool for educational institutions demonstrating the power of a real-time PCR as seeing is believing. The system throughput can be doubled using a single channel multiplexing method as demonstrated earlier[30].

Acknowledgements

P. Neuzil acknowledges partial financial support from the Central European Institute of Technology (CEITEC), grant number CZ.1.05/1.1.00/02.0068. The authors gratefully acknowledge the NIST CNST NanoFab staff for helpful discussions and assistance with device fabrication. This article identifies certain commercial equipment, instruments, and materials to specify the experimental procedure. Such identification does not imply recommendation or endorsement by the National Institute of Standards and Technology, nor does it imply that the equipment, instruments, and materials identified are necessarily the best available for the purpose.

3.4 Author contributions

Christian Ahrberg conducted experiments and designed the experiments and did the data processing. Bojan Robert Ilic and Pavel Neuzil fabricated the silicon chip and Pavel Neuzil produced the layouts for the printed circuit boards. Andreas Manz advised on experiment design. All authors reviewed the manuscript.

3.5 Conclusion

The contribution in this chapter demonstrates that it is feasible to conduct polymerase chain reactions in VRCs. It was shown that the miniaturized chip design works and provides means for real time detection by the same device. An efficiency of 0.91 ± 0.05 was found from the standard curve, which is in the range desirable for real-time PCR and similar to values obtained from commercial, bench-top machines. Furthermore the standard curves have shown that a single copy of template can be detected by the device. As no concentrations lower than one copy per reaction volume occur in real samples this shows that the lowest sample concentration possible is detectable by the system. Additionally the contribution shows the first integration of VRCs, a bespoken silicon heating chip, and real time fluorescence detection on the same handheld device, making it one of the smallest real-time PCR cyclers at this point in time. The device is capable of amplifying up to four samples in parallel which can be used for a positive and negative control as well as two actual samples in a point-of-care situation.

As discussed previously the accuracy of the real-time results provided by the handheld device is significantly effected by pipetting. The volumes used for the VRCs are very close to the lowest volumes commercial pipettes are capable of handling, which is an inherent source of error for this system. Furthermore droplet positioning ontop of the heaters and detectors also influences the results. Although the extend of this error sources can be reduced through user training and experience it still limits the user to user comparability of results.
Since only four positions are available for PCR standard curves required for absolute quantification can not be conducted in parallel with the analysis of the sample. This makes the device less suitable for absolute quantifications, however relative quantifications can be easily done using the handheld qPCR cycler. As shown in the next chapter one position can be used for a positive control for both the gene in question and a reference. The second position can be used as the negative control and in the remaining two positions can be used for the analysis of the two genes in the sample.

Thus a system for the controlled temperature manipulation and fluoresence measurement of virtual reaction chambers has been introduced in this chapter. It was demonstrated how the chip can be used for a portable device for qPCR. Due to the small size of the instrumentation the chip and detection introduced here can easily be mounted under a microscope for further analysis. These properties make the system an ideal tool for further analysis of VRCs in the context of this thesis.

Bibliography

[1] P. Neuzil, J. Pipper, and T.M. Hsieh. Disposable real-time microPCR device: lab-on-a-chip at a low cost. *Mol. BioSyst.*, 2:292–298, 2006.

[2] P. Neuzil, C. Zhang, J. Pipper, S. Oh, and L. Zhuo. Ultra fast miniaturized real-time PCR: 40 cycles in less than six minutes. *Nucleic Acids Research*, 34(11):e77, 2006.

[3] J. Pipper, M. Inoue, L. F. Ng, P. Neuzil, Y. Zhang, and L. Novak. Catching bird flu in a droplet. *Nat Med*, 13(10):1259–63, 2007.

[4] J. Pipper, Y. Zhang, P. Neuzil, and T.-M. Hsieh. Clockwork PCR Including Sample Preparation. *Angewandte Chemie*, 120(21):3964–3968, 2008.

[5] K. Mullis, F. Faloona, S. Scharf, R. Saiki, G. Horn, and H. Erlich. Specific enzymatic amplification of DNA in vitro: the polymerase chain reaction. *Cold Spring Harb Symp Quant Biol*, 51 Pt 1:263–73, 1986.

[6] R. K. Saiki, D. H. Gelfand, S. Stoffel, S. J. Scharf, R. Higuchi, G. T. Horn, K. B. Mullis, and H. A. Erlich. Primer-directed enzymatic amplification of DNA with a thermostable DNA polymerase. *Science*, 239 (4839):487–91, 1988.

[7] S. Yang and R. E. Rothman. PCR-based diagnostics for infectious diseases: uses, limitations, and future applications in acute-care settings. *Lancet Infectious Diseases*, 4(6):337–348, 2004.

[8] R. Decorte and J. J. Cassiman. Forensic Medicine and the Polymerase Chain-Reaction Technique. *Journal of Medical Genetics*, 30(8):625–633, 1993.

[9] M. A. Jobling and P. Gill. Encoded evidence: DNA in forensic analysis. *Nature Reviews Genetics*, 5(10):739–751, 2004.

[10] M. A. Jobling, A. Pandya, and C. TylerSmith. The Y chromosome in forensic analysis and paternity testing. *International Journal of Legal Medicine*, 110(3):118–124, 1997.

[11] S. S. Iqbal, M. W. Mayo, J. G. Bruno, B. V. Bronk, C. A. Batt, and J. P. Chambers. A review of molecular recognition technologies for detection of biological threat agents. *Biosensors and Bioelectronics*, 15 (11-12):549–578, 2000.

[12] M.A. Valasek and J.J. Repa. The power of real-time PCR. *Advances in Physiology Education*, 29(3):151–159, 2005.

[13] P. Belgrader, J. K. Smith, V. W. Weedn, and M. A. Northrup. Rapid PCR for identity testing using a battery-powered miniature thermal cycler. *Journal of Forensic Sciences*, 43(2):315–319, 1998.

[14] P. Belgrader, S. Young, B. Yuan, M. Primeau, L. A. Christel, F. Pourahmadi, and M. A. Northrup. A battery-powered notebook thermal cycler for rapid multiplex real-time PCR analysis. *Analytical Chemistry*, 73 (2):391–391, 2001.

[15] N. Agrawal, Y. A. Hassan, and V. M. Ugaz. A pocket-sized convective PCR thermocycler. *Angew Chem Int Ed Engl*, 46(23):4316–9, 2007.

[16] P. Neuzil, S. Giselbrecht, K. Laenge, T.J. Huang, and A. Manz. Revisiting lab-on-a-chip technology for drug discovery. *Nature Reviews Drug Discovery*, 11(8):620–632, 2012.

[17] M. U. Kopp, A. J. DeMello, and A. Manz. Chemical amplification: continuous-flow PCR on a chip. *Science*, 280(5366):1046–8, 1998.

[18] P. Neuzil, T.M. Hsieh, and J. Pipper. Apparatus for regulating the temperature of a biological and/or chemical sample and method of using the same, 2012.

[19] J. Pipper, T.M. Hsieh, and P. Neuzil. Method of processing a biological and/or chemical sample, 2012.

[20] P. Neuzil, L. Novak, J. Pipper, S. Lee, L. F. Ng, and C. Zhang. Rapid detection of viral RNA by a pocket-size real-time PCR system. *Lab Chip*, 10(19):2632–4, 2010.

[21] L. Novak, P. Neuzil, J. Pipper, Y. Zhang, and S. Lee. An integrated fluorescence detection system for lab-on-a-chip applications. *Lab on a Chip*, 7(1):27–29, 2007.

[22] P. Neuzil, L. Novak, and J. Pipper. Compact optical detection system, 2008.

[23] P. Neuzil, W. Sun, T. Karasek, and A. Manz. Nanoliter-sized overheated reactor. *Applied Physics Letters*, 106(2), 2015.

[24] V.M. Corman, M. Eickmann, O. Landt, T. Bleicker, S. Bruenink, M. Eschbach-Bludau, M. Matrosovich, S. Becker, and C. Drosten. Specific detection by real-time reverse-transcription reaction assays of a novel avian influenza A(H7N9) strain associated with human spillover infections in China. *Euro Surveill.*, 18(16), 2013.

[25] G.H. Reed and C.T. Wittwer. Sensitivity and Specificity of Single-Nucleotide Polymorphism Scanning by High-Resolution Melting Analysis. *Clin Chem*, 50(10):1748–1754, 2004.

[26] L. Zhou, J. Vandersteen, L. Wang, T. Fuller, M. Taylor, B. Palais, and C. T. Wittwer. High-resolution DNA melting curve analysis to establish HLA genotypic identity. *Tissue Antigens*, 64(2):156–164, 2004.

[27] P. Neuzil, C. Zhang, J. Pipper, S. Oh, and L. Zhuo. Ultra fast miniaturized real-time PCR: 40 cycles in less than six minutes. *Nucleic Acids Research*, 34(11), 2006.

[28] J. S. Farrar and C. T. Wittwer. Extreme PCR: efficient and specific DNA amplification in 15-60 seconds. *Clin Chem*, 61(1):145–53, 2015.

[29] P. Neuzil, J. Pipper, and T. M. Hsieh. Disposable real-time microPCR device: lab-on-a-chip at a low cost. *Mol Biosyst*, 2(6-7):292–8, 2006.

[30] C.D. Ahrberg and P. Neuzil. Doubling Throughput of a Real-Time PCR. *Scientific Reports*, 5:12595, 2015.

Chapter 4

Reverse Transcription on Handheld PCR

4.1 Motivation and relation to the thesis

Many application of PCR require the detection of RNA instead of DNA, for example in the detection of RNA-viruses or expression rates of specific genes. As polymerase chain reaction can only amplify DNA targets, complementary DNA targets have to be synthesised from RNA prior to amplification. The enzyme reverse transcriptase is usually used for this purpose. Commercial thermal cyclers can perform the reverse transcription step followed by PCR through simple modifications, like the addition of a reverse transcription temperature step before amplification and use of the reverse transcriptase in the reaction mix.

Here it is demonstrated that the handheld PCR device, introduced previously, is also capable of the detection of RNA. For this the temperature profile and reaction mix is modified in a similar manner done in commercial devices allowing reverse transcription with consecutive real-time PCR without the need for manual sample manipulation. Furthermore it will be shown how the device can be used for relative quantifications by the utilization of all four sample positions.

4.2 State of the art

Reverse transcriptase was already discovered in 1963 when researching the *Rous sarcoma* virus [1]. Furthermore the concept of relative quantification using the $2\Delta\Delta C_T$-Method is known and used for PCR for some time[2]. Both concepts have been employed extensively, nowadays reverse transcription followed by PCR is routinely done in laboratories without intermediate sample manipulation. In one example 1100 samples were tested for infection

with the Ebola virus by reverse transcription qPCR on established commercial machines [3]. Additionally RNA detection for bird flue was already shown in virtual reaction chambers using a previous iteration of the heating chip [4].

The work shown in this chapter strives to demonstrate that the techniques and methods for the detection of RNA can be used with the handheld device constructed. In contrast to the previous paper showing real time detection of bird flu RNA, fluorescence is measured by the handheld device instead of an external microscope. Additionally four samples are analysed in parallel showing a portable relative quantification, not demonstrated previously with virtual reaction chambers.

4.3 Palm-sized device for point-of-care Ebola detection

Prepared for publication

We show the utilization of a recently developed cellphone-sized, real-time polymerase chain reaction (PCR) device to detect RNA of an Ebola virus using single-step reverse transcription PCR (RT-PCR). The device was shown to concurrently perform four PCRs each with a volume of 100 nL: one positive control with both Ebola and GAPDH RNA, one negative control. The last two positions were used to measure the GAPDH and the Ebola content of a sample. The comparison of critical thresholds from the two samples provided relative quantification. The entire process, which consisted of reverse transcription, PCR amplification, and melting curve analysis, was conducted in less than 37 minutes. The next step will be integration with a sample preparation unit to form an integrated sample-to-answer system for point-of-care infectious disease diagnostics.

Introduction

The recent epidemic of Ebola in West Africa has been one of the largest and most complex in history of this virus [5]. The origin of this virus is still a mystery, regardless of the utilization of DNA sequencing techniques[6].
Many infectious diseases native to this particular region of the world show similar symptoms as Ebola. This greatly exacerbates the difficulties in patient management and treatment decisions. Some reports even found more than half of suspected Ebola cases in a treatment facility eventually had an alternate diagnosis [5]. A rapid, sensitive and accurate detection method is crucial to verify the Ebola infection making decision to start quarantine and treatment immediately. Both false negative as well as false positive test results are highly undesirable with potentially damaging impact on the patient. Reverse transcription polymerase chain reaction (RT-PCR) method is clinically proven to be the test of choice [7]. The world health organization (WHO) currently suggests the diagnosis of Ebola either using RT-PCR or antigen tests [8]. Laboratories capable of safe handling of potentially highly contagious samples need to fulfill biosafety hazard level 3 or 4. Their number and their access to the samples is limited, especially in remote locations. Logistics are complicated as the samples have to be transferred triple-packed in cooled containers, often for long distances. Mobile laboratories were specifically designed to solve this problem by testing samples in effected remote location and thus to contain the spreading of respective infectious diseases [9]. The mobile laboratories solve the problem only par-

tially, as their number is limited so they have to be placed in centralized locations and clinical samples shipped to them. Even though there are some solutions that help to cope with the situation, such as shipping samples in dried form [10] and developed antigen-antibody based point-of-care (POC) tests suitable for remote location [11] [12], a robust Ebola diagnostics method suitable for remote location is still a challenge.
The worst Ebola disease outbreak is over today. Affected countries are now facing the biggest number of Ebola survivors in history. Patients with negative results of the RT-PCR test were released from hospitals and treatment units as healthy [13], although many of them were reporting health problems later on. Among the most common were joint pain, eye problems, severe fatigue and headaches as well as mental health problems and depressions[14]. They are often described as post-Ebola virus disease syndrome and very little is known about their origin. Nevertheless, the virus RNA was recently discovered in the semen and eye-liquid of survivors discovered so it is assumed that the virus might be harbored in immunologically privileged sites like joint cartilage and gonads [15]. More studies of the Ebola virus presence using readily available and robust technique such as RT-PCR to understand its behavioral patterns is urgently needed.
Recently a handheld, real-time PCR device was presented [16]. In this contribution, we show how our device can be used for RT-PCR to diagnose the presence of Ebola ribonucleic acid (RNA) for its diagnoses (Figure 4.1). This simple device could be readily available to perform quantitative analysis of patients' samples to determine viral load and effectiveness of the Ebola treatment. Presence of such devices in remote locations is urgently required during epidemic outbreaks, such as the last one with the Ebola virus. Here we demonstrate this device to quickly identify presence of a RNA of Ebola virus in a small sample. This would work regardless of patients exhibiting Ebola symptoms or not. The device could also detect minute quantities of RNA in joint cartilages.
This real-time PCR device is $\approx$ 100 mm by $\approx$ 60 mm by $\approx$ 33 mm and weighs less than 80 g. It is powered by an external 12 V power supply provided by a car battery or a charger. The device is capable of concurrently processing four $\approx$ 100 nL samples, designed for positive and negative control as well as two actual samples.

Samples placed on a hydrophobically coated disposable microscope cover slip are covered with mineral oil ($\approx 1\mu$L) to form a virtual reaction chamber (VRC) [17][18]. Only the disposable glass microscope coverslip is in contact with the sample. New glass for every four samples guarantees no run to run cross contamination. A micro-machined silicon heater under the VRC provides heating of the samples through the glass, achieving heating rates $\approx 20^{\circ}C/s$ while a rate of $\approx -20^{\circ}C/s$ was accomplished by passive cooling. We integrated a miniaturized fluorescence housing to monitor the progress

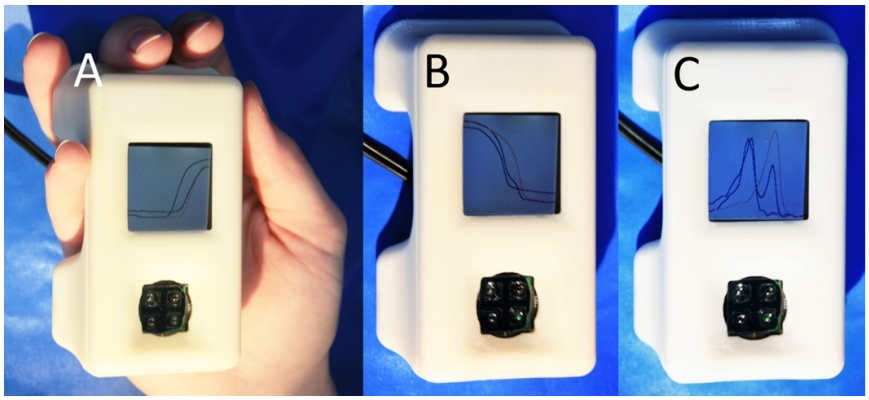

Figure 4.1: (A) Smartphone-size real time PCR capable of four reactions at a time, demonstrated here to detect RNA of an Ebola virus performing real-time RT-PCR, (B) followed by melting curve analysis (C) and its derivation.

of PCR in real-time in each VRC. Blue light was emitted by light emitting diodes (LED), the samples were illuminated and excited fluorescence light was processed by fluorescein isothiocyanate (FITC) filter set. The fluorescence amplitude was detected by photodiodes. The light from LED was modulated, and together with photocurrent induced in photodiodes, the signal was processed using an embedded lock-in amplifier, achieving the system immunity with respect to ambient light.
Viral loads are usually determined by comparison with a housekeeping gene. Human transcript glyceraldehyde-3-phosphate dehydrogenase (GAPDH) has constant expression at moderate levels inside human cells [19] which is one of the reasons why we choose it. Out of four samples processed by the device, two were used for control. One contained RNA from both Ebola and GAPDH as a positive control and one was a no template control (NTC), a negative control. The two remaining locations were utilized to measure the number of copies of Ebola RNA (first one) and GAPDH RNA (second one). A relative quantification of Ebola to GAPDH expression can be used to determine the viral load in the patient's sample.

Materials and Methods

Synthesis of RNA template

To synthesis RNA templates for the reverse transcription PCR reaction 10μL of aqueous solution containing $5 * 10^{-5}$ ng/μL frame shifted cDNA of Ebola (ATG Biosynthesis) virus were added to a solution consisting out of 10μL of 5x Transcription Buffer (ThermoFisher) and 1.5μL of T3 RNA polymerase (20U/μL) (ThermoFisher). Furthermore, 10μL of a nucleotide triphosphates (dNTP) solution containing 10 mM of each of the four nucleotides adenosine

triphosphate (ATP), guanosine triphosphate (GTP), cytidine triphosphate (CTP), and uridine triphosphate (UTP) (all by ThermoFisher) and 1.25μL of RiboLock RNAse Inhibitor (40U/μL) (Thermo Scientific) were added. The solution volume was adjusted to 50μL by adding deionized (DI) water prepared by Prograd T3 column system (Millipore) and incubated at 37°C for 2 h. Afterwards 1μL of HL-ds DNAse (ArcticZymes) and 5μL of 10x Reaction Buffer (ArcticZymes) were added to remove the complementary deoxyribonucleic acid (cDNA) template.
The mixture was incubated at 37°C for 10 min followed by a second incubation step at 58°C for 5 min to deactivate the DNAse. Complete removal of cDNA was checked using standard quantitative PCR (qPCR) without a reverse-transcription step.
RNA for GAPDH was prepared in a similar manner starting with a synthetic cDNA (ATG Biosynthesis) solution with a concentration of $5 * 10^{-6}$ ng/μL. For the GAPDH / EBOLA control reactions both RNAs were prepared in the same vial starting from the mentioned cDNA stock solutions.

Reverse Transcription PCR

The prepared RNA samples were analyzed through reverse transcription qPCR. For this 5μL of 4x One-Step Grand Master Mix (TATAA), 1μL of one-step reverse transcriptase mix (TATAA), and 1μL of 20x EvaGreen in DI water (TATAA) were prepared. Forward (GGTCAGTTTCTATC-CTTTGC) and reverse primers (CATGTGTCCAACTGATTGCC) (Eurofins MWG Operon) for Ebola[3] were added to a final concentration of 1.8μM. Lastly RNA template was added and the entire solution adjusted to a volume of 20μL using again DI water. For the one step reverse transcription qPCR a 5 min reverse-transcription step at 50°C was carried out first followed by a hot start at 95°C for 30 s. Consecutively 40 cycles consisting out of a 5 s denaturation step at 95°C, a 10 s annealing step conducted at 55°C, and a 30 s extension step at 60°C. Finally melting curve analysis (MCA) was performed to identify the products of the reaction to make sure that no nonspecific PCR amplification took place. We used forward (AGCC-CACATCGCTCAGACAC) and reverse (CGAGCAAGACGTTCAGTCCT) primers (Eurofines MWG Operon) to amplify the GAPDH gene in final concentration of 1.8μM. The concentration of both primers for co-amplification of EBOLA and GAPDH was also used in final concentrations of 1.8μM for each primer.
We performed control qPCR experiment in 20μL glass capillaries using the Light Cycler (Roche). Experiments on the hand-held device were carried out in the form of a virtual reaction chamber (VRC). The sample volume was 100nL covered with 2μL of M5904 light mineral oil from Sigma Aldrich. Both sample as well as the oil were pipetted onto a hydrophobicaly coated disposable glass slide.

Results

During 40 cycles of PCR the fluorescence amplitude were extracted at the end of an extension step and stored in an internal device memory. Once the PCR was completed the MCA was also performed and results displayed at its display (Figure 4.1). The overall analysis time for reverse transcription ($\approx$ 5 min), amplification ($\approx$ 30 min), and melting curve analysis ($\approx$ 90 s) was less than $\approx$ 37 min. The PCR results can be also normalized and plotted as function of cycle number (Figure 4.2). Intersects with an arbitrary threshold of 0.05 were used to extract threshold cycles (C_T) resulting in a C_T of 21.3 for the positive control of Ebola RNA and GAPDH RNA, 26.6 for the Ebola RNA test sample and 27.9 for the GAPDH RNA test sample. As expected the no template control did not result in any amplification and thus no C_T could be extracted, showing no contamination of the NTC. The difference in threshold cycle of PCR amplification between Ebola and GAPDH RNA was $\Delta C_T = 1.3$. We can conclude that for every copy of RNA of GAPDH gene in the starting sample there is statistically 2.5 copies of RNA of Ebola virus ($(1+E)^{\Delta C_T}$). The PCR amplification efficiency (E) is assumed to be equal for both cDNAs.

The extracted melting curves (Figure 4.3) and their negative derivative (Figure 4.3) show the purity of the RT-PCR product. The melting temperature (T_M) of Ebola RNA amplicon was $78.58 \pm 0.04°C$ (fitted value and standard error) and GAPDH DNA amplicon had $83.08 \pm 0.04°C$ (fitted value and standard error). Both T_M correspond to the temperatures extracted from LightCycler using the sample samples. The positive control containing Ebola RNA as well as GAPDH DNA amplicons had two distinct steps in the melting curve resulting in two peaks after derivation. The first peak T_M is at $78.72 \pm 0.05°C$ (fitted value and standard error) and the second at $83.06 \pm 0.05°C$ (fitted value and standard error), respectively, corresponding to the melting temperature of Ebola RNA and GAPDH DNA amplicons.

Discussion

Here we show the performance of a handheld, real-time PCR device capability of performing RT-PCR to detect RNA of an Ebola virus with a housekeeping gene for quantification and MCA to confirm the RT-PCR specificity. The total time for this analysis was less than 37 minutes. This time could be shortened by the employment of different polymerase or optimization of the system.
The device processed four samples concurrently, sufficient number for POC applications. Once a sample would be suspected of containing RNA of Ebola virus, a second sample containing a house keeping gene such as RNA of

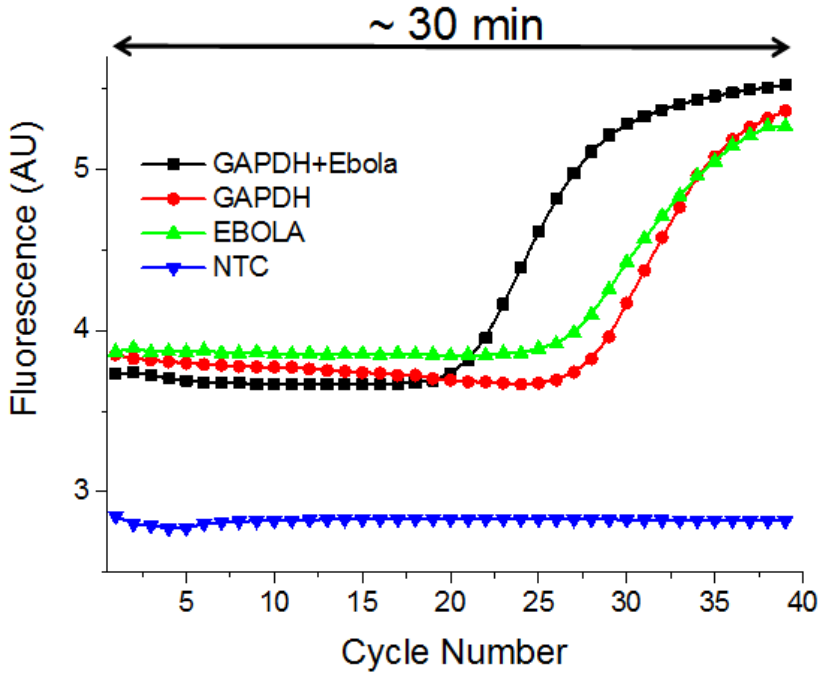

Figure 4.2: A normalized PCR amplification curves for the positive control containing Ebola and GAPDH (black squares), a sample with GAPDH RNA (red circles) and Ebola RNA (green upward triangles and the no template control (NTC) (blue downward triangles). An arbitrary threshold is set, resulting in a threshold cycle of 21.25 for the GAPDH + Ebola, 27.93 for the GAPDH RNA sample and 26.64 for the Ebola RNA sample.

GAPDH, third sample combination of both RNAs (positive control) and the last one would be NTC (negative control). Once the positive control is conducted by multiplexing in the same VRC of both Ebola RNA and a RNA of a reference gene GAPDH, the relative viral load of the target RNA with respect to the reference RNA can be estimated. This option could be especially useful for determining viral loads required for monitoring the post-Ebola disease syndrome.

We estimated that the Ebola RNA was 2.5 times more present than the GAPDH RNA reference gene. We used 10x times higher amount of template for Ebola RNA than the one form GAPDH so one might expect corresponding difference in C_T of the PCRs. We can hypothesize that there might be two main reasons for this discrepancy. First, we assumed that the amplification efficiency of both amplicons is the same as well as both reserve transcriptions. We performed standard PCR curve of both cDNAs were recorded using the Roche LightCycler. Amplification efficiency of Ebola cDNA was close to unity ($E \approx 0.99$), the efficiency of GAPDH cDNA was

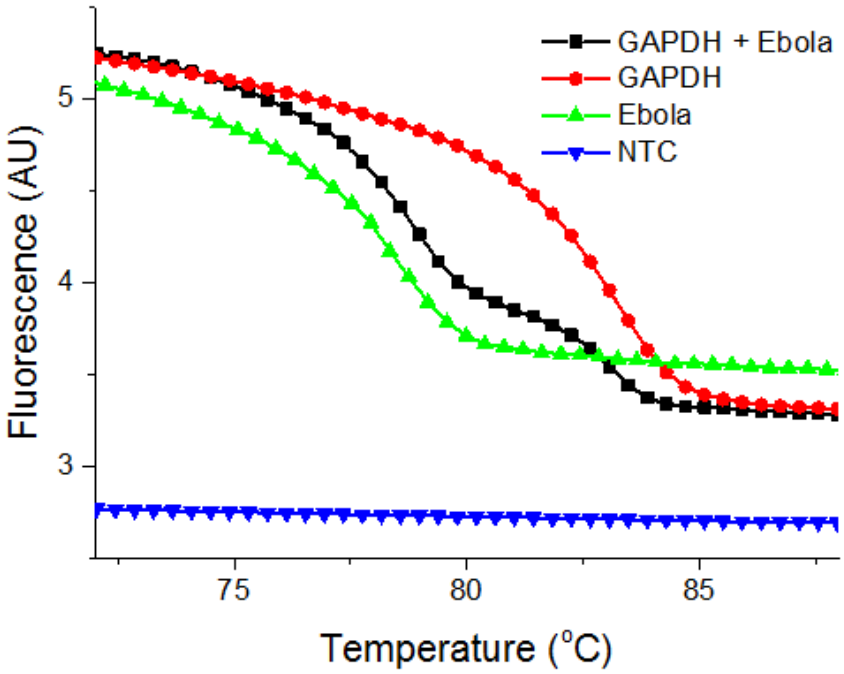

Figure 4.3: Melting curves recorded after 40 cycles of PCR amplification for samples containing GAPDH RNA (red circles), Ebola RNA (green upward triangles) and a positive control containing both genes (black squares). The no template control (NTC) (magenta) does not exhibit any nonlinearity at the melting curve, proving the absence of amplified DNA.

only ≈ 0.89. However, these differences in PCR efficiencies cannot not explain the significantly lower C_T than expected. We suspect that there were also differences in efficiency in reverse-transcription steps.

Conclusion

Here we show that the smartphone-size device is capable of detecting RNA of an Ebola virus and compares its viral loads to a housekeeping gene in less than 37 min using single step real-time RT-PCR including the MCA. T_M of both amplicons confirmed specificity of the PCR. The device is battery powered with a size of only ≈ 100 mm by ≈ 60 mm by ≈ 33 mm and weighing less than 80 g. The system can be further integrated with a previously developed sample preparation module [4] [20] into an integrated sample-to-answer system suitable for decentralized laboratories to tackle the next Ebola virus or any other infectious disease outbreak. Due to its simplicity and small size, it could be then distributed in large numbers into areas with infectious disease outbreaks or even just suspected of the disease.

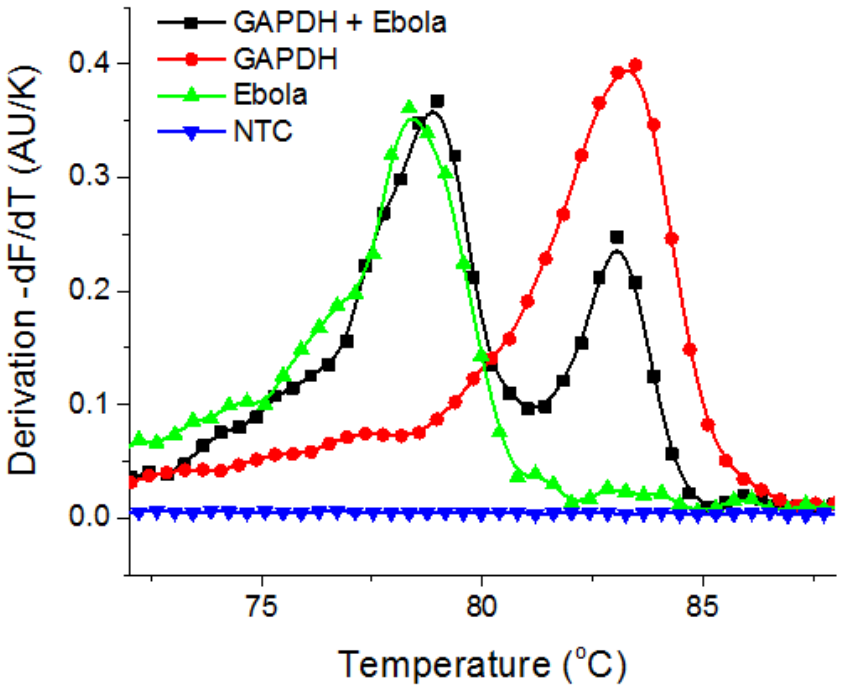

Figure 4.4: The first derivative of fluorescence with respect to temperature for the recorded melting curves. The Ebola RNA (green upward triangles) and GAPDH RNA (red circles) samples each show an individual peak, indicating melting temperatures of $78.58 \pm 0.04°C$ (fitted value and standard error) and $83.08 \pm 0.04°C$ (fitted value and standard error) respectively, as extracted using curve fitting with Gaussian function. The positive control with both Ebola and GAPDH present (black squares) presents both melting peaks at $78.72 \pm 0.05°C$ (fitted value and standard error) and $83.06 \pm 0.05°C$ (fitted value and standard error) respectively, demonstrating the successful amplification of both targets with nearly identical T_M as the individual samples. No template control (NTC) (blue downwards triangles) shows no peaks at the MCA.

4.4 Conclusion

The contribution in this chapter illustrates that the portable, VRC based qPCR instrument can be used for both the analysis of DNA and RNA as commercial, bench-top cyclers can be. Furthermore an example is given for how the system can be used for a relative quantification under utilization of all sample positions. As indicated in the previous chapter the ability to perform relative quantifications needed to be demonstrated, especially as relative quantifications are often more relevant for medical diagnosis. Lastly it is demonstrated here that two targets can be amplified in parallel in the same VRC and more importantly melting curve analysis on the handheld device is able to differentiate the two targets.

While the instrument developed here is shown to be suitable for point of care applications for both DNA and RNA, sample preparation is an issue. Although there are numerous polymerization enzymes and PCR master mixes immune to inhibitors available, transport of these remains a problem. Furthermore for field applications samples like water, soil, blood or saliva samples would have to be prepared and possibly concentrated. It should be possible to perform these steps in a simple and possibly equipment free manner in field. Solutions to these problems could lie in the lyophilization of reagents or in the development of simple microfluidic chips for sample preparation. However, a demonstration of these would be out of the aim of the thesis.

Overall the results shown in this chapter have shown the suitability of the handheld device for the analysis of RNA and DNA. Thus the feasibility of using virtual reaction chambers has been illustrated. It has been demonstrated that two different amplicons can be amplified in parallel and differentiated afterwards by melting curve analysis in the same virtual reaction chamber.

Bibliography

[1] H.M. Temin. The effects of actinomycin D on growth of Rous sarcoma virus in vitro. *Virology*, 20(4):577 – 582, 1963.

[2] K.J. Livak and T.D. Schmittgen. Analysis of Relative Gene Expression Data Using Real-Time Quantitative PCR and the $2 - \Delta\Delta C_T$ Method. *Methods*, 25(4):402 – 408, 2001. ISSN 1046-2023.

[3] J.S. Towner, P.E. Rollin, D.G. Bausch, A. Sanchez, S.M. Crary, M. Vincent, W.F. Lee, C.F. Spiropoulou, T.G. Ksiazek, M. Lukwiya, F. Kaducu, R. Downing, and S.T. Nichol. Rapid Diagnosis of Ebola Hemorrhagic Fever by Reverse Transcription-PCR in an Outbreak Setting and Assessment of Patient Viral Load as a Predictor of Outcome. *Journal of Virology*, 78(8):4330–4341, 2004.

[4] J. Pipper, M. Inoue, L.F. P. Ng, P. Neuzil, Y. Zhang, and L. Novak. Catching bird flu in a droplet. *Nature Medicine*, 13(10):1259–1263, 2007.

[5] M.K. O'Shea, K.A. Clay, D.G. Craig, S.W. Matthews, R.L.C. Kao, T.E. Fletcher, M.S. Bailey, and E. Hutley. Diagnosis of Febrile Illnesses Other Than Ebola Virus Disease at an Ebola Treatment Unit in Sierra Leone. *Clinical Infectious Diseases*, 61(5):795–798, 2015.

[6] T.T.-Y. Lam, H. Zhu, Y.L. Chong, E.C. Holmes, and Y. Guan. Puzzling Origins of the Ebola Outbreak in the Democratic Republic of the Congo, 2014. *Journal of Virology*, 89(19):10130–10132, 2015.

[7] C. Drosten, S. Gottig, S. Schilling, M. Asper, M. Panning, H. Schmitz, and S. Gunther. Rapid detection and quantification of RNA of Ebola and Marburg viruses, Lassa virus, Crimean-Congo hemorrhagic fever virus, Rift Valley fever virus, Dengue virus, and Yellow fever virus by real-time reverse transcription-PCR. *Journal of Clinical Microbiology*, 40(7):2323–2330, 2002.

[8] WHO. Laboratory diagnosis of Ebola virus disease, 2015.

[9] S. D. Pas, C. Reusken, B. L. Haagmans, and M. P. Koopmans. Deployment of Dutch mobile laboratories in the West African Ebola virus response. *Journal of Clinical Virology*, 70:S3–S3, 2015.

[10] S. Sarkar, M. P. Singh, and R. K. Ratho. Dried blood spot for Ebola testing in developing countries. *Lancet Infectious Diseases*, 15(9):1005–1005, 2015.

[11] N. Bhadelia. Rapid diagnostics for Ebola in emergency settings. *Lancet*, 386(9996):833–835, 2015.

[12] M.J. Broadhurst, J.D. Kelly, A. Miller, A. Semper, D. Bailey, E. Groppelli, A. Simpson, T. Brooks, S. Hula, W. Nyoni, A.B. Sankoh, S. Kanu, A. Jalloh, Q. Ton, N. Sarchet, P. George, M.D. Perkins, B. Wonderly, M. Murray, and N.R. Pollock. ReEBOV Antigen Rapid Test kit for point-of-care and laboratory-based testing for Ebola virus disease: a field validation study. *Lancet*, 386(9996):867–874, 2015.

[13] A.I. Qureshi, M. Chughtai, T.O. Loua, J. Pe Kolie, H.F.S. Camara, M.F. Ishfaq, C.T. N'Dour, and K. Beavogui. Study of Ebola Virus Disease Survivors in Guinea. *Clinical Infectious Diseases*, 61(7):1035–1042, 2015.

[14] A. Gulland. Thousands of Ebola survivors experience serious medical complications. *Bmj-British Medical Journal*, 351, 2015.

[15] F.J. Carod-Artal. Post-Ebolavirus disease syndrome: what do we know? *Expert Review of Anti-infective Therapy*, 13(10):1185–1187, 2015.

[16] C.D. Ahrberg, B.R. Ilic, A. Manz, and P. Neuzil. Handheld Real-Time PCR Device. *Lab on a Chip*, 2016.

[17] Z. Guttenberg, H. Muller, H. Habermuller, A. Geisbauer, J. Pipper, J. Felbel, M. Kielpinski, J. Scriba, and A. Wixforth. Planar chip device for PCR and hybridization with surface acoustic wave pump. *Lab on a Chip*, 5(3):308–317, 2005.

[18] P. Neuzil, J. Pipper, and T.M. Hsieh. Disposable real-time microPCR device: lab-on-a-chip at a low cost. *Molecular Biosystems*, 2(6-7):292–298, 2006.

[19] S. Tan, C.A. Carr, K. Yeoh, C.J. Schofield, K. Davies, and K. Clarke. Identification of valid housekeeping genes for quantitative RT-PCR analysis of cardiosphere-derived cells preconditioned under hypoxia or with prolyl-4-hydroxylase inhibitors. *Molecular Biology Reports*, 39(4): 4857–4867, 2012.

[20] J. Pipper, Y. Zhang, P. Neuzil, and T.-M. Hsieh. Clockwork PCR including sample preparation. *Angewandte Chemie-International Edition*, 47(21):3900–3904, 2008.

Chapter 5

Multiplexing using two different Dyes

5.1 Motivation and relation to the thesis

The concurrent amplification, detection and quantification of two or more genes is required for many applications. In medical diagnostics for example the amount of virus is often determined with respect to an internal reference gene, like a transcript gene for example. Thus it is desirable to be able to perform simultaneous amplification and detection within the same VRC on the hand-held device for it to be suitable in point-of-care diagnostics. While the parallel amplification of two amplicons is no problem and can be simply achieved through the addition of a second set of primers, detection and quantification provide a problem. As already explained in the introduction most methods for the quantification of two or more genes employ TaqMan-probes of different emission wavelength. This is not possible with our device since it only has one excitation light source and filters for one fluorophore.
The aim of this chapter is to develop a simple method able to detect and quantify two amplificons using only one excitation and one emission wavelength. The method is simple and does not require additional equipment and can easily be implementable to our hand-held device and other qPCR machines.
A possible solution to this problem is the combination of sequence specific TaqMan probes with unspecific intercalating dyes, both having the same excitation and emission characteristics.

5.2 State of the art

Most techniques for multiplexing either employ end point detection methods like gel electrophoresis or melting curve analysis. Alternatively they use probes with different emission wavelength. The approach of using an

intercalating dye in combination with a TaqMan probe has been used in few examples in the past. The first reported use of this combination of dyes was done by Lind et al. [1] who used a sequence dependent TaqMan probe in the same reaction as an intercalating dye. To differentiate between the two dyes, FAM, which emits green light, was used as reporter for the TaqMan probe and BOXTO, which emits yellow light, was used for the intercalator. Hence the two dyes were detected using different filter sets making the signals simple to differentiate. The method used one set of primers corresponding to the single target of the amplification. The TaqMan probe was used to detect and quantify this target. After complete amplification a melting curve analysis was performed using the BOXTO dye to detect unspecific by-products. This first report demonstrated that using both dye chemistries in combination does not inhibit the reaction.

The early approach by Lind et al. which had only a single target and used the intercalating dye to detect for unspecific amplification was soon taken up and improved. An assay was developed which used the dye combination to detect two different targets. However, the assay was not used for quantification [2]. Two primer sets for two different amplicons (*M. tuberculosis* with and without a deletion) were used in combination with a TaqMan probe for one of the two amplicons. The TaqMan probe used either 6-Carboxyl-X-Rhodamine (ROX), with an emission maximum at $610nm$, or diSulfo - Cy5 carboxylic acid (Cy5), with an emission maximum at $669nm$, as a reporter. The intercalator SYBR Green I, with an emission maximum at $520nm$, was used in the same reaction and detected through a separate set of optical filters from the TaqMan probe. After amplification fluorescence was measured once on the emission wavelength of the TaqMan dye and the intercalator. To avoid a signal from unspecific by-products from SYBR green the measurement was carried out at an elevated temperature of $84°C$ where unspecific by-products are denatured.

This resulted in a Boolean outcome of signals with either a TaqMan signal and a SYBR green signal present, only a SYBR green signal or no signal from either dye. Through this the subtype of the bacteria could be determined (Fig. 5.2).

Both methods introduced here so far use dyes with distinctively different emission spectra and hence different optical filter sets for the detection of probe and intercalator. The possibility to measure the intercalator and the probe on the same fluorescence channel was introduced in 2012 by Van Poucke et al. [3]. The approach used four different dyes (FAM, HEX, Texas Red and Cy5) in combination with SYBR green which shares its excitation and emission properties with FAM. During thermal cycling four targets could be quantified and detected through the TaqMan probes. To isolate the FAM signal from the SYBR green signal fluorescence measurements

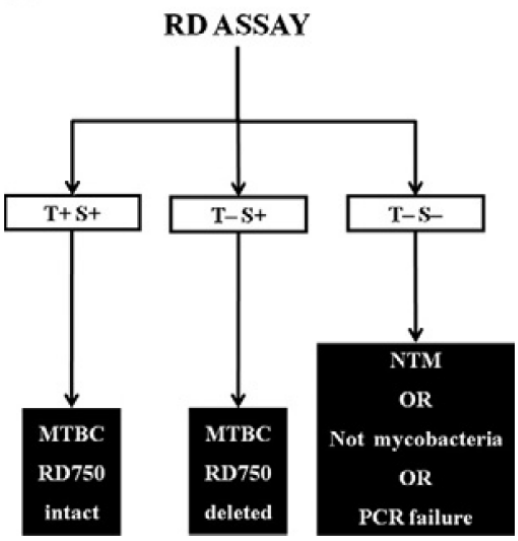

Figure 5.1: In the assay the presence of the TaqMan signal (T+) and the SYBR green signal (S+) indicates the presence of *M. tuberculosis* without the deletion, which is the target of the TaqMan probe. If only the *M. tuberculosis* with the deletion is present no signal from the TaqMan probe is obtained (T-), but one gets a signal from SYBR green (S+) due to the second set of primers. The last option is that neither TaqMan (T-) nor SYBR green (S-) result in a signal. In this case *M. tuberculosis* is either not present, or the reaction has failed *Cheah E.S.G.,* ***Journal of Molecular Diagnostics****, vol. 12 (250 - 256), 2010.*

were conducted during the denaturation step. As no double stranded DNA is present in denaturation, SYBR green can not bind to dsDNA and thus is not fluorescent. After complete amplification melting curve analysis could be performed using SYBR green to check for unspecific amplification and by-products. Here it is not necessary to separate the intercalators signal from the FAM-signal as the probe signal decreases linearly with temperature and thus only shifts the baseline in the differentiated fluorescence signal. This method was picked up for some applications [4] but not developed further.

The approach shown in the following will use a probe and an intercalator with the same excitation and emission wavelength but in contrast to existing methods it will utilize the isolated TaqMan signal as well as the combined TaqMan intercalator signal during cycling. This makes it possible to detect and quantify two amplicons with only one probe and one set of optical filters. As in previous methods melting curve analysis can be conducted after amplification to verify purity of reaction products.

5.3 Paper: Doubling Throughput of a Real-Time PCR

As published in: *Christian D. Ahrberg and Pavel Neuzil, Doubling Throughput of a Real-Time PCR,* ***Scientific Reports*** *5, 12595 (2015)*

The invention of polymerase chain reaction (PCR) in 1983 revolutionized many areas of science, due to its ability to multiply a number of copies of DNA sequences (known as amplicons). Here we report on a method to double the throughput of quantitative PCR which could be especially useful for PCR based mass screening. We concurrently amplified two target genes using only a single fluorescent dye. A FAM probe labelled olionucleotide was attached to a quencher for one amplicon while the second one was without a probe. The PCR was performed in the presence of the intercalating dye SYBR Green I. We collected the fluorescence amplitude at two points per PCR cycle, at the denaturation and extension steps. The signal at denaturation is related only to the amplicon with the FAM probe while the amplitude at the extension contained information from both amplicons. We thus detected two genes within the same well using a single fluorescent channel. Any commercial realtime PCR systems can use this method doubling the number of detected genes. The method can be used for absolute quantification of DNA using a known concentration of housekeeping gene at one fluorescent channel.

The first demonstration of polymerase chain reaction (PCR) in 1983 is considered one of the greatest scientific achievements of the 20th century [5]. It revolutionized many areas of science, due to its ability to multiply a number of copies of DNA sequences (known as amplicons), using either DNA directly or complementary DNA after reverse transcription from RNA. The PCR cocktail called master mix contains free nucleotides, sets of primers and other compounds, besides the polymerase enzyme. The primers are short DNA sequences, one complementary to the DNA strand of interest in a forward direction and the second one complementary in reverse. The classic PCR method required the employment of a post-processing step such as electrophoresis or hybridization to verify the presence and purity of an amplicon.

A few years after the first PCR demonstration, a fluorescent marker was added to the PCR mixture to monitor the reaction in real time [6]. It also allows the determination of an initial DNA concentration. Thus, this method is often called a quantitative PCR (qPCR). The most popular qPCR is based

on intercalating dyes, such as SYBR Green I. The dye produces its fluorescence only in the presence of double-stranded DNA. Thus, researchers can monitor the concentration of amplicons. Another outcome of this method is the melting curve analysis (MCA), typically conducted once the PCR is completed. The sample is slowly warmed up while its fluorescence is monitored. At elevated temperatures, the double stranded DNA amplicons start to convert to single stranded (melt) and consequently the amplitude of the fluorescence drops. When half of the DNA melts from double stranded into single stranded, the temperature is called the melting temperature (T_M). It is characteristic of the DNA amplicon length and its sequence. The intercalating dye-based methods are frequently used as they are not specific to any particular DNA sequence.

Another popular qPCR method is based on a probe such as 6-carboxyfluorescein (FAM) [7]. This probe has to be chemically bound to the oligonucleotides next to a quencher such as TAMRA or a black hole quencher. This PCR method is often called TaqMan or TaqMan chemistry [8]. Once the primers bind to the DNA template, the quencher typically gets separated from the fluorophore and its fluorescence amplitude increases. This method is gene specific but requires oligonucleotides to be synthesised with attached dye and a quencher. Fluorescence resonance energy transfer (FRET)-based methods are also popular [9].

A method to detect more than one target sequence in a single sample is called multiplexing. It offers significant advantages compared to single PCR, such as more information per reaction and therefore time saving. Applications for multiplex PCR can be found in food sciences [10], agricultural sciences [11] or in human medicine. In human medicine, the method is often used to determine ratios of housekeeping genes for normalization [12], assessing viral loads [13] or determining the species [14] or subspecies in bacterial [15] and viral infections [16]. Researchers used end-point multiplex detection to identify different amplicons by the differences in their melting temperature by MCA [17] in the presence of an intercalating dye [10]. This method requires amplicons with different melting temperature caused by different DNA lengths and sequences [18]. Alternatively, a gel electrophoresis can be performed after PCR to separate and detect the different DNA amplicons [19]. This method requires amplicons with different number of base pairs (length), resulting in different electrophoretic mobilities for each amplicon. Both methods are based on post-processing after PCR. Thus, they provide qualitative information as to whether the DNA sequence of interest was present or absent in the original sample. There is limited knowledge obtained about the quantity of DNA templates in the original sample.

The probe-based methods belong to the real-time PCR family. The

results give quantitative information, thus also called quantitative PCR (qPCR). The most common approach is performing PCR with oligonucleotides attached to probes with different emission wavelengths and detect them using several fluorescence channels [20]. The number of genes identifiable per fluorescence channel can be further increased by creating colour codes [21] for the different genes and extracting information on amplicon concentrations via linear combinations on the individual fluorescence channels [22]. Theoretically, the number of genes concurrently detectable is unrestricted, but there are various limits imposed through the optical filter system required and through the dye assays. Selecting an appropriate probe for the assay also becomes increasingly difficult and assay costs increase with the number of used probes.

What will happen if TaqMan probes, such as FAM, and intercalating dyes, like SYBR Green I, are combined in the same experiment? One of the earliest work reports combination of TaqMan probe with emission in the FAM spectrum and the asymmetric cyanine dye BOXTO (TATAA) [1]. BOXTO has an emission maximum at 552 nm, thus requiring a different filter set from FAM to be detected. In their work, they combined the dyes to quantify and detect the gene of interest using the TaqMan dye. Once the PCR was completed, they performed melting curve analysis (MCA) to detect nonspecific product formation by monitoring the fluorescence signal from BOXTO.

A few years later, PCR was performed with a primer set labeled with TaqMan probes 6-Carboxyl-X-Rhodamine (ROX) or diSulfo - Cy5 carboxylic acid (Cy5) in presence of SYBR Green I intercalating dye to detect polymorphism in *Mycobacterium tuberculosis culture 21.* Both those dyes have different fluorescent distinctively different excitation/emission wavelength from SYBR Green I thus different filters have to be used for detection of each dye. With this combination of dyes and using primer sets for two different amplicons, the authors got three possible Boolean outcomes after completing the PCR. They either got a signal from the TaqMan probe and the intercalating dye, a signal from the intercalating dye or no signal. In the first case, they could conclude that *M. tuberculosis* was present and the polymorphism had not occurred. In the second case, *M. tuberculosis* was present and the polymorphism did occurred and in the last case either *M. tuberculosis* was not present or the PCR failed. The Boolean approach described by authors allows specifying which of the two phenotypes is present, as long as there is no mixture of the two phenotypes. Both works [2] [1] used different fluorescent channels to detect the probe and to detect the intercalating dye.

Recently, it was shown that two dyes with the same emission wavelengths

could be combined [3]. Researchers used four different TaqMan probes labelled with FAM dye, phosphoramidite (HEX), Texas Red and Cy5 dyes combined with the intercalating dye SYBR Green I, which exhibits nearly identical excitation/emission spectra as FAM. They extracted quantitative data during the PCR from individual signals from TaqMan probes above the melting temperature of the amplicons to eliminate signal from the intercalating dye. Once the PCR was completed the MCA was performed to detect the unspecific amplification due to possible primer interactions.

In our approach, we take this idea one step further by measuring both the signal of the TaqMan probe as well as the combined signal of the TaqMan probe and intercalating dye during thermal cycling. This allows us to detect and quantify two different genes in the FAM fluorescent channel. We used primer sets for two different genes, a FAM based probe complementary to only one of the genes and SYBR Green I as an intercalating dye. Both genes contributed to the total fluorescence amplitude in the presence of an intercalating dye such as SYBR Green I, as long as the temperature of the mixture was below the T_M. The FAM-labelled probe separated from the quencher also contributed to the total fluorescence. Once the temperature was increased above the T_M, only FAM-based fluorescence contributed to the total fluorescence amplitude. We could then extract two amplification curves: the probe-based amplicon at the denaturation temperature (here called a denaturation curve) and the second one at the end of the extension step (here called an extension curve). This second amplification curve contains both DNA templates together. The concentration of the probe-linked amplicon is already known and can be subtracted from the extension curve, resulting in the concentration of the second amplicon. We can then determine the threshold cycle (C_T) and via comparison with the PCR standard curve also the corresponding original template concentration of both DNAs. The major advantage of this method is the ability of simultaneous, quantitative detection of two DNA templates, using only a single fluorescent channel.

There are two mechanisms of fluorescence contributing to the extension curve: intercalating dye and the probe. The amplitude of this composite fluorescent signal always has to be higher than the one originating only from TaqMan probe extracted at the denaturation curve. Another reason why the signal originated from TaqMan probe is lower is its sensitivity to temperature. Its amplitude is inversely proportional to temperature and the denaturation curve is taken at $93°C - 95°C$, while the extension curve is captured at about $60°C$. The method described above works even in extreme cases with one DNA template having significantly higher number of copies than the second one. Once the number of copies of the DNA linked to TaqMan probe is dominating the C_T value extracted from denaturation curve will be slightly higher than the C_T value extracted from extension curve.

In the opposite case with non-TaqMan template number of DNA copies is dominating, the CT extracted from the extension curve will be significantly lower than the corresponding C_T extracted from the denaturation curve. In both cases, the difference in both C_T determined the number of copies of the second DNA template. We performed two sets of experiments. First, we used two common housekeeping genes: Glyceraldehyde 3-phosphate dehydrogenase (GAPDH) and hypoxanthine-guanine phosphoribosyltransferase (HPRT). The results could be used to calculate a normalization factor by method shown earlier [12] [23][24] [25]. In the second experiment, we determined a viral load in the sample of haemagglutinin (HA) with both HPRT and GAPDH as housekeeping genes [26].

Material and Methods

Experiments

Synthetic DNA templates for GAPDH, HPRT and HA (ATG Biosynthetics) were used for the experiments. The primers were designed using Roche Universal Probe Library Assay Design Center and purchased from Eurofins MWG Operon (Table 5.1). Universal probe #73 (Roche Molecular Systems) was used as TaqMan probe corresponding to HPRT together with the Roche LightCycler TaqMan Master Mix. The reaction mixture consisted of $4\mu L$ master mix, $1\mu L$ of SYBR Green I 10,000 x solution (Lonza) diluted by a factor of 500. The primers and probe were added with concentrations of $1.8\mu M$ and $200nM$, respectively. A sample template was then pipetted in and the mixture volume was increased up to $20\mu L$ by adding de-ionized water produced by a Milli-Q PrograT3 (Millipore) column after autoclaving. Data collection and thermal cycling were done by Roche LightCycler Carousel-Based system using a temperature profile according to the master mix specifications. We used continuous fluorescence measurement mode to capture the data. The measurement can be simplified by collecting fluorescence amplitude data only at the end of the extension and denaturation step with the same quality of results.

Standard curves were recorded in two sets of experiments. In the first set, the concentration of the TaqMan gene was constant while the concentration of non-TaqMan gene was varied (Table 5.2 and Table 5.3). In the second experiment set concentration of non-TaqMan gene was constant while the TaqMan gene concentration was varied (Table 5.4 and Table 5.5). Lastly, an experiment was conducted to determine the concentration of both genes in the presence of a third one. The sample contained HPRT with concentrations of $3.1 * 10^{-7} ng \setminus \mu L$, GAPDH with a concentration of $3.1 * 10^{-6} ng \setminus \mu L$ and HA with a concentration of $6.25 * 10^{-6} ng \setminus \mu L$. We only used two primers at a time, either HPRT and GAPDH primers or HPRT and HA

Gene	Direction	Sequence
HPRT	Forward	5'-TGACCTTGATTTATTTTGCATACC-3'
HPRT	Reverse	5'-CGAGCAAGACGTTCAGTCCT-3'
GAPDH	Forward	5'-AGCCACATCGCTCAGACAC-3'
GAPDH	Reverse	5'-GCCAATACGACCAAATCC-3'
HA	Forward	5'-GGGACTCAACAATTATGAAAAGTGAA-3'
HA	Reverse	5'-GGGTGTATATTGTGGAATGGCAT-3'

Table 5.1: List of primers and their corresponding sequences.

primers. A second sample with the concentrations of $1.6 * 10^{-7} ng \setminus \mu L$ HPRT, $6.25 * 10^{-6} ng \setminus \mu L$ GAPDH and $1.6 * 10^{-5} ng \setminus \mu L$ HA was also tested in the same manner.

Experiment Name	Concentration of HPRT in $ng \setminus \mu L$	Concentration of GAPDH in $ng \setminus \mu L$	Denaturation C_T	Extension C_T
1:0	$6.25 * 10^{-7}$	0	27.4	20.9
1:1	$6.25 * 10^{-7}$	$6.25 * 10^{-7}$	27.7	19.4
1:2	$6.25 * 10^{-7}$	$12.5 * 10^{-7}$	27.6	18.4
1:10	$6.25 * 10^{-7}$	$6.25 * 10^{-6}$	26.8	17.8
1:20	$6.25 * 10^{-7}$	$12.5 * 10^{-6}$	26.0	16.7

Table 5.2: Experiments with excess GAPDH and extracted threshold cycles (C_T).

Experiment Name	Concentration of HPRT in $ng \setminus \mu L$	Concentration of HA in $ng \setminus \mu L$	Denaturation C_T	Extension C_T
1:0	$6.25 * 10^{-7}$	0	26.5	21.3
1:1	$6.25 * 10^{-7}$	$6.25 * 10^{-7}$	26.3	19.3
1:2	$6.25 * 10^{-7}$	$12.5 * 10^{-7}$	26.2	18.2
1:10	$6.25 * 10^{-7}$	$6.25 * 10^{-6}$	26.3	17.9
1:20	$6.25 * 10^{-7}7$	$12.5 * 10^{-6}$	24.9	15.8

Table 5.3: Experiments with excess HA and extracted threshold cycles (C_T).

Data Analysis

We captured all fluorescent data during the entire PCR protocol (Fig. 5.2(a)) and processed them in Matlab, a numerical computing software. We ex-

Experiment Name	**Concentration of HPRT in** $ng \setminus \mu L$	**Concentration of GAPDH in** $ng \setminus \mu L$	**Denaturation** C_T	**Extension** C_T
1:1	$6.25 * 10^{-7}$	$6.25 * 10^{-7}$	29.0	18.2
2:1	$12.5 * 10^{-7}$	$6.25 * 10^{-7}$	26.4	18.2
10:1	$6.25 * 10^{-6}$	$6.25 * 10^{-7}$	24.0	17.0
20:1	$12.5 * 10^{-6}$	$6.25 * 10^{-7}$	22.6	16.3
100:1	$6.25 * 10^{-5}$	$6.25 * 10^{-7}$	20.4	13.9

Table 5.4: Experiments with excess HPRT and extracted threshold cycles (C_T).

Experiment Name	**Concentration of HPRT in** $ng \setminus \mu L$	**Concentration of HA in** $ng \setminus \mu L$	**Denaturation** C_T	**Extension** C_T
1:1	$6.25 * 10^{-7}$	$6.25 * 10^{-7}$	28.6	19.2
2:1	$12.5 * 10^{-7}$	$6.25 * 10^{-7}$	26.3	18.3
10:1	$6.25 * 10^{-6}$	$6.25 * 10^{-7}$	23.3	16.6
20:1	$12.5 * 10^{-6}$	$6.25 * 10^{-7}$	22.7	15.9
100:1	$6.25 * 10^{-5}$	$6.25 * 10^{-7}$	19.6	14.1

Table 5.5: Experiments with excess HPRT and extracted threshold cycles (C_T).

tracted data from Roche LightCycler in two blocks, temperature as a function of time and fluorescence as a function of time. We then used temperature data to determine the beginning of each cycle. Next, we extracted fluorescence amplitude during denaturation and extension steps for each cycle. Each point was formed as a mean from the last five fluorescence measurements in the step. This data processing resulted in two amplification curves denaturations and extensions as a function of cycle number.

We defined the cycle threshold (C_T) as a value of the cycle number when fluorescence amplitude is equal to the background mean (from first 10 cycles) plus five times the standard deviation of the average. We calculated the C_T values for both curves for denaturation as well as extension. As the last step of data processing, both amplification curves were normalized by subtracting the initial fluorescence signal and then dividing all numbers by the fluorescence amplitude. We also performed MCA (Fig. 5.2(b)).
Concentrations were determined by performing PCR with different template concentrations by creating standard curves.

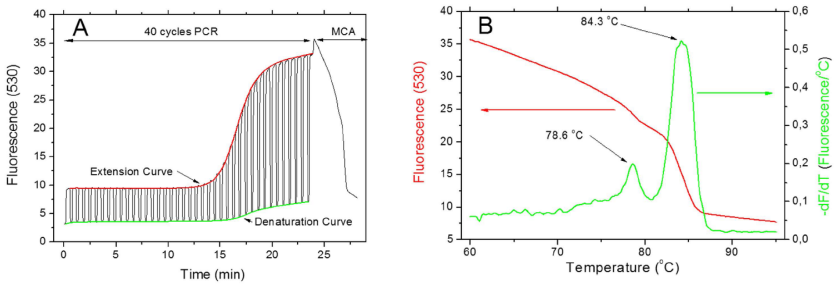

Figure 5.2: (A) A typical data set with both amplification curves extracted from a 40-cycle PCR. The fluorescence amplitude recorded at the end of the extension (red) and denaturation (green) step are shown here. The normalized amplification curves are shown as inset. At the end of the PCR we performed the MCA. (B) The results of the MCA analysis showing DNA templates with two different melting temperatures, 78.6°C and 84.3°C.

Results

The captured data from PCR with different DNA template concentrations are shown in process in figure 5.3. Normalized PCR amplification curves are shown in figure 5.4. As an example, we performed an experiment with a constant concentration of HPRT and a varied concentration of GAPDH.

Non-TaqMan Gene in excess

Housekeeping genes. First, we kept the TaqMan gene (HPRT) concentration constant while the concentration of GAPDH gene was varied. The C_T values extracted from denaturation curves remained constant, as shown in figure 5.5 A. The C_T values extracted from the extension curves decreased with increasing concentration of the non-TaqMan gene (GAPDH).

Viral Load. Second, we also kept the TaqMan gene (HPRT) concentration constant while we varied concentration of cDNA of HA gene. The CT values extracted from denaturation curves again remained constant as shown in figure 5.5 B and the C_T values extracted from the extension curves decreased with increasing concentration of the non-TaqMan gene (HA).

TaqMan Gene in excess

Housekeeping genes. In the two experiments we conducted, the TaqMan gene is in higher concentrations than the non-TaqMan gene. Figure 5.5 C shows the results of experiments using a varied concentration of the HPRT

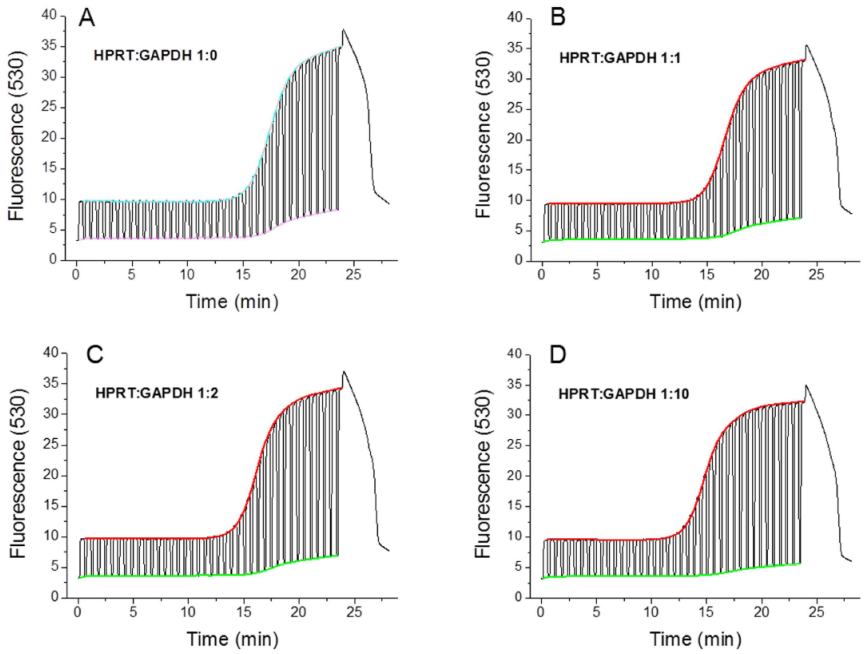

Figure 5.3: Raw fluorescence data from LightCycler for experiments with different ratios between HPRT and GAPDH genes. (A) Shows HPRT gene alone, (B) ratio 1:1, (C) ratio 1:2 and (D) ratio 1:10. We extracted both denaturation (green) and extension (red) curves from all graphs. No template control (NTC) expressed no amplification and its average fluorescence amplitude was 0.113 with a standard deviation of 0.002.

(TaqMan gene) and using a constant concentration of the GAPDH (non-TaqMan gene). The extracted C_T values from the denaturation and extension curves both decreases with an increasing HPRT concentration. However, the rate of change of the C_T values extracted from the denaturation curve is higher than the one from the extension curve. Quantitative information on both genes can be determined from the difference between both curves at a particular total DNA concentration.

Viral Load. As for the housekeeping gene, we have varied concentration of HPRT (TaqMan gene) and constant concentration of HA (non-TaqMan gene). The results (fig. 5.5 D) are similar to the previous ones.

Typical determination of DNA template concentrations.

A C_T value extracted from denaturation curve in the first sample had an amplitude of 26.9. It corresponded only to the concentration of the HPRT gene. A C_T value was also extracted from two extension curves, one with

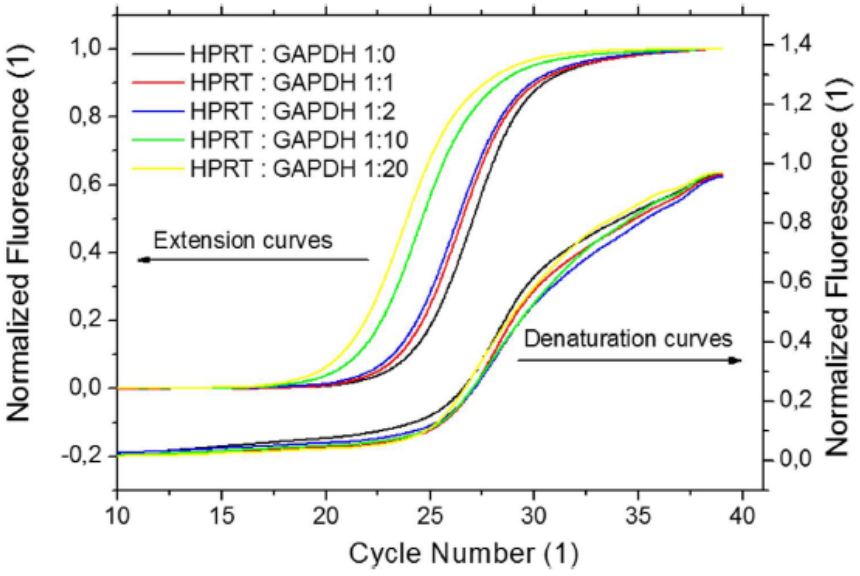

Figure 5.4: (left axis) Extracted normalized extension curves. The curves amplitude was divided by its maximum amplitude and the slope was also subtracted for easier curve to curve comparison. (right axis) The normalized denaturation curves. The normalization was done in a similar fashion as for extension curves.

primers for the GAPDH gene ($C_T = 18.1$) and one with primers for the HA gene ($C_T = 17.5$). Those three C_T values corresponded to a concentration of $6.25 * 10^{-7} ng \setminus \mu L$ for HPRT, $3.49 * 10^{-6} ng \setminus \mu L$ for GAPDH and $4.52 * 10^{-6} ng \setminus \mu L$ for HA. The C_T values extracted from the second sample gave an amplitude of 26.5 for HPRT, 18.4 for GAPDH and 16.8 for HA. Those C_T values corresponded to a concentration of $6.25 * 10^{-7} ng \setminus \mu L$ for HPRT, $2.61 * 10^{-6} ng \setminus \mu L$ for GAPDH and $7.55 * 10^{-6} ng \setminus \mu L$ for HA.

Discussion

The ability to perform quantitative multiplexed PCR is of particular interest for a number of applications. Typically, it is performed by probe-based PCR with a number of probes using specific dyes and with corresponding fluorescent channels for each dye. Here, we have demonstrated a novel method enabling the simultaneous detection of two DNA templates, using only a single fluorescent channel.

We combined a FAM type of TaqMan probe for the first DNA template with an intercalating dye for the second DNA template. We recorded a continuous fluorescence signal for 40-cycle PCR protocol, followed by MCA.

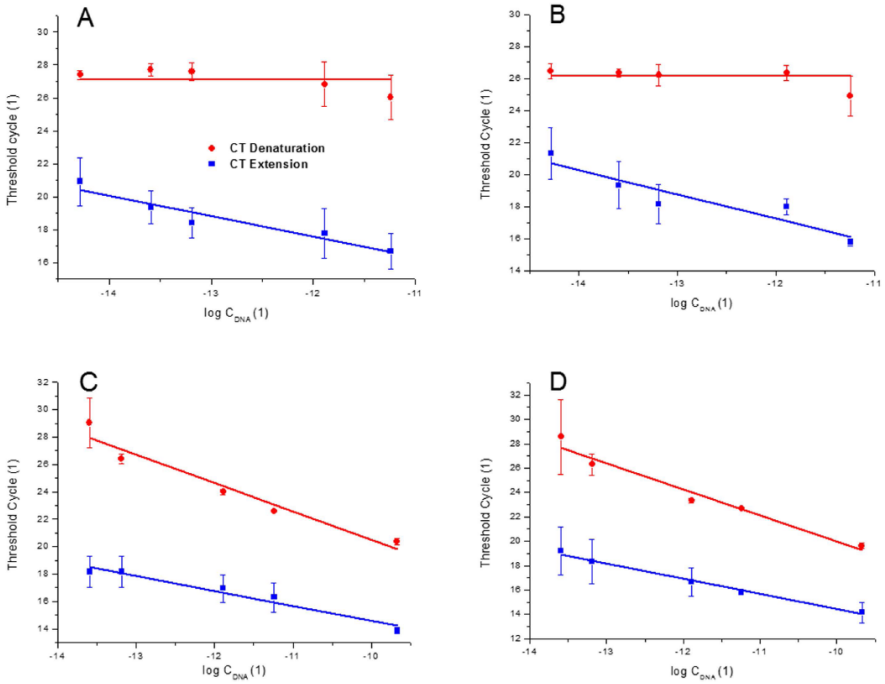

Figure 5.5: Extracted threshold cycles (C_T) for experiments with fixed concentration of either HPRT (A,B), GAPDH (C) or HA (D) genes and varying concentrations of GAPDH (A), HA (B) or HPRT (C,D). Each experiment was repeated three times. The varied concentration was calculated by subtracting the constant value of concentration ($6.25 * 10^{-7} ng \setminus \mu L$) from the total DNA concentration. The red circles correspond to C_T extracted from the denaturation curves while the blue squares from the extension curves.

From the fluorescent signal, we extracted two amplification curves. One was at the end of the denaturation step corresponding only to the TaqMan probe and the second one was at the end of the extension step. The second curve consisted of information from both genes. We then subtracted a TaqMan probe-based data from the second curve resulting in only the non-TaqMan template amplification curve. This extraction was conducted by a script in Matlab. The possibility of detecting and quantifying more than two genes was demonstrated by running several experiments with different primers within the same sample.
An easy way of extracting information on the concentration ratio between two or more genes was demonstrated based on the PCR standard curve. The method feasibility was demonstrated for a concentration difference of up to four orders of magnitude. Results with higher concentration differences are most likely hindered by the depletion of the master mix due to the amplification of one gene.

This method can be implemented for DNA template quantification using TaqMan probe-based gene with a known concentration as the internal standard. In such a case, the standard PCR curve would not be required.
Examples for this can be seen in the experiments in which the concentrations of the three genes were determined. The concentration of the TaqMan gene was the same as for the standard curves in the first sample. This and the fact that the all concentrations were within one order of magnitude allowed a relatively accurate determination of the concentrations of all genes. In the second sample, the concentration of the TaqMan gene deviated significantly from the standard curves. Furthermore, the difference in concentrations between the genes was more than two orders of magnitude. Because of this, the estimate of concentrations became less accurate.
The described method might an option to increase the number of detected genes concurrently without expanding the number of fluorescent channels of commercial real-time PCR devices. Even here, we only tested a single tube, and an identical experiment could be done in all 96 wells of a standard plate system to expand into the detection of 192 genes, 384 into 768 and 1536 into 3072. Furthermore, the method could also be further optimized by research into the binding properties of the intercalating dyes.
In this contribution, the C_T values were extracted from a continuous fluorescent signal. Identical information can be also extracted from only two measurement points during each amplification cycle, at the end of the denaturation step and at the end of the extension step. This way, practically any commercial real-time PCR system is capable of doubling the throughput by performing the multiplexing described in this contribution.

5.4 Authors contribution

Christian Ahrberg came with the idea of combining probe and intercalating dye, prepared all chemicals conducted the experiment and extracted data. Pavel Neuzil prepared figures and wrote the main manuscript text. Both authors reviewed the manuscript.

5.5 Conclusion

The aim of developing a method of detecting and quantifying to different targets with only one set of optical filters was achieved. Through the simplicity of the method it could be integrated into our portable real-time PCR device through a simple software modification. No hardware modification would be required since only a second measurement of fluorescence amplitude in the denaturation step would be required. For this reasons the method can also be used in already existing commercial thermal cylcers. Furthermore the temperature profile does not require alternation hence the total run time of the device remains the same. Thus the number of targets that can be measured by only one filter set during a single run is doubled compared to previous methods.

As shown absolute quantification with this method needs at least two calibration curves making it more complex than calibrations for only one target. However, other multiplex methods also require more rigorous calibration compared to single target reactions. This in mind, the method could be especially useful for relative quantification applications, for example when measuring viral loads compared to a reference gene. On our handheld device a relative quantification could be done with the four VRCs as follows: the first VRC contains the positive control for both the TaqMan and the SYBR green target, the second contains the no template control for both, the third contains a positive control for the SYBR green target and the last VRC contains the actual sample.

For best accuracy the binding properties of the intercalator to both targets should be known so that it is possible to derive accurate predictions about target concentrations from the difference in signal. As this is hard to predict from theory, assays would have to be calibrated before use. This, however, is no issue for point-of-care applications or diagnostics as in these applications the use of pre-designed assays is the norm.

Lastly it should be noted that while the method can be used on the hand-held device as well as commercial devices it does not utilize any of the benefits offered through virtual reaction chambers or miniaturization apart from a lower sample consumption. Thus for further development a modification of the method or an alternative method making use of the advantages of the system would be desirable.

Bibliography

[1] K. Lind, A. Stahlberg, N. Zoric, and M. Kubista. Combining sequence-specific probes and DNA binding dyes in real-time PCR for specific nucleic acid quantification and melting curve analysis. *BioTechniques*, 40:315–319, 2006.

[2] E.S.G. Cheah, J. Malkin, R.C. Free, S.-M. Lee, N. Perera, G. Woltmann, H. Patel, P.T. Kimmitt, R.J. Smith, K. Rajakumar, and M.R. Barer. A Two-Tube Combined TaqMan/SYBR Green Assay to Identify Mycobacteria and Detect Single Global Lineage-Defining Polymorphisms in Mycobacterium tuberculosis. *The Journal of Molecular Diagnostics*, 12(2):250–256, 2010.

[3] M. Van Poucke, A. Van Zeveren, and L.J. Peelman. Combined FAM-labeled TaqMan probe detection and SYBR green I melting curve analysis in multiprobe qPCR genotyping assays. *BioTechniques*, 52:81–86, 2012.

[4] M. Polinski, D.B. Hamilton, B. Nowak, and A. Bridle. SYBR, TaqMan, or both: Highly sensitive, non-invasive detection of Cardicola blood fluke species in Southern Bluefin Tuna (Thunnus maccoyii). *Molecular and Biochemical Parasitology*, 191(1):7 – 15, 2013.

[5] R.K. Saiki, S. Scharf, F. Faloona, K.B. Mullis, G.T. Horn, H.A. Erlich, and N. Arnheim. Enzymatic amplification of beta-globin genomic sequences and restriction site analysis for diagnosis of sickle cell anemia. *Science*, 230(4732):1350–1354, 1985.

[6] R. Higuchi, C. Fockler, G. Dollinger, and R. Watson. Kinetic PCR Analysis: Real-time Monitoring of DNA Amplification Reactions. *Nat Biotech*, 11(9):1026–1030, 1993.

[7] P. K. Witham, C. T. Yamashiro, K. J. Livak, and C. A. Batt. A PCR-based assay for the detection of Escherichia coli Shiga-like toxin genes in ground beef. *Appl Environ Microbiol*, 62(4):1347–53, 1996.

[8] P. M. Holland, R. D. Abramson, R. Watson, and D. H. Gelfand. Detection of Specific Polymerase Chain-Reaction Product by Utilizing the 5'-3' Exonuclease Activity of Thermus-Aquaticus DNA-Polymerase. *Proc Natl Acad Sci U S A*, 88(16):7276–7280, 1991.

[9] A. Andrus, S. Cox, S. Beavers, A. Parker, J. Anuskiewicz, and B. Mullah. High-throughput synthesis of functionalized oligonucleotides. *Nucleic Acids Symp Ser*, 37:317–8, 1997.

[10] M. Safdar and M. F. Abasiyanik. Simultaneous identification of pork and poultry origins in pet foods by a quick multiplex real-time PCR assay using EvaGreen florescence dye. *Appl Biochem Biotechnol*, 171 (7):1855–64, 2013.

[11] A. Abd-Elmagid, P.A. Garrido, R. Hunger, J.L. Lyles, M.A. Mansfield, B.K. Gugino, D.L. Smith, H.A. Melouk, and C.D. Garzon. Discriminatory simplex and multiplex PCR for four species of the genus Sclerotinia. *Journal of Microbiological Methods*, 92(3):293–300, 2013.

[12] J. Vandesompele, K. De Preter, F. Pattyn, B. Poppe, N. Van Roy, A. De Paepe, and F. Speleman. Accurate normalization of real-time quantitative RT-PCR data by geometric averaging of multiple internal control genes. *Genome biology*, 3(7):0034, 2002.

[13] F. Osman, E. Hodzic, A. Omanska-Klusek, T. Olineka, and A. Rowhani. Development and validation of a multiplex quantitative PCR assay for the rapid detection of Grapevine virus A, B and D. *Journal of Virological Methods*, 194(1-2):138–145, 2013.

[14] Y. Kim, Y. Choi, B.-Y. Jeon, H. Jin, S.-N. Cho, and H. Lee. A Simple and Efficient Multiplex PCR Assay for the Identification of Mycobacterium Genus and Mycobacterium tuberculosis Complex to the Species Level. *Yonsei Med J*, 54(5):1220–1226, 2013.

[15] J. F. Mehrabadi, P. Morsali, H. R. Nejad, and A. A. Imani Fooladi. Detection of toxigenic Vibrio cholerae with new multiplex PCR. *J Infect Public Health*, 5(3):263–7, 2012.

[16] C. L. Lo, S. P. Yip, P. K. Cheng, T. S. To, W. W. Lim, and P. H. Leung. One-step rapid reverse transcription-PCR assay for detecting and typing dengue viruses with GC tail and induced fluorescence resonance energy transfer techniques for melting temperature and color multiplexing. *Clin Chem*, 53(4):594–9, 2007.

[17] S. D. Bohling, T. C. King, C. T. Wittwer, and K. S. Elenitoba-Johnson. Rapid simultaneous amplification and detection of the MBR/JH chromosomal translocation by fluorescence melting curve analysis. *Am J Pathol*, 154(1):97–103, 1999.

[18] H. Gudnason, M. Dufva, D.D. Bang, and A. Wolff. Comparison of multiple DNA dyes for real-time PCR: effects of dye concentration and sequence composition on DNA amplification and melting temperature. *Nucleic Acids Research*, 35(19):e127, 2007.

[19] M.S. Noorani, P. Awasthi, M.P. Sharma, R. Ram, A.A. Zaidi, and V. Hallan. Simultaneous detection and identification of four cherry

viruses by two step multiplex RT-PCR with an internal control of plant nad5 mRNA. *Journal of Virological Methods*, 193(1):103–107, 2013.

[20] Q. Huang, L. Zheng, Y. Zhu, J. Zhang, H. Wen, J. Huang, J. Niu, X. Zhao, and Q. Li. Multicolor Combinatorial Probe Coding for Real-Time PCR. *PLoS ONE*, 6(1):e16033, 2011.

[21] I. Nazarenko, B. Lowe, M. Darfler, P. Ikonomi, D. Schuster, and A. Rashtchian. Multiplex quantitative PCR using self-quenched primers labeled with a single fluorophore. *Nucleic Acids Res*, 30(9):e37, 2002.

[22] A. Rajagopal, A. Scherer, A. Homyk, and E. Kartalov. Supercolor Coding Methods for Large-Scale Multiplexing of Biochemical Assays. *Analytical Chemistry*, 85(16):7629–7636, 2013.

[23] M. Rienzo, C. Schiano, A. Casamassimi, V. Grimaldi, T. Infante, and C. Napoli. Identification of valid reference housekeeping genes for gene expression analysis in tumor neovascularization studies. *Clinical and Translational Oncology*, 15(3):211–218, 2013.

[24] S. Tan, C.A. Carr, K. Yeoh, C.J. Schofield, K.E. Davies, and K. Clarke. Identification of valid housekeeping genes for quantitative RT-PCR analysis of cardiosphere-derived cells preconditioned under hypoxia or with prolyl-4-hydroxylase inhibitors. *Molecular Biology Reports*, 39(4): 4857–4867, 2012.

[25] S. Moniotte, J. L. Vaerman, M. M. Kockx, D. Larrouy, D. Langin, P. Noirhomme, and J. L. Balligand. Real-time RT-PCR for the Detection of Beta-adrenoceptor Messenger RNAs in Small Human Endomyocardial Biopsies. *Journal of Molecular and Cellular Cardiology*, 33 (12):2121–2133, 2001.

[26] C. L. Ward, M. H. Dempsey, C. J. A. Ring, R. E. Kempson, L. Zhang, D. Gor, B. W. Snowden, and M. Tisdale. Design and performance testing of quantitative real time PCR assays for influenza A and B viral load measurement. *Journal of Clinical Virology*, 29(3):179–188, 2004.

Chapter 6

Multiplexing - Fast Melting Curve Analysis

6.1 Motivation and relation to the thesis

A combination of probe and intercalator with similar emission wavelength is a possibility of performing multiplexed PCR on the hand-held device as demonstrated in the last chapter. Nevertheless the method demonstrated previously does not utilise the advantages presented through the use of microfluidics. Virtual reaction chambers as our microfluidic reaction volume have the advantage of offering a low sample consumption. More importantly VRCs provide a very homogeneous temperature distribution within their volume. The low thermal mass combined with the heating chip give access to fast temperature ramping rates ($> 20°C/s$) while maintaining the homogeneous temperature distribution.
The aim of this chapter is to introduce a way of conducting quantitative multiplexing polymerase chain reactions while being restricted to only one set of fluorescence filters. Additionally the method exploits the advantages offered through virtual reaction chambers. This can be achieved by conducting a fast melting curve analysis when changing from extension to denaturation temperature at the end of each cycle. To not elongate the time required for the entire reaction the melting curves are recorded with the normal temperature transition rate between the two steps. To prevent broadening of melting peaks this method prerequisites no temperature gradients to be present in the sample.

6.2 State of the art

Most quantitative multiplexing approaches rely on probes labelled with different dyes as described in previous chapters. When using an intercalating dye for real-time detection the most common method of differentiating prod-

ucts is melting curve analysis or high resolution melting curve analysis. A variety of intercalating dyes have been used for this purpose, like SYBR green[1]. Later on different dyes were used as well, for example the SYBR green derivative EvaGreen [2]. MCA can be performed on the same device the real-time PCR is done, without requiring manual manipulation of the sample, preventing contamination. Furthermore the same optical filters can be used since only one dye is used. The main disadvantage is that is possible to quantify and detect only one target using this method, but as soon as MCA detects more than one product no quantitative information can be derived any more.
To tackle this problem some protocols suggest measuring fluorescence during cycling not at extension temperature but instead at a higher temperature [3]. The higher temperature is chosen in such a manner that unspecific by-products are denatureated and the specific product is still present in double stranded form. Following this suggestion the quantitative data collected during the reaction corresponds to the single specific product. If subsequent MCA reveals a unspecific by-product, the quantitative data is still usable for the quantification of specific product.
This idea can be taken further by measuring fluorescence at more temperatures between extension and denaturation temperature during thermal cycling. If increments of $1°C$ or less are taken one would finally arrive at a melting curve recorded after each cycle. The issue is that in the paper by Cheah et al. the one additional step to measure fluorescence already takes 20 seconds. So if one would measure fluorescence at an additional 20 points after every cycle the total reaction time would increase by 400 seconds per cycle.

The approach shown in the following will record a melting curve after every cycle as proposed. In order to keep total reaction times short normal temperature profiles as used for standard real-time PCR will be used with heating and cooling rates around $20°C/s$. This will be achieved by exploiting the advantages microfluidics and especially VRCs provide regarding detection and especially thermal transfer.

6.3 Paper: Single Fluorescence Channel-based Multiplex Detection of Avian Influenza Virus by Quantitative PCR with Intercalating Dye

As published in: *Christian D. Ahrberg, Andreas Manz and Pavel Neuzil, Single Fluorescence Channel-based Multiplex Detection of Avian Influenza Virus by Quantitative PCR with Intercalating Dye* ***Scientific Reports*** *5, 11479 (2015)*

Since its invention in 1985 the polymerase chain reaction (PCR) has become a well-established method for amplification and detection of segments of double-stranded DNA. Incorporation of fluorogenic probes or DNA intercalating dyes (such as SYBR Green) into the PCR mixture allowed real-time reaction monitoring and extraction of quantitative information (qPCR). Probes with different excitation spectra enable multiplex qPCR of several DNA segments using multi-channel optical detection systems. Here we show multiplex qPCR using an economical EvaGreen-based system with single optical channel detection. Previously reported non quantitative multiplex realtime PCR techniques based on intercalating dyes were conducted once the PCR is completed by performing melting curve analysis (MCA). The technique presented in this paper is both qualitative and quantitative as it provides information about the presence of multiple DNA strands as well as the number of starting copies in the tested sample. Besides important internal control, multiplex qPCR also allows detecting concentrations of more than one DNA strand within the same sample. Detection of the avian influenza virus H7N9 by PCR is a well established method. Multiplex qPCR greatly enhances its specificity as it is capable of distinguishing both haemagglutinin (HA) and neuraminidase (NA) genes as well as their ratio.

The influenza A virus is composed of eight RNA segments of negative-sense single-stranded RNA where segment 4 encodes the haemagglutinin (HA) gene, and segment 6 the neuraminidase (NA) gene. In order to increase specificity of H7N9 detection, besides the detection of the virus itself, one should also detect both HA and NA individually as well as their ratio. PCR is the method of choice to detect the virus as it can deliver results in tens of minutes compared to traditional methods such as ELISA where the testing takes a few days.
The polymerase chain reaction (PCR) was invented in 1985 [4] [5] to amplify double stranded DNA segments. Adding fluorogenic probe or DNA intercalating dyes (such as SYBR Green) allowed real-time [6] reaction progress

monitoring and extracting of quantitative information (qPCR) [7] [8]. A typical PCR process consists of three steps conducted at different temperatures: denaturation at $95°C$, annealing at $50-60°C$ and extension at $72°C$. Using the Taqman probe-based PCR system the annealing and extension steps are combined into one and performed at a temperature of about $60°C$[8]. The presence of end-point PCR products can be confirmed by agarose gel electrophoresis or by capillary electrophoresis (CE) [9]. However, an end-point measurement does not necessarily correlate with the original number of copies of the amplified DNA sequence. Real-time PCR allows precise quantitative information to be extracted from the exponential phase of the reaction [7] [10]. The Taqman probe-based assay format, for example the FAM (fluorophore) and TAMRA (quencher) labeled probe, is specific to its target gene, whereas the SYBR Green-based format is non-specific. To determine the specificity of the PCR products using SYBR Green, a subsequent melting curve analysis (MCA) [11] has to be implemented. MCA is often preferred over CE as it is performed in the PCR system immediately once the PCR is completed by sweeping samples temperature while monitoring amplitude of fluorescence and thus no sample manipulation is required.
Multiplex quantitative PCR (qPCR) methods based on Taqman probes as well as FRET-based systems have been demonstrated [12]. Currently, it is routinely done with probes, such as the popular FITC, JOEL, ROX and Cy5, using multiple optical channels. Each channel requires its corresponding light source, filter set and a detector. Can multiplex qPCR be conducted in one channel, while demultiplexing the results in real-time? Probe-based systems cannot be used as there is no technique capable of distinguishing the PCR products in a real time. On the other hand intercalating dye based PCR has shown promising results as the products can be demultiplexed using melting curve analysis (MCA) once the PCR is completed[13]. However, this method can determine serotype of the DNA or RNA but does not provide quantitative information. Continuous monitoring of the amplitude of the fluorescent signal is a powerful technique with a number of different applications [14]. One of them was product differentiation during PCR where a number of MCAs were performed individually after several thermal cycles of PCR[1].
In this contribution we propose and demonstrate a method to dynamically extract melting curves within each thermal cycle of a real-time PCR based on a single intercalating dye. This was accomplished by processing captured data without changing the PCR protocol, resulting in a set of 40 MCAs. From this set we were able to demultiplex quantitative data for different segments of DNA. The proposed method allows multiplex internal positive controls using a single intercalating dye and is an alternative for probe based systems used to detect HA to NA gene ratios. It employs only a single fluorescent optical channel. Typical MCA for intercalating dye-based

PCR is performed by scanning the temperature of the sample at the rate of $1°C/s$ or lower while recording the corresponding amplitude of fluorescence signal. The slow scanning rate is an important factor as every system with temperature control such as PCR exhibits a delay between temperature at the sensor and the sample. PCR systems can have a delay as long as a few seconds or more which is why slow temperature scanning for precise determination of a melting curve is essential.
During PCR the sample is cycled between different temperatures. Especially interesting is the transition from extension to denaturation as it covers the range of expected melting temperatures. All that is needed, then, is to detect the fluorescence amplitude from the sample and determine the corresponding temperature during this phase.
The first task has been demonstrated earlier by continuous fluorescence monitoring during the PCR cycling [14]. However the precise temperature monitoring of the sample during temperature transitions is not straightforward as there is discrepancy between sample and heater temperature as explained above. Is there another way to monitor actual sample temperature during ramping from annealing step to denaturation step?
We believe there is a method to measure the sample temperature with high precision. This temperature is given by a thermal control system typically using proportional integrated derivative (PID) method of feedback, the thermal mass of the sample H and the thermal conductance G between the heating block and the sample. The time constant τ of the temperature delay is given by $\tau = H/G$. Values of H, G and PID constants do not change during the PCR process so the temperature profile of the sample is a repetitive function of time during the PCR cycling. This implies that it is sufficient to determine the temperature profile of the sample only during a single cycle. We have used a modified version (Fig. 6.1) of the virtual reaction chamber (VRC) system for this experiment[15]. The heat transfer and the sample temperature profile was simulated by finite element analysis (FEA) and the results were experimentally verified [16]. The model gave us a correlation between the temperature of the heater and the sample during transition from annealing step to denaturation step required for the MCA extraction. The real sample experiment exhibited faster response than the model probably due to convection in the aqueous sample decreasing the temperature gradient minimally in the transition period. This also provided a homogenous temperature distribution, crucial to the method, since it suppresses data smearing.

Here we introduce a method of multiplex qPCR using a single fluorescence channel in the presence of Eva-Green intercalator. It is based on recording both temperature T and fluorescence F as a function of time t and cycle number n. From both functions [$F = f(t, n)$ and $T = f(t, n)$] we have then eliminated time and generated fluorescence as function of temper-

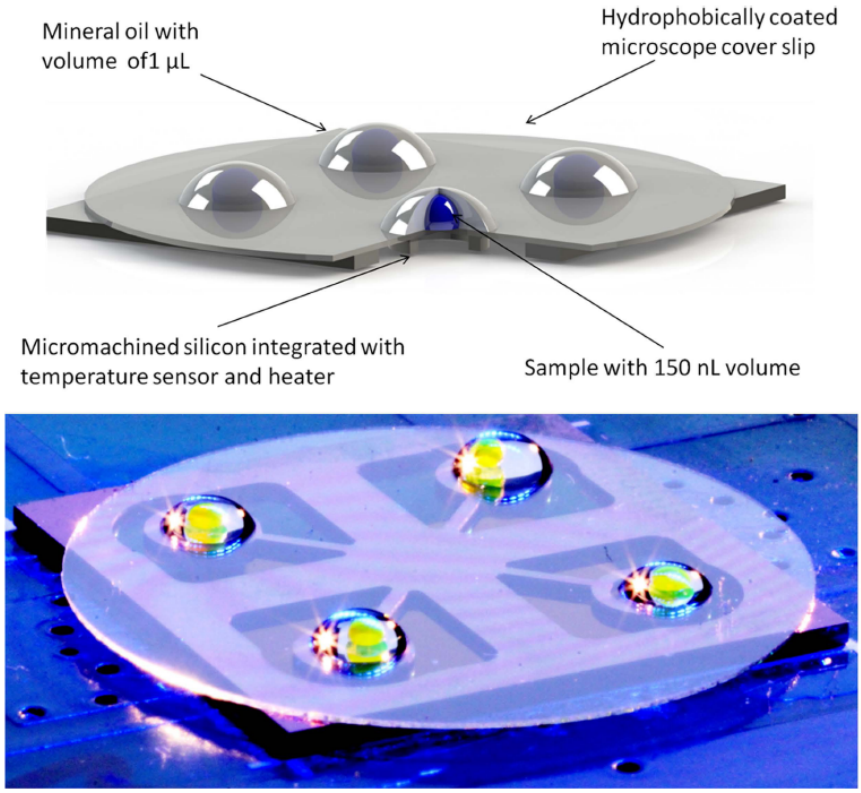

Figure 6.1: (Top) Schematic diagram of the sample and heater. (Bottom) Photograph of four VRCs on silicon chip with sample replaced with fluorescein solution for visualization purpose.

ature $[F = f(T, n)]$ with PCR cycle number as a parameter. We have thus performed a melting curve analysis (MCA) during each PCR cycle. Subsequently we plotted the first negative derivative of fluorescence with respect to temperature as a function of temperature $-dF/dT = f(T)$. For each amplicon a distinct melting temperature was obtained, with its amplitude corresponding to its concentration at each cycle. PCR amplification curves were then created by plotting the amplitude of the respective amplicon as function of cycle number. This way we can quantitatively detect one or more different amplicons using only a single intercalating dye. We only need to perform continuous fluorescence detection at an acquisition rate at or above $1kHz$, thus conventional reagents and protocols can be still used.
The only prerequisite for the methods are a high enough data acquisition rate of fluorescence amplitude, a small sample volume and a sufficiently large difference in melting temperature of the genes for differentiation.

Materials and Methods

Preparation of PCR mixture and thermal cycling.

PCR mixture consisted of $6\mu L$ Roche LightCycler TaqMan Master Mix (Roche Diagnostics, Germany), $1\mu L$ 20X EvaGreen Dye in water (TATAA, Sweden) as well as forward and reverse primers[17] (Table 6.1)(MWG Eurofines, Germany) at a final concentration of $1.8\mu M$. To this solution synthetic complementary DNA (cDNA) templates (ATG Biosynthesis, Germany) for haemagglutinin (HA) and neuraminidase (NA) for the avian influenza virus (H7N9) were added at different concentrations (Table 6.1). Lastly the solution was adjusted to a volume of $20\mu L$ using water obtained from a Milli-Q ProgradT3 column (Millipore, Germany).

Target gene	**Primer name**	**Primer sequence (5'-3')**	**Primer size (bp)**	**Amplicon size (bp)**
H7N9 HA	HA-Forward	TACAGGGAAGAGG CAATGCA	20	103
H7N9 HA	HA-Reverse	AACATGATGCCCC GAAGCTA	20	103
H7N9 NA	NA Forward	CCAGTATCGCGCC CTGATA	19	70
H7N9 NA	NA Reverse	GCATTCCACCCTG CTGTTGT	20	70

Table 6.1: Primers used in this study

A droplet with a volume of $150nL$ of the PCR solution was placed on a hydrophobically coated microscope glass cover slip and covered with $1.5\mu L$ of mineral oil 9405 (Sigma Aldrich, Germany) thus forming a VRC. This glass was then placed on a micromachined silicon chip integrated with both a heater and a sensor, similar to a design shown earlier[15]. Here the silicon chip has a size of only 15 x $15mm$ to better fit a handheld PCR device we are developing (see Fig. 6.1). The small thermal mass of the VRC together with the silicon heater resulted in heating rates $> 20°C/s$ and similar cooling rates achieved only by passive cooling. The PCR protocol consisted of a hot start for 10 min at $95°C$ followed by 40 cycles each consisting of two steps, denaturation for 5 s at $95°C$ and annealing/extension for 30 s at $60°C$.
Fluorescence amplitude was continuously monitored using an Axiotron II microscope (Zeiss, Germany). We have used a blue LED model M470L3-C4 LED with principal wavelength of 470 nm (Thorlabs, Germany) for excitation. The LED was powered with square wave pulses at a frequency of

2710 Hz and a duty cycle of 5%. Light from the LED as well as emitted light from the specimen was filtered with a filter set model 49002 - ET - EGFP (FITC/Cy2) (Chroma Optical Corp, USA). Emitted light was captured by a PMT photosensor module H10722-20 (Hamamatsu Photonics K.K., Germany). The PMT signal was processed by a lock-in amplifier 7230 DSP (Ametek, USA) and its output recorded by a digital oscilloscope model DPO 3014 (Tektronix, Germany) with data rate of 2500 measurements per second. The temperature of the PCR chip was also recorded by the oscilloscope at the same data rate.
For comparison, samples were also analyzed using the Roche LightCycler Carousel-Based system (Roche Diagnostics, Germany) followed by a standard melting curve after thermal cycling.

Data Analysis

Captured fluorescence data were analyzed using a custom written Matlab-script. First the data were filtered by a fast Fourier transform filter (FFTF). Subsequently, the fluorescence signal was divided into the individual cycles based on the captured temperature profile. The fluorescence amplitude during transition from extension/annealing step to denaturation step was then extracted for each cycle and fluorescence as function of temperature was plotted with cycle number as a parameter. MCA was formed by numerical differentiation of the fluorescence with respect to temperature and its negative value was plotted as a function of temperature. The melting curve captured at the first cycle was subtracted from all melting curves to suppress a background fluorescence effect we have observed. This background fluorescence could be caused by autofluorescence from the adjacent printed circuit board as well as fluorescence of the temperature dependence of the fluorophore as well as unspecific binding of the dye onto single stranded DNA[18]. PCR amplification curves were created by plotting amplitudes at the MCA of each amplicon as a function of the cycle number.

Results and Discussion

We have run a 40 cycle PCR using the master mix manufacturer's specifications. A typical fluorescence profile was obtained (see Fig. 6.2 A). In figure **??** B we show the single cycle number 23 to demonstrate the extracted data for the MCA.

This procedure was applied to a sample containing only a single amplicon (HA) with a melting temperature of $76°C$ (see fig. **??** A,B). We have then added to the sample a second amplicon (NA) with a melting temperature of $68°C$. A second peak corresponding to this amplicon can be observed in the respective MCA (Fig. **??** C,D). Increasing the amount of NA added

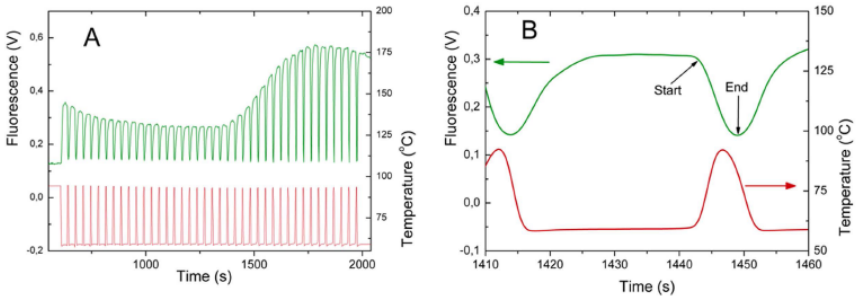

Figure 6.2: (A) Continuous fluorescence profile and corresponding temperature captured of entire PCR experiment. The 10 minutes of hot start is not completely shown, thermal cycling starts after 600 seconds. (B) Single PCR step number 23 showing fluorescence amplitude (green, left axis) and temperature (red, right axis). Start and end of data recording for MCA is shown by arrows.

compared to HA lead to an even faster increase of the magnitude of peak at $68°C$ (Fig. **??** E,F). Extracting the fluorescence amplitude from the derived curves for each cycle at $68°C$ and $76°C$ respectively, results in two PCR amplification curves. Figure 6.4 A shows the two amplification curves extracted for the experiments with a higher concentration of NA than HA (experiments A1 to A5 in Table 6.2).

The sample spiked with the cDNA of the HA gene yielded only a single amplification curve with melting temperature of $76°C$, which was expected. For all other experiments we were able to extract two amplification curves, one at a temperature of $68°C$ and the second one at temperature of $76°C$. Threshold cycles (C_T) were defined in the usual way. It was found that the difference in C_T (ΔC_T) of the two curves corresponded to the expected difference according to the ratio of concentrations of HA and NA. An overview of all conducted experiments is presented in table 6.2. The results indicate that ΔC_T corresponds to the expected values. We can then conclude that the method can be used for multiplexed quantitative PCR. As an example, (see Table 6.2) sample A5 has the concentration of NA 19 times higher than the concentration of HA. With 100% PCR efficiency one would expect a ΔC_T of $4.25(log_2 19)$. We have found the ΔC_T value to be 4.0 ± 0.4 which corresponds to an efficiency of 84%, reasonably close to the ideal value.
We have observed MCA peak broadening in our experiment due to applied conditions. It is necessary to run several replicates of the same experiment to suppress random errors and improve the result precision. The MCAs are recorded at a scanning rate of over $20°C/s$ while the commercial systems for high resolution melting curve analysis (HRMCA)[19] are usually operating with low temperature scan rates between $0.1°C/s$ and $0.5°C/s$. Differen-

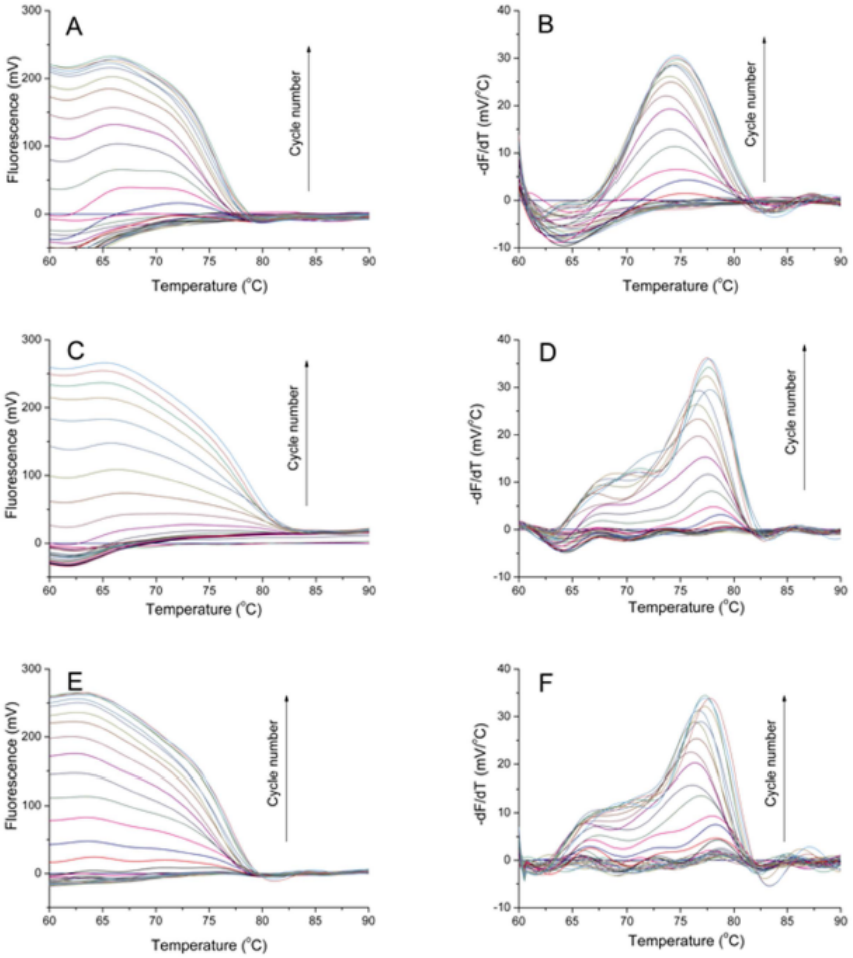

Figure 6.3: Melting curves (A, C, E) and corresponding to their first negative derivative (B, D, F) for all 40 cycles with cycle number as parameter. A and B are data from sample containing only HA. C and D are data from sample containing HA and twice more of NA. E and F are data from sample containing HA and ten times more NA.

tiation of amplicons with melting point differences ΔT_m as small as $1.2°C$ have been demonstrated in HRMCA. However the method presented in this contribution requires greater ΔT_m due to peak broadening caused by the high heating rate.
We assume that a difference in amplicons melting temperatures of at least $5°C$ would be sufficient to differentiate them from each other. This could be achieved by primer design since the melting temperature is a function of amplicon length and ratio of CG/AT content. Therefore an extension temperature of $60°C$ and a denaturation temperature of $95°C$ would allow for

Experiment Code	**Concentration of HA** ($ng/\mu L$)	**Concentration of NA** ($ng/\mu L$)	C_T **at** $68°C$ **(NA)**	C_T **at** $76°C$ **(HA)**	**Difference between** C_T **at** $68°C$ **and** $76°C$
A1	$1.0 * 10^{-7}$	0	-	22.5	-
A2	$5.0 * 10^{-7}$	$5.0 * 10^{-7}$	22.8	22.4	0.4 ± 0.3
A3	$3.2 * 10^{-7}$	$6.4 * 10^{-7}$	25.8	24.7	1.0 ± 0.5
A4	$9.0 * 10^{-8}$	$9.1 * 10^{-7}$	23.7	20.9	2.8 ± 0.3
A5	$5.0 * 10^{-8}$	$9.5 * 10^{-7}$	25.7	29.5	4.0 ± 0.4
B1	0	$1.0 * 10^{-7}$	27.5	-	-
B2	$5.0 * 10^{-7}$	$5.0 * 10^{-7}$	23.1	22.9	-0.1 ± 0.8
B3	$6.4 * 10^{-7}$	$3.2 * 10^{-7}$	23.4	24.6	-1.2 ± 0.1
B4	$9.1 * 10^{-7}$	$9.0 * 10^{-8}$	26.7	30	-3.3 ± 0.3
B5	$9.5 * 10^{-7}$	$5.0 * 10^{-8}$	23.4	27	-3.5 ± 0.1

Table 6.2: Overview of conducted experiments, found threshold cycles (C_T) for both melting temperatures as well as the difference between both threshold cycles.

6 different amplicons to be detected in the same droplet, assuming a ΔT_m of $5°C$.
Furthermore, the temperature measured by the sensor in HRMCA corresponds practically to the sample temperature due to the slow scanning rate. In our approach the sample temperature lags behind the temperature measured by the sensor underneath the sample[20]. This can be seen from the comparative end point HRMCA done with the LightCycler, Figure 6.4 B shows the fluorescence amplitude plotted as function of temperature with a temperature gradient of $0.1°C/s$. In figure 6.4 C the first negative derivative of this curve with respect to temperature is shown, displaying two distinct peaks. Both melting temperatures found on the LightCycler are $8°C$ higher than the temperatures we measured in our system. Nevertheless this T_m offset has no influence on quality of the results especially when this lag is known and the resulting temperature offset is calibrated.

Ideally the test should be performed with a clinical sample containing H7N9 virus starting with sample preparation followed with reverse transcription. VRC-based RT-PCR demonstrating almost all those steps was shown earlier, detecting both RNA from H5N1 avian influenza virus [21] as well as from virus of severe acute respiratory syndrome (SARS) [22]. Processing clinical sample containing virus of avian influenza or SARS would also require laboratory classified as biosafety hazard level 3 which we do not have available. In previous work we developed the system based on spiking

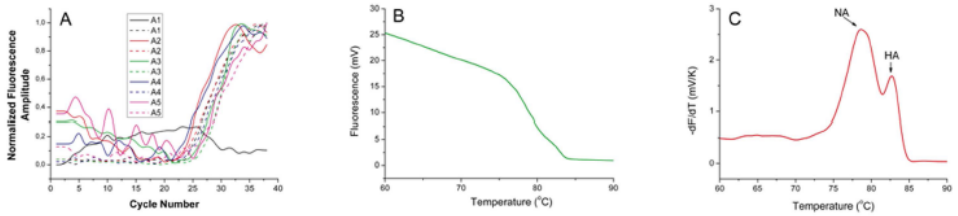

Figure 6.4: Amplification curves extracted for samples A1-A5 (referring to experiment codes in Table 6.2) at $68°C$ (solid lines) and $76°C$ (dashed lines). Sample A1 shows no amplification at $68°C$ (black line) as expected (A), end point high resolution melting curve analysis of sample A2 after 40 cycles on the LightCycler (B-C)

blood sample with RNA, here in this work we spiked PCR master mix with two types of cDNA.

Conclusion

We have developed a method for quantitative, multi target PCR using only a single intercalating dye and thus only one fluorescence channel. Our approach allows researchers to perform affordable multiplex PCR using simple tools as well as reagents. Another advantage compared to conventional methods is small consumption of reagents due to small sample volume. Fluorescent amplitude sampling at a rate above 100 samples per second is, however, required for constructing MCA during transition from annealing/extension to denaturation. This method might be particularly interesting for determination of serotype of virus such as dengue fever or an avian influenza. Other potential applications include measurement of viral loads in a sample, differentiation between H7N9 and H7N5, and quantitative detection of co-infections. We have experimentally verified the method using a homemade PCR system primarily for convenience as we have 100% control of the tool. In principle any commercial real-time PCR device would be capable of performing the same protocol as long as it has available fluorescent amplitude sampling rate of $1kHz$ or higher and can process samples with small volume of a $1\mu L$ or below.

6.4 Authors contribution

Christian Ahrberg ran the lab experiment and prepared all necessary reagents as well as the data processing in Matlab environment, Andreas Manz helped with the experiment preparation and Pavel Neuzil came with the original idea of realtime multiplexing using intercalating dye. All authors reviewed the manuscript.

6.5 Conclusion

It was demonstrated in this chapter that it is possible to extract melting curves from the transition of the extension to the denaturation step after every cycle. Due to the homogeneous temperature distribution and the low thermal mass of the virtual reaction chamber heating rates of $20°C/s$ could be used. By plotting the amplitude of the melting peaks with respect to cycle number it was shown that it is possible to detect and quantify two different targets using only a single fluorescence dye. This is a significant improvement compared to standard melting curve analysis since the method described here is qualitative as well as quantitative, unlike conventional melting curve analysis which provides only qualitative results. It is conceivable to extent the method to more than two targets if targets are chosen with melting temperatures far enough apart for differentiation.

When using larger sample volumes temperature gradients inside the sample would lead to peak broadening making a fast recording of melting curves infeasible. Thus it is a necessity to work with small volumes and VRCs are ideal for this purpose as they provide a simple solution to this problem. As the method uses only a single intercalating dye all fluorescence measurements can be made with the same optical filter set. These two factors make this method suited for the hand-held device, however it can not be integrated for two reasons. Firstly the number of fluorescence measurements that can be done per second is not high enough to obtain melting curves of high enough resolution. Secondly due to having only one Lock-In amplifier on the printed circuit board of the hand-held device means that only temperature or fluorescence can be measured at any instance in time. Thus when going from extension to denaturation temperature fluorescence can not be measured as the temperature needs to be monitored. Hence to integrated the method to the hand-held device a modification of the hardware would be required.

The method can be easily realised by mounting the heating chip of the hand-held device under a fluorescence microscope. This way VRCs can be used as containers for the sample, the chip can be used exclusively for heating and the microscope does the detection. Fluorescence measurements can be realised at much greater rates than required using a photomultiplier tube, Lock-in amplifier and oscilloscope. This makes the method especially feasible for research laboratories, many of which already have fluorescence microscopes and the required accessories.

Bibliography

[1] K. M. Ririe, R. P. Rasmussen, and C. T. Wittwer. Product differentiation by analysis of DNA melting curves during the polymerase chain reaction. *Analytical Biochemistry*, 245(2):154–60, 1997.

[2] V. Marotta Roberta, O. Turri, A. Morandi, M. Murano, G. Melzi d'Eril, and M. Luisa Biondi. High resolution melting analysis to genotype the most common variants in the HFE gene. *Clin Chem Lab Med*, 49(9): 1453, 2011.

[3] E.S.G. Cheah, J. Malkin, R.C. Free, S.-M. Lee, N. Perera, G. Woltmann, H. Patel, P.T. Kimmitt, R.J. Smith, K. Rajakumar, and M.R. Barer. A Two-Tube Combined TaqMan/SYBR Green Assay to Identify Mycobacteria and Detect Single Global Lineage-Defining Polymorphisms in Mycobacterium tuberculosis. *The Journal of Molecular Diagnostics*, 12(2):250–256, 2010.

[4] R. K. Saiki, S. Scharf, F. Faloona, K. B. Mullis, G. T. Horn, H. A. Erlich, and N. Arnheim. Enzymatic amplification of beta-globin genomic sequences and restriction site analysis for diagnosis of sickle cell anemia. *Science*, 230(4732):1350–4, 1985.

[5] R. K. Saiki, D. H. Gelfand, S. Stoffel, S. J. Scharf, R. Higuchi, G. T. Horn, K. B. Mullis, and H. A. Erlich. Primer-directed enzymatic amplification of DNA with a thermostable DNA polymerase. *Science*, 239 (4839):487–91, 1988.

[6] R. Higuchi, C. Fockler, G. Dollinger, and R. Watson. Kinetic PCR analysis: real-time monitoring of DNA amplification reactions. *Biotechnology (N Y)*, 11(9):1026–30, 1993.

[7] L. G. Lee, C. R. Connell, and W. Bloch. Allelic discrimination by nick-translation PCR with fluorogenic probes. *Nucleic Acids Res*, 21(16): 3761–6, 1993.

[8] M. Kubista, J. M. Andrade, M. Bengtsson, A. Forootan, J. Jonak, K. Lind, R. Sindelka, R. Sjoback, B. Sjogreen, L. Strombom, A. Stahlberg, and N. Zoric. The real-time polymerase chain reaction. *Mol Aspects Med*, 27(2-3):95–125, 2006.

[9] J. Cheng, M. A. Shoffner, K. R. Mitchelson, L. J. Kricka, and P. Wilding. Analysis of ligase chain reaction products amplified in a silicon-glass chip using capillary electrophoresis. *J Chromatogr A*, 732(1):151–8, 1996.

[10] Q. Huang, L. Zheng, Y. Zhu, J. Zhang, H. Wen, J. Huang, J. Niu, X. Zhao, and Q. Li. Multicolor combinatorial probe coding for real-time PCR. *PLoS One*, 6(1):e16033, 2011.

[11] M. Fixman and J. J. Freire. Theory of DNA melting curves. *Biopolymers*, 16(12):2693–704, 1977.

[12] A. Andersson, M. Hoglund, B. Johansson, C. Lassen, R. Billstrom, S. Garwicz, P. G. Nilsson, F. Mitelman, and T. Fioretos. Paired multiplex reverse-transcriptase polymerase chain reaction (PMRT-PCR) analysis as a rapid and accurate diagnostic tool for the detection of MLL fusion genes in hematologic malignancies. *Leukemia*, 15(8):1293–300, 2001.

[13] A. J. Gubala. Multiplex real-time PCR detection of Vibrio cholerae. *J Microbiol Methods*, 65(2):278–93, 2006.

[14] C. T. Wittwer, M. G. Herrmann, A. A. Moss, and R. P. Rasmussen. Continuous fluorescence monitoring of rapid cycle DNA amplification. *Biotechniques*, 22(1):130–1, 134–8, 1997.

[15] P. Neuzil, J. Pipper, and T. M. Hsieh. Disposable real-time microPCR device: lab-on-a-chip at a low cost. *Mol Biosyst*, 2(6-7):292–8, 2006.

[16] P. Neuzil, T. Karasek, W. Sun, and A. Manz. Nanoliter-sized Overheated Reactor. *Applied Physics Letters*, X, 2014.

[17] V.M. Corman, M. Eickmann, O. Landt, T. Bleicker, S. Bruenink, M. Eschbach-Bludau, M. Matrosovich, S. Becker, and C. Drosten. Specific detection by real-time reverse- transcription reaction assays of a novel avian influenza A(H7N9) strain associated with human spillover infections in China. *Euro Surveill.*, 18(16), 2013.

[18] F. Mao, W.-Y. Leung, and X. Xin. Characterization of EvaGreen and the implication of its physicochemical properties for qPCR applications. *BMC Biotechnology*, 7(1):76, 2007.

[19] C. Pasay, L. Arlian, M. Morgan, D. Vyszenski-Moher, A. Rose, D. Holt, S. Walton, and J. McCarthy. High-resolution melt analysis for the detection of a mutation associated with permethrin resistance in a population of scabies mites. *Medical and Veterinary Entomology*, 22(1): 82–88, 2008.

[20] P. Neuzil, F. Cheng, J. B. Soon, L. L. Qian, and J. Reboud. Non-contact fluorescent bleaching-independent method for temperature measurement in microfluidic systems based on DNA melting curves. *Lab Chip*, 10(20):2818–21, 2010.

[21] J. Pipper, M. Inoue, L. F. P. Ng, P. Neuzil, Y. Zhang, and L. Novak. Catching bird flu in a droplet. *Nat Med*, 13(10):1259–1263, 2007.

[22] J. Pipper, Y. Zhang, P. Neuzil, and T. M. Hsieh. Clockwork PCR including sample preparation. *Angew Chem Int Ed Engl*, 47(21):3900–4, 2008.

Chapter 7

Modelling of PCR

7.1 Motivation and relation to the thesis

The previous chapters deal with the applications of VRCs in combination with a self constructed thermal cycler for PCR. However to enhance specificity and yield of the polymerase chain reaction the influence of various parameters have to be understood. The parameters easiest to control are the denaturation, annealing and extension temperature. The denaturation temperature is undemanding to optimise, it should be chosen in such a manner that all double stranded DNA denaturates into single strands. As the melting temperatures rarely exceed $85°C$ temperatures between $90°C$ and $95°C$ are ideally suited for this purpose. The annealing temperature should be chosen in such a manner that the primer only binds specifically and does not bind to mismatched sequences. This temperature can easily be optimized by conducting a set of experiments with different annealing temperatures followed by melting curve analysis. Afterwards the temperature is selected which had the lowest amount of side product. Often the extension temperature does not require optimization. Usually the temperature with the highest polymerase activity is picked here. More critical are the concentrations of primers, nucleotides and enzyme used in the reaction. For these an optimum can often only be found by screening large sets of different concentration ratios.

The aim of this chapter is to develop a simple mathematical model to enhance the understanding of the processes during the PCR. Furthermore the model helps to choose concentrations for primers, nucleotides as well as the polymerase enzyme.

7.2 State of the art

Throughout the years different models have been constructed describing either PCR or single steps of the PCR. The common aim of these models is to increase specificity, assist with analysis of results or enhance the understanding of the reaction. An example for an early model is a simulation of annealing step for complex templates [1]. This model used database of DNA sequences to find positions on which primers could possibly bind, initiating a polymerization. The model took into account mismatch between the primers and the unspecific binding site as well as the length of the by-product. By using this model primers can be designed in a better manner helping to increase the specificity of the reaction, especially when using complex samples.
Other models are constructed to predict the accumulation of product with the PCR cycles. The most popular model here predicts the the amount of product after the n-th cycle simply by $N_n = N_0(1 + E)^n$, where N_n is the number of dsDNA molecules after the n-th cycle, N_0 the initial number of molecules and E the efficiency of the reaction. While these models are only rarely used for optimization purposes they find frequent application in the analysis of real-time PCR results. An example here would be relative quantification of one target compared to a second one [2].

Since these models usually assume an unchanged efficiency for all cycles, often equal to unity, more sophisticated models were constructed explaining the change in efficiency throughout the cycles. One model, for example, divides the model of the reaction in three parts: Denaturation, annealing and extension [3]. While the denaturation is simply considered to have perfect efficiency, hence all double stranded DNA denaturates into single strands, annealing is considered in a more complex manner. For annealing the hybridization of primers to their target DNA as well as the combination of two single strands of DNA into a double strand and the formation of primer dimers from two primers were considered. These processes were expressed either through equilibria or kinetic rate equations in the model. The extension step was divided into two substeps. First a complex was formed from a ssDNA-primer template and the polymerase enzyme. In the next step chain growth occurred. While the first step was assumed to be in quasi equilibrium and the chain growth processes were described kinetically by ordinary differential equations (ODEs).
As the model introduced previously is able to provide information on the development of cycle efficiency during cycling and does not describe the development of nucleotide concentration during the reaction further models were developed. Sarika Mehra and Wei-Shou Hu[4] suggested a model that, like the previous one, divided the cycles into three subunits. The denaturation and annealing part were treated like in the previous model with the

annealing part being strictly described by kinetic equations. In the extension part the formation of a primer-enzyme-ssDNA complex was again the first step. Unlike the other model a nucleotide had to be added to the complex before the chain growth could occur. It was assumed that the addition of enzyme as well as nucleotide to the complex are irreversible and that the reactions involved are in quasi-equilibrium. Through this addition it was possible to draw conclusions on the influence of nucleotide concentration on the outcome of the reaction.

In this chapter a model is suggested that extends the model by Mehra and Hu by accounting for all reactions involved in the extension step with kinetic descriptions. In exchange the annealing process is only described by a simple statistic approach. This allows to make predictions on the development of cycle efficiency as well as estimate the influence of concentrations of the single reagents. Unlike the other models the effect of concentrations on the length of the produced products can be researched using this model.

7.3 Modelling of PCR: Kinetic explanation for Primer dimers

Prepared for publication

A simple mathematical model based on step growth processes to describe the polymerase chain reaction (PCR) is introduced. It has been used to analyse different reaction conditions to predict the distribution of the chain lengths of the products of a PCR. The model suggests that choosing the initial concentrations in such a way that the primers are the limiting reagent in the reaction will produce narrow chain length distributions around the target length, whereas conditions in which the yield of the reaction is limited through the concentration of the nucleotides produce shorter side products and thus a wider distribution. Furthermore, the model proposes that the time that should be spent in each cycle is mainly determined by the enzyme concentration. Experiments were carried out to confirm the predictions made by the model. Due to its simplicity, the model is useful for choosing the reaction conditions before conducting PCR experiments, so as to prevent the formation of unspecific products.

Introduction

The polymerase chain reaction (PCR) is a widely used tool for the detection, quantification and amplification of DNA or RNA sequences. Applications can be found in many areas, such as clinical diagnostics [5] [6], food science [7], and the agricultural sciences [8]. While primers and targets are selected very carefully [9], the reaction conditions and reagent concentrations are rarely optimized. Often, heuristics are followed for choosing temperature profiles, and ready made master mixes are used for the reactions. Carefully designing those aspects could help to reduce the amount of unwanted side products made in the reaction and decrease the reaction time. Mathematical models could provide a simple way to cater to these design criteria.

Several models describing various aspects of PCR have been published in the past. For example, Hsu et al. [10] proposed a model based on rate equations describing the kinetics of the thermal deactivation of the Taq polymerase. Furthermore, they investigated the effects of enzyme deactivation on the efficiency of the reaction as well as the extension times in the individual cycles. Another model [3] focused on the annealing process, also exploring the effects on the reaction's efficiency. Using a kinetic and a thermodynamic equilibrium model to describe primer-template annealing as well

as the template-template, primer-primer annealing and side processes, predictions about the cycle specific efficiency throughout the PCR were made. While these models focus on only a very few processes, still, predictions about the reaction can be made using them. Through the consideration of more processes, more accurate predictions should be possible as well as a better fine tuning of the reaction conditions.
A kinetic description of PCR was suggested by Mehra et al. [4], who also considered reactions in the extension phase, for example, the formation of enzyme-primer-ssDNA complexes or the addition of nucleotides to one of these. Furthermore, extension (chain growth) was considered in the form of a step growth process. Most processes were treated using mass-action kinetics, giving a system of ordinary differential equations to be solved. However, some other processes were described using pseudo steady-state equilibria, such as the reactions describing nucleotide addition. This extended model allowed optimizing the primer concentrations as well as accurately predicting the cycle efficiencies, through the large number of parameters incorporated.

Other models have been written to obtain a deeper understanding of the mechanism of the reaction. These models usually focus on the reaction at the molecular level [1], or treat only single stages of the reaction, such as denaturation, for example [11] [12].

The aim of our model is to use chemical reaction engineering to produce a simple model focusing on a kinetic description of the the chain growth process. For simplicity, the number of processes involved in our model is kept as low as possible, while covering the most important reactions. Furthermore, including parameters for the four main reagents of the reaction, the DNA, the enzyme, the primers, and the nucleotides, is desirable for the design of PCR experiments.

Model derivation

The PCR process typically has three different temperature steps. In the first step, called denaturation and typically conducted around 95°C, double stranded DNA melts into two single strands. Then an annealing step (usually 50–60°C) follows, in which primers, which are short DNA sequences typically 15 to 20 base pairs long, bind to the single strands. Lastly, an extension step is conducted, where the DNA polymerase attaches to the DNA-primer construct and synthesizes a second complementary strand of DNA. This step is normally conducted at temperatures of around 72°C. It is not unusual to use the same temperature as for the annealing step, especially when using fluorescence TaqMan probes for detection.
Thus, assuming perfect efficiency, the amount of double stranded DNA will double every cycle and large quantities of DNA can be synthesized by re-

peating the three steps several times.

Denaturation

For our model, we consider only one process during the denaturation step, namely the melting of double stranded DNA into two single strands:

$$\text{dsDNA} \longrightarrow 2\text{ssDNA} \tag{7.1}$$

Since all double stranded DNA is denatured after 5 seconds [3], we accounted for this process by setting the concentration of ssDNA to double that of the dsDNA of the last cycle. The concentration of dsDNA subsequently is defined as zero for the cycle.

Annealing

In the annealing step, two different processes are considered, namely the binding of the ssDNA to a complementary primer and the binding of the ssDNA to a complementary strand of the ssDNA, resulting in dsDNA:

$$\begin{gathered}\text{ssDNA} + \text{P} \longrightarrow \text{ssDNA} \cdot \text{P} \\ \text{ssDNA} + \text{ssDNA} \longrightarrow \text{dsDNA}\end{gathered}$$

These two process have been modelled with a simple probability-based model, where the concentration of the $ssDNA \cdot P$ complex formed is given by (7.2) and the concentration of the dsDNA is given by (7.3), where $Prop$ is the probability of annealing with a primer (7.4).

$$[ssDNA \cdot P] = [ssDNA]Prop \tag{7.2}$$

$$[dsDNA] = [ssDNA](1 - Prop) \tag{7.3}$$

$$Prop = \frac{[P]}{[P] + [ssDNA]} \tag{7.4}$$

Thus the concentrations of the primers after the annealing step can be calculated by Equation (7.5).

$$[P] = [P]' - [ssDNA \cdot P] \tag{7.5}$$

Here, $[P]'$ denotes the primer concentration from the last cycle. This approach was chosen to model the processes taking place during the annealing step because experimental measurements of the kinetics of this process are difficult, thus only very few have been reported in the literature. On the other hand, the modelled rate constants for annealing as well as melting

tend to be in the nanosecond range [12] and thus orders of magnitude faster than the other processes considered in this model. Therefore the reactions associated to these have reached a steady state long before the other reactions involved in PCR. Thus these annealing steps are unlikely to be rate limiting in the PCR reaction.

Extension

The first step in extension that is employed in the model is the reversible formation of a complex consisting of single stranded DNA, primer, and polymerase. Next, a nucleotide has to join the complex. Now the primer could grow by one base into a chain C_1.

$$\begin{aligned} \mathrm{ssDNA \cdot P + E} &\rightleftharpoons \mathrm{ssDNA \cdot P \cdot E} \\ \mathrm{ssDNA \cdot P \cdot E + N} &\rightleftharpoons \mathrm{ssDNA \cdot P \cdot E \cdot N} \\ \mathrm{ssDNA \cdot P \cdot E \cdot N} &\longrightarrow \mathrm{C_1 \cdot E} \end{aligned}$$

Now the process of nucleotide addition to the complex and incorporation into the chain is repeated until the length of the original template is reached. Due to the reversibility of the the formation of the complex of ssDNA, chain, and enzyme, the enzyme can dissociate.

$$\begin{aligned} \mathrm{C_i + E} &\rightleftharpoons \mathrm{C_i \cdot E} \\ \mathrm{C_i \cdot E + N} &\rightleftharpoons \mathrm{C_i \cdot E \cdot N} \\ \mathrm{C_i \cdot E \cdot N} &\longrightarrow \mathrm{C_{i+1} \cdot E} \end{aligned}$$

These steps are repeated until the chain reaches the full length of the template. Once this length is reached, the only process that can occur is the reversible dissociation of the polymerase enzyme from the newly formed double stranded DNA (C_n):

$$\begin{aligned} \mathrm{C_{n-1} + E} &\rightleftharpoons \mathrm{C_{n-1} \cdot E} \\ \mathrm{C_{n-1} \cdot E + N} &\rightleftharpoons \mathrm{C_{n-1} \cdot E \cdot N} \\ \mathrm{C_{n-1} \cdot E \cdot N} &\longrightarrow \mathrm{C_n \cdot E} \\ \mathrm{C_n \cdot E} &\rightleftharpoons \mathrm{C_n + E} \end{aligned}$$

The reactions described above are described by the following rate equations in the model:

$$r_E = k_E[C_i][E] \tag{7.6}$$

$$r_{-E} = k_{-E}[C_i \cdot E] \tag{7.7}$$

$$r_N = k_N[C_i \cdot E][N] \tag{7.8}$$

$$r_{-N} = k_{-N}[C_i \cdot E \cdot N] \tag{7.9}$$

$$r_G = k_G[C_i \cdot E \cdot N] \tag{7.10}$$

The addition of the enzyme to the ssDNA-chain complex is described by (7.6), while the reverse process is described by (7.7), where k_E and k_{-E} are the rate constants for the reaction and reverse reaction, respectively. Similarly, (7.8) and (7.9) describe the addition of a nucleotide and the reverse process. Again, k_N and k_{-N} are the rate constants for the forward and reverse reactions. Lastly, the rate of chain growth is described by equation (7.10), with k_G being the rate constant for this reaction. $[C_i]$, $[E]$, $[N]$, $[C_i \cdot E]$ and $[C_i \cdot E \cdot N]$ are the concentrations of the chains of length i, the enzyme, the nucleotides, the chain-enzyme complexes, and the chain-enzyme-nucleotide complexes, respectively.
For simplicity, the rate constants for all four bases (A,T,C,G) are treated the same, i.e. the same concentration is used for all of them and rate constants do not differentiate between the different bases. This assumption can be made because in a long enough piece of DNA all four bases are present in the same amount statistically. Furthermore an incorporation of, for example, a C in one strand requires the incorporation of a G in the reverse complement strand. Thus if a differentiation between the bases should be necessary, it should be enough to only differentiate between A,T and G,C as long as one is interested in the processes happening in the bulk solution.

Other reactions considered

In addition to the reactions modelled that describe the most important processes in the PCR, the inactivation of the polymerase was also accounted for by the model through a simple first order reaction (7.11) described by the rate (7.12)

$$\mathrm{E} \longrightarrow \mathrm{E_{inact}} \tag{7.11}$$

$$r_{inact} = k_{inact}[E] \tag{7.12}$$

where k_{inact} is the rate constant for the reaction and $[E]$ is the enzyme concentration.

Cycle transition

The system of ordinary differential equations (ODEs) described above was solved for each cycle. For the initial concentration of dsDNA, the sum of the final concentrations of dsDNA and fully extended chains from the

last cycle was taken. For the primer and nucleotide concentration in the beginning of a cycle, the concentration of each of them at the end of the last cycle was taken. Primers that had annealed to an ssDNA template and not extended as well as chains that had started extending but had not reached the template length by the end of the cycle, were assumed inactive and ignored for all subsequent cycles. This seems a strong assumption but from the solution of the model as well as experiments it can be seen that these cases only occur when either nucleotides have run out or the concentration of the active enzyme is very low. Under these conditions, there is almost no amplification or extension in subsequent cycles, and thus this assumptions should not influence the validity of the model.

The parameters used for the model

The following parameters were used for the model:

Rate constant	Value	Unit	Source
k_E	0.06	s^{-1}	[13]
k_{-E}	$1.2 * 10^7$	$M^{-1}s^{-1}$	[13]
k_N	50	s^{-1}	[13]
k_{-N}	$1.0 * 10^7$	$M^{-1}s^{-1}$	[13]
k_G	60	s^{-1}	[13]
k_{inact}	10^{-4}	s^{-1}	Estimated from half life

Table 7.1: Values used for the rate constants during modeling

The following table lists the concentrations used for the stoichiometric ratio between the primer and the nucleotides. For simulations with an excess of the primer or of the nucleotide, the concentrations were adjusted accordingly.

Concentration	Value	Unit	
$[dsDNA]$	$1.24 * 10^{-10}$	M	dsDNA
$[P]$	$3.19 * 10^{-6}$	M	Primers
$[E]$	$1.0 * 10^{-5}$	M	Polymerase
$[N]$	$1.5 * 10^{-4}$	M	Nucleotides

Table 7.2: Concentrations used for the stoichiometric ratio of nucleotides to primers

Model predictions

There are three main components that influence the distribution of products after each cycle. The first two are the primers and nucleotides, the two reagents in this model. The concentrations of these not only influence the

rate of the reaction but, more importantly, the ratio of the two determines the distribution of the products. Furthermore, due to the eventual depletion of one or both of these reagents, amplification does not continue endlessly. The third main component consists of the polymerase enzyme, which acts as a catalyst in this model and plays an important role in determining the reaction rate.
Three cases were analysed: Primers limiting, nucleotides limiting, and the effect of different concentrations of the polymerase enzyme. To understand the effects of the concentrations of the primer and the nucleotide, one should first analyse the case in which both are present in a stoichiometric ratio.

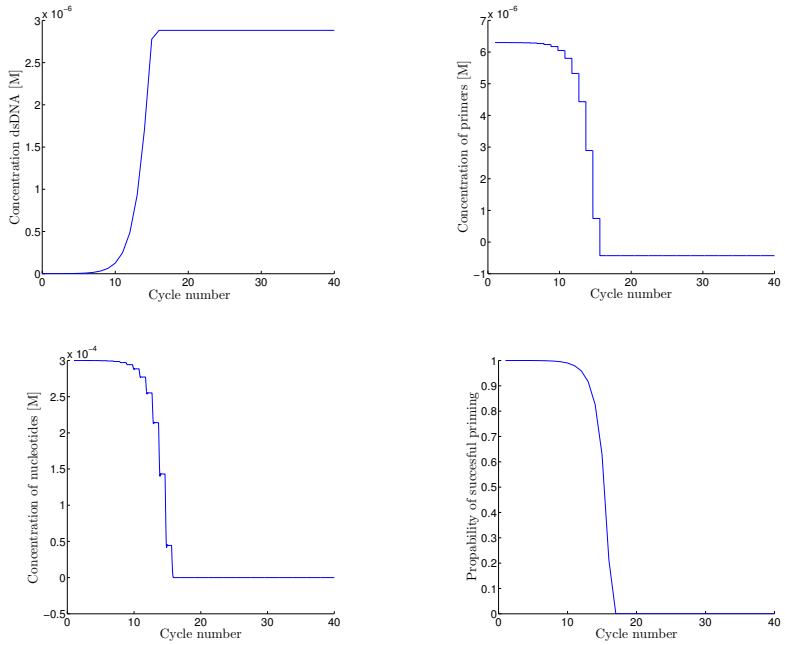

Figure 7.1: Plots of modelled concentration of dsDNA (top left (a)), primers (top right (b)) as well as nucleotides (bottom left (c)) against cycle number. The probability of successful priming against cycle number is shown in the last graph (bottom right (d)). Initial concentrations were chosen for a case with a stoichiometric ratio of primers to nucleotides.

As Figure 7.1 illustrates, the concentration of double stranded DNA increases exponentially until cycle 15. In the subsequent cycle, both the nucleotides as well as the primers are depleted, as can be seen from Figure 7.1(c) and Figure 7.1(b). At the same time, the probability of a successful priming event decreases rapidly to zero (Fig. 7.1(d)) due to the depletion of primers. The simulation predicts that during the first 15 cycles, only fully elongated chains are formed. In the 16th cycle, small concentrations of shorter chains are formed, due to the depletion of the nucleotides (Fig.

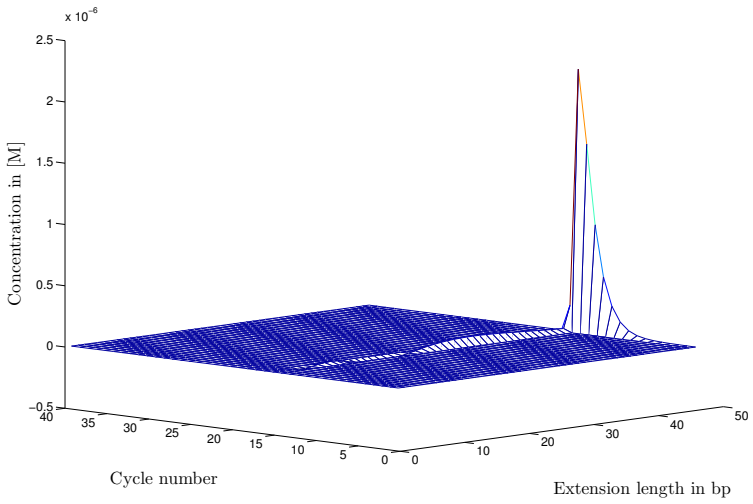

Figure 7.2: Graph showing the length of products formed during thermal cycling for a case of stoichiometric ratio of primers to nucleotides according to the model.

7.2). In the following cycles, no new chains are formed, due to the depletion of the nucleotides as well as the primers.

Nucleotides Limiting

Simulations were carried out with nucleotides as the limiting reagent. For this purpose, primer concentrations two, ten, and twenty times as high as stoichiometricly necessary were considered. All conditions showed the same trend, hence in the following, the most extreme case considered will be discussed. In this case, the primer concentration is twenty times higher than stoichiometricly required by the nucleotide concentration.

As observed before for a stoichiometric ratio betwen the primers and nucleotides, the concentration of double stranded DNA increases until the 15th cycle in the case of a nucleotide limited reaction (Fig. 7.3(a)). Figure 7.3(c) shows that the nucleotides are depleted by this cycle, while there is still a considerable concentration of free primer. The concentration of unbound polymerase during the cycles decreases exponentially until cycle 16. Afterwards, it remains constant due to the constant amount of DNA templates that are present in the subsequent cycles. A slight decrease in concentration is due to the inactivation of the polymerase. The probability of successful priming decreases in two steps, as illustrated by Figure 7.3(d). Until cycle 15, this is due to the annealing of the primer to template, followed by subsequent elongation. Afterwards, the probability decreases due to the

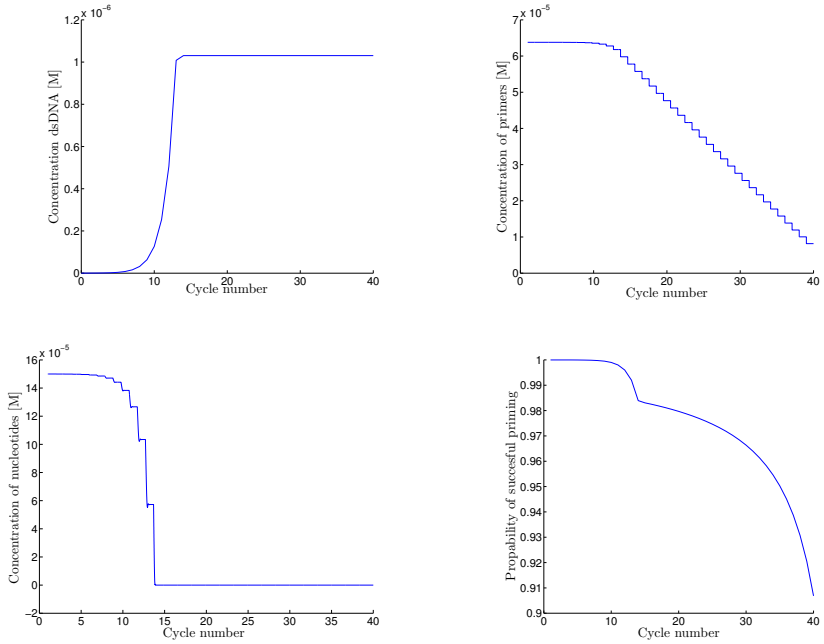

Figure 7.3: Plots of modelled concentration of dsDNA (top left (a)), primers (top right (b)) as well as nucleotides (bottom left (c)) against cycle number. The probability of successful priming against cycle number is shown in the last graph (bottom right (d)). Initial concentrations were chosen for a case with a 20-fold excess of primers over nucleotides.

model's assuming that the primers are bound to template once as chains, and not as primers any more, even when those primers have not been elongated. Therefore, those primers are removed from the pool of available primers and the probability of successful priming decreases.

Based on the distribution of chain lengths produced during cycling, displayed in Figure 7.4, various observations can be made. First of all, it can be seen that after cycle 15, once all the nucleotides have been consumed, priming events still occur at a constant rate. The constant rate is dependent on the amount of template produced until cycle 15. Due to the depletion of the nucleotides, these primers are no longer elongated, and so are considered to be produced chains of length zero. Furthermore, it can be seen that until the cycle in which the nucleotides run out, only fully elongated chains are formed. In the cycle in which the nucleotides run out, a large amount of not fully elongated chains are formed, but almost no fully extended chains.

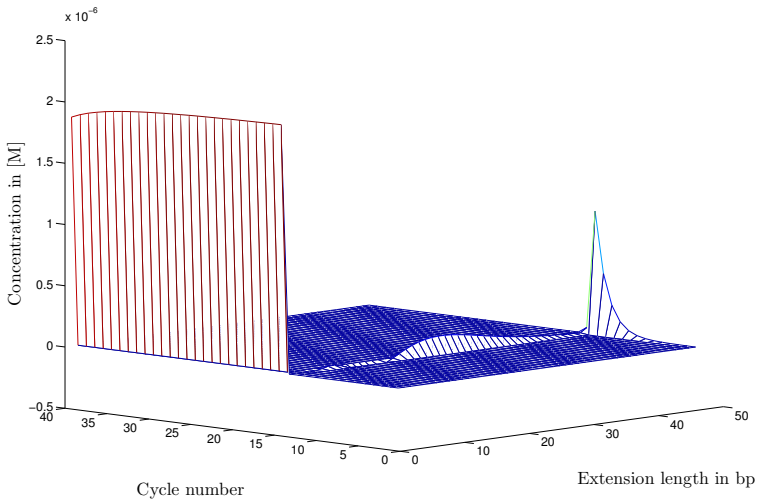

Figure 7.4: Figure illustrating the concentration of chains of different length produced during each cycle for conditions under which the reaction is limited through the nucleotide concentration according to the model.

Primers Limiting

In another set of simulations, the nucleotide was in excess over the primer concentration. Simulations were carried out with a 5-, 10-, 50-, and 100-fold excess of nucleotides over primers. Again, the trend shown by all simulations is similar and therefore only the extreme case, with a 100-fold excess of nucleotides over primers, is discussed here.

Exponential amplification for the first 15 cycles can be observed under these conditions (Fig. 7.5(a)). After the 15th cycle, the primer concentration has dropped to zero (Fig. 7.5(b)) and the probability of successful priming consequently has dropped to zero as well (Fig. 7.5(d)). In subsequent cycles, the concentration of nucleotide remains constant (Fig.7.5(c)), since no reactions consuming nucleotides can occur any more.

The chain length distribution in the case of an excess of primers is significantly different from the cases considered previously. As Figure 7.6 shows, the initial cycles produce only fully extended chains. Once the primers are depleted, in cycle 15, no new chains are formed as no new priming events can occur. During the entire cycling, the model predicts no development of short-chained side products.

Effects of Polymerase

During PCR, the polymerase enzyme acts as a catalyst for the reaction, given that it is in the same state before and after the reaction and is not

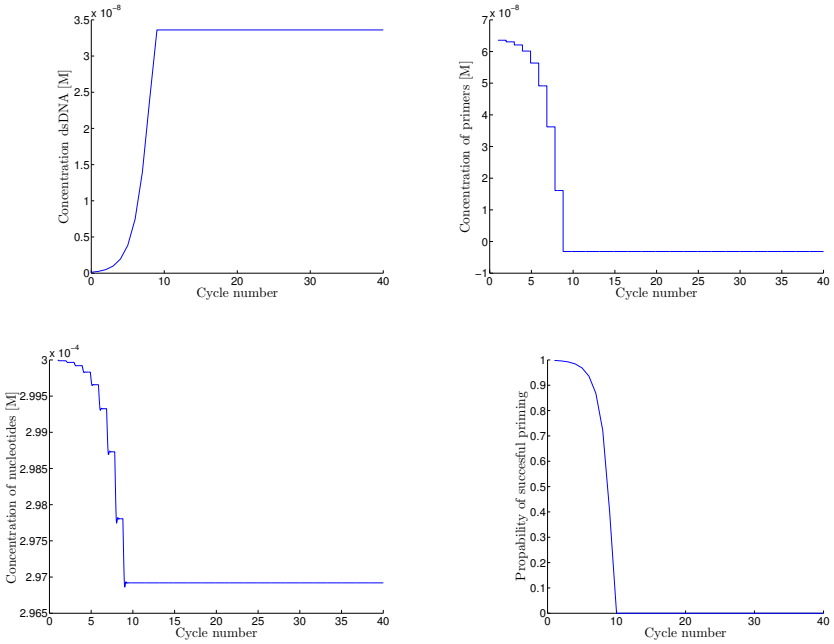

Figure 7.5: Plots of modelled concentration of dsDNA (top left (a)), primers (top right (b)) as well as nucleotides (bottom left (c)) against cycle number. The probability of successful priming against cycle number is shown in the last graph (bottom right (d)). Initial concentrations were chosen for a case with a 100-fold excess of nucleotide over primer concentration.

consumed during the reaction. As long as conditions are chosen such that the reaction reaches completion after each cycle, the enzyme concentration does not have an effect on the product distribution. Figure 7.7 shows the concentration of nucleotide for the first 11 cycles. The parameters for the simulation were chosen as in the stoichiometric case considered initially. As can be seen, the nucleotide concentration reaches a plateau before the next cycle begins, indicating that the reaction has run to completion.

Next, conditions were simulated in which the concentration of the enzyme was increased by three orders of magnitude, while keeping all other parameters the same. Figure 7.8 shows that the nucleotide concentration plateaus before the next cycle is started. In contrast to the simulation carried out before, the plateau is reached faster.

When, on the other hand, the polymerase enzyme concentration is decreased to the point of the reaction time's no longer being sufficient for the reaction to reach completion, the situation becomes more interesting. This case was studied by decreasing the enzyme concentration for the simulation by two orders of magnitude compared to the stoichiometric case studied. As can be seen in Figure 7.9(a), the dsDNA concentration increases exponen-

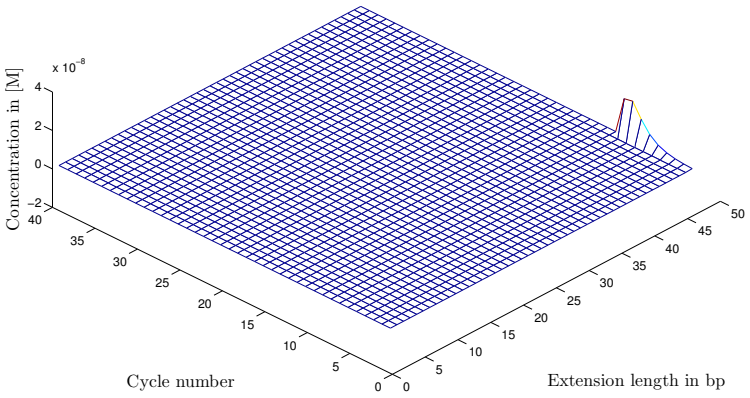

Figure 7.6: Figure illustrating the concentration of chains of different lengths produced during each cycle for conditions limited by the primer concentration according to the model.

tially until the reaction rate becomes limited through the enzyme concentration. At this point, the rate of dsDNA only increases linearly. The limiting rate is defined by the maximum throughput achievable through the polymerase during the elongation time. This in turn leads to linear decreases in the primer and nucleotide concentrations once the enzyme is saturated (Figs 7.9(b) and 7.9(c)).

The limiting reaction rate (through the enzyme) also has significant effects on the chain length distribution of the product. As Figure 7.10 illustrates, only a very small fraction of chains becomes fully elongated. Many priming events occur without subsequent chain growth. Since this effect is not due to a depletion of the nucleotides, and no significant amount of shorter chain side products is formed, it can be concluded that with the rate constants chosen, it is far more likely for an enzyme to complete chain growth than for it to dissociate before complete elongation has occurred. By choosing longer times for chain elongation, the effects on product distribution can be countered easily.

Experimental verification

In order to verify the predictions made by the model, experiments were conducted with different ratios of primers to nucleotides. The predictions of the model regarding the effects of enzyme concentration were not verified, since measurements of the reaction rate during thermal cycling are difficult

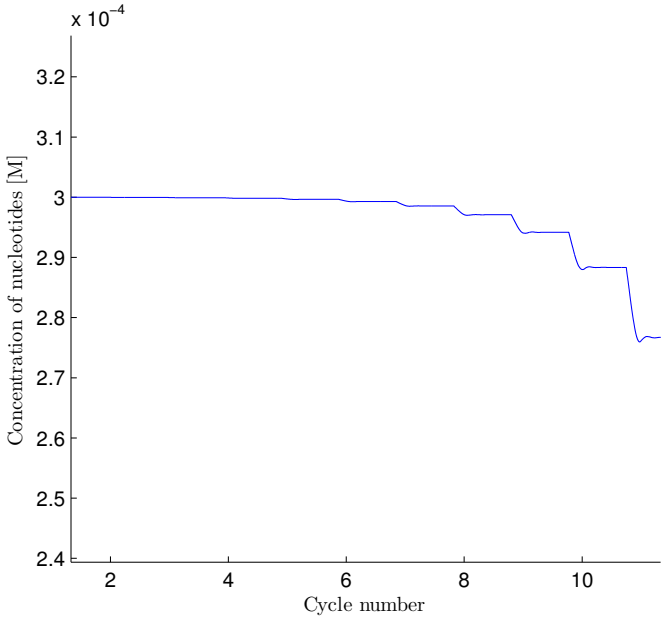

Figure 7.7: Modelled concentration of nucleotides against cycle number for the first 11 cycles. The concentration plateaus before starting the next cycle, indicating that the reaction has gone to completion.

and require more sophisticated setups than conventional real-time thermal cyclers.

Experimental conditions

For all experiments, a solution containing 2 μL of magnesium free PCR buffer (Thermo Fisher), 0.6 μL of 50 mM $MgCl_2$ solution (Thermo Fisher), 1 μL 20x EvaGreen (Tataa) and 0.1 μL 500U Platinum Taq DNA Polymerase (Thermo Fisher) were used. A nucleotide mixture containing all four bases in a concentration of 2.5 mM (GeneAmp dNTP Blend, Thermo Fisher) and forward (agccacatcgctcagacac) and reverse (gcccaatacgaccaaatcc) primers (Eurofines Genomics) were added in varying amounts depending on the experiment. As a template, 2 μL of a solution consisting of $5 * 10^{-6}$ ng/μL (12500 copies per μL) of synthetic DNA (ATG Biosynthesis) template for the human transcript GAPDH were added. Finally, the volume of the solution was adjusted to 20 μL using Millipore-water. The concentrations of primers and nucleotides used for the experiments can be found in Table 7.3.

Experiments were conducted on the Roche LightCycler (Capillary based) using a 30 seconds hot start at $95°C$ followed by 40 cycles of $95°C$ for 10 seconds, $56°C$ for 30 seconds, and $72°C$ for 30 seconds. After thermal cycling,

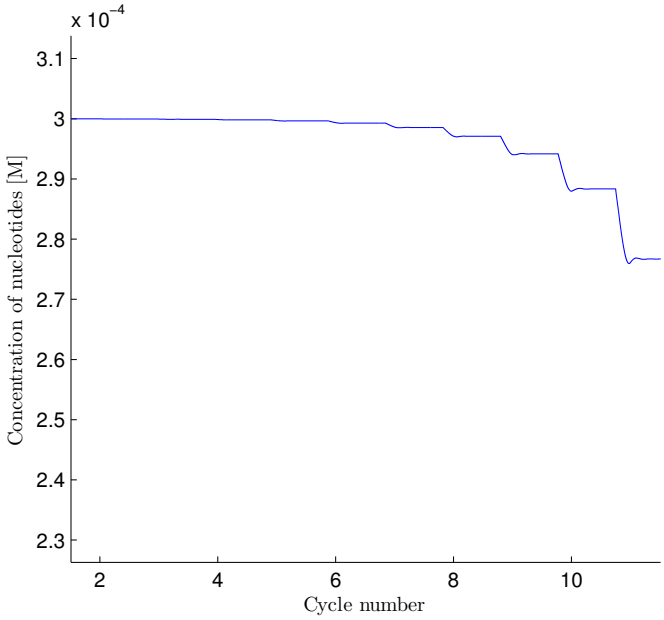

Figure 7.8: Modelled concentration of nucleotides against cycle number for the first 11 cycles. The concentration plateaus before starting the next cycle, indicating that the reaction has gone to completion. For this simulation the polymerase concentration was increased by a factor of 1000 above the concentration usually used.

a melting curve analysis was performed by heating the sample to $95°C$, and then cooling to $55°C$ to finally heat up to $95°C$ with a gradient of $0.1°$ C/s while continuously measuring the fluorescence.

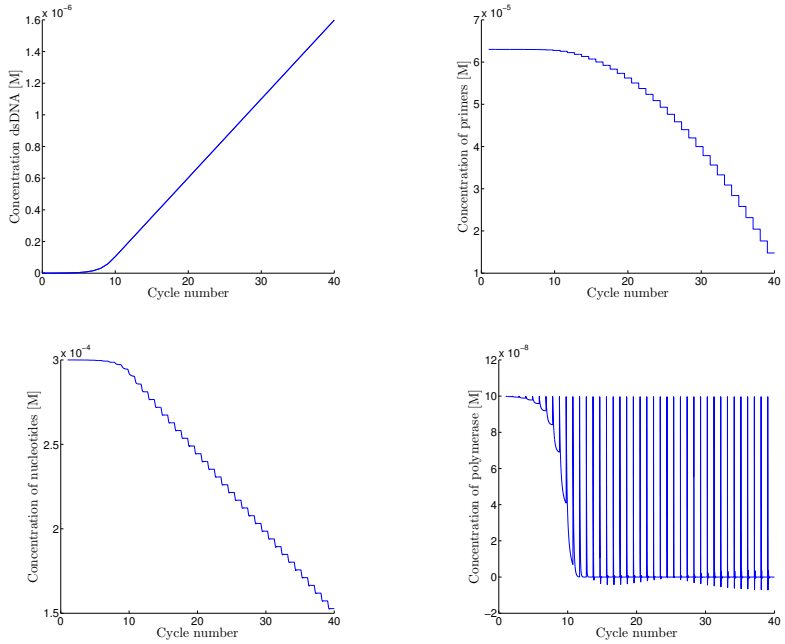

Figure 7.9: Plots of modelled concentration of dsDNA (top left (a)), primers (top right (b)) as well as nucleotides (bottom left (c)) against cycle number. The concentration of free enzyme against cycle number is shown in the bottom right graph (d). Initial concentrations were chosen for a case with a polymerase enzyme concentration three orders of magnitude lower than for the stoichiometric case originally considered.

Primer Concentration in mM	Nucleotide Concentration in mM	Ratio Nucleotides : Primers	Comment
0.3	$6.38 * 10^{-3}$	1:1	Stoichiometric case
0.3	$3.19 * 10^{-3}$	2:1	Primers limiting
0.3	$6.38 * 10^{-4}$	10:1	Primers limiting
0.3	$1.28 * 10^{-4}$	50:1	Primers limiting
0.3	$6.38 * 10^{-5}$	100:1	Primers limiting
0.15	$6.38 * 10^{-3}$	1:2	Nucleotides limiting
0.15	$3.19 * 10^{-2}$	1:10	Nucleotides limiting
0.15	$6.38 * 10^{-2}$	1:20	Nucleotides limiting
0.15	$3.19 * 10^{-1}$	1:100	Nucleotides limiting

Table 7.3: Table showing primer and nucleotide concentrations for the experiments conducted

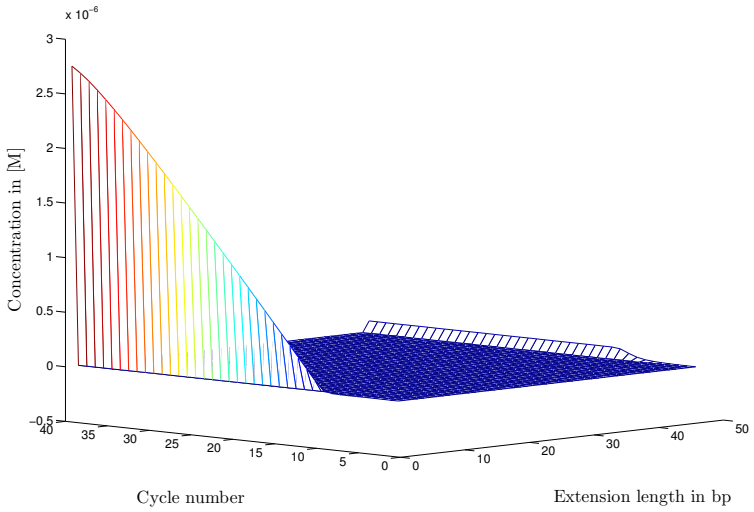

Figure 7.10: Figure illustrating the concentration of chains of different lengths produced during each cycle according to the model.

As the concentration of dsDNA is not detected directly through the LightCycler, it rather detects the fluorescence emitted by the EvaGreen bound to the dsDNA, comparing the threshold cycles predicted by the model to the threshold cycles obtained through experiments is difficult. Furthermore, background noise is not considered in the model.

Stoichiometric case

Conducting experiments with a stoichiometric ratio of primer to nucleotide resulted in a normal amplification (Fig. 7.11) curve as predicted by the model. In the experimental curve, the end of exponential growth is less abrupt than predicted, indicating that the statistical priming approach becomes less suitable for late exponential growth. For this reason, a plateau like that predicted by the model could not be observed.

The product chain length distribution was analysed by a melting curve analysis at the end of the PCR run. The melting curve analysis revealed a single main product, indicated through the one peak at $80°C$ in Figure 7.12(b). There might be shorter chain side products, but their concentrations are insufficient for detection through a melting curve analysis. The results confirm the predictions made by the model for the chain length distribution.

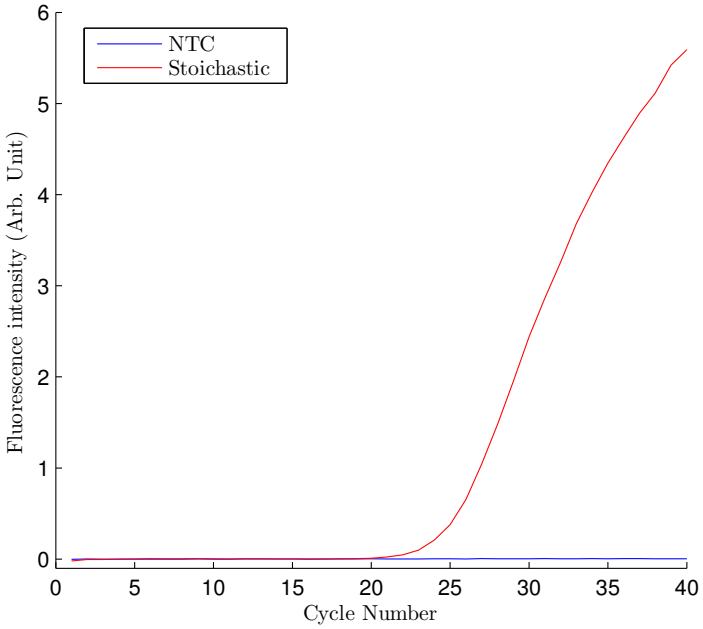

Figure 7.11: Fluorescence signal as function of cycle number for experiments where the concentration of primers and nucleotides are in a stoichiometric ratio to each other.

Primers limiting

Other experiments were carried out with an excess of nucleotides, hence the primer concentration limited the reaction. Figure 7.13 shows the amplification curves obtained in these experiments. As expected from the model, normal amplification curves were obtained. It can be observed that the closer the ratio of primers and nucleotides is to the stoichiometric case, the higher the fluorescence intensity and thus the product yield.

The results of the melting curve analysis conducted for these experiments can be seen in Figure 7.14. Especially from the first derivative of the fluorescence signal with respect to temperature (Fig. 7.14(b)), it can be seen that the product peak at $85°C$ is the most dominant peak. Furthermore, it is recognizable that the amount of short chain by-products is decreasing with increasing nucleotide to primer ratio. This is indicated through the shoulder to the left of the product peak, representing shorter chain products, decreasing with higher nucleotide concentrations. Thus the predictions made by the model regarding the product chain-length distribution for these cases are confirmed.

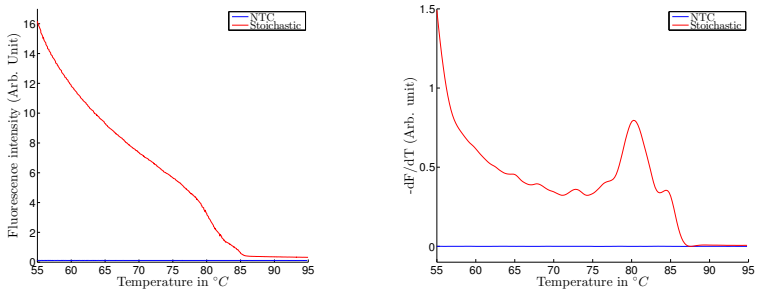

Figure 7.12: Plot of the melting curve analysis of the experiments with a stoichiometric ratio of nucleotides to primers. Fluorescence signal as function of temperature (left) and first negative derivative with respect to temperature as a function of temperature (right). As can be seen, only small amounts of unspecific by-products with melting temperatures below $75°C$ are formed.

Nucleotides limiting

Lastly, experiments were conducted in which the amount of product formed was limited by the nucleotide concentration, while primers were in excess. Figure 7.15 shows the amplification curves obtained. As expected from the model, the amplification curves are regularly shaped with a normal exponential increase. Plateaus were not reached for the experiments conducted, unlike the prediction of the model. This is most likely due to the loss of validity, in the late cycles, of the statistical approach used for the annealing of the primers.

The model predicts a large amount of shorter chain side products for this case. Our experiments confirmed this prediction, as can be seen through the carried out melting curve analysis (Fig. 7.16). It can be seen that next to the product peak at $80°C$ there is a second prominent peak at $60°C$. This peaks corresponds to primers extended only by a couple of base pairs. Compared to the other experiments conducted with a stoichiometric ratio of primers to nucleotides or an excess of nucleotides, this is a significant increase in the amount of side product.

Discussion

The experiments have shown that the predictions made by the model regarding the chain length distribution of the reaction products appear to be valid. Furthermore, it has been demonstrated that the accumulation of double stranded DNA is modelled reasonably well up to the point where the reaction leaves the exponential phase. At that point, the statistical annealing approach starts losing validity, and a more rigorous modelling of the annealing processes would be required to make predictions in these late

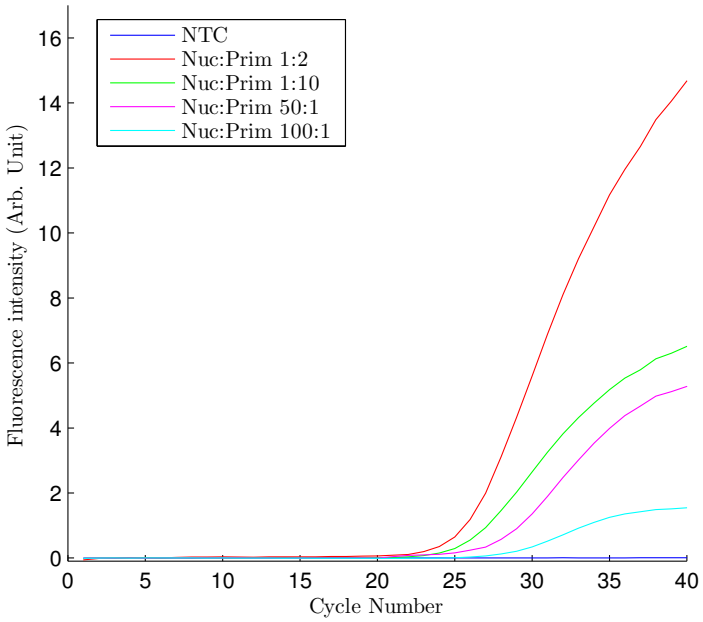

Figure 7.13: Fluorescence signal as function of cycle number for experiments where the reaction is limited through the amount of primers present in the reaction mixture

stages of amplification.
Predictions about the threshold cycles are difficult to verify from experimental data since dsDNA is often detected through fluorescence. Thus a correlation between dsDNA concentration and fluorescence intensity from the dye would have to be made in the model. Furthermore, the baseline noise of the thermal cycler would have to be taken into account. Since these extensions of the model would not provide additional guidance for experimental design, they were, for the sake of simplicity, not included.

The model has also been used to make predictions of the effect of Taq polymerase concentration. It has been seen that the polymerase concentration has little effect on the chain length distribution of the products, when extension times are sufficently long. It mainly influences the time individual cycles require to reach completion. Since it is very difficult to measure the enzyme activity or the dynamic development of the dsDNA concentration during a cycle, no experiments were conducted to verify those predictions. Farrar et al. [14] recently attempted to run 35 cycles of PCR in as little as 15 to 60 seconds. In order to achieve that, the concentration of the enzyme was increased, ensuring completion of the reaction in every single

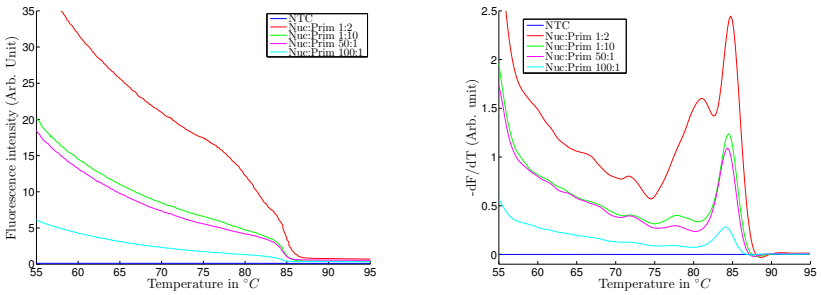

Figure 7.14: Plot of the melting curve analysis of the experiments with excess nucleotides. Fluorescence signal as function of temperature (left) and first negative derivative with respect to temperature as a function of temperature (right). As can be seen, only small amounts of unspecific by-products with melting temperatures below 75 $°C$ are formed.

cycle. This confirms the prediction of our model that a higher enzyme concentration would allow faster cycles. An important question arising here is what the ideal amount of enzyme would be. As most commercial machines are not able to run 35 cycles of PCR in 60 seconds, and time is often not a critical parameter for many applications, there is little reason to use high enzyme concentrations. The ideal enzyme concentration would probably be such that all the enzyme is saturated in the last cycles of the exponential amplification. This compromise allows, on the one hand, reasonable times for each cycle and, on the other hand, reduces the cost of the enzyme employed.
To be able to run PCR cycles in times of around one second, Farrar et al. also had to significantly increase the concentration of primers. According to our model predictions, this should have negative effects on the product distribution. In their experiments, this step seems to be necessary to achieve rapid cycle times. This suggest that at very fast cycle times, a more rigorous modelling of the annealing is necessary to obtain accurate predictions. An extension of the model to a more rigorous description of the annealing processes as well as introducing temperature dependences of the enzyme activity and other reactions has been tested. Since it is difficult to find rate constants for these and the rate constants reported in the literature are often estimated, it was decided not to include this in the model since it would depart from the scope of a simple model. Furthermore, the annealing rate constants found in the literature are in the nanosecond range, inducing a stiffness in the system of ordinary differential equations.

Unspecific products not only arise through a suboptimal choice of primer and nucleotide concentrations: the so-called primer dimers can also arise

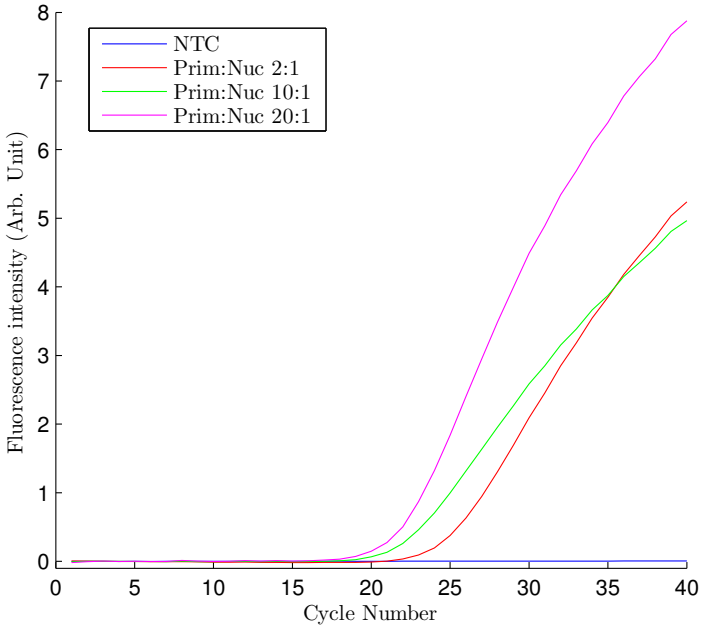

Figure 7.15: Fluorescence signal as function of cycle number for experiments where the reaction is limited through the amount of nucleotides present in the reaction mixture

through the unspecific binding of primers and extension of these [15]. As synthetic DNA and pure primers have been used for the experiments conducted here, it can be assumed that there is no unspecific binding of the primers. Hence, different mechanisms of primer dimer formation can be excluded as a source of primer dimers in the experiments conducted, but should be considered for more complex samples.

A simple model has been presented in this paper able to help in the optimization of PCR reactions. Choosing the primer and nucleotide concentrations in the right ratio helps reduce unspecific short chain by-products and hence improves the outcome of the PCR. The model furthermore can help determine the enzyme concentration for the reaction. Due to the simplicity of the model, it can be used to help design conditions for conventional PCR reactions. If the aim is a high-speed PCR, the model should be extended to provide better predictions.

Acknowledgement

For help with preparing the reagent and conducting the experiments, the author would like to thank Yoojung Lee and Jaewon Hwang. This work was

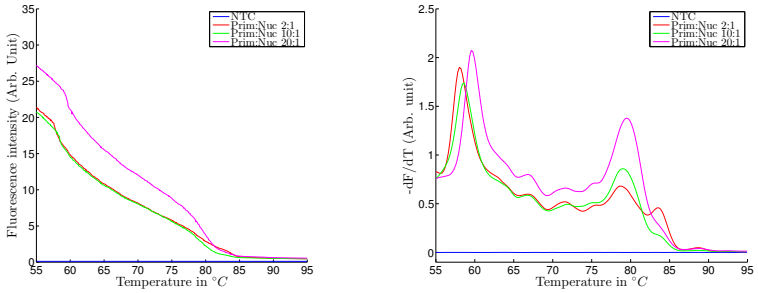

Figure 7.16: Plot of the melting curve analysis of the experiments with excess primers. Fluorescence signal as function of temperature (left) and first negative derivative with respect to temperature as a function of temperature (right). The formation of unspecific short chain products is easily recognizable from the graphs through peaks in the derived plot around 60 $^{\circ}C$.

financed by the Korea Institute of Science and the Technology-Europe basic research program.

Authors contribution

Christian Ahrberg wrote the model an carried out the simulations. Experiments to verify the model were designed by Christian Ahrberg and carried out with the assistance of Yoojung Lee and Jaewon Hwang. The manuscript was written by Christian Ahrberg.

7.4 Conclusion

As was the aim of this chapter, a simple kinetic model has been developed describing the polymerase chain reaction. With aid of the model concentrations for the main reagents of the reaction, nucleotides, primers and the enzyme, can be optimised before starting experiments. Through this optimization of reaction conditions is greatly simplified. Furthermore the understanding of the processes during PCR and the interactions of the components was enhanced through the construction of this model.

Under certain conditions the model predicts shorter chained side products. As no unspecific amplification is taken into account this provides an alternative explanation for primer dimers. In most cases the formation of primer dimers is explained by unspecific binding of primers with consecutive amplification, but as is shown here the wrong kinetic or stochastic conditions can also lead to side products. This underlines the importance of consequent and rigorous experiment design. While other published models do not look at the size distribution of products, they often address the annealing process. Since the model shown here takes a simplified approach to model annealing the last cycles of amplification are more abrupt than observed in reality. Although this has only very limited influence on the predictive capabilities of the model under regular conditions, a more rigorous description would be desirable when going to very fast PCR for example.

For future development of the model it would be desirable to explore the effects of taking templates which are thousands of base-pairs long. Furthermore exploring the effect of having a template significantly longer than the amplicon could be of interest, especially the effects on the product length distribution. The coamplification of two different targets in the same reaction would also be of interest since the situation is often occurring under practical conditions. Lastly the model could be used to predict the optimum length of each extension step. In PCR all cylces are usually the same, however, it is conceivable that early cycles could require less time compared to later ones. Through a slight modification of the model and the introduction of more accurate rate constants this question could be answered, possibly reducing the time required for reaction.

Overall the model introduced here fulfils the purpose it was written for and allows for an optimization of reagent concentrations before starting experiments. Furthermore a cause for short chain side products was found and can be prevented in experiments by adequate design.

Bibliography

[1] E. Rubin and A.A. Levy. A Mathematical Model and a Computerized Simulation of PCR Using Complex Templates. *Nucleic Acids Research*, 24(18):3538–3545, 1996.

[2] M.W. Pfaffl. A new mathematical model for relative quantification in real-time RT-PCR. *Nucleic Acids Research*, 29(9):e45, 2001.

[3] J.L. Gevertz, S.M. Dunn, and C.M. Roth. Mathematical model of real-time PCR kinetics. *Biotechnology and Bioengineering*, 92(3):346–355, 2005.

[4] S. Mehra and W.-S. Hu. A kinetic model of quantitative real-time polymerase chain reaction. *Biotechnology and Bioengineering*, 91(7): 848–860, 2005. ISSN 1097-0290.

[5] J. Vandesompele, K. De Preter, F. Pattyn, B. Poppe, N. Van Roy, A. De Paepe, and F. Speleman. Accurate normalization of real-time quantitative RT-PCR data by geometric averaging of multiple internal control genes. *Genome Biology*, 3(7):0034, 2002.

[6] F. Osman, E. Hodzic, A. Omanska-Klusek, T. Olineka, and A. Rowhani. Development and validation of a multiplex quantitative PCR assay for the rapid detection of Grapevine virus A, B and D. *Journal of Virological Methods*, 194(1-2):138–145, 2013.

[7] M. Safdar and M.F. Abasiyanik. Simultaneous Identification of Pork and Poultry Origins in Pet Foods by a Quick Multiplex Real-Time PCR Assay Using EvaGreen Florescence Dye. *Applied Biochemistry and Biotechnology*, 171(7):1855–1864, 2013.

[8] A. Abd-Elmagid, P.A. Garrido, R. Hunger, J.L. Lyles, M.A. Mansfield, B.K. Gugino, D.L. Smith, H.A. Melouk, and C.D. Garzon. Discriminatory simplex and multiplex PCR for four species of the genus Sclerotinia. *Journal of Microbiological Methods*, 92(3):293–300, 2013.

[9] C.W. Dieffenbach, T.M. Lowe, and G.S. Dveksler. General concepts for PCR primer design. *Genome Research*, 3(3):S30–S37, 1993.

[10] J.T. Hsu, S. Das, and S. Mohapatra. Polymerase chain reaction engineering. *Biotechnology and Bioengineering*, 55(2):359–366, 1997. ISSN 1097-0290.

[11] T.S. Van Erp and M. Peyard. The dynamics of the DNA denaturation transition. *arXiv:1204.5585v1 [physics.bio-ph]*, 2012.

[12] O. Dahlen and T.S. Van Erp. Mesoscopic modeling of DNA denaturation rates: Sequence dependence and experimental comparison. *The Journal of Chemical Physics*, 142(23):235101, 2015. doi: http://dx.doi.org/10.1063/1.4922519. URL `http://scitation.aip.org/content/aip/journal/jcp/142/23/10.1063/1.4922519`.

[13] A. Agah, M. Aghajan, F. Mashayekhi, S. Amini, R.W. Davis, J.D. Plummer, M. Ronaghi, and P.B. Griffin. A multi-enzyme model for pyrosequencing. *Nucleic Acids Research*, 32(21):e166, 2004.

[14] J.S. Farrar and C.T. Wittwer. Extreme PCR: Efficient and Specific DNA Amplification in 15-60 Seconds. *Clinical Chemistry*, 61(1):145–153, 2015.

[15] J. Brownie, S. Shawcross, J. Theaker, D. Whitcombe, R. Ferrie, C. Newton, and S. Little. The elimination of primer-dimer accumulation in PCR. *Nucleic Acids Research*, 25(16):3235–3241, 1997.

Chapter 8

Protein Melting Curve Analysis

8.1 Motivation and relation to the thesis

In the last chapters it was shown how virtual reaction chambers combined with a heating system and fluorescence detection can be used for the polymerase chain reaction of DNA and RNA. However, the working systems range of applications can be extended, especially as VRCs offer a simple method of superheating small aqueous samples. Thus an application requiring the thermal manipulation of samples and fluorescent measurements thereof was searched. If possible the application should utilise the superheating capabilities of the system and benefit of the small sample volumes.

The central dogma of molecular biology explains the relation between DNA, RNA and proteins. Since DNA and RNA both can be analysed using VRCs an analysis method for proteins is interesting. Indeed the thermal stability of proteins can be probed through the addition of a hydrophobic dye and application of a temperature gradient. In this chapter it will be shown how VRCs can be used to perform these measurements. The advantage they provide over conventional measurements are the capability of superheating, allowing the testing of thermal stable proteins. The low sample consumption makes the system suitable for screening applications and quick tests regarding protein identity and purity.

8.2 State of the art

Denaturation of proteins through the application of a thermal gradient has been known for some time and is commonly used probe the thermal stability of proteins or to characterise protein ligand interactions. The introduction of hydrophobic dyes, such as Nile Red [1] or ANS and bis-ANS [2], allowed

these measurements to be carried out by fluorescence measurements. Commercial real time thermal cyclers are often used for this purpose as they offer ways of manipulating the temperature of the sample while monitoring fluorescence. The main disadvantage here is the relatively large sample consumptions between $5\mu L$ and $1mL$. Therefore a microfluidic device was introduced to reduce sample consumption [3]. Here the sample, green fluorescence protein (GFP), was flown through a capillary which was heated by an infrared laser. Through the fast heating provided by the laser the rate constant for the thermally induced unfolding process could be determined. Although this approach allowed a significantly smaller sample consumption ($\sim 1 - 2\mu L$) the maximum temperature reached in these experiments was $85°C$, and thus within the temperature-range accessible by commercial machines.
Virtual reaction chambers offer the advantage of providing an easy access to superheating and could thus increase the accessible temperature range, while maintaining a low sample consumption. Previously superheated VRCs have already been used to break spores for the preparation of PCR samples [4] as well as the fragmentation of peptides for sequencing by mass spectroscopy [5]. For both of these applications the aqeous sample had to be superheated. For spore breaking a temperature of $180°C$ for at least 20 seconds was necessary while peptide sequencing required $200°C$ for 10 seconds.

Here it will be shown how VRCs can be used as a tool in protein thermal stability analysis using hydrophobic dyes for detection. Through their small volume they help reducing sample consumption. In addition the ability to superheat gives access to a larger temperature range not accessible by standard real time thermal cyclers. This will allow researching thermostable proteins without the need to pressurize the sample up to the point were the proteins start fragmenting as demonstrated earlier.

8.3 A novel method for protein thermal stability analyses using superheated droplets

Prepared for publication

Here we describe a novel method for the study of protein thermal stability using superheated aqueous samples within virtual reaction chambers. Virtual reaction chambers consist of an aqueous sample droplet encapsulated by an oil droplet on a hydrophobic surface. Such samples can be superheated due to the lack of nucleation sites. The thermal denaturation of proteins is induced through the application of a temperature gradient using a bespoke silicon heating chip. The unfolding of proteins is followed through the addition of a hydrophobic dye that attaches to protein hydrophobic domains that become exposed during denaturation. Using this method, we investigated the thermal stability of green fluorescence protein and Taq-polymerase. A possible screening application of the method was demonstrated by evaluating the effect of ionic concentration on the thermal stability of bovine serum albumin.

Introduction

During the early part of the 20th century, it was established that proteins lose their function when heated, although the cause for this was as yet unknown. Around 1930, several groups began predicting the secondary and tertiary structures of proteins, among them Dorothy Wrinch[6] and Linus Pauling[7]. With these models in place, the first experimental validations were attempted by denaturating proteins through the addition of reagents that selectively break bonds or weaken intra-molecular attractions[8]. Today protein structures are mainly determined using X-ray crystallography[9], cryo electron-microscopy[10] or NMR[11].

While methods such as NMR, X-ray crystallography and cryo electron-microscopy are good for determining the structure of a protein, they provide only limited information on protein interactions with other molecules. Furthermore, the thermodynamics of these interactions are often important when screening for potential drug candidates[12]. To access this thermodynamic information, a variety of thermodynamic methods (e.g., isothermal titration calorimetry (ITC) or differential scanning calorimetry (DSC)) have been developed[13].

Because of the highly sensitive nature of fluorescence spectroscopy, fluorescent dye-based approaches have been developed to research proteins.

These dyes typically interact non-covalently with the protein or protein degradation products through hydrophobic or electrostatic interactions. Thus, protein aggregation, fibrillation, chemical degradation and conformational changes can be detected optically[14]. 1-anilinonaphtalene-8-sulfonate (ANS), 4,4'-Dianilino-1,1'-binaphthyl-5,5'-disulfonic acid (bis-ANS)[15] and Nile Red[1] are examples of dyes used for this purpose. Due to their ability to control temperature while measuring fluorescence, real-time polymerase chain reaction (qPCR) thermocyclers, which are commonly available in research laboratories, are often used for these experiments.

Recently, our group has introduced a micro-machined, silicon chip for heating PCR samples, mountable to a fluorescence microscope[16]. The sample is placed as a droplet with a volume of 100 nL on a hydrophobic surface, thus forming a virtual reaction chamber (VRC)[17] (Fig. 8.1). Superheating within VRCs has already been applied to peptide analysis[5]. Here, we demonstrated how this system can be used to investigate the thermal stability of proteins. The use of a micro-fabricated heating chip and VRCs has the advantage of having significantly lower sample consumption (100-300 nL) compared to real time PCR cyclers (5-20 μL) or calorimeters (0.1-1 mL). Furthermore, aqueous samples in VRCs can be superheated to temperatures of up to $200°C$[17]. This is due to the sample being completely encapsulated through the oil phase, preventing the formation of the nucleation sites necessary for boiling[18]. Through this feature it is possible to study proteins stable at $100°C$ or more, a temperature range not accessible by real-time PCR cyclers due to sample boiling. Thus, the combination of miniaturization with VRCs helps to reduce sample volumes and allows samples to be heated to temperatures in excess of the boiling temperature of water, without the need of pressurization.

To demonstrate the usefulness of VRCs, initial experiments were made using green fluorescent protein (GFP). Since GFP has an intrinsic fluorescence dependent on its folded state, its denaturation can be easily observed, without the requirement of adding a dye. For comparison, these experiments were carried out on a chip and in a commercial RT-PCR cycler. Second, a screening application was demonstrated by testing the influence of the ionic strength of the buffer on the stability of bovine serum albumin. Lastly, experiments were carried out measuring the thermal denaturation of Taq polymerase. As Taq polymerase is stable at $95°C$, super-heating of the solution is necessary for observing the unfolding of this protein.

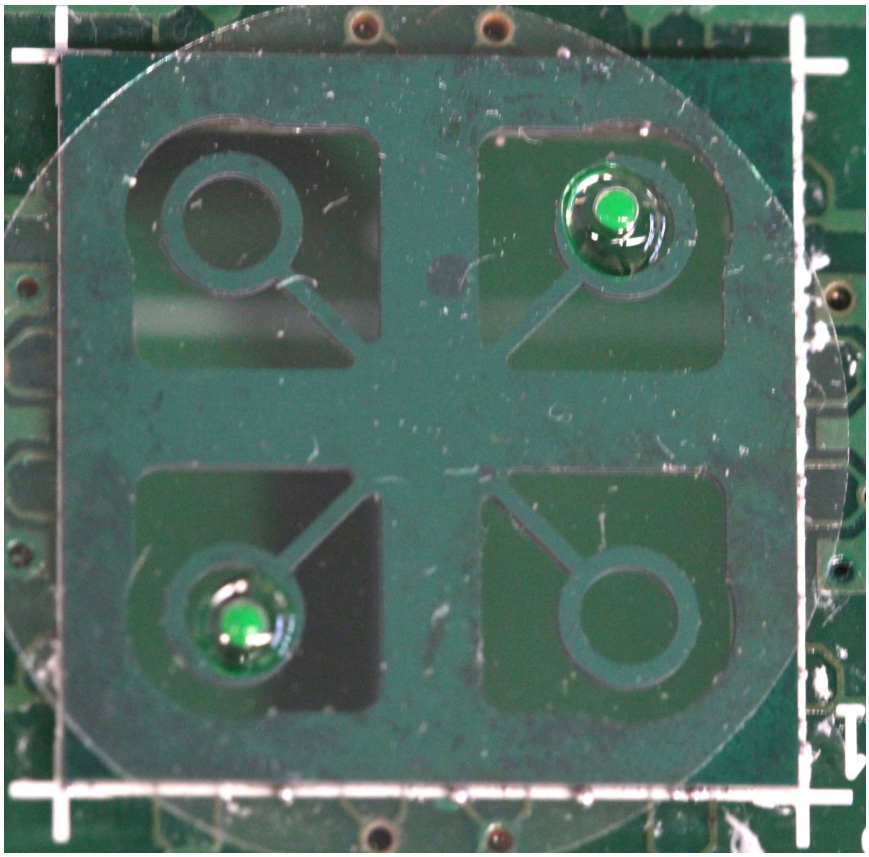

Figure 8.1: Image of the heating chip and two VRCs. The chip was designed for the parallel heating of up to four samples in parallel. For experiments only one heating position was used at a time. For visualisation purposes the sample has been replaced with fluorescein solution in this image.

Experimental Section

Setup

The virtual reaction chambers were prepared by pipetting 300 nL of sample onto a microscope cover slip coated with (1H,1H,2H,2H-perfluorooctyl) trichlorosilane (Sigma-Aldrich)[17]. To prevent evaporation samples were covered with 2 μL of a mixture consisting out of 5 g of FC-40 (Sigma-Aldrich) and 5 g FC-70 (Sigma-Aldrich). The viscosity of the oil mixture was increased through the dissolution of 3wt% Teflon-beads (Sigma-Aldrich). Prepared VRCs were placed on a custom made, micro-machined silicon heater developed for a portable PCR device[16]. A temperature ramp of $0.5°C/s$ starting from $25°C$ was applied while fluorescence was continuously monitored. The temperature was measured with a resistive sensor next to the heater on the bespoke silicon chip. The temperature correlation

between the measured temperature and sample temperature was determined earlier[17].

Fluorescence amplitude was captured using a fluorescence microscope (Zeiss) equipped with a blue LED (ThorLabs) and FAM-Filterset (Chroma) for experiments with GFP or an amber LED (ThorLabs) with corresponding filters (Chroma) for all other experiments. Detection was done using a photomultiplier tube (Hamamatsu) and oscilloscope (Tektronix). The LEDs for excitation were modulated and a LockIn amplifier (AmTek) was used for detection to increase the signal to noise ratio.

Samples consisted of 5 μL of Protein Thermal Shift Buffer (ThermoFischer) and 5 μL of 4X Protein Thermal Shift Dye (ThemoFischer). Either 2 μL of bovine serum albumin solution (200 mg/mL) (Sigma-Aldrich), 1 μL of native polymerase (5 U/μL) (ThermoFischer) or 4 μL of extracted GFP were added. To the BSA samples, aqueous sodium chloride solution (Sigma-Aldrich) was added to achieve final concentrations of 0, 0.15, 0.3, 0.5 and 1 M. Finally, volumes were adjusted to 20 μL using Milli-Q water (PrograqdT3 column, Millipore). For samples containing GFP the Protein Thermal Shift Dye was replaced with water.

When applicable, samples were also measured using a Roche LightCycler (Roche Molecular Diagnostics) with a temperature ramp of $0.5°C/s$ ranging from 37 to $95°C$ with continuous fluorescence measurement.

Isolation of GFP

Green fluorescent protein was harvested from *Escherichia coli* transfected with GFP by first washing the culture with water, followed by centrifugation at 3,250 g for 10 min. The resulting cell pellet was resuspended in 1 mL of Laemmli lysis buffer and sonicated on ice 6 times for 30 sec. The cell debris were removed from the solution through centrifugation (10 min, 12,100 g at $4°C$). The supernatant was transferred into another microcentrifuge tube and diluted with a mixture of acetone (Sigma-Aldrich) and methanol (Sigma-Aldrich) (8:1) cooled to $-20°C$. After 2 h of incubation at $-80°C$, proteins were pelleted by centrifugation (10 min, 1,000 g at $4°C$). Pellets were washed with acetone (Sigma-Aldrich) at $-20°C$ three times before resuspension in difference gel electrophoresis [DIGE] label buffer.

Results and Discussion

For comparison, experiments were first carried out on both our custom-made chip and a LightCycler. When GFP was heated, protein unfolding results in a loss of its fluorescence (Fig. 8.2). On both systems, the loss of fluo-

rescence occurs in a single step, as recognizable from the single peak in the derived signals. This confirms reports of a single domain unfolding in the denaturation of GFP[3]. The peak maximums from both the light cycler and the chip were at $\sim 82°C$, indicating the comparability of results from the two systems. The graphs also show how a broader temperature range can be accessed by the chip approach than by the LightCycler. While the minimum temperature achievable by the LightCyler is $37°C$, the lower limit of the chip is ambient temperature. To prevent boiling in the capillaries, the LightCyclers maximum temperature is limited to $95°C$. Whereas, through the use of VRCs, the chip aqueous samples can be superheated to temperatures in excess of $100°C$ (up to $125°C$ in this study).

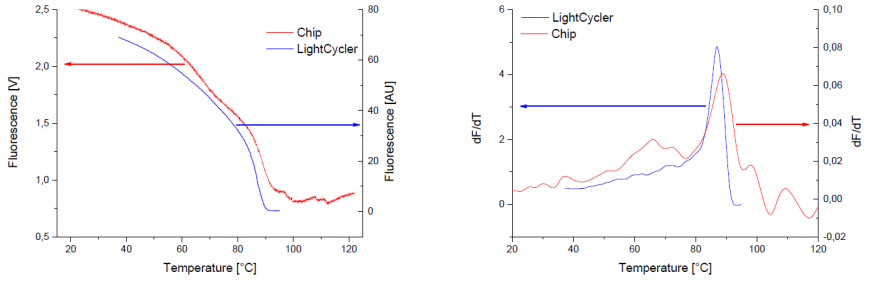

Figure 8.2: Fluorescence signal as function of temperature as recorded by the LightCycler (blue curve) and out chip (red) (left graph). First derivative of fluorescence signals with respect to temperature for the LightCycler (blue) and our chip (red) (right graph). The single step in which GFP denatures can be recognized from the single peak in the derived fluorescence signal.

To demonstrate the usefulness of the chip approach for screening applications, we tested the influence of ionic strength on the thermal stability of bovine serum albumin. In these experiments, a dye was necessary to follow the unfolding process. Figure 8.3 shows how the fluorescence increases at different buffer concentrations of sodium chloride, as well as the first derivative with respect to temperature. As the concentration of sodium chloride increases, the ionic strength of the buffer also increases, thus delaying the rise in fluorescence to a higher temperature. Hence, the peak maximums of the derived fluorescence increases from $72°C$ with no sodium chloride to $87.5°C$ at sodium chloride concentrations of 1 M. The strong stabilizing effect of sodium chloride was previously reported by DSC[19].

The ability of VCRs to superheat aqueous samples was used for the analysis of Taq polymerase. As it is used for polymerase chain reaction, and thus repeatedly heated to $95°C$, the stability of this protein is well-known. Therefore, super-heating is necessary to thermally denature the

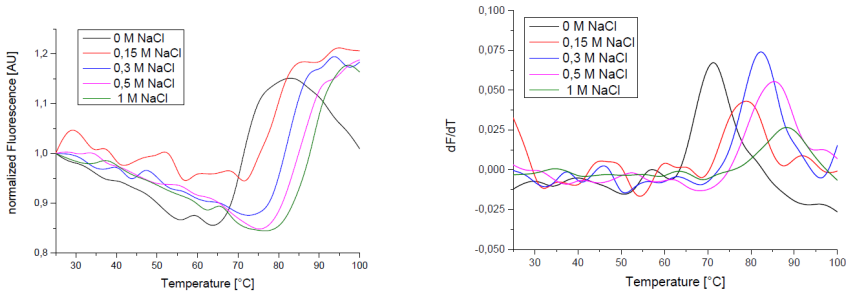

Figure 8.3: Normalized fluorescence signals as function of temperature for experiments with BSA protein and different concentrations of sodium chloride (left). First derivative of fluorescence with respect to temperature for experiments with BSA and various concentrations of sodium chloride (right). The graphs show how a higher ionic strength of the solution leads to a thermal stabilization of the protein.

protein. Through calorimetric measurements the denaturation of Taq polymerase in two distinctive steps was reported with the first domain unfolding at 88.9°C and the second at 99.1°C[20]. As the first domain denatures at temperatures exceeded during polymerase chain reaction, this unfolding process is thought to be reversible[20]. In the experiments conducted with our chip, an unfolding process in two steps was observed (Fig. 8.4). The first derivative of the fluorescence signal with respect to temperature shows two peaks, one at 81°C and the second one at 104°C. The presence of the two peaks confirms the observations made by differential scanning calorimetry of a two-step denaturation process[20]. The denaturation temperatures found by differential scanning calorimetry could not be reproduced, however, the divergence is most likely due to differences in the pH and ionic strength of the buffers used. Furthermore, it is possible that the proteins were extracted from different strains of *Thermus aquaticus*. However, we confirmed that the second, irreversible, denaturation step occurs at a temperature higher than the boiling temperature of water and thus is not reached during PCR.

Conclusion

Here we have shown how VRCs to analyse the thermal stability of proteins. It was demonstrated that thermostable proteins can be easily analysed using the ability of VRCs to superheat water to temperatures $> 100°C$. While other methods (e.g., scanning calorimetry) require extensive pressurized set-ups to measure above 100°C, the experimental set-up used here is relatively simple and measurements could be performed in as little as 3 to 5 min, depending on the temperature range investigated. Furthermore, sample consumption is much lower using VRCs with sample volumes (in the range

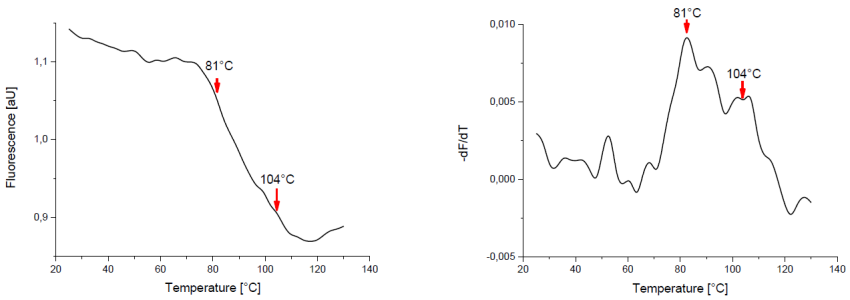

Figure 8.4: Diagram showing fluorescence amplitude as a function of temperature for experiments conducted with native Taq polymerase (left). First derivative of the fluorescence signal with respect to temperature for experiments with Taq polymerase (right). In the derivative two peaks can be seen corresponding to the denaturation of two separate domains of Taq polymerase.

of 100 to 300 nL) than for other fluorescence methods performed using commercial machines.

Through the use of the hydrophobic dye the extraction of thermodynamic data is hardly possible. Furthermore, fluorescence measurements are more prone to noise due to temperature effects on fluorescence yield and unspecific binding of the dye, especially at low temperatures.

However, this novel chip system is suitable for screening tasks, for example when searching for buffer conditions stabilising or destabilising for a protein or when screening for the effects of mutations on stability. Because of the low sample consumption, fast analysis and simple set-up, potential candidates can be screened first using the chip method, with promising candidates being subsequently analysed by DSC.

Acknowledgement

The authors would like to thank Ahyeon Gyeon and Mathias Altmeyer for help with bacteria culture and protein extraction. This work was financed by Korea Institute of Science and Technology - Europe basic research program.

8.4 Conclusion

An application for the virtual reaction chambers capability to superheat aqueous samples has been shown in here with the analysis of the thermostable Taq-polymerase enzyme. To analyse this enzyme the sample had to be heated to $110°C$ which could be done without pressurizing the system due to the VRCs. Furthermore the anlysis of proteins in VRCs in combination with the heating chip used throughout this thesis provides the means to analyse all three biomolecules mentioned in the central dogma of molecular biology (DNA, RNA and proteins).
For the conducted experiments the bespoke chip was mounted beneath a fluorescence microscope, as can be found in many laboratories. As demonstrated in the screening experiments of buffer conditions for bovine serum albumin only very low amounts of sample are required. This, the simplicity of conducting experiments and the set-up as well as the large temperature range accessible make VRCs and the heating chip a good tool for screening experiments.

In conclusion it has been illustrated here how the advantages provided by virtual reaction chambers and the bespoke chip for temperature control can be used for the analysis of the thermal stability of proteins. This illustrates the versatility of VRCs as an analysis tool.

Bibliography

[1] D.L. Sackett and J. Wolff. Nile red as a polarity-sensitive fluorescent probe of hydrophobic protein surfaces. *Analytical Biochemistry*, 167(2): 228–234, 1987.

[2] B. Asim, B. Anusree, M. Chaitali, B. Kankan, and R. Siddhartha. A Fluorescence Spectroscopic and Molecular Dynamics Study of bis-ANS/Protein Interaction. *Journal of Biomolecular Structure and Dynamics*, 15(5):959–966, 1998.

[3] D.M. Sagar, S. Aoudjane, M. Gaudet, G. Aeppli, and P.A. Dalby. Optically Induced Thermal Gradients for Protein Characterization in Nanolitre-scale Samples in Microfluidic Devices. *Sci. Rep.*, 3, 2013.

[4] A. Pribylka, A.V. Almeida, M.O. Altmeyer, J. Petr, J. Sevcik, A. Manz, and P. Neuzil. "fast spore breaking by superheating". *Lab Chip*, 13: 1695–1698, 2013.

[5] M.O. Altmeyer, A. Manz, and P. Neuzil. Microfluidic Superheating for Peptide Sequence Elucidation. *Analytical Chemistry*, 87(12):5997–6003, 2015.

[6] D. M. Wrinch. The Pattern of Proteins. *Nature*, 137:411–412, 1936.

[7] Linus Pauling, Robert B. Corey, and H. R. Branson. The structure of proteins: Two hydrogen-bonded helical configurations of the polypeptide chain. *Proceedings of the National Academy of Sciences*, 37(4): 205–211, 1951.

[8] W. Kauzmann. *Some Factors in the Interpretation of Protein Denaturation1*, volume Volume 14, pages 1–63. Academic Press, 1959.

[9] A.T. Gres, K.A. Kirby, V.N. KewalRamani, J.J. Tanner, O. Pornillos, and S.G. Sarafianos. X-ray crystal structures of native HIV-1 capsid protein reveal conformational variability. *Science*, 349(6243):99–103, 2015.

[10] R.Y.-R. Wang, M. Kudryashev, X. Li, E.H. Egelman, M. Basler, Y. Cheng, D. Baker, and F. DiMaio. De novo protein structure determination from near-atomic-resolution cryo-EM maps. *Nat Meth*, 12 (4):335–338, 2015.

[11] L. Brown, C. Cox, J. Baptiste, H. Summers, R. Button, K. Bahlow, V. Spurrier, J. Kyser, B. Luttge, L. Kuo, E. Freed, and M. Summers. NMR Structure of the Myristylated Feline Immunodeficiency Virus Matrix Protein. *Viruses*, 7(5):2210, 2015.

[12] N.C. Garbett and J.B. Chaires. Thermodynamic studies for drug design and screening. *Expert Opinion on Drug Discovery*, 7(4):299–314, 2012.

[13] N.C. Garbett. *The Use of Calorimetry to Study Ligand-DNA Interactions*, chapter 12, pages 299–324. Springer Vienna, 2011.

[14] A. Hawe, M. Sutter, and W. Jiskoot. Extrinsic Fluorescent Dyes as Tools for Protein Characterization. *Pharmaceutical Research*, 25(7): 1487–1499, 2008.

[15] B. Asim, B. Anusree, M. Chaitali, B. Kankan, and R. Siddhartha. A Fluorescence Spectroscopic and Molecular Dynamics Study of bis-ANS/Protein Interaction. *Journal of Biomolecular Structure and Dynamics*, 15(5):959–966, 1998.

[16] C.D. Ahrberg, A. Manz, and P. Neuzil. Single Fluorescence Channel-based Multiplex Detection of Avian Influenza Virus by Quantitative PCR with Intercalating Dye. *Scientific Reports*, 5:11479, 2015.

[17] P. Neuzil, T. Karasek, W. Sun, and A. Manz. Nanoliter-sized Overheated Reactor. *Applied Physics Letters*, X, 2014.

[18] D. Zahn. How Does Water Boil? *Physical Review Letters*, 93(22): 227801, 2004.

[19] C. Giancola, C. De Sena, D. Fessas, G. Graziano, and G. Barone. DSC studies on bovine serum albumin denaturation Effects of ionic strength and SDS concentration. *International Journal of Biological Macromolecules*, 20(3):193–204, 1997.

[20] I. Karantzeni, C. Ruiz, C.-C. Liu, and V.J. Licata. Comparative thermal denaturation of Thermus aquaticus and Escherichia coli type 1 DNA polymerases. *Biochemical Journal*, 374(Pt 3):785–792, 2003.

Chapter 9

Conclusion

The aim of this thesis was to evaluate virtual reaction chambers as a tool for the analysis of biomolecules. Applications focused on the analysis of DNA and RNA, through polymerase chain reaction and reverse transcription PCR, as well as the analysis of thermal stability of proteins. In a first step a device for the thermal manipulation of VRCs and fluorescent measurement of these was constructed. The bespoke silicon chip in combination with a miniaturized fluorescence detection system was used to create of a hand-held, real time PCR device.

In subsequent experiments it was shown that VRCs can also be used to perform reverse transcription PCR. As experiments were carried out on the hand-held device constructed previously this demonstrates the feasibility of the system to be used in point-of-care environments, for the detection of virus infections for example.

Two methods for conducting multiplex PCR, using only a single fluorescence channel, were developed, as many real world applications of quantitative polymerase chain reaction require the quantification of two or more genes, like in the determination of viral loads.
In the first method a sequence specific probe was used in combination with an intercalating dye of the same emission wavelength. Through two fluorescence measurements, one during the extension and one in the denaturation step, two genes could be amplified and quantified in the same reaction. The method is simple and can be integrated into the hand-held device and most commercial real-time thermal cyclers by software modification.
The second method utilized the advantages virtual reaction chambers offer, namely a homogeneous temperature distribution and a low thermal mass. Mounting the silicon chip developed for the hand-held device under a fluorescent microscope it was possible to record a melting curve after every extension step. It was demonstrated that it is possible to detect and quan-

tify two amplicons using only one intercalating dye with this method.

To facilitate the understanding of the reaction and allow for better experiment design a mathematical model was written describing the polymerase chain reaction. Although the model describes all three steps of the reaction it focuses on the kinetics in the extension step in particular. With aid of the model a source for so called primer dimers was found, that can be eliminated by good experiment design.

The last section of the thesis centres on the thermal stability analysis of proteins in VRCs. For these experiments the silicon heating chip was mounted underneath of a fluorescent microscope. A hydrophobic dye was added to the samples in VRCs and a thermal gradient applied. Due to the superheating capability of VRCs even thermostable proteins like Taq polymerase could be analysed.

Concluding it was shown that virtual reaction chambers are an excellent tool for the analysis of DNA, RNA and proteins. Through their special properties experiments with VRCs can be conducted with very little sample consumption. Furthermore the temperature of VRCs can be manipulated easily with simple means due to their low thermal mass. This makes them particularly useful for point-of-care or screening applications. The superheating capabilities of the VRCs can be used for applications usually only accessible with more complicated, pressurized equipments.

9.1 Outlook

With the usefulness of virtual reaction chambers for the analysis of DNA and RNA demonstrated in this thesis there are a variety of different ideas to continue the work. Firstly the developed hand-held device should be tested under real-world conditions, outside of a laboratory. Ideally this would be done in a point-of-care environment with real samples like blood, urine or water from rivers or ponds. Further experiments should be conducted to make the PCR-reagents portable, by lyophilizing them to the glass slide for example.
Secondly the mathematical model developed for the description of the PCR could be extended in future work. One possibility for this would be an extension of the model towards the coamplification of several targets to describe multiplexing. Another possibility would be a more rigid model for denaturation and annealing processes, which should be able to describe late cycles more accurately.

Lastly further applications of the superheating capabilities of the VRC

could be tested. Here chemical synthesis requiring an autoclave or crystallisation would be interesting candidates for further experiments.

Chapter 10

List of Abbreviations

Abbreviation	Description
A	Adenosine
ADC	Analog-to-digital converter
ANS	1-anilinonaphtalene-8-sulfonate
BSA	Bovine Serum Albumins
C	Cytidine
CAD	Computer assisted design
CCD	Charge-coupled device
cDNA	Complementary DNA
CE	Capillary electrophoresis
CMOS	Complementary metal-oxide-semiconductor
CP	Crossing point
CPU	Central processing unit
C_t	Threshold cycle
Cy5	diSulfo - Cy5 carboxylic acid
diFET	Dielectrically-isolated field effect transistor
DNA	Deoxyribonucleic acid
DSC	Differential scanning calorimetry
dsDNA	double stranded deoxyribonucleic acid
ELISA	Enzyme-linked Immunosorbent Assay
EtBr	Ethidium Bromide
FAM	6-carboxyfluorescein
FEA	Finite Element Analysis
FRET	Fluorescence Resonance Energy Transfer
G	Guanosine
GAPDH	Glyceraldehyde 3-phosphate dehydrogenase
GFP	Green Fluorescence Protein
HA	Haemagglutinin
HEX	Phosphoramidite
HRMCA	High Resolution melting curve analysis

Abbreviation	Description
HPRT	Hypoxanthine-guanine phosphoribosyltransferase
JOE	6-carboxy-4',5'-dichloro-2',7'-dimethoxyfluoresceine
LCD	Liquid Crystal display
LED	Light emitting diode
MCA	Melting Curve Analysis
NA	Neuraminidase
NMR	Nuclear magnetic resonance spectroscopy
NTC	No template control
ODEs	Ordinary differential equations
PCB	Printed circuit board
PCR	Polymerase Chain Reaction
PID	Proportional integral derivative
PMT	Photomultiplier tube
POC	Point-of-care
PWM	Pulse-width modulation
Q	Quencher
qPCR	Quantitative PCR
R	Reporter
RNA	Ribonucleic acid
RTD	Resistance temperature detector
rtPCR	reverse transcription PCR
ROX	6-Carboxyl-X-Rhodamine
SNPs	Single nucleotide polymorphisms
ssDNA	Single stranded deoxyribonucleic acid
T	Thymidine
T_M	Melting temperature
Taq	*Thermus aquaticus*
TEC	Thermoelectric cooler
VRC	Virtual Reaction Chamber
USB	Universal serial bus
WHO	World health organization

Table 10.1: Table of abbreviations used in this thesis

Chapter 11

Appendix

11.1 Terms and definitions

11.1.1 Segmented Flow

In the initial years of microfluidics only single phase flows were used leading exclusively continuous flows. With the introduction of a second phase the participation of the two phases became important. In principle there are two options, in the first option the two phases flow parallel to each other, resembling two continuous flows next to each other. This option is often chosen for extraction purposes but rarely finds applications in other tasks due to difficulties in creating stable flow profiles. The other option is segmenting one phase (called the segmented phase) by the second phase (the so called continuous phase). This can be done in the form of slugs or droplets (Fig. 11.1). While in slug flow both phases have contact to the walls of the channel, only the continuous phase has wall contact in droplet mode. Both modes can be generated using gas/liquid systems or liquid/liquid systems like oil/water for example.

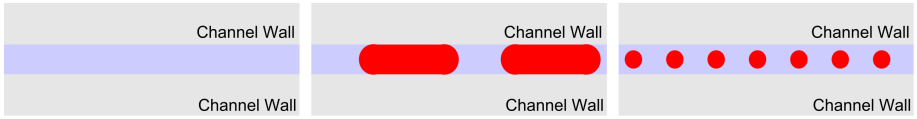

Figure 11.1: Drawings of one phase continuous flow (left), two phase segmented flow in slug mode (middle) and two phase segmented mode in droplet mode (right). It can be seen that in slug mode both phases have contact to the channel wall, while in droplet mode only the continuous phase has contact to the channel wall.

If slugs or droplets are generated and which phase is the segmented and continuous is determined through flow rates as well as the affinities of the two phases to the channel walls. Furthermore stability can be influenced by

the addition of surfactants to one of the two phases. Slugs, like droplets, can be generated by sheer force in the Herz to kiloHerz range with monodispersed volumes ranging down to picoliter volumes.

Droplets and slugs have a number of advantages compared to conventional continuous flow. Firstly they provide a big number of discrete reaction volumes that can be loaded with different reagents or reagent ratios which is of big importance in screening applications. Secondly, unit operations like droplet generation, splitting, merging, dilution, mixing and incubation can be done with ease. Furthermore droplets have no contact to the channel surface preventing side reactions with the reactor material or contamination through impurities in the reactor. Lastly flow in slugs/droplets does not feature the usual parabolic flow profile of continuous flow (Fig. 11.2). This prevents dispersion in mass transport which can lead to unwanted side products in reactions.

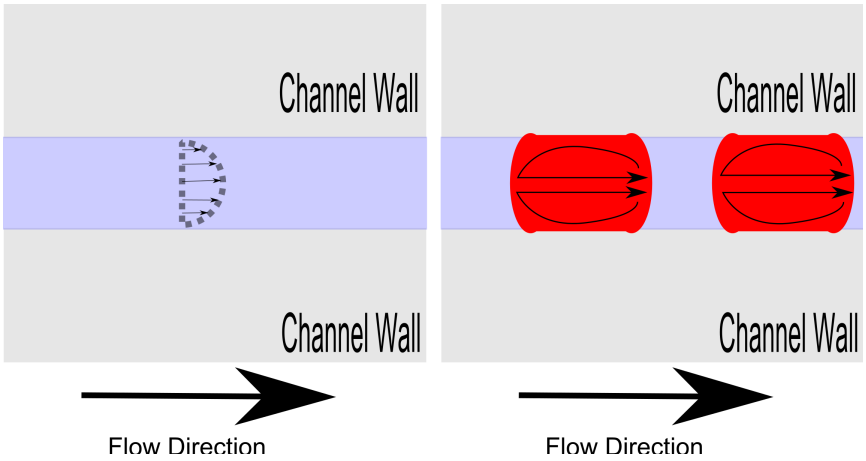

Figure 11.2: Drawings of flow profiles in continuous flow (left) and segmented slug flow (right). A parabolic flow profile is present in continuous flow, typical for laminar flow at low Reynolds numbers. In segmented flow, however, shear between the droplet and the stationary phase leads to an internal convection / recirculating flow inside the droplets. Similar internal flows would be observed in droplet-mode segmented flow.

11.1.2 DNA

Deoxyribonucleic acids (DNA) are long, linear biomolecules that can have a molecular weight of several million Dalton. During cell devision exact copies of the DNA molecules are made and transferred to the daughter cell. The DNA is used as a method of information transfer here. The other task of DNA is the storage of information inside the cell. Due to these reasons DNA is often described as the code of life.

DNA is made from three basic components, nucleobases, β-D-deoxyribose (a sugar) and phosphoric acid (Fig.11.3).

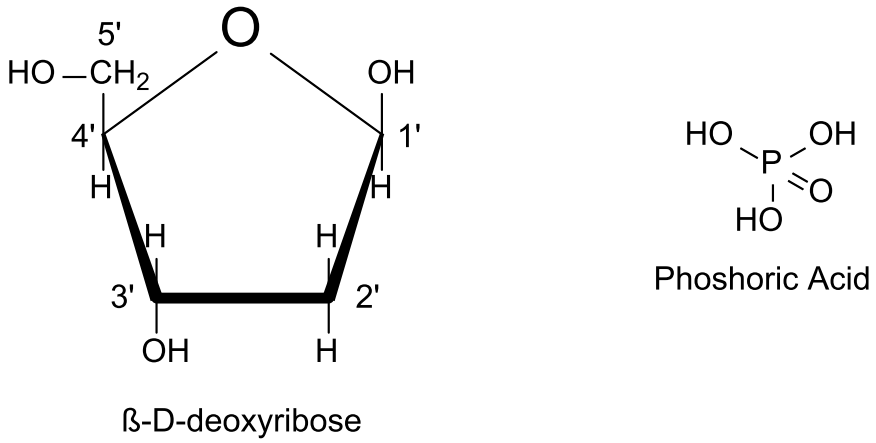

Figure 11.3: Molecular structure of the sugar β-D-deoxyribose (left) and Phosphoric acid (right).

A nucleoside is formed by the covalent bonding of a nucleobase and a sugar. Through the covalent attachment of a phosphate to the 5‘-end of the sugar a nucleotide is created. Now a chain can be synthesized by attaching the phosphate group at the 5-end of the sugar to the 3‘-end of a sugar of another nucleotide (Fig. 11.4).

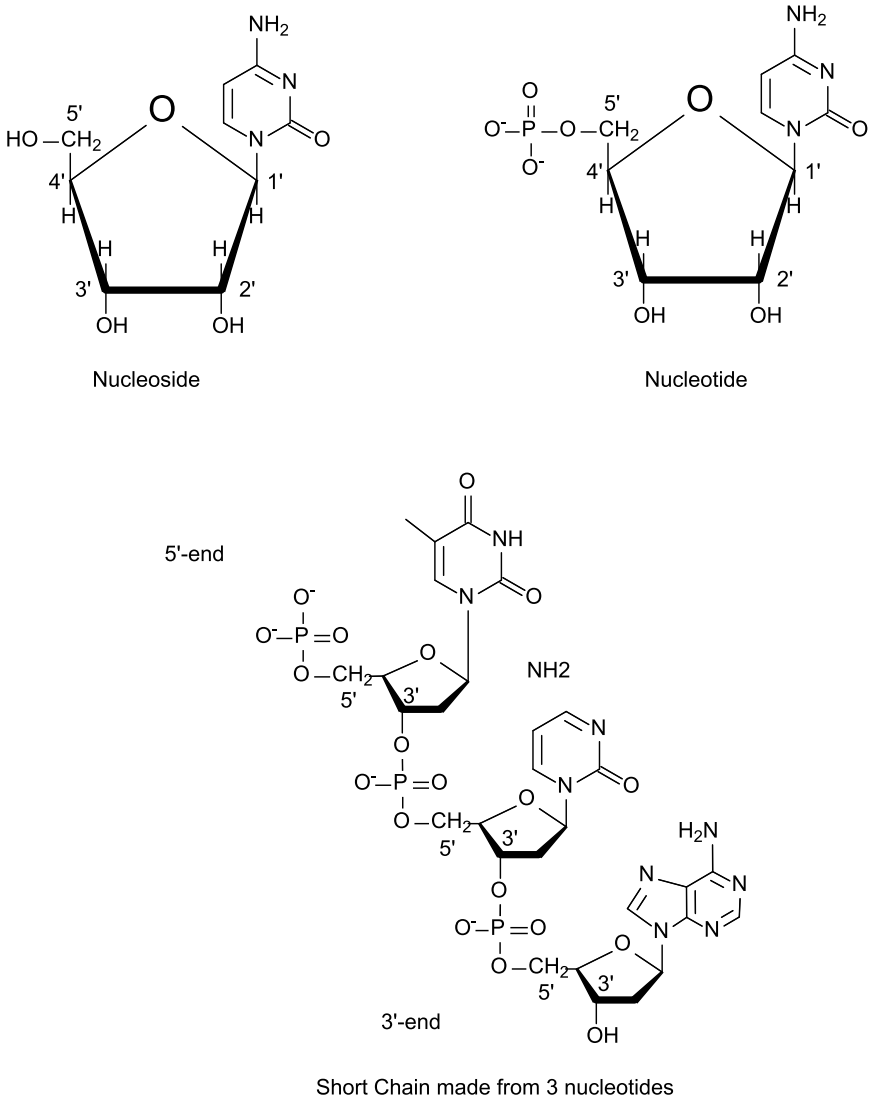

Figure 11.4: Molecular structure of a nucleoside composed of a sugar and a nucleobase (top left). Example of a nucleotide which is formed through the addition of phosphoric acid to a nucleoside (top right) and an example of a short chain formed from three different nucleotides (bottom).

In 1953 Watson and Cricks discovered the double helix-structure in which DNA is usually present. To form this right-twisted double helix two strands of the polynucleotide chain described above combine. While the sugar-phosphate backbone is hydrophobic and forms the outside of the helix the hydrophilic bases point to the inside. The strands align in such a manner that the first strand runs from 5‘-end to 3‘-end while the other strand goes in the opposite direction from 3‘-end to 5‘-end.

The aromatic rings of the base pairs align parallel to each other forming a twisted structure similar to a ladder.

Figure 11.5: Photograph of a DNA model created by Watson and Crick exhibited at the Science Museum in London. From the model the double helix as well as the ladder structure formed through the base-pairs can be recognized.

For steric reasons only two pairs of base pairs out of the possible six can form a stable connection with hydrogen bonds. One of these combinations is

adenine-thymine (A - T), the other one is guanine and cytosine (G - C). Due to this requirement the sequence of the first strand determines the sequence of the second complementary strand.
In solution DNA only rarely exists as a linear double helix structure, it rather forms turns and twisted. This is often called supercoiling and forms the tertiary structure of DNA.

11.1.3 RNA

Like DNA ribonucleic acids (RNA) are long, linear biomolecules. They are also made from the three basic components phosphoric acid, nucleobase and sugar. Unlike in DNA the sugar used for RNA is β-D-ribose (Fig. 11.6). Furthermore instead of thymine, uracil is used as one of the bases. The main purpose of RNA is the transport of information from DNA, which is often centered inside the nucleus, to the cytoplasm and where proteins are synthesized. Furthermore it is involved in several control processes in cells.

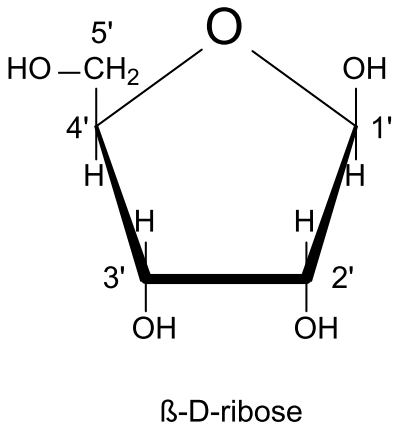

Figure 11.6: Molecular structure of the sugar β-D-ribose that is incoperated into RNA instead of β-D-deoxyribose.

As for DNA nucleosides, nucleotides and chains are formed in the same manner. Unlike DNA the additional OH-groups on the sugar provide to much steric hinderance to form a double strand, preventing the formation of a double helix. Thus RNA can only exist in a single stranded form. The single strand however can fold, loop and form limited base pairing with itself allowing some three dimensional structure to be present.

11.1.4 Nucleotides

Nucleotides for DNA and RNA consist out of a phosphate, which is phosphoric acid in both cases, a sugar and a nucleobase. As explained in the

previous section the sugar in DNA is β-D-deoxyribose and in RNA β-D-ribose. The nucleobases can be divided in two groups: the ones derived from purine and the ones derived from pyrimidine. The purine derivatives adenine (A) and guanine (G) are used for both DNA and RNA (Fig. 11.7).

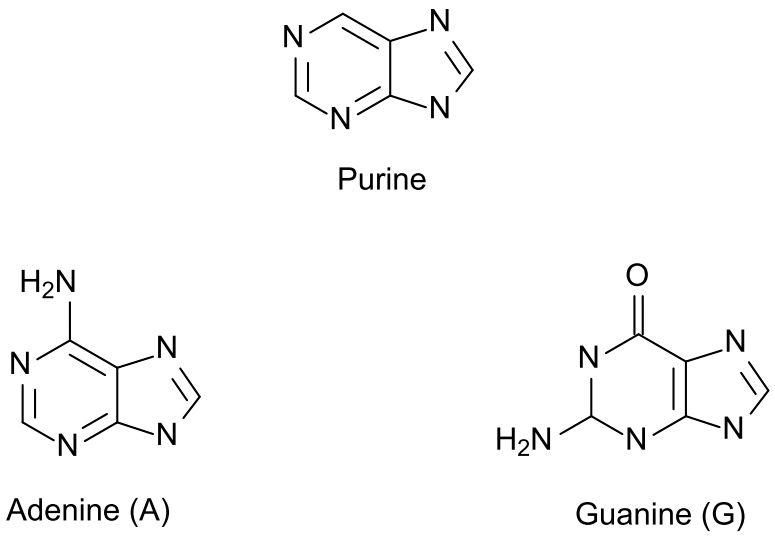

Figure 11.7: Molecular structure of purine and the two nucleobases adenine as well as guanine derived from purine.

From the pyrimidine derivatives only cytosine (C) is used in RNA and DNA, while thymine (T) is exclusively occurring in DNA and replaced with uracil (U) in DNA (Fig. 11.8).

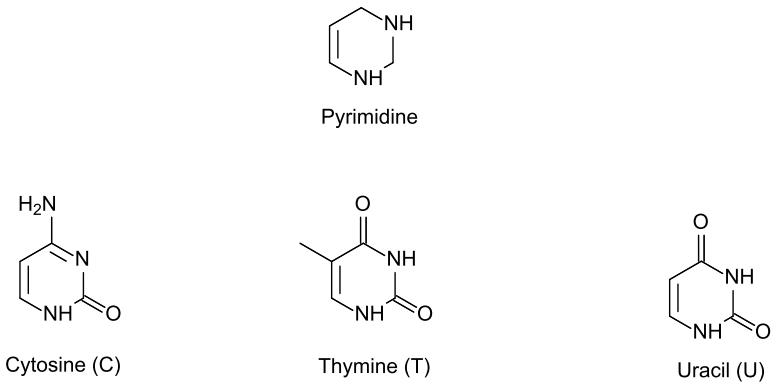

Figure 11.8: Molecular structure of pyrimidine.Furthermore the nucleobase cytosine, used in DNA and RNA, thymine, only occurring in DNA, and uracil, occurring in RNA instead of thymine, are shown. All three are derived from pyrimidine.

11.1.5 Polymerase

One of the enzyme universally used for PCR is Taq-Polymerase. It is named after *Thermus aquaticus* a thermophile bacteria found in hot springs, like in the yellow stone national park. The main advantage of this polymerase is its thermal stability, with a half life greater than two hours at $92.5°C$, 40 minutes at $95°C$ and 9 minutes at $97.5°C$. Due to this property Taq-polymerase is not deactivated during the denaturation step.

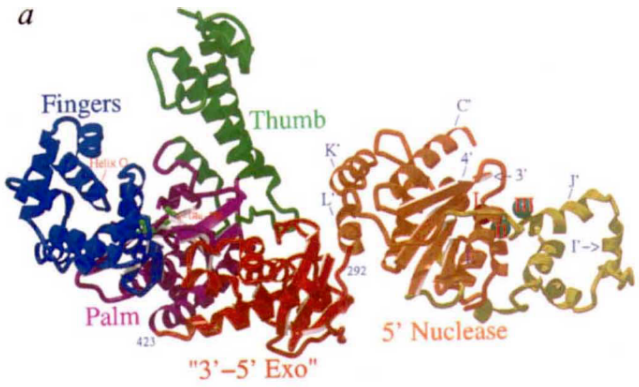

Figure 11.9: 3D-Model of the structure of Taq-Polymerase showing the different domains of the protein *Y. Kim et al.* ***Nature****, vol. 376 (612 - 616), 1995.*

The enzyme reaches its optimum activity between 70 and $80°C$ depending on buffer conditions and can replicate 1000 base pairs of DNA in 10

seconds at this temperature. The main drawbacks of the polymerase are the relatively high error rate of 1 in 9000 nucleotides in-cooperated incorrectly. Furthermore Taq-polymerase does not feature a proofreading functionality. Therefore Pfu-Polymerase from *Pyrococcus furiosus* and Vent-polymerase from *Thermococcus litoralis* are sometimes used as an alternative.

11.1.6 SYBR-Green

SYBR-Green I (Fig. 11.10) is a dye for DNA introduced in the 1990s for gel electrophoresis with similar optical properties as fluorescine. It is reversible included into the grooves that are formed by the dsDNA double helix structure by a process called intercalation. As it is temperature stable, has favorable photo-physical properties, a high selectivity for dsDNA as well as a high sensitivity SYBR green is commonly used for real-time PCR instead of the carcinogenic ethedium-bromide.

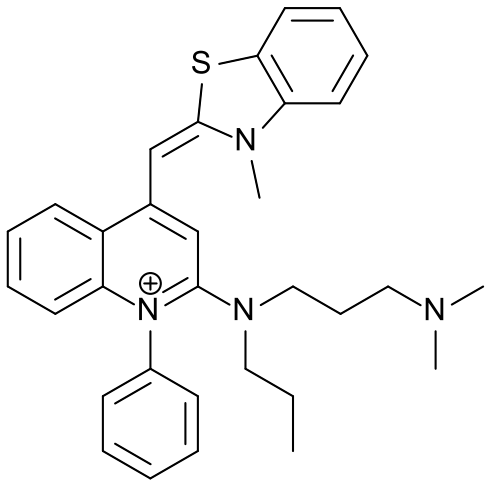

Figure 11.10: Molecular structure of SYBR green I.

SYBR green is only fluorescent when intercalated into double stranded DNA allowing to perform melting curve analysis. Its excitation maximum is at 494 nm and the emission maximum is at 521 nm. This allows detection to be performed with the same optical filters used for fluorescine which are commonly available.

11.1.7 Threshold cycle / Crossing point cycle

The threshold cycle, sometimes also referred to as crossing point cycle, is the cycle in which the fluorescence signal exceeds a threshold value during real-time PCR. The threshold is usually arbitrarily chosen in such a manner that

any signal above the threshold indicates a significant amplification. Popular choices include arbitrary values above the baseline value or the sum of the mean value of the baseline and 3, 5 or 10 times the standard deviation of the baseline noise.

11.1.8 Protein Structure

Proteins account for up to half of the dry weight of a cell and carry out many of the basic functions within the cell. They are involved in metabolite and ion transport, catalyse chemical reactions or serve as a sensor for certain molecules for example. The functionality of a protein is often linked to its structure, which is subdivided into four different levels. The four levels of protein structure will be explained in the following.

Primary Structure

Proteins are a chain of amino acids, of which there are twenty occurring in nature. Usually chains of 20 or less amino acids are refereed to as peptides while longer chains are refereed to as proteins. The sequence in which the amino acids occur in the chain are defined through the DNA, respectively RNA, template. The amino acids are linked by peptide bonds which are formed by a condensation reaction from two amino acids, linking them and eliminating a water molecule in the process (Fig. 11.11).

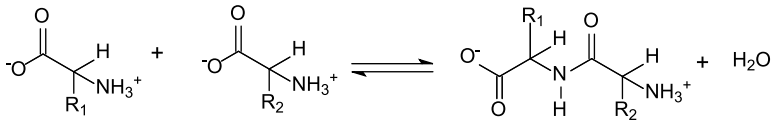

Figure 11.11: Example of a peptide coupling reaction in which a dipeptide is formed from two arbitrary amino acids denoted by R_1 and R_2. As can be seen a water molecule is eliminated through the reaction.

The sequence of amino acids in a protein is referred to as the primary structure of the protein. Due to the direction of the chain and number of available building blocks even short sequences of amino acids can be arranged in enormous numbers of mutations. For example a dipeptide can be formed in 400 different ways (20^2), and a chain of 5 amino acids already provides more than a million possible sequences ($20^5 = 3.200.000$).

Secondary Structure

The primary structure of proteins folds up into regularly occurring helixes and sheets named α-helix and β-pleated sheets respectively (Fig. 11.12). This is called secondary structure of proteins. Both, the helixes and sheets,

are stably hold together with hydrogen bonds. In an α-helix, which is similar to a right-handed coil, a hydrogen bond is formed between the R-CO group of one amino acid with an R-NH group of an amino acid residue four acids down the chain. In β-pleated sheets hydrogen bonds are formed between the amino acid substitutes brought in proximity through folding of the backbone. Depending on whether the backbone runs in the same direction or in opposite directions this is referred to as parallel or anti-parallel β-folding.

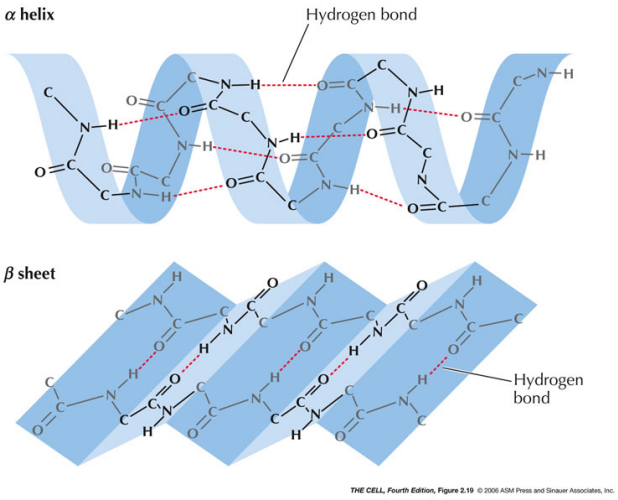

Figure 11.12: Structure of an α-helix (top) and β-sheet (bottom) ***The Cell**, Fourth Edition (Fig.2.19), 2006* ASM Press and Sinauer Associates.

Sometimes the amino acid chain can form random loops or coils. However, these are often not stable and not regularly occurring. Thus they are often excluded when speaking about secondary structure.

Tertiary Structure

The complete three dimensional structure of a protein is called the tertiary structure of the protein. It contains the folding of the secondary structure as well as the interactions between the single amino acids.

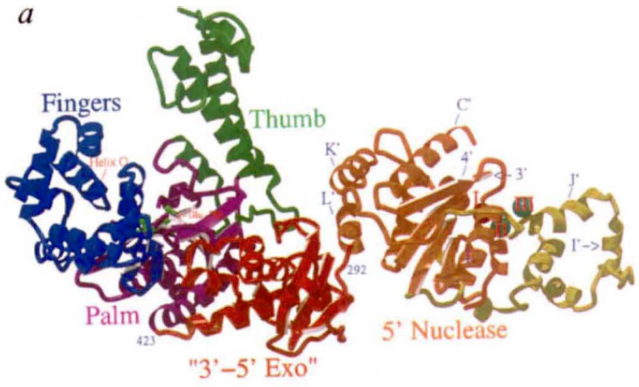

Figure 11.13: 3D-Model of the structure of Taq-Polymerase showing the different domains of the protein *Y. Kim et al.* ***Nature****, vol. 376 (612 - 616), 1995.*

The tertiary structure is formed with the help of hydrogen bonds, ionic interactions, Van der Waals forces as well as sulphur bridges. Sulphur bridges are covalent bonds that can be formed between two cysteines, an amino acid.

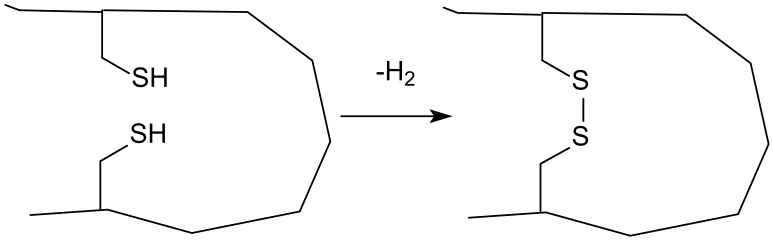

Figure 11.14: Example of a sulphur bridge being formed between two cysteines on the same polypetide chain. During the process hydrogen is eliminated.

The tertiary structure of a protein is usually only stable in a narrow range of salt concentration, pH of the solution and temperature. Leaving these conditions can lead to an unfolding of the protein which leads to a loss of protein function.

Quaternary Structure

The three dimensional arrangement of a single polypeptide chain is described by the tertiary structure. However, there are proteins, like insulin, consisting out of more than one polypeptide chain. The quaternary structure describes the interactions between the two chains when folding. Like for tertiary structures the most important forces during folding are hydrogen bonds as

well as electrostatic interactions. Furthermore sulphur bridges can form covalently attaching both chains to each other.

11.2 Original Paper - Handheld real-time PCR device

Lab on a Chip

PAPER

View Article Online
View Journal

Handheld real-time PCR device†

Christian D. Ahrberg,[a] Bojan Robert Ilic,[b] Andreas Manz[a] and Pavel Neužil*[acd]

Cite this: DOI: 10.1039/c5lc01415h

Received 18th November 2015,
Accepted 16th December 2015

DOI: 10.1039/c5lc01415h

www.rsc.org/loc

Here we report one of the smallest real-time polymerase chain reaction (PCR) systems to date with an approximate size of 100 mm × 60 mm × 33 mm. The system is an autonomous unit requiring an external 12 V power supply. Four simultaneous reactions are performed in the form of virtual reaction chambers (VRCs) where a ≈200 nL sample is covered with mineral oil and placed on a glass cover slip. Fast, 40 cycle amplification of an amplicon from the H7N9 gene was used to demonstrate the PCR performance. The standard curve slope was −3.02 ± 0.16 cycles at threshold per decade (mean ± standard deviation) corresponding to an amplification efficiency of 0.91 ± 0.05 per cycle (mean ± standard deviation). The PCR device was capable of detecting a single deoxyribonucleic acid (DNA) copy. These results further suggest that our handheld PCR device may have broad, technologically-relevant applications extending to rapid detection of infectious diseases in small clinics.

The invention of polymerase chain reaction (PCR) 32 years ago is considered to be one of the greatest inventions of the last century.[1] Over the years, many variants of the original system have been developed. One of the most important advancements is the real-time PCR analysis system.[2] The approach enables real-time PCR amplification, monitoring, and quantification of the number of deoxyribonucleic acid (DNA) copies in the sample under consideration. This method is commonly referred to as quantitative PCR (qPCR).[2] The main advantage of real-time PCR is the elimination of any post-processing, such as electrophoresis or hybridization to detect the PCR product.

The PCR reaction is performed by thermal cycling in the presence of specific oligonucleotides, the enzyme polymerase, free nucleic acids and bivalent salts such as $MgSO_4$ or $MgCl_2$. This cocktail is commonly referred to as the PCR master mix. The detection of PCR product amplification is conducted by monitoring the fluorescence amplitude during the PCR. In the presence of an intercalating dye, such as SYBR Green I, the fluorescence amplitude is proportional to the concentration of the DNA amplicon, the product of the PCR. In order to verify amplification specificity, upon PCR completion, employment of an intercalating dye enables performing melting curve analysis (MCA). Another improvement of the PCR is the addition of the reverse transcriptase enzyme to the PCR cocktail, forming reverse transcription PCR (RT-PCR).

PCR has become the method of choice for the detection of DNA and RT-PCR to detect RNA. These two reactions have revolutionized genetics. Furthermore, PCR has many diverse applications in infectious disease diagnostics for detection of viruses or bacteria,[3] in forensic science,[4,5] paternity tests,[6] security applications[7] and myriad other commercial applications.[8] Commercial systems are typically rather large tabletop tools used for high throughput mass screenings and are impractical for use in point-of-care applications (POC), where the most important system parameters are portability and power consumption. The quest for a miniaturized PCR version suitable for POC diagnostics was initiated at Lawrence Livermore Laboratories[9,10] more than two decades ago. Agrawal *et al.* have developed a pocket-sized conventional PCR system[11] that requires extensive sample post-processing to identify the presence of an amplicon. In contrast, real-time PCR eliminates the need for sample processing once PCR is completed.

Real-time PCR systems consist of a heater, temperature sensor, and fluorescence excitation and detection unit. Temperature cycling is performed by heating and cooling of samples. Within the PCR process, the cooling rate is one of the primary limiting factors. Bulky commercial systems have large heat capacities, hence heat removal is challenging, and is typically accomplished by using a thermoelectric cooler (TEC), commonly known as the Peltier element. Since these bulky systems consume a considerable amount of power, they are generally unsuitable for field testing POC applications.

[a] KIST-Europe, Microfluidics Group, Campus E7.1, 66111 Saarbrücken, Germany. E-mail: pavel.neuzil@gmail.com
[b] National Institute of Standard and Technology (NIST), Center for Nanoscale Science and Technology, 100 Bureau Drive, MS 6201, Gaithersburg, MD 20899-6201, USA
[c] Brno University of Technology (BUT), Central European Institute of Technology (CEITEC), Technická 3058/10, CZ-616 00 Brno, Czech Republic
[d] Northwestern Polytechnical University (NPU), School of Mechanical Engineering, Department of Microsystem Engineering, 127 West Youyi Road, Xi'an Shaanxi, 710072, PR China

† Electronic supplementary information (ESI) available. See DOI: 10.1039/c5lc01415h

Small PCR instruments are often based on microfluidic devices, so-called "lab-on-a-chip" devices.[12] These systems comprise two major groups, spatial-domain and time-domain PCRs. On the one hand, time-domain PCRs have a single heater with samples placed in direct contact. Here, temperature cycling is carried out by changing the heater element temperature. On the opposite end of the spectrum, the spatial-domain PCR has several heaters, each held at a different temperature. In this scenario, temperature cycling is accomplished by moving samples between heaters.

A typical representative of a spatial-domain system is the continuous PCR-on-a-chip.[13] Within this system, the sample flow in the microfluidic chip is positioned over the heaters, each kept at a different temperature. The sample flows through tubes, thereby achieving thermal cycling. Here, PCR duration is only limited by the flow rate and the heat transfer between the sample and the side walls, for both heating and cooling. The two major drawbacks of a flow-through PCR are system complexity and a high likelihood of sample-to-sample cross-contamination.

An alternative version was introduced a few years ago where the sample was in the form of a virtual reaction chamber (VRC).[14–16] The VRC self-assembly system consists of a water droplet covered with mineral oil, preventing water evaporation from the sample. In this scenario, the water droplet contained the PCR master mix with a pre-determined number of DNA copies. Here, the VRC with DNA was separated from the micromachined silicon heaters by a disposable, hydrophobically-coated microscope cover slip. To eliminate sample-to-sample contamination, the glass cover slip was a disposable part of the system, and therefore each cover slip was a single use component. The sample contained magnetic particles which facilitated sample motion between heaters.[17] A pocket-size real-time PCR system capable of processing a single sample was introduced a few years later.[18] The system had an integrated miniaturized optical detection unit, LCD display and control electronics. One of the key features was the implementation of lock-in amplification for optical signal processing.[17] The lock-in amplification feature allowed for ambient system operation without light protection, thereby rendering the system robust and user-friendly. One of the system drawbacks was processing a single sample at a time and furthermore, the device was bulky.

A practical system to conduct PCR for POC applications requires simultaneous processing of 4 or more samples. Diagnoses of clinical samples should be concurrently conducted with positive and negative control samples, thereby eliminating false negative or positive events.

In our work, we introduce a new portable PCR system (Fig. 1) capable of concurrently analyzing four ≈200 nL volume samples. The system speed is determined by the heating and cooling rates. The heating rate collectively arises from the VRC thermal capacitance (H) and the dissipated Joule heat. The rate of passive cooling applied within our system is given by the thermal time constant (τ) of the system, which is given by H/G, where G is the thermal conductance. Since the specific heat of water is exceptionally large, the thermal properties of our system are strongly dependent on the sample water volume. Consequently, a smaller sample size results in a faster system.[19]

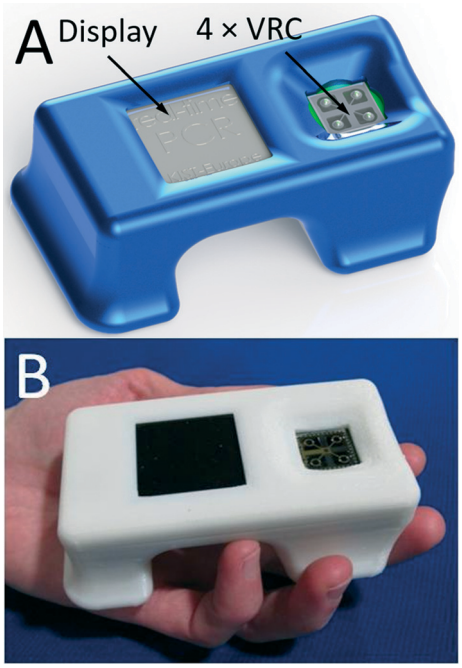

Fig. 1 (A) CAD design drawing of the handheld PCR. The illustration shows a display with a compartment accommodating 4 samples in the VRC form. (B) Fabricated and assembled complete real-time PCR device packaged within a 3D printed casing.

System samples consist of a negative control, also called no template control (NTC), a positive control, and two samples of interest. The four sample system architecture represents the minimal number of samples required for practical applications. Our system conducts 40 PCR cycles in less than ≈35 min, while simultaneously processing the results. Furthermore, our portable real-time PCR is capable of detecting a single DNA copy.

The PCR performance was evaluated by detecting a complementary DNA from the avian influenza virus (H7N9) as well as two human transcripts, hypoxanthine phosphoribosyltransferase (HPRT) and glyceraldehyde-3-phosphate dehydrogenase (GAPDH). To the best of our knowledge, our system platform represents the smallest real-time PCR system.

Our PCR instrument has two key features:

1. The four samples are in the VRC form and are placed on a disposable glass cover slip over micromachined silicon heaters. Upon PCR completion, the single-use, disposable glass element is removed and a new glass cover slip is placed on top of the silicon heater.

2. The fluorescence excitation/detection system is based on a lock-in amplifier, thereby rendering the system immune to ambient light. The PCR instrument is equipped with a graphical 84 × 48 pixel liquid crystal display (LCD) with a diagonal size of ≈38.1 mm to show the reaction progress and

final results. The captured data is stored in an internal memory and can be uploaded for external processing *via* a universal serial bus (USB). The system is powered by an external 12 V battery.

System setup

Our current system has two new key features: an integrated optical head and simplified control electronics.

1. Integrated optical head

A fluorescence detection system for a single spot requires a light source, three filters (excitation, dichroic mirror and emission) and a detector. We redesigned the original head[20,21] with 5 filters for the four units (see Fig. 2). Each measurement spot is illuminated with a light emitting diode (LED) with a principal emission wavelength of 470 nm and a luminous intensity in the range of 7.2 cd to 12 cd. Light passes through an excitation band pass filter with a center wavelength of ≈470 nm and a band pass of ≈40 nm, blocking light from the LED with wavelengths longer than ≈490 nm. Light is then reflected off of a long pass dichroic mirror with a cut-off wavelength of ≈495 nm, and focused by a lens with a focal length of ≈3.1 mm, a numerical aperture of ≈0.68 and an antireflective coating in the range of ≈350 nm to ≈700 nm. The emitted fluorescence (F) is collimated by the same lens, passing through the dichroic mirror. The residual blue light is suppressed by a long pass emission filter with a cut-off wavelength of ≈510 nm, and fluorescence is captured by the conventional silicon photodiode with a radiant sensitive area of ≈7.5 mm.^{2} The cross section schematic of the handheld PCR system illustrating the optical path is shown in Fig. S1 (ESI†). The resulting photocurrent is converted into voltage using an ultra-low bias current operational amplifier with dielectrically-isolated field effect transistor inputs (diFET) as a transconductance amplifier. In this configuration, the four sample systems share optical filters. Four LEDs are mounted in two pairs. Within each pair, the LEDs were parallel, thus requiring only two excitation and two dichroic filters for all 4 LEDs. Finally, there is only a single emission filter for all photodiodes. A potential expansion to eight systems would require additional LEDs and photodiodes with amplifiers.

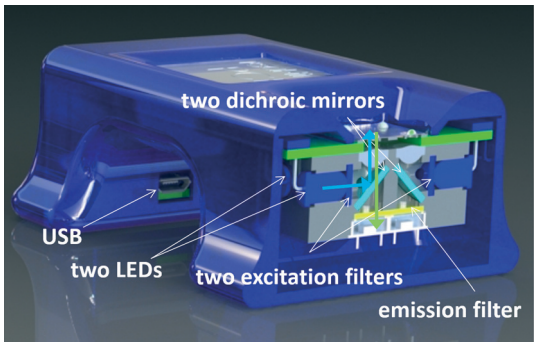

Fig. 2 Schematic illustration of the integrated optical head. Blue arrows show the optical path from one LED with filters to the VRC. The green arrow shows the optical path of excited fluorescence to the photodiode. Light emitted from a blue LED passes through the blue filter in order to remove the green portion of emitted light, then reflects off of the dichroic mirror through a donut-shaped heater and is focused on the sample by an aspherical lens. Excited fluorescence is collimated by the same lens, passing through the dichroic mirror with the blue portion filtered out by a green filter. Residual green light interacts with a photodiode and induces a photocurrent, which is further processed.

2. Control electronics

A previously published system[18] had one lock-in amplifier for a single fluorescence detection system and a second one for temperature measurement. This scenario was very inefficient since fluorescence was monitored for ≈2 s during each PCR cycle. The second lock-in amplifier for temperature measurement was used during the entire PCR operation. Our current system employs a single lock-in amplifier to monitor the sample temperature and capture fluorescence from all four spots.

The system heaters were connected in a serial–parallel combination, wherein the system controlled the average temperature of all four heaters. We used a similar AC biased Wheatstone bridge to convert the resistance of the resistance temperature detector (RTD) into a DC voltage as previously described.[18]

The control electronics for the optical system was a simplified version of our previous work.[18] Here, each PCR system (spot) had its own LED, collimating lens and a photodiode with a respective transconductance amplifier while the optical filters are shared. We activated one LED at a time, thereby feeding the signal to a single, corresponding transconductance amplifier. Outputs of the four amplifiers were connected together and processed as one signal. The complete schematic of the PCR system is shown in Fig. S2 (ESI†).

The incident photocurrents from the photodiodes were converted into voltage using four dedicated operational amplifiers. The amplifier outputs were connected together and a single composite signal was further processed. The cross talk between four measured spots was minimized since one LED was activated at a time; therefore the resulting total amplitude of the processed photocurrent originated from a single dedicated PCR reaction. All important devices are listed in Table S1 (ESI†).

Experimental

A typical real-time PCR protocol with an intercalating dye such as SYBR-Green I initiates with a hot start to activate the polymerase. PCR cycles consist of denaturation, annealing and extension steps. The fluorescence amplitude is measured at the end of the extension step for a period of ≈2 s. We controlled the heater temperature using the proportional integrative-derivative (PID) closed feedback loop method. The amount of heat delivered through dissipated Joule heating was controlled using a pulse-width modulation (PWM) technique. The last ≈2 s of the amplification cycle were used for

fluorescence monitoring (see Fig. 3). In this step, following temperature stabilization, we monitored the duty cycle of the PWM and calculated its average. During the last ≈2 s, the feedback loop was disconnected, the temperature was not monitored and the average value of the PWM was employed. During the system development phase, we monitored the heater temperature and found that the method described above gives us a temperature variation of less than ±0.5 °C over a ≈2 s time interval. The sample temperature follows the heater temperature with a ≈1.5 s delay,[22] therefore a ±0.5 °C temperature variation at the heater does not affect the PCR performance. The measured temperature profile from ≈6 PCR steps is shown within the system liquid crystal display (LCD) in Fig. 4A.

During the last two seconds of the extension step, the fluorescence measurement system was activated. Sequentially, each LED was individually powered for ≈0.5 s and the emitted fluorescence was captured by the respective photodiode and lock-in amplifier. At the completion of an amplification cycle, the system was switched back into the temperature measurement mode, initiating the start of a new cycle. The PCR amplification curves were plotted for each spot and the captured amplitude of fluorescence was displayed on the LCD display. The typical PCR amplification curve is shown in Fig. 4B. Directly following the PCR process, melting curve analysis (MCA) was performed. Since temperature measurement during the MCA is time consuming, we performed this step without a feedback loop. In the course of the PCR, we monitored and recorded the PWM duty cycle of three fixed temperature points: denaturation, annealing and extension temperatures. These three points were used to calculate the required duty cycle for temperature scans ranging from

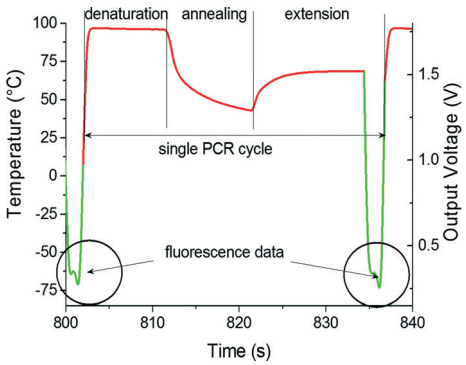

Fig. 3 PCR thermal profile of a single amplification step. The heater temperature (red part) is linearly proportional to the built-in lock-in amplification output, which was captured with an oscilloscope. While performing denaturation at ≈93 °C, annealing at ≈56 °C and most of the extension step at ≈72 °C, the built-in lock-in amplifier is utilized to measure the average temperature of all four heaters. In the last two seconds of the extension step, the lock-in amplifier is used to sequentially process the fluorescence signal (green part) from the 4 measurement spots (circled area). These data are stored in their original format in analog-to-digital converter units (ADC units) within the memory of a microcontroller. Once fluorescence is measured, the heater is powered by the average value of pulse width modulation obtained during the extension phase.

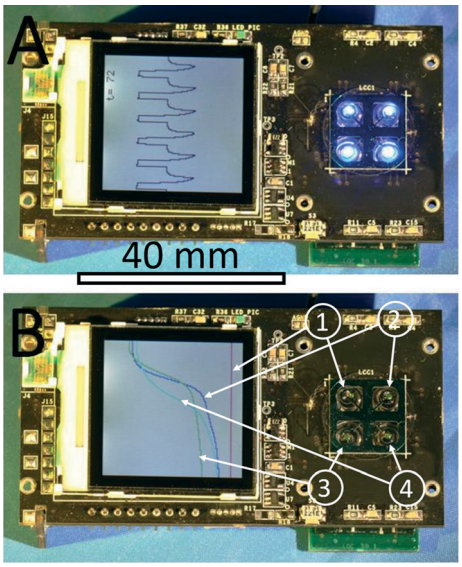

Fig. 4 (A) An assembled PCR system with four VRCs, each consisting of a ≈0.5 μL sized sample covered with ≈1.5 μL of M5904 mineral oil, showing the PCR temperature profile (protocol) within the LCD display. The device size is 82 mm × 45 mm × 20 mm (length, width and height). Scale bar is 40 mm. The protocol started by a "hot start" to activate the polymerase enzyme for ≈10 min at ≈95 °C, followed by 40 cycles of PCR amplification. Each amplification cycle consisted of 3 steps. First, denaturation for ≈10 s at ≈95 °C, then annealing for ≈10 s at ≈50 °C and the last step was extension for ≈15 s at ≈68 °C (instead of typical ≈72 °C), during which fluorescence was measured. The LCD display shows 6 cycles. At the completion of each PCR amplification cycle, fluorescence amplitude at each spot was calculated and amplification curves were plotted in (B). We placed NTC at position 1, a low concentration of complementary DNA (cDNA) from H7N9 HA gene at position 3, a medium concentration at position 2 and the highest concentration (positive control) at position 4. The results show that the PCR reaction was successfully accomplished without PCR amplification of the NTC sample. Furthermore, the results prove that the samples were not cross contaminated, thereby eliminating false positive outcomes. Positive control results at position 4 indicate the absence of false negative results, thereby showing a successful PCR amplification process.

≈68 °C to ≈94 °C without a closed feedback loop. The system was stabilized at ≈68 °C. The temperature of each heater was then gradually increased to ≈95 °C while the fluorescence in each of the four spots was sequentially measured. The measurement of each spot required a duration of ≈0.5 s, hence ≈2 s was required to measure all 4 VRCs. This measurement setup allowed for fluorescence measurement from each spot with an offset of ≈0.25 °C between adjacent VRCs. Once the MCA was completed, we stabilized the sample at the assumed temperature of ≈95 °C and then measured the actual temperature. Directly following this, the system's central processing unit (CPU) performed two corrections. First, the MCA was recalculated based on the actual final temperature. Second, the correction accounts for the temperature offset between individual VRCs. Consequently, the MCAs for each spot were recalculated accordingly. Finally, a negative derivative value of fluorescence with respect to temperature ($-dF/dT$) was calculated.

The device performance was evaluated using synthetic complementary DNA (cDNA) for the hemagglutinin of the H7N9 avian influenza virus. Forward and reverse primers were chosen as suggested earlier:[23] forward primer: TACAGGGAAGAGGCAATGCA, reverse primer: AACATGATGCCCCGAAGCTA, giving a total amplicon length of 104 base pairs with a melting temperature of ≈81.1 °C, as measured using a commercial real time PCR system.

The PCR master mix was prepared by mixing ≈2 μL of FastStart DNA Master SYBR Green I, ≈2 μL of $MgCl_2$ solution, ≈2 μL of sample HA (5×10^{-5} ng μL^{-1}), ≈0.3 μL of ≈400 mg mL^{-1} BSA solution and primers in a final concentration of $\approx 1.8 \times 10^{-6}$ mol L^{-1}. We added deionized (DI) water with a resistivity higher than 18 MΩ cm at 25 °C to create the final volume of ≈20 μL. The NTC sample had ≈2 μL HA gene volume replaced with DI water.

First, we performed basic real-time PCR with different contents of cDNA per μL as shown in Table 1 with NTC at position 1 and different contents at positions 2 to 4. The amplification curves are shown in Fig. 5A. Once the PCR process was completed, we also conducted a MCA (not shown here). The MCA shape is not suitable for performing high-resolution analysis;[24] nevertheless, it does show that a specific DNA was amplified with the melting temperature of 83.36 ± 0.63 °C (mean ± standard deviation), in close proximity to the measured value of $T_M \approx 81.1$ °C. The marginal difference in the T_M values is due to the uncertainty of calibration precision of the commercial PCR system used as a benchmark tool. The T_M resolution is sufficient to verify specific DNA amplification; however, it may not be suitable for performing high-resolution melting curve analysis.[25]

We then performed a series of four identical measurements using an HA content of $\approx 5 \times 10^{-5}$ ng in a μL of cDNA (see data in Table 2 and a graphical representation in Fig. 5B). Different PCR locations resulted in performance variation, consequently producing mean C_T values in the range of ≈8 to ≈9.6 with a standard deviation ranging between ≈0.8 and ≈1.5. The difference in C_T values at positions 2 to 4 might be caused by imperfections due to manual VRC placement. The VRC at position 1 appears to have a lower heat transfer rate than VRCs at other positions. We attribute the variation to a slower transition from amplification to saturation of the DNA amplification curve (Fig. 5B). We further presume that heater defects at position 1 could give rise to a temperature that is different in comparison with the other three positions, consequently leading to a differing PCR efficiency. Additionally, this discrepancy could be attributed to the stress induced during chip-to-PCB soldering, giving rise to bending of the chip. The silicon chip deformations could cause both variations in the intermediate oil layer thickness and a differing heat rate.

Finally, we obtained standard PCR curves. The samples were prepared by the following procedure. We mixed a sample with cDNA corresponding to 12 500 copies per 200 nL volume. This sample was diluted 10×, yielding 1250 copies per 200 nL volume; the next dilution yielded 125 copies per 200 nL volume. The last two dilutions had a statistical number of 12.5 copies per 200 nL and 1.25 copy per 200 nL volume, respectively. The PCR results as well as the normalized data are shown in Fig. 5C and D, demonstrating that our portable real-time PCR is able to detect a single DNA copy with an excellent efficiency of 0.91 ± 0.05 per cycle (mean ± standard deviation), which is well within the required range of PCR efficiency between 0.8 and 1.0.

Table 1 Typical results with NTC (position one) serving as negative control and three different sample concentrations at positions 2 to 4. The sample at position 4 serves as positive control

Position	Mean C_T	Standard deviation	Concentration HA (ng μL^{-1})
1	—	—	—
2	28.7	1.5	$\approx 5.0 \times 10^{-8}$
3	27.0	1.0	$\approx 7.5 \times 10^{-8}$
4	20.0	1.0	$\approx 5.0 \times 10^{-6}$

Discussion

The PCR protocol consisted of a ≈10 min hot start at ≈95 °C, followed by 40 cycles of ≈10 s at ≈95 °C, ≈10 s at ≈50 °C and ≈15 s at ≈68 °C. Once the PCR amplification was completed, we conducted an MCA with a scan rate of ≈0.2 °C s^{-1}. This protocol required a total time for amplification of less than 35 minutes with an additional ≈150 s for the MCA. The ultimate speed of the PCR was not the primary target of this work. Nevertheless, the time required for DNA amplification can be shortened by using different types of hot starts, Taqman chemistry (or both)[19] or even not using the hot start at all.[26]

Here we used the same heater as in our previous work. The dissipated Joule heat P depends on the square of voltage V: $P = V^2/R$, where R is the heater resistance. The Joule heat dissipation and the consequent heating rate were enhanced with either an increased voltage bias or by lowering the heater resistance. In a previous work,[22] we increased the bias voltage up to 20 V using an external power supply. Here, the heater is powered using a 12 V external power supply in either an AC/DC converter or a battery type configuration. A change in this voltage would require additional space for a step up voltage converter. The additional feature would further require either a redesign of the heater on a micromachine, requiring a new mask for the metal lithography level, or the use of a thicker metal layer with a lower sheet resistance. Both cases would require the fabrication of new PCR chip architectures.[14] The current PCR chip layout is shown in Fig. S3 (ESI†) and the chip fabrication process in section 5 (ESI†).

In principle, the fundamental limitation in the speed of the device is determined by the heat transfer between the heater and the sample, which is ≈1.5 s for each temperature step. Nevertheless, the device can still run as fast as its predecessor achieving ≈9.5 s per PCR cycle, still being considered as one of the fastest real-time PCRs demonstrated at that point in time.[19]

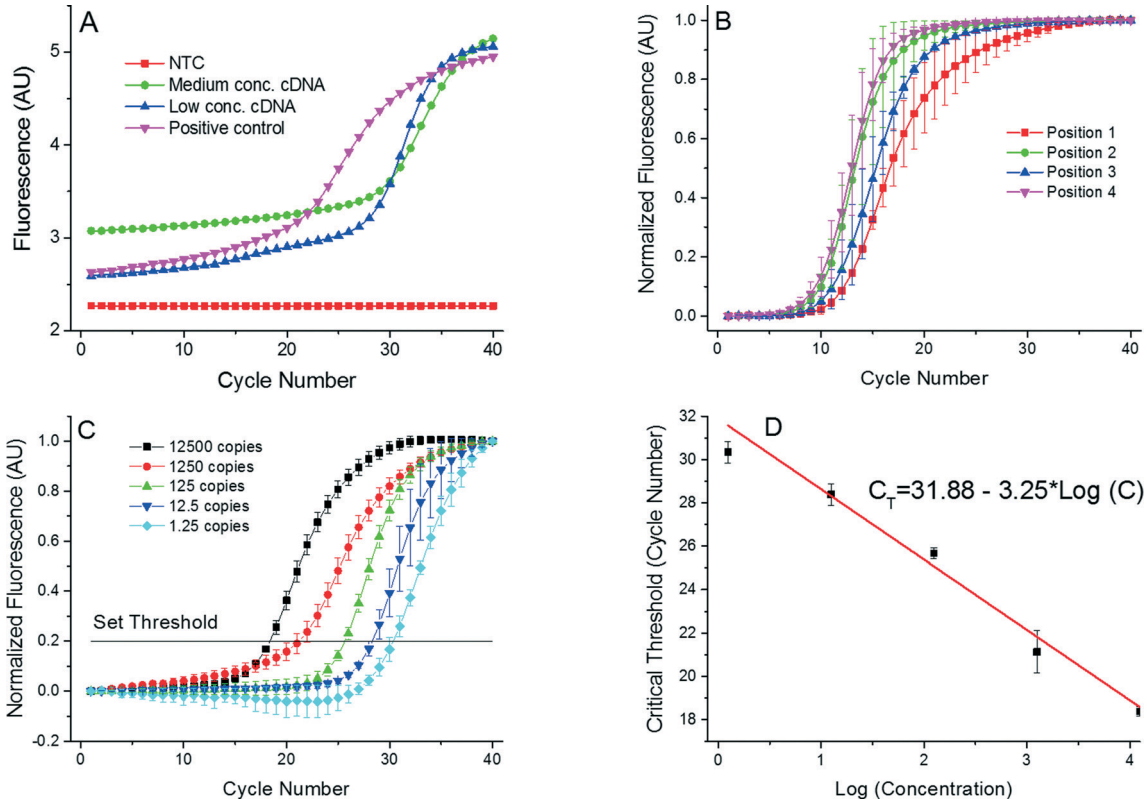

Fig. 5 (A) Single PCR run as it appears in the PCR display. These PCR amplification curves show results from the 4 positions of the PCR device. We used complementary DNA (cDNA) from the H7N9 HA gene for testing purposes. AU stands for arbitrary units. Once the PCR was completed, the MCAs were performed with a melting temperature value of 83.36 ± 0.63 °C (mean ± standard deviation). Measurement uncertainties emanate from the manual placement of the droplet. Slight droplet misalignments at the heater cause temperature variations between various experimental runs, thereby affecting the overall PCR efficiency. Also, due to these temperature variations, we readily observe a slight shift in the measured melting temperature. (B) Measurements performed at the 4 positions with identical concentration of all samples performed three times to suppress random error. The corresponding extracted critical thresholds (C_T) are shown in Table 2. A greater value of C_T at position 4 suggests a lower amplification efficiency at that position. This may be caused by a temperature variation due to a non-optimized bonding process of the silicon chip to the PCB. (C) PCR results from position 1 with the calculated number of cDNA copies in the sample from ≈12 500 down to ≈1.25. These numbers are calculated by a 10× dilution starting from ≈12500. Since only whole numbers of cDNA copies per sample exist, fractional values imply the statistically most probable value. Each experiment was performed three times. (D) Extracted standard real-time PCR curve from results in Fig. 5C showing the C_T value as a function of LOG (cDNA concentration). The slope of −3.02 ± 0.16 cycles at threshold per decade (mean ± standard deviation) corresponds to the PCR efficiency of 0.91 ± 0.05 per cycle (mean ± standard deviation).

Furthermore, we enhance the system robustness by not incorporating moving parts. The system light source consists of 4 LEDs with an estimated lifetime of more than 50 000 hours. A single 40 cycle PCR run requires each LED to operate for less than 1 min. The most vulnerable part is the micromachined silicon chip mounted directly on the main PCB. We envision a new version of our system, currently under development, with the brittle silicon chip mounted on a dedicated PCB. Therefore, if the fragile part is damaged, a replacement silicon chip can be easily exchanged. In order to limit interference between PWM pulses and temperature sensing signals, the layout of the micromachined silicon chip will incorporate electrical shielding between integrated heaters and sensors. In this scenario, the chip size will increase to ≈18 mm × 18 mm. Also, this configuration provides additional space in order to further modify the optical housing and facilitate the removal of the PCB from the optical path. The current version of the system exhibited a large self-induced fluorescence due to the PCB being illuminated by the blue LEDs. Finally, we plan to reduce the complexity of the optical housing by reducing the number of parts. This would also allow us to replace the silicon chip once variations in PCR efficiency are discovered.

Table 2 Results of critical threshold from 4 measurements at each PCR location with identical concentration of the HA gene. The graphical output is shown in Fig. 5B. The discrepancy between results from individual samples was probably caused by sample misalignment with respect to the heater as they were placed manually

Position	Mean C_T	Standard deviation	Concentration HA (ng μL^{-1})
1	9.6	1.5	$\approx 5.0 \times 10^{-5}$
2	9.0	1.2	$\approx 5.0 \times 10^{-5}$
3	9.5	0.6	$\approx 5.0 \times 10^{-5}$
4	8.0	0.8	$\approx 5.0 \times 10^{-5}$

Furthermore, in future experiments, we plan to use either microscope glass cover slips with upfront lyophilized PCR or a single step RT-PCR master mix. In this configuration, the pipetted ≈200 nL volume sample will be entirely composed of DNA (RNA).

Conclusions

We designed and tested one of the smallest real-time PCR devices. It has a length of ≈100 mm, a width of ≈60 mm and a height of ≈33 mm and weighs only ≈90 g. The device measured 4 PCRs simultaneously in less than ≈35 min, including MCA. The sample was processed in the form of a virtual reaction chamber (VRC) where 200 nL of a sample was placed on a disposable glass cover slip covered with mineral oil to prevent water evaporation from the sample. The sample only interacts with the glass cover slip to eliminate possibilities of sample-to-sample cross-contamination; the glass element was a single-use, disposable system component. Our negative control tests further demonstrate the lack of cross contamination between samples. The system depicted in Fig. 4 was successfully utilized for at least 100 distinct PCR runs. We have demonstrated its performance by amplifying the cDNA of an HA gene of the H7N9 avian influenza virus and displayed the results on an integrated LCD display. We demonstrated the capability of simultaneously running 4 samples at a time with good reproducibility. The PCR efficiency was demonstrated by obtaining a PCR standard curve in the range of 12500 to 1.25 copies with an achieved slope of −3.02 ± 0.16 cycles at threshold per decade (mean ± standard deviation). The value corresponds to a PCR efficiency of 0.91 ± 0.05 per cycle (mean ± standard deviation). The system was also capable of detecting a single DNA copy within the sample.

The captured data was subsequently transferred to a personal computer (PC) *via* a USB interface for further processing. This tiny real-time PCR device is a promising diagnostic system for remote clinics as well as a tool for educational institutions demonstrating the power of a real-time PCR as "seeing is believing". The system throughput can be doubled using a single channel multiplexing method as demonstrated earlier.[27]

Acknowledgements

P. Neužil acknowledges partial financial support from the Central European Institute of Technology (CEITEC), grant number CZ.1.05/1.1.00/02.0068. The authors gratefully acknowledge the NIST CNST NanoFab staff for helpful discussions and assistance with device fabrication. This article identifies certain commercial equipment, instruments, and materials to specify the experimental procedure. Such identification does not imply recommendation or endorsement by the National Institute of Standards and Technology, nor does it imply that the equipment, instruments, and materials identified are necessarily the best available for the purpose.

References

1 K. Mullis, F. Faloona, S. Scharf, R. Saiki, G. Horn and H. Erlich, *Cold Spring Harbor Symp. Quant. Biol.*, 1986, **51**(Pt 1), 263–273.
2 R. K. Saiki, D. H. Gelfand, S. Stoffel, S. J. Scharf, R. Higuchi, G. T. Horn, K. B. Mullis and H. A. Erlich, *Science*, 1988, **239**, 487–491.
3 S. Yang and R. E. Rothman, *Lancet Infect. Dis.*, 2004, **4**, 337–348.
4 R. Decorte and J. J. Cassiman, *J. Med. Genet.*, 1993, **30**, 625–633.
5 M. A. Jobling and P. Gill, *Nat. Rev. Genet.*, 2004, **5**, 739–751.
6 M. A. Jobling, A. Pandya and C. TylerSmith, *Z. Rechtsmed.*, 1997, **110**, 118–124.
7 S. S. Iqbal, M. W. Mayo, J. G. Bruno, B. V. Bronk, C. A. Batt and J. P. Chambers, *Biosens. Bioelectron.*, 2000, **15**, 549–578.
8 M. A. Valasek and J. J. Repa, *Adv. Physiol. Educ.*, 2005, **29**, 151–159.
9 P. Belgrader, J. K. Smith, V. W. Weedn and M. A. Northrup, *J. Forensic Sci.*, 1998, **43**, 315–319.
10 P. Belgrader, S. Young, B. Yuan, M. Primeau, L. A. Christel, F. Pourahmadi and M. A. Northrup, *Anal. Chem.*, 2001, **73**, 391–391.
11 N. Agrawal, Y. A. Hassan and V. M. Ugaz, *Angew. Chem., Int. Ed.*, 2007, **46**, 4316–4319.
12 P. Neuzil, S. Giselbrecht, K. Laenge, T. J. Huang and A. Manz, *Nat. Rev. Drug Discovery*, 2012, **11**, 620–632.
13 M. U. Kopp, A. J. Mello and A. Manz, *Science*, 1998, **280**, 1046–1048.
14 P. Neuzil, J. Pipper and T. M. Hsieh, *Mol. BioSyst.*, 2006, **2**, 292–298.
15 P. Neuzil, T. M. Hsieh and J. Pipper, *US Pat.*, 8216855, 2012.
16 J. Pipper, T. M. Hsieh and P. Neuzil, *US Pat.*, 8124033, 2012.
17 J. Pipper, M. Inoue, L. F. Ng, P. Neuzil, Y. Zhang and L. Novak, *Nat. Med.*, 2007, **13**, 1259–1263.
18 P. Neuzil, L. Novak, J. Pipper, S. Lee, L. F. Ng and C. Zhang, *Lab Chip*, 2010, **10**, 2632–2634.
19 P. Neuzil, C. Zhang, J. Pipper, S. Oh and L. Zhuo, *Nucleic Acids Res.*, 2006, **34**, e77.
20 L. Novak, P. Neuzil, J. Pipper, Y. Zhang and S. Lee, *Lab Chip*, 2007, **7**, 27–29.
21 P. Neuzil, L. Novak and J. Pipper, *Pat. Appl.*, WO2008024080A, 2008.
22 P. Neuzil, W. Sun, T. Karasek and A. Manz, *Appl. Phys. Lett.*, 2015, 106.
23 V. M. Corman, M. Eickmann, O. Landt, T. Bleicker, S. Brünink, M. Eschbach-Bludau, M. Matrosovich, S. Becker and C. Drosten, *Euro Surveill.*, 2013, **18**(16), 20461. Available online: http://www.eurosurveillance.org/ViewArticle.aspx?ArticleId=20461.
24 G. H. Reed and C. T. Wittwer, *Clin. Chem.*, 2004, **50**, 1748–1754.
25 L. Zhou, J. Vandersteen, L. Wang, T. Fuller, M. Taylor, B. Palais and C. T. Wittwer, *Tissue Antigens*, 2004, **64**, 156–164.
26 J. S. Farrar and C. T. Wittwer, *Clin. Chem.*, 2015, **61**, 145–153.
27 C. D. Ahrberg and P. Neuzil, *Sci. Rep.*, 2015, **5**, 12595.

11.2.1 Supplemental Material- Handheld real-time PCR device

Electronic Supplementary Material (ESI) for Lab on a Chip.

Supplementary data:

1. Cross section of the optical housing

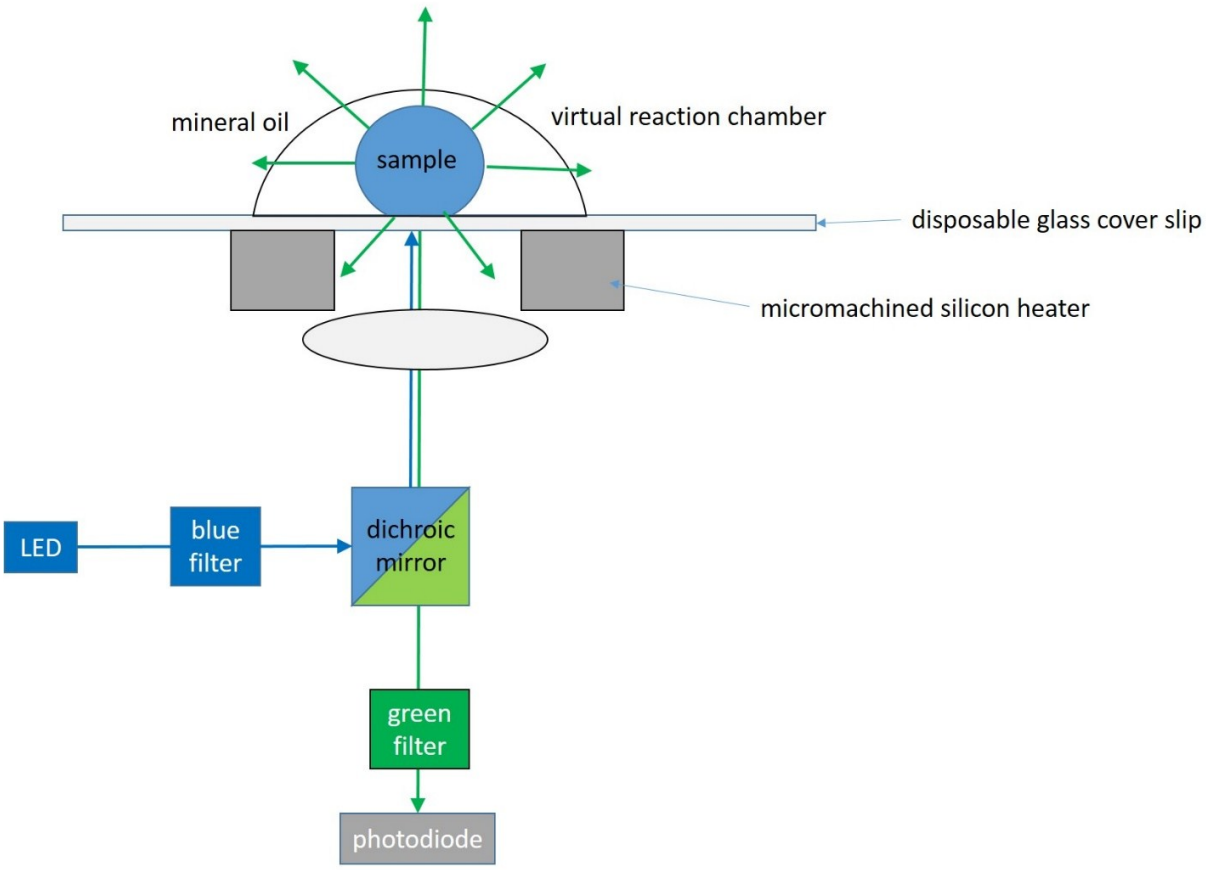

Figure 1: Cross section schematic of the handheld PCR system illustrating the optical path. Light emanating from the LEDs is filtered, then deflected by a dichroic mirror, and focused via lenses onto the VRC. A disposable glass slide separates the VRC from the micromachined silicon chip. The emitted fluorescence is collimated (using the same set of lenses), then passes through the dichroic mirror and a green filter prior to being captured by the photodiode.

2. Schematic of the PCR system

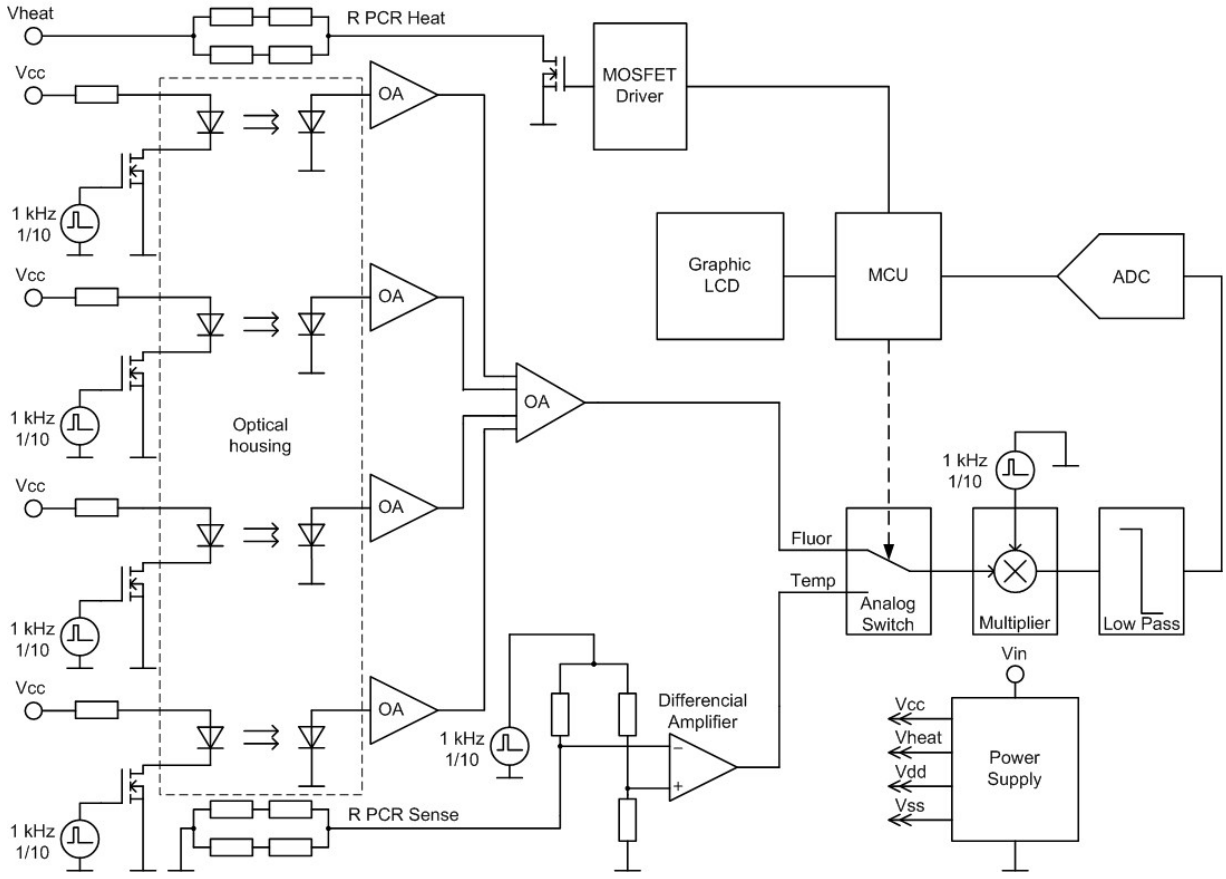

Figure 2: PCR electrical schematic showing four blocks of the fluorescent system inside the optical housing followed by transconductance operation amplifiers, by a generic amplifier and a Wheatstone bridge for temperature monitoring. The analog selector was used for further processing either the fluorescence or the temperature signals by the microcomputer (MCU) via an analog to digital converter (ADC). The processor also controls the dissipated Joule heat within the PCR chip and its temperature via a MOSFET driver.

3. List of components: Table 1

category	type	parameters	number
electrical	Square wave generator	Frequency: 1 kHz duty cycle: 10 %	6
	Power MOSFET	N-channel MOSFET with $R_{DS(on)}$ = 170 mΩ	4
	Power MOSFET	N-channel MOSFET with $R_{DS(on)}$ = 30 mΩ	1
	LED	Wavelength: 470 nm Luminous intensity: 7.2 – 12 cd Diameter: 5 mm	4
	photodiode	7.4 mm^2	4
	Operation amplifier	diFET with bias current < 100 fA	4
	Operation amplifier	Noise < 15 nV/√Hz @ 1 kHz	1
	Differential amplifier	Noise < 8 nV/√Hz @ 1 kHz	1
	Analog switch/analog to digital converter	16 bit resolution, 2 selectable differential inputs	1
	Analog multiplier	4-quadrant analog multiplier	1
	Low pass filter	2 Hz cut off	1
	MCU	16 bit microprocessor	1
	Graphic display	84 × 42 pixels	1
	Switched power supply	Generating DC voltages: +5V, ±12V, +18V	1
thermomechanical	Micromachined silicon chip	Custom layout, integrated with thin film heater and RTD sensor	1
optical	Optical housing	Made by CNC	1
	Low pass filter	490 nm	2
	Dichroic mirror	495 nm	2
	Long pass filter	510 nm	1
	Lens	Diameter: 6.35 mm N.A.: 0.68 Focal length: 3.1 mm	4

4. PCR chip layout

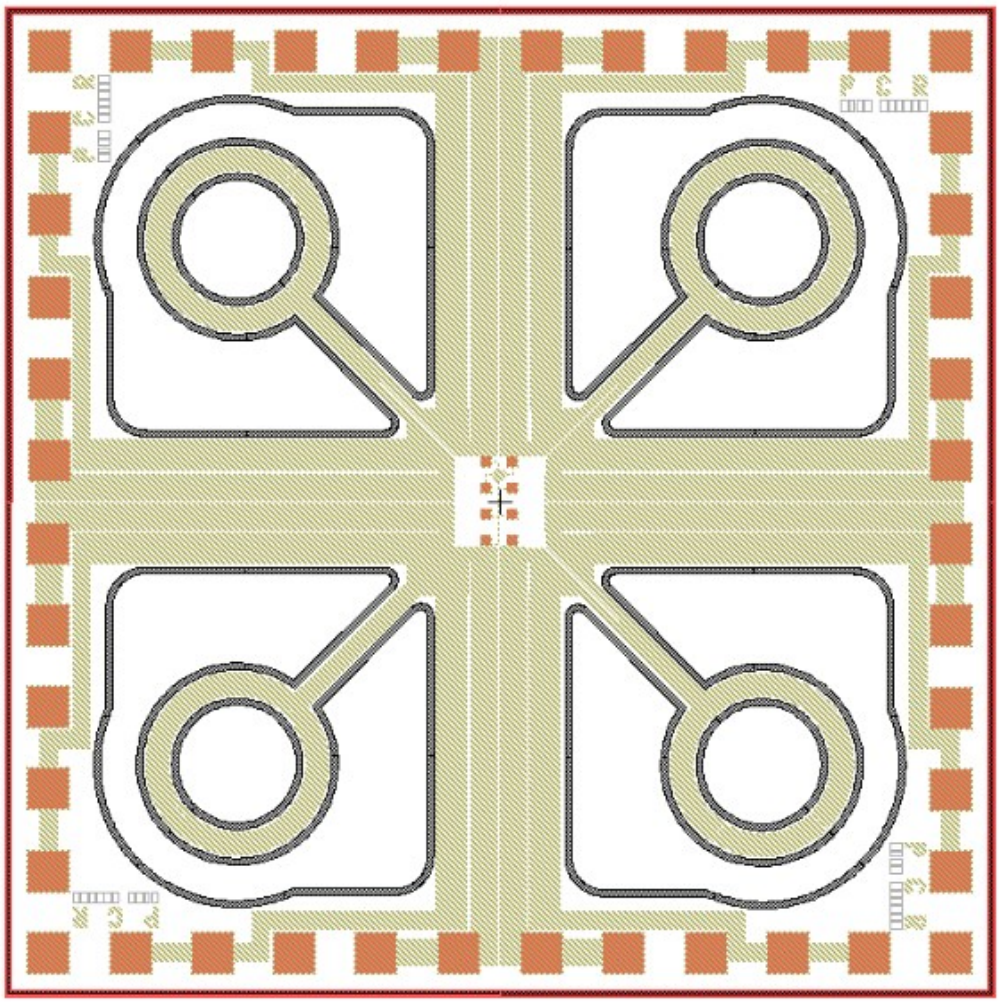

Figure 3 Layout of the PCR chip. The chip is square size with side of ≈ 15 mm. The distance between heater centers is ≈ 8mm.

5. PCR chip fabrication process
    a. Starting substrate silicon wafers with diameter of ≈ 100 mm
    b. SiO_2 deposition by plasma enhanced chemical vapor deposition (PECVD) process with thickness of ≈ 0.5 μm
    c. Au/Cr deposition by sputtering with thickness of ≈ 200 nm and ≈ 5 nm for Au and Cr, respectively
    d. Contact lithography (Au/Cr patterning)
        i. Positive photoresist (PR) spincoating with PR thickness between 1 and 2 μm
        ii. PR pre-bake
        iii. Soft contact exposure
        iv. Postbake
        v. PR developing
        vi. Wafer spin drying
    e. Au/Cr patterning by ion milling with secondary ion mass spectroscopy (SIMS) end point detection
    f. PR removal by acetone and 2-n propyl alcohol or stripper
    g. SiO_2 deposition by plasma enhanced chemical vapor deposition (PECVD) process with thickness of ≈ 0.5 μm.
    h. Contact lithography (bond pads opening)
        i. PR spincoating with PR thickness between 1 μm and 2 μm
        ii. PR pre-bake
        iii. Soft contact exposure
        iv. Postbake
        v. PR developing
        vi. Wafer spin drying
    i. SiO_2 etching by ≈ 40 % NH_4F and ≈ 49 % HF in ratio of ≈ 7 : 1 (BOE 7:1)
    j. PR removal by acetone and 2-n propyl alcohol or stripper
    k. Contact lithography (silicon etching)
        i. PR spincoating with PR thickness between 8 and 12 μm
        ii. PR pre-bake
        iii. Soft contact exposure
        iv. PR developing
        v. Postbake
        vi. Wafer spin drying
    l. SiO_2 etching by BOE 7:1
    m. Silicon etching by Bosch process through silicon water
    n. PR removal by acetone and 2-n propyl alcohol or stripper
    o. Chips drying by N_2
    p. Soldering chips to the printed circuit boards

11.3 Original Paper - Doubling Throughput of a Real-Time PCR

SCIENTIFIC REPORTS

OPEN

Doubling Throughput of a Real-Time PCR

Christian D. Ahrberg[1] & Pavel Neužil[1,2,3]

Received: 14 September 2014
Accepted: 03 July 2015
Published: 27 July 2015

The invention of polymerase chain reaction (PCR) in 1983 revolutionized many areas of science, due to its ability to multiply a number of copies of DNA sequences (known as amplicons). Here we report on a method to double the throughput of quantitative PCR which could be especially useful for PCR-based mass screening. We concurrently amplified two target genes using only single fluorescent dye. A FAM probe labelled olionucleotide was attached to a quencher for one amplicon while the second one was without a probe. The PCR was performed in the presence of the intercalating dye SYBR Green I. We collected the fluorescence amplitude at two points per PCR cycle, at the denaturation and extension steps. The signal at denaturation is related only to the amplicon with the FAM probe while the amplitude at the extension contained information from both amplicons. We thus detected two genes within the same well using a single fluorescent channel. Any commercial real-time PCR systems can use this method doubling the number of detected genes. The method can be used for absolute quantification of DNA using a known concentration of housekeeping gene at one fluorescent channel.

The first demonstration of polymerase chain reaction (PCR) in 1983 is considered one of the greatest scientific achievements of the 20th century[1]. It revolutionized many areas of science, due to its ability to multiply a number of copies of DNA sequences (known as amplicons), using either DNA directly or complementary DNA after reverse transcription from RNA. The PCR cocktail called master mix contains free nucleotides, sets of primers and other compounds, besides the polymerase enzyme. The primers are short DNA sequences, one complementary to the DNA strand of interest in a forward direction and the second one complementary in reverse. The classic PCR method required the employment of a post-processing step such as electrophoresis or hybridization to verify the presence and purity of an amplicon.

A few years after the first PCR demonstration, a fluorescent marker was added to the PCR mixture to monitor the reaction in real time[2]. It also allows the determination of an initial DNA concentration. Thus, this method is often called a quantitative PCR (qPCR). The most popular qPCR is based on intercalating dyes, such as SYBR Green I. The dye produces its fluorescence only in the presence of double-stranded DNA. Thus, researchers can monitor the concentration of amplicons. Another outcome of this method is the melting curve analysis (MCA), typically conducted once the PCR is completed. The sample is slowly warmed up while its fluorescence is monitored. At elevated temperatures, the double stranded DNA amplicons start to convert to single stranded (melt) and consequently the amplitude of the fluorescence drops. When half of the DNA melts from double stranded into single stranded, the temperature is called the melting temperature (T_M). It is characteristic of the DNA amplicon length and its sequence. The intercalating dye-based methods are frequently used as they are not specific to any particular DNA sequence.

Another popular qPCR method is based on a probe such as 6-carboxy-fluorescein (FAM)[3]. This probe has to be chemically bound to the oligonucleotides next to a quencher such as TAMRA or a black hole quencher. This PCR method is often called TaqMan or TaqMan chemistry[4]. Once the primers bind to the

[1]Kist-Europe, Saarbrücken, Saarland, 66123, Germany. [2]Central European Institute of Technology, Brno University of Technology, Technická 3058/10, CZ-616 00 Brno, Czech Republic. [3]Northwestern Polytechnical University, School of Mechanical Engineering, 127 West Youyi Road, Xi'an, Shaanxi, 710072, P.R.China. Correspondence and requests for materials should be addressed to P.N. (email: pavel.neuzil@gmail.com)

DNA template, the quencher typically gets separated from the fluorophore and its fluorescence amplitude increases. This method is gene specific but requires oligonucleotides to be synthesised with attached dye and a quencher. Fluorescence resonance energy transfer (FRET)-based methods are also popular[5].

A method to detect more than one target sequence in a single sample is called multiplexing. It offers significant advantages compared to single PCR, such as more information per reaction and therefore time saving. Applications for multiplex PCR can be found in food sciences[6], agricultural sciences[7] or in human medicine. In human medicine, the method is often used to determine ratios of housekeeping genes for normalization[8], assessing viral loads[9] or determining the species[10] or subspecies in bacterial[11] and viral infections[12]. Researchers used end-point multiplex detection to identify different amplicons by the differences in their melting temperature by MCA[13] in the presence of an intercalating dye[14]. This method requires amplicons with different melting temperature caused by different DNA lengths and sequences[15]. Alternatively, a gel electrophoresis can be performed after PCR to separate and detect the different DNA amplicons[16]. This method requires amplicons with different number of base pairs (length), resulting in different electrophoretic mobilities for each amplicon. Both methods are based on post-processing after PCR. Thus, they provide qualitative information as to whether the DNA sequence of interest was present or absent in the original sample. There is limited knowledge obtained about the quantity of DNA templates in the original sample.

The probe-based methods belong to the real-time PCR family. The results give quantitative information, thus also called quantitative PCR (qPCR). The most common approach is performing PCR with oligonucleotides attached to probes with different emission wavelengths and detect them using several fluorescence channels[17]. The number of genes identifiable per fluorescence channel can be further increased by creating colour codes[18] for the different genes and extracting information on amplicon concentrations via linear combinations on the individual fluorescence channels[19]. Theoretically, the number of genes concurrently detectable is unrestricted, but there are various limits imposed through the optical filter system required and through the dye assays. Selecting an appropriate probe for the assay also becomes increasingly difficult and assay costs increase with the number of used probes.

What will happen if TaqMan probes, such as FAM, and intercalating dyes, like SYBR Green I, are combined in the same experiment? One of the earliest work reports combination of TaqMan probe with emission in the FAM spectrum and the asymmetric cyanine dye BOXTO (TATAA)[20]. BOXTO has an emission maximum at 552 nm, thus requiring a different filter set from FAM to be detected. In their work, they combined the dyes to quantify and detect the gene of interest using the TaqMan dye. Once the PCR was completed, they performed melting curve analysis (MCA) to detect nonspecific product formation by monitoring the fluorescence signal from BOXTO.

A few years later, PCR was performed with a primer set labeled with TaqMan probes6-Carboxyl-X-Rhodamine (ROX) or diSulfo - Cy5 carboxylic acid (Cy5) in presence of SYBR Green I intercalating dye to detect polymorphism in *Mycobacterium (M) tuberculosis* culture[21]. Both those dyes have different fluorescent distinctively different excitation/emission wavelength from SYBR Green I thus different filters have to be used for detection of each dye. With this combination of dyes and using primer sets for two different amplicons, the authors got three possible Boolean outcomes after completing the PCR. They either got a signal from the TaqMan probe and the intercalating dye, a signal from the intercalating dye or no signal. In the first case, they could conclude that M. tuberculosis was present and the polymorphism had not occurred. In the second case, M. tuberculosis was present and the polymorphism did occurred and in the last case either M. tuberculosis was not present or the PCR failed. The Boolean approach described by authors allows specifying which of the two phenotypes is present, as long as there is no mixture of the two phenotypes. Both works[20,21] used different fluorescent channels to detect the probe and to detect the intercalating dye.

Recently, it was shown that two dyes with the same emission wavelengths could be combined[22]. Researchers used four different TaqMan probes labelled with FAM dye, phosphoramidite (HEX), Texas Red and Cy5 dyes combined with the intercalating dye SYBR Green I, which exhibits nearly identical excitation/emission spectra as FAM. They extracted quantitative data during the PCR from individual signals from TaqMan probes above the melting temperature of the amplicons to eliminate signal from the intercalating dye. Once the PCR was completed the MCA was performed to detect the unspecific amplification due to possible primer interactions.

In our approach, we take this idea one step further by measuring both the signal of the TaqMan probe as well as the combined signal of the TaqMan probe and intercalating dye during thermal cycling. This allows us to detect and quantify two different genes in the FAM fluorescent channel. We used primer sets for two different genes, a FAM based probe complementary to only one of the genes and SYBR Green I as an intercalating dye.

Both genes contributed to the total fluorescence amplitude in the presence of an intercalating dye such as SYBR Green I, as long as the temperature of the mixture was below the T_M. The FAM-labelled probe separated from the quencher also contributed to the total fluorescence. Once the temperature was increased above the $T_{M,}$ only FAM-based fluorescence contributed to the total fluorescence amplitude. We could then extract two amplification curves: the probe-based amplicon at the denaturation temperature (here called a denaturation curve) and the second one at the end of the extension step (here called an extension curve). This second amplification curve contains both DNA templates together. The concentration of the probe-linked amplicon is already known and can be subtracted from the extension curve,

Gene	Direction	Sequence
HPRT	Forward	5′-TGACCTTGATTTATTTTGCATACC-3′
HPRT	Reverse	5′-CGAGCAAGACGTTCAGTCCT-3′
GAPDH	Forward	5′-AGCCACATCGCTCAGACAC-3′
GAPDH	Reverse	5′-GCCAATACGACCAAATCC-3′
HA	Forward	5′-GGGACTCAACAATTATGAAAAGTGAA-3′
HA	Reverse	5′-GGGTGTATATTGTGGAATGGCAT-3′

Table 1. List of primers and their corresponding sequences.

Experiment Name	Concentration HPRT in ng/μl	Concentration GAPDH in ng/μl	Denaturation C_T	Extension C_T
1:0	6.25×10^{-7}	0	27.4	20.9
1:1	6.25×10^{-7}	6.25×10^{-7}	27.7	19.4
1:2	6.25×10^{-7}	12.5×10^{-7}	27.6	18.4
1:10	6.25×10^{-7}	6.25×10^{-6}	26.8	17.8
1:20	6.25×10^{-7}	12.5×10^{-6}	26.0	16.7

Table 2. Experiments with excess GAPDH and extracted threshold cycles (C_T).

resulting in the concentration of the second amplicon. We can then determine the threshold cycle (C_T) and via comparison with the PCR standard curve also the corresponding original template concentration of both DNAs. The major advantage of this method is the ability of simultaneous, quantitative detection of two DNA templates, using only a single fluorescent channel.

There are two mechanisms of fluorescence contributing to the extension curve: intercalating dye and the probe. The amplitude of this composite fluorescent signal always has to be higher than the one originating only from TaqMan probe extracted at the denaturation curve. Another reason why the signal originated from TaqMan probe is lower is its sensitivity to temperature. Its amplitude is inversely proportional to temperature and the denaturation curve is taken at 93 °C–95 °C, while the extension curve is captured at about 60 °C.

The method described above works even in extreme cases with one DNA template having significantly higher number of copies than the second one. Once the number of copies of the DNA linked to TaqMan probe is dominating the C_T value extracted from denaturation curve will be slightly higher than the C_T value extracted from extension curve. In the opposite case with non-TaqMan template number of DNA copies is dominating, the C_T extracted from the extension curve will be significantly lower than the corresponding C_T extracted from the denaturation curve. In both cases, the difference in both C_T determined the number of copies of the second DNA template.

We performed two sets of experiments. First, we used two common housekeeping genes: Glyceraldehyde 3-phosphate dehydrogenase (GAPDH) and hypoxanthine-guanine phosphoribosyltransferase (HPRT). The results could be used to calculate a normalization factor by method shown earlier[8,23–25].

In the second experiment, we determined a viral load in the sample of haemagglutinin (HA) with both HPRT and GAPDH as housekeeping genes[26].

Material and Methods

Experiments. Synthetic DNA templates for GAPDH, HPRT and HA (ATG Biosynthetics) were used for the experiments. The primers were designed using Roche Universal Probe Library Assay Design Center and purchased from Eurofins MWG Operon (Table 1). Universal probe #73 (Roche Molecular Systems) was used as TaqMan probe corresponding to HPRT together with the Roche LightCycler TaqMan Master Mix. The reaction mixture consisted of 4 μL master mix, 1 μL of SYBR Green I 10,000 x solution (Lonza) diluted by a factor of 500. The primers and probe were added with concentrations of 1.8 μM and 200 nM, respectively. A sample template was then pipetted in and the mixture volume was increased up to 20 μL by adding de-ionized water produced by a Milli-Q ProgradT3 (Millipore) column after autoclaving. Data collection and thermal cycling were done by Roche LightCycler Carousel-Based system using a temperature profile according to the master mix specifications. We used continuous fluorescence measurement mode to capture the data. The measurement can be simplified by collecting fluorescence amplitude data only at the end of the extension and denaturation step with the same quality of results.

Experiment Name	Concentration HPRT in ng/μl	Concentration HA in ng/μl	Denaturation C_T	Extension C_T
1:0	6.25×10^{-7}	0	26.5	21.3
1:1	6.25×10^{-7}	6.25×10^{-7}	26.3	19.3
1:2	6.25×10^{-7}	12.5×10^{-7}	26.2	18.2
1:10	6.25×10^{-7}	6.25×10^{-6}	26.3	17.9
1:20	6.25×10^{-7}	12.5×10^{-6}	24.9	15.8

Table 3. Experiments with excess HA and extracted threshold cycles (C_T).

Experiment Name	Concentration HPRT in ng/μl	Concentration GAPDH in ng/μl	Denaturation C_T	Extension C_T
1:1	6.25×10^{-7}	6.25×10^{-7}	29.0	18.2
2:1	12.5×10^{-7}	6.25×10^{-7}	26.4	18.2
10:1	6.25×10^{-6}	6.25×10^{-7}	24.0	17.0
20:1	12.5×10^{-6}	6.25×10^{-7}	22.6	16.3
100:1	6.25×10^{-5}	6.25×10^{-7}	20.4	13.9

Table 4. Experiments with excess HPRT and extracted threshold cycles (C_T).

Experiment Name	Concentration HPRT in ng/μl	Concentration HA in ng/μl	Denaturation C_T	Extension C_T
1:1	6.25×10^{-7}	6.25×10^{-7}	28.6	19.2
2:1	12.5×10^{-7}	6.25×10^{-7}	26.3	18.3
10:1	6.25×10^{-6}	6.25×10^{-7}	23.3	16.6
20:1	12.5×10^{-6}	6.25×10^{-7}	22.7	15.9
100:1	6.25×10^{-5}	6.25×10^{-7}	19.6	14.1

Table 5. Experiments with excess HPRT and extracted threshold cycles (C_T).

Standard curves were recorded in two sets of experiments. In the first set, the concentration of the TaqMan gene was constant while the concentration of non-TaqMan gene was varied (Tables 2 and 3). In the second experiment set concentration of non-TaqMan gene was constant while the TaqMan gene concentration was varied (Tables 4 and 5).

Lastly, an experiment was conducted to determine the concentration of both genes in the presence of a third one. The sample contained HPRT with concentrations of 3.1×10^{-7} ng/μl, GAPDH with a concentration of 3.1×10^{-6} ng/μl and HA with a concentration of 6.25×10^{-6} ng/μl. We only used two primers at a time, either HPRT and GAPDH primers or HPRT and HA primers. A second sample with the concentrations of 1.6×10^{-7} ng/μl HPRT, 6.25×10^{-6} ng/μl GAPDH and 1.6×10^{-5} ng/μl HA was also tested in the same manner.

Data Analysis. We captured all fluorescent data during the entire PCR protocol (see Fig. 1A) and processed them in Matlab, a numerical computing software. We extracted data from Roche LightCycler in two blocks, temperature as a function of time and fluorescence as a function of time. We then used temperature data to determine the beginning of each cycle. Next, we extracted fluorescence amplitude during denaturation and extension steps for each cycle. Each point was formed as a mean from the last five fluorescence measurements in the step. This data processing resulted in two amplification curve denaturations and extensions as a function of cycle number.

We defined the cycle threshold (C_T) as a value of the cycle number when fluorescence amplitude is equal to the background mean (from first 10 cycles) plus five times the standard deviation of the average. We calculated the C_T values for both curves for denaturation as well as extension. As the last step of data processing, both amplification curves were normalized by subtracting the initial fluorescence signal and then dividing all numbers by the fluorescence amplitude. We also performed MCA (see Fig. 1B).

Concentrations were determined by performing PCR with different template concentrations by creating standard curves.

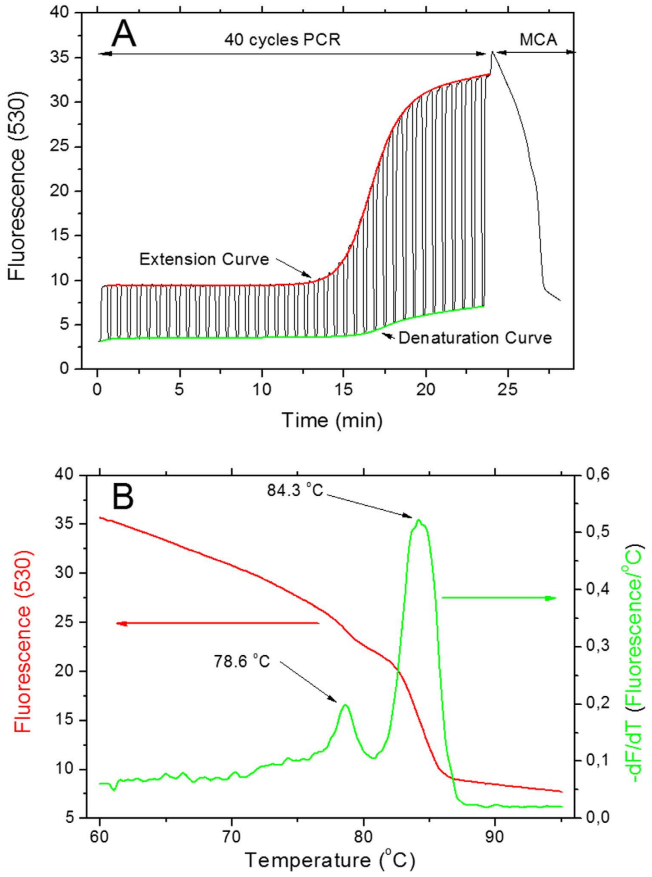

Figure 1. (**A**) A typical data set with both amplification curves extracted from a 40-cycle PCR. The fluorescence amplitude recorded at the end of the extension (red) and denaturation (green) step are shown here. The normalized amplification curves are shown as inset. At the end of the PCR we performed the MCA. (**B**) The results of the MCA analysis showing DNA templates with two different melting temperatures, 78.6 °C and 84.3 °C.

Results

The captured data from PCR with different DNA template concentrations are shown in process in Fig. 2. Normalized PCR amplification curves are shown in Fig. 3. As an example, we performed an experiment with a constant concentration of HPRT and a varied concentration of GAPDH.

Non-TaqMan Gene in excess. *Housekeeping genes.* First, we kept the TaqMan gene (HPRT) concentration constant while the concentration of GAPDH gene was varied. The C_T values extracted from denaturation curves remained constant, as shown in Fig. 4A. The C_T values extracted from the extension curves decreased with increasing concentration of the non-TaqMan gene (GAPDH).

Viral load. Second, we also kept the TaqMan gene (HPRT) concentration constant while we varied concentration of cDNA of HA gene. The C_T values extracted from denaturation curves again remained constant as shown in Fig. 4B and the C_T values extracted from the extension curves decreased with increasing concentration of the non-TaqMan gene (HA).

TaqMan Gene in excess. *Housekeeping genes.* In the two experiments we conducted, the TaqMan gene is in higher concentrations than the non-TaqMan gene. Figure 4C shows the results of experiments using a varied concentration of the HPRT (TaqMan gene) and using a constant concentration of the GAPDH (non-TaqMan gene). The extracted C_T values from the denaturation and extension curves both decreases with an increasing HPRT concentration. However, the rate of change of the C_T values extracted from the denaturation curve is higher than the one from the extension curve. Quantitative information on both genes can be determined from the difference between both curves at a particular total DNA concentration.

Viral load. As for the housekeeping gene, we have varied concentration of HPRT (TaqMan gene) and constant concentration of HA (non-TaqMan gene). The results (see Fig. 4D) are similar to the previous ones.

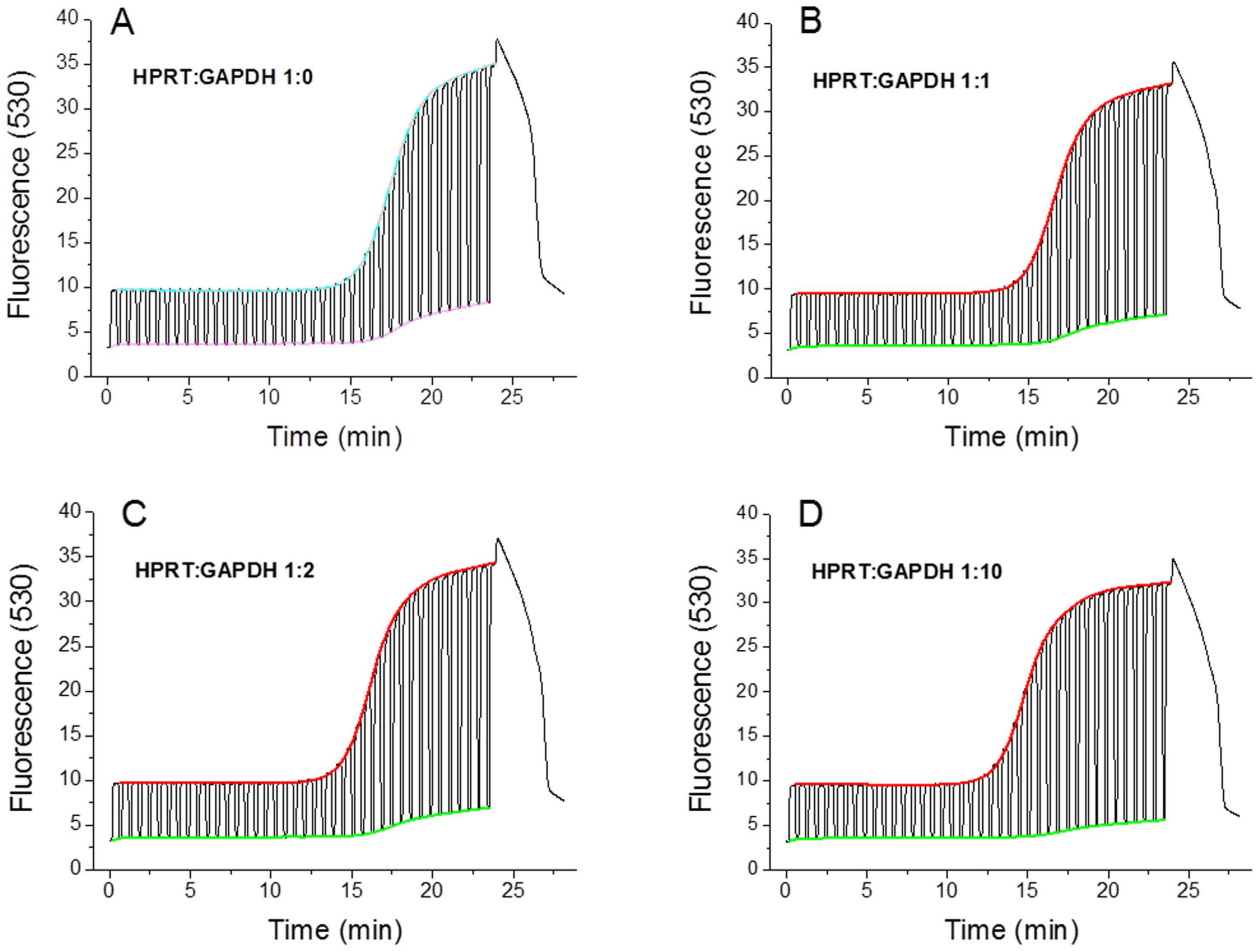

Figure 2. Raw fluorescence data from LightCycler for experiments with different ratios between HPRT and GAPDH genes. (**A**) Shows HPRT gene alone, (**B**) ratio 1:1, (**C**) ratio 1:2 and (**D**) ratio 1:10. We extracted both denaturation (green) and extension (red) curves from all graphs. No template control (NTC) expressed no amplification and its average fluorescence amplitude was 0.113 with a standard deviation of 0.002.

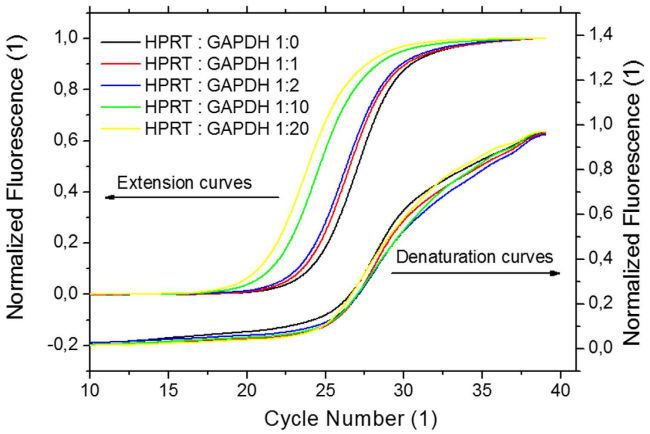

Figure 3. (left axis) Extracted normalized extension curves. The curves' amplitude was divided by its maximum amplitude and the slope was also subtracted for easier curve to curve comparison. (right axis) The normalized denaturation curves. The normalization was done in a similar fashion as for extension curves.

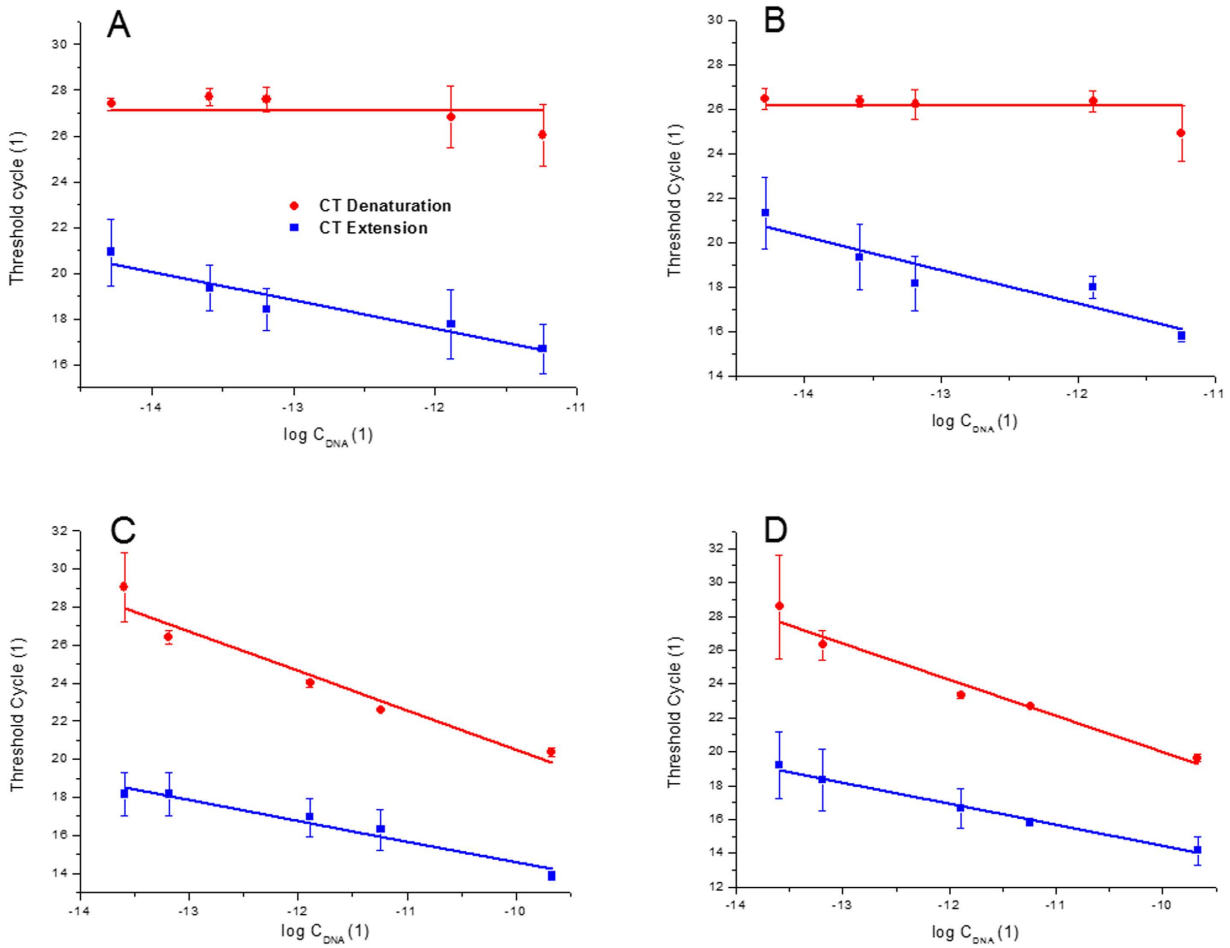

Figure 4. Extracted threshold cycles (C_T) for experiments with fixed concentration of either HPRT (A,B), GAPDH (C) or HA (D) genes and varying concentrations of GAPDH (A) HA (B) or HPRT (C,D). Each experiment was repeated three times. The varied concentration was calculated by subtracting the constant value of concentration (6.25×10^{-7} ng/μL) from the total DNA concentration. The red circles correspond to CT extracted from the denaturation curves while the blue squares from the extension curves.

Typical determination of DNA template concentrations. A C_T value extracted from denaturation curve in the first sample had an amplitude of 26.9. It corresponded only to the concentration of the HPRT gene. A C_T value was also extracted from two extension curves, one with primers for the GAPDH gene ($C_T = 18.1$) and one with primers for the HA gene ($C_T = 17.5$). Those three C_T values corresponded to a concentration of 6.25×10^{-7} for HPRT, 3.49×10^{-6} ng/μl for GAPDH and 4.52×10^{-6} ng/μl for HA.

The C_T values extracted from the second sample gave an amplitude of 26.5 for HPRT, 18.4 for GAPDH and 16.8 for HA. Those C_T values corresponded to a concentration of 6.25×10^{-7} ng/μl for HPRT, 2.61×10^{-6} ng/μl for GAPDH and 7.55×10^{-6} ng/μl for HA.

Discussion

The ability to perform quantitative multiplexed PCR is of particular interest for a number of applications. Typically, it is performed by probe-based PCR with a number of probes using specific dyes and with corresponding fluorescent channels for each dye. Here, we have demonstrated a novel method enabling the simultaneous detection of two DNA templates, using only a single fluorescent channel.

We combined a FAM type of TaqMan probe for the first DNA template with an intercalating dye for the second DNA template. We recorded a continuous fluorescence signal for 40-cycle PCR protocol, followed by MCA. From the fluorescent signal, we extracted two amplification curves. One was at the end of the denaturation step corresponding only to the TaqMan probe and the second one was at the end of the extension step. The second curve consisted of information from both genes. We then subtracted a TaqMan probe-based data from the second curve resulting in only the non-TaqMan template amplification curve. This extraction was conducted by a script in Matlab. The possibility of detecting and quantifying more than two genes was demonstrated by running several experiments with different primers within the same sample.

An easy way of extracting information on the concentration ratio between two or more genes was demonstrated based on the PCR standard curve. The method feasibility was demonstrated for a concentration difference of up to four orders of magnitude. Results with higher concentration differences are most likely hindered by the depletion of the master mix due to the amplification of one gene.

This method can be implemented for DNA template quantification using TaqMan probe-based gene with a known concentration as the internal standard. In such a case, the standard PCR curve would not be required.

Examples for this can be seen in the experiments in which the concentrations of the three genes were determined. The concentration of the TaqMan gene was the same as for the standard curves in the first sample, This and the fact that the all concentrations were within one order of magnitude allowed a relatively accurate determination of the concentrations of all genes. In the second sample, the concentration of the TaqMan gene deviated significantly from the standard curves. Furthermore, the difference in concentrations between the genes was more than two orders of magnitude. Because of this, the estimate of concentrations became less accurate.

The described method might an option to increase the number of detected genes concurrently without expanding the number of fluorescent channels of commercial real-time PCR devices. Even here, we only tested a single tube, and an identical experiment could be done in all 96 wells of a standard plate system to expand into the detection of 192 genes, 384 into 768 and 1536 into 3072. Furthermore, the method could also be further optimized by research into the binding properties of the intercalating dyes.

In this contribution, the C_T values were extracted from a continuous fluorescent signal. Identical information can be also extracted from only two measurement points during each amplification cycle, at the end of the denaturation step and at the end of the extension step. This way, practically any commercial real-time PCR system is capable of doubling the throughput by performing the multiplexing described in this contribution.

References

1. Saiki, R. *et al.* Enzymatic amplification of beta-globin genomic sequences and restriction site analysis for diagnosis of sickle cell anemia. *Science* **230,** 1350–1354 (1985).
2. Higuchi, R., Fockler, C., Dollinger, G. & Watson, R. Kinetic PCR Analysis: Real-time Monitoring of DNA Amplification Reactions. *Nat Biotech* **11,** 1026–1030 (1993).
3. Witham, P. K., Yamashiro, C. T., Livak, K. J. & Batt, C. A. A PCR-based assay for the detection of Escherichia coli Shiga-like toxin genes in ground beef. *Applied and environmental microbiology* **62,** 1347–1353 (1996).
4. Holland, P. M., Abramson, R. D., Watson, R. & Gelfand, D. H. Detection of Specific Polymerase Chain-Reaction Product by Utilizing the 5′-]3′ Exonuclease Activity of Thermus-Aquaticus DNA-Polymerase. *P Natl Acad Sci USA* **88,** 7276–7280 (1991).
5. Andrus, A. *et al.* High-throughput synthesis of functionalized oligonucleotides. *Nucleic acids symposium series*, 317–318 (1997).
6. Safdar, M. & Abasiyanik, M. F. Simultaneous identification of pork and poultry origins in pet foods by a quick multiplex real-time PCR assay using EvaGreen florescence dye. *Applied biochemistry and biotechnology* **171,** 1855–1864 (2013).
7. Abd-Elmagid, A. *et al.* Discriminatory simplex and multiplex PCR for four species of the genus Sclerotinia. *Journal of Microbiological Methods* **92,** 293–300 (2013).
8. Vandesompele, J. *et al.* Accurate normalization of real-time quantitative RT-PCR data by geometric averaging of multiple internal control genes. *Genome biology* **3,** research0034 (2002).
9. Osman, F., Hodzic, E., Omanska-Klusek, A., Olineka, T. & Rowhani, A. Development and validation of a multiplex quantitative PCR assay for the rapid detection of Grapevine virus A, B and D. *Journal of Virological Methods* **194,** 138–145 (2013).
10. Kim, Y. *et al.* A Simple and Efficient Multiplex PCR Assay for the Identification of Mycobacterium Genus and Mycobacterium tuberculosis Complex to the Species Level. *Yonsei Med J* **54,** 1220–1226 (2013).
11. Mehrabadi, J. F., Morsali, P., Nejad, H. R. & Imani Fooladi, A. A. Detection of toxigenic Vibrio cholerae with new multiplex PCR. *Journal of infection and public health* **5,** 263–267 (2012).
12. Lo, C. L. *et al.* One-step rapid reverse transcription-PCR assay for detecting and typing dengue viruses with GC tail and induced fluorescence resonance energy transfer techniques for melting temperature and color multiplexing. *Clinical chemistry* **53,** 594–599 (2007).
13. Bohling, S. D., King, T. C., Wittwer, C. T. & Elenitoba-Johnson, K. S. Rapid simultaneous amplification and detection of the MBR/JH chromosomal translocation by fluorescence melting curve analysis. *The American journal of pathology* **154,** 97–103 (1999).
14. Safdar, M. & Abasıyanık, M. F. Simultaneous Identification of Pork and Poultry Origins in Pet Foods by a Quick Multiplex Real-Time PCR Assay Using EvaGreen Florescence Dye. *Applied biochemistry and biotechnology* **171,** 1855–1864 (2013).
15. Gudnason, H., Dufva, M., Bang, D. D. & Wolff, A. Comparison of multiple DNA dyes for real-time PCR: effects of dye concentration and sequence composition on DNA amplification and melting temperature. *Nucleic Acids Research* **35,** e127 (2007).
16. Noorani, M. S. *et al.* Simultaneous detection and identification of four cherry viruses by two step multiplex RT-PCR with an internal control of plant nad5 mRNA. *Journal of Virological Methods* **193,** 103–107 (2013).
17. Huang, Q. *et al.* Multicolor Combinatorial Probe Coding for Real-Time PCR. *PLoS ONE* **6,** e16033 (2011).
18. Nazarenko, I. *et al.* Multiplex quantitative PCR using self-quenched primers labeled with a single fluorophore. *Nucleic Acids Res* **30,** e37 (2002).
19. Rajagopal, A., Scherer, A., Homyk, A. & Kartalov, E. Supercolor Coding Methods for Large-Scale Multiplexing of Biochemical Assays. *Analytical Chemistry* **85,** 7629–7636 (2013).
20. Lind, K., Stahlberg, A., Zoric, N. & Kubista, M. Combining sequence-specific probes and DNA binding dyes in real-time PCR for specific nucleic acid quantification and melting curve analysis. *BioTechniques* **40,** 315–319 (2006).
21. Cheah, E. S. *et al.* A two-tube combined TaqMan/SYBR Green assay to identify mycobacteria and detect single global lineage-defining polymorphisms in Mycobacterium tuberculosis. *J Mol Diagn* **12,** 250–256 (2010).
22. Van Poucke, M., Van Zeveren, A. & Peelman, L. J. [Letter to the editor] Combined FAM-labeled TaqMan probe detection and SYBR green I melting curve analysis in multiprobe qPCR genotyping assays. *BioTechniques* 52, 81–86 (2012).
23. Rienzo, M. *et al.* Identification of valid reference housekeeping genes for gene expression analysis in tumor neovascularization studies. *Clin Transl Oncol* **15,** 211–218 (2013).

24. Tan, S. *et al.* Identification of valid housekeeping genes for quantitative RT-PCR analysis of cardiosphere-derived cells preconditioned under hypoxia or with prolyl-4-hydroxylase inhibitors. *Mol Biol Rep* **39,** 4857–4867 (2012).
25. Moniotte, S. *et al.* Real-time RT-PCR for the Detection of Beta-adrenoceptor Messenger RNAs in Small Human Endomyocardial Biopsies. *Journal of Molecular and Cellular Cardiology* **33,** 2121–2133 (2001).
26. Ward, C. L. *et al.* Design and performance testing of quantitative real time PCR assays for influenza A and B viral load measurement. *Journal of Clinical Virology* **29,** 179–188 (2004).

Acknowledgements

We would like to thank Dr. Philip Day and Elaheh Shekaramiz for their support with assay selection and primer design. P. Neužil acknowledges partial support by Central European Institute of Technology (CEITEC), grant number CZ.1.05/1.1.00/02.0068.

Author Contributions

C.A. came with the idea of combining probe and intercallating dye, prepared all chemicals conducted the experiment and extracted data. P.N. prepared figures and wrote the main manuscript text. Both authors reviewed the manuscript.

Additional Information

Competing financial interests: The authors declare no competing financial interests.

How to cite this article: Ahrberg, C. D. and Neužil, P. Doubling Throughput of a Real-Time PCR. *Sci. Rep.* **5**, 12595; doi: 10.1038/srep12595 (2015).

11.4 Original Paper - Single Fluorescence Channel-based Multiplex Detection of Avian Influenza Virus by Quantitative PCR with Intercalating Dye

SCIENTIFIC REPORTS

OPEN

Single Fluorescence Channel-based Multiplex Detection of Avian Influenza Virus by Quantitative PCR with Intercalating Dye

Received: 21 January 2015
Accepted: 30 March 2015
Published: 19 June 2015

Christian D. Ahberg[1], Andreas Manz[1] & Pavel Neuzil[1,2,3]

Since its invention in 1985 the polymerase chain reaction (PCR) has become a well-established method for amplification and detection of segments of double-stranded DNA. Incorporation of fluorogenic probe or DNA intercalating dyes (such as SYBR Green) into the PCR mixture allowed real-time reaction monitoring and extraction of quantitative information (qPCR). Probes with different excitation spectra enable multiplex qPCR of several DNA segments using multi-channel optical detection systems. Here we show multiplex qPCR using an economical EvaGreen-based system with single optical channel detection. Previously reported non quantitative multiplex real-time PCR techniques based on intercalating dyes were conducted once the PCR is completed by performing melting curve analysis (MCA). The technique presented in this paper is both qualitative and quantitative as it provides information about the presence of multiple DNA strands as well as the number of starting copies in the tested sample. Besides important internal control, multiplex qPCR also allows detecting concentrations of more than one DNA strand within the same sample. Detection of the avian influenza virus H7N9 by PCR is a well established method. Multiplex qPCR greatly enhances its specificity as it is capable of distinguishing both haemagglutinin (HA) and neuraminidase (NA) genes as well as their ratio.

The influenza A virus is composed of eight RNA segments of negative-sense single-stranded RNA where segment 4 encodes the haemagglutinin (HA) gene, and segment 6 the neuraminidase (NA) gene. In order to increase specificity of H7N9 detection, besides the detection of the virus itself, one should also detect both HA and NA individually as well as their ratio. PCR is the method of choice to detect the virus as it can deliver results in tens of minutes compared to traditional methods such as ELISA where the testing takes a few days.

The polymerase chain reaction (PCR) was invented in 1985[1,2] to amplify double stranded DNA segments. Adding fluorogenic probe or DNA intercalating dyes (such as SYBR Green) allowed real-time[3] reaction progress monitoring and extracting of quantitative information (qPCR)[4,5]. A typical PCR process consists of three steps conducted at different temperatures: denaturation at 95 °C, annealing at 50–60 °C and extension at 72 °C. Using the Taqman probe-based PCR system the annealing and extension steps are combined into one and performed at a temperature of about 60 °C[5]. The presence of end-point PCR products can be confirmed by agarose gel electrophoresis or by capillary electrophoresis (CE)[6]. However, an end-point measurement does not necessarily correlate with the original number of copies of the amplified DNA sequence. Real-time PCR allows precise quantitative information to be extracted from the exponential phase of the reaction[4,7]. The Taqman probe-based assay format, for example the FAM™ (fluorophore) and TAMRA™ (quencher) labeled probe, is specific to its target gene, whereas the

[1]Kist-Europe, Campus E7.1, Saarbruecken, Germany D-66123. [2]Brno University of Technology, Technická 10, Brno, Czech Republic. [3]Institute of Bioengineering and Nanotechnology, 31 Biopolis Way, The Nanos, #04-01, 138669 Singapore. Correspondence and requests for materials should be addressed to P.N. (email: pavel.neuzil@gmail.com)

SYBR Green-based format is non-specific. To determine the specificity of the PCR products using SYBR Green, a subsequent melting curve analysis[8] (MCA) has to be implemented. MCA is often preferred over CE as it is performed in the PCR system immediately once the PCR is completed by sweeping samples' temperature while monitoring amplitude of fluorescence and thus no sample manipulation is required.

Multiplex quantitative PCR (qPCR) methods based on Taqman probes as well as FRET-based systems have been demonstrated[9]. Currently, it is routinely done with probes, such as the popular FITC, JOEL, ROX and Cy5, using multiple optical channels. Each channel requires its corresponding light source, filter set and a detector. Can multiplex qPCR be conducted in one channel, while demultiplexing the results in real-time? Probe-based systems cannot be used as there is no technique capable of distinguishing the PCR products in a real time. On the other hand intercalating dye based PCR has shown promising results as the products can be demultiplexed using melting curve analysis (MCA) once the PCR is completed[10]. However, this method can determine serotype of the DNA or RNA but does not provide quantitative information. Continuous monitoring of the amplitude of the fluorescent signal is a powerful technique with a number of different applications[11]. One of them was product differentiation during PCR where a number of MCAs were performed individually after several thermal cycles of PCR[12].

In this contribution we propose and demonstrate a method to dynamically extract melting curves within each thermal cycle of a real-time PCR based on a single intercalating dye. This was accomplished by processing captured data without changing the PCR protocol, resulting in a set of 40 MCAs. From this set we were able to demultiplex quantitative data for different segments of DNA. The proposed method allows multiplex internal positive controls using a single intercalating dye and is an alternative for probe based systems used to detect HA to NA gene ratios. It employs only a single fluorescent optical channel.

Typical MCA for intercalating dye-based PCR is performed by scanning the temperature of the sample at the rate of 1 °C/s or lower while recording the corresponding amplitude of fluorescence signal. The slow scanning rate is an important factor as every system with temperature control such as PCR exhibits a delay between temperature at the sensor and the sample. PCR systems can have a delay as long as a few seconds or more which is why slow temperature scanning for precise determination of a melting curve is essential.

During PCR the sample is cycled between different temperatures. Especially interesting is the transition from extension to denaturation as it covers the range of expected melting temperatures. All that is needed, then, is to detect the fluorescence amplitude from the sample and determine the corresponding temperature during this phase.

The first task has been demonstrated earlier by continuous fluorescence monitoring during the PCR cycling[11]. However the precise temperature monitoring of the sample during temperature transitions is not straightforward as there is discrepancy between sample and heater temperature as explained above. Is there another way to monitor actual sample temperature during ramping from annealing step to denaturation step?

We believe there is a method to measure the sample temperature with high precision. This temperature is given by a thermal control system typically using proportional integrated derivative (PID) method of feedback, the thermal mass of the sample H and the thermal conductance G between the heating block and the sample. The time constant τ of the temperature delay is given by $\tau = H/G$. Values of H, G and PID constants do not change during the PCR process so the temperature profile of the sample is a repetitive function of time during the PCR cycling. This implies that it is sufficient to determine the temperature profile of the sample only during a single cycle. We have used a modified version (see Fig. 1) of the virtual reaction chamber (VRC) system for this experiment[13]. The heat transfer and the sample temperature profile was simulated by finite element analysis (FEA) and the results were experimentally verified[14]. The model gave us a correlation between the temperature of the heater and the sample during transition from annealing step to denaturation step required for the MCA extraction. The real sample experiment exhibited faster response than the model probably due to convection in the aqueous sample decreasing the temperature gradient minimally in the transition period. This also provided a homogenous temperature distribution, crucial to the method, since it suppresses data smearing.

Here we introduce a method of multiplex qPCR using a single fluorescence channel in the presence of Eva-Green intercalator. It is based on recording both temperature T and fluorescence F as a function of time t and cycle number n. From both functions [$F = f(t,n)$ and $T = f(t,n)$] we have then eliminated time and generated fluorescence as function of temperature [$F = f(T,n)$] with PCR cycle number as a parameter. We have thus performed a melting curve analysis (MCA) during each PCR cycle. Subsequently we plotted the first negative derivative of fluorescence with respect to temperature as a function of temperature $-dF/dT = f(T)$. For each amplicon a distinct melting temperature was obtained, with its amplitude corresponding to its concentration at each cycle. PCR amplification curves were then created by plotting the amplitude of the respective amplicon as function of cycle number. This way we can quantitatively detect one or more different amplicons using only a single intercalating dye. We only need to perform continuous fluorescence detection at an acquisition rate at or above 1 kHz, thus conventional reagents and protocols can be still used.

The only prerequisite for the methods are a high enough data acquisition rate of fluorescence amplitude, a small sample volume and a sufficiently large difference in melting temperature of the genes for differentiation.

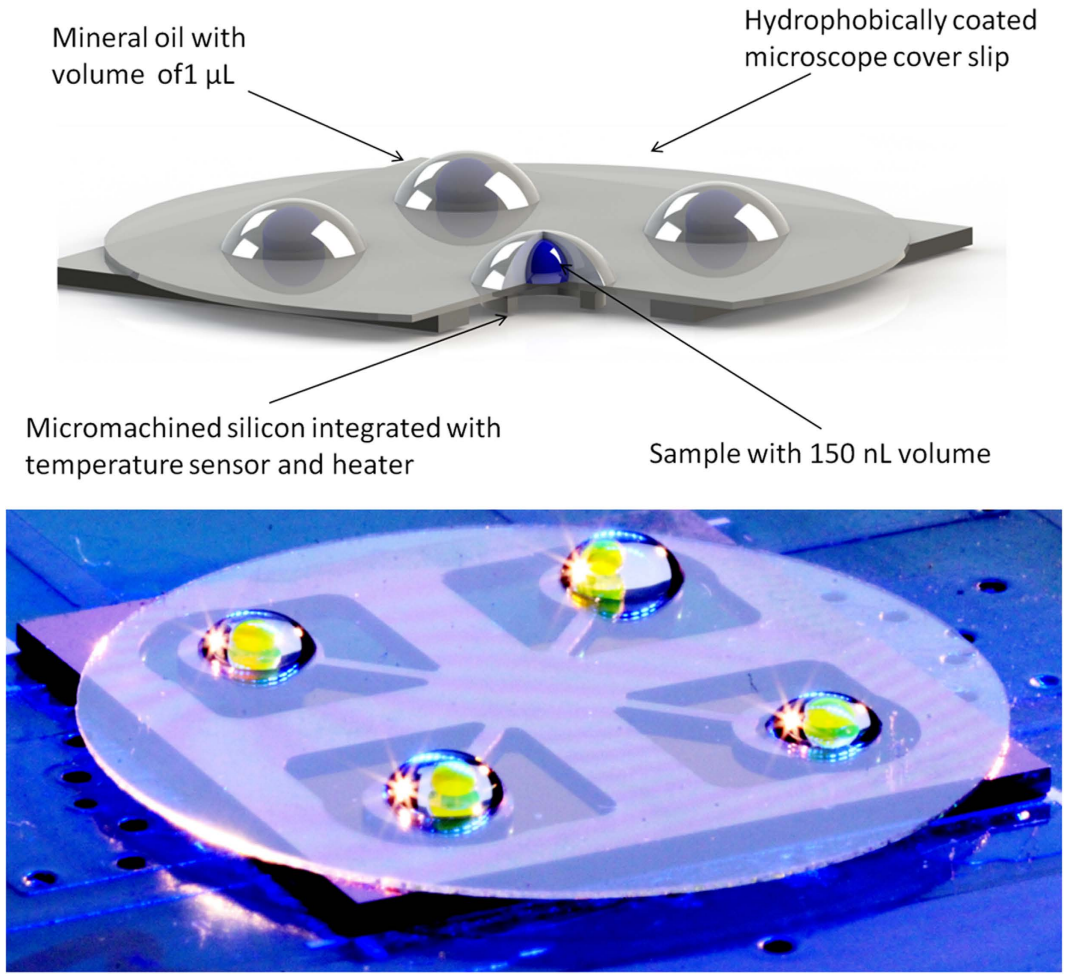

Figure 1. (**A**) Schematic diagram of the sample and heater. (**B**) Photograph of four VRCs on silicon chip with sample replaced with fluorescein solution for visualization purpose.

Target gene	Primer name	Primer sequence (5'-3')	Primer size (bp)	Amplicon size (bp)
H7N9 HA	HA-Forward	TACAGGGAAGAGGCAATGCA	20	103
	HA-Reverse	AACATGATGCCCCGAAGCTA	20	
H7N9 NA	NA Forward	CCAGTATCGCGCCCTGATA	19	70
	NA Reverse	GCATTCCACCCTGCTGTTGT	20	

Table 1. Primers used in this study.

Materials and Methods

Preparation of PCR mixture and thermal cycling. PCR mixture consisted of 6µL Roche LightCycler TaqMan Master Mix (Roche Diagnostics, Germany), 1µL 20X EvaGreen Dye in water (TATAA, Sweden) as well as forward and reverse primers[15] (Table 1)(MWG Eurofines, Germany) at a final concentration of 1.8µM. To this solution synthetic complementary DNA (cDNA) templates (ATG Biosynthesis, Germany) for haemagglutinin (HA) and neuraminidase (NA) for the avian influenza virus (H7N9) were added at different concentrations (see Table 1). Lastly the solution was adjusted to a volume of 20µL using water obtained from a Milli-Q PrograDT3 column (Millipore, Germany).

A droplet with a volume of 150 nL of the PCR solution was placed on a hydrophobically coated microscope glass cover slip and covered with 1.5µL of mineral oil 9405 (Sigma Aldrich, Germany) thus forming a VRC. This glass was then placed on a micromachined silicon chip integrated with both a heater and a sensor, similar to a design shown earlier[13]. Here the silicon chip has a size of only 15 × 15 mm to better fit a handheld PCR device we are developing (see Fig. 1). The small thermal mass of the VRC together with the silicon heater resulted in heating rates >20 °C/s and similar cooling rates achieved only

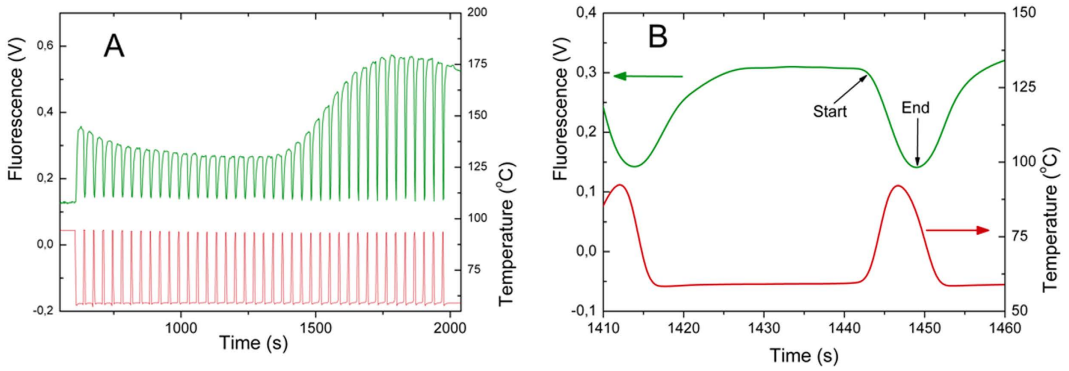

Figure 2. (**A**) Continuous fluorescence profile and corresponding temperature captured of entire PCR experiment. The 10 minutes of hot start is not completely shown, thermal cycling starts after 600 seconds. (**B**) Single PCR step number 23 showing fluorescence amplitude (green, left axis) and temperature (red, right axis). Start and end of data recording for MCA is shown by arrows.

by passive cooling. The PCR protocol consisted of a hot start for 10 min at 95 °C followed by 40 cycles each consisting of two steps, denaturation for 5 s at 95 °C and annealing/extension for 30 s at 60 °C.

Fluorescence amplitude was continuously monitored using an Axiotron II microscope (Zeiss, Germany). We have used a blue LED model M470L3-C4 LED with principal wavelength of 470 nm (Thorlabs, Germany) for excitation. The LED was powered with square wave pulses at a frequency of 2710 Hz and a duty cycle of 5%. Light from the LED as well as emitted light from the specimen was filtered with a filter set model 49002 - ET - EGFP (FITC/Cy2) (Chroma Optical Corp, USA). Emitted light was captured by a PMT photosensor module H10722-20 (Hamamatsu Photonics K.K., Germany). The PMT signal was processed by a lock-in amplifier 7230 DSP (Ametek, USA) and its output recorded by a digital oscilloscope model DPO 3014 (Tektronix, Germany) with data rate of 2500 measurements per second. The temperature of the PCR chip was also recorded by the oscilloscope at the same data rate.

For comparison, samples were also analyzed using the Roche LightCycler Carousel-Based system (Roche Diagnostics, Germany) followed by a standard melting curve after thermal cycling.

Data analysis. Captured fluorescence data were analyzed using a custom written Matlab-script. First the data were filtered by a fast Fourier transform filter (FFTF). Subsequently, the fluorescence signal was divided into the individual cycles based on the captured temperature profile. The fluorescence amplitude during transition from extension/annealing step to denaturation step was then extracted for each cycle and fluorescence as function of temperature was plotted with cycle number as a parameter. MCA was formed by numerical differentiation of the fluorescence with respect to temperature and its negative value was plotted as a function of temperature. The melting curve captured at the first cycle was subtracted from all melting curves to suppress a background fluorescence effect we have observed. This background fluorescence could be caused by autofluorescence from the adjacent printed circuit board as well as fluorescence of the temperature dependence of the fluorophore as well as unspecific binding of the dye onto single stranded DNA[16]. PCR amplification curves were created by plotting amplitudes at the MCA of each amplicon as a function of the cycle number.

Results and Discussion. We have run a 40 cycle PCR using the master mix manufacturer's specifications. A typical fluorescence profile was obtained (see Fig. 2A). In Fig. 2B we show the single cycle number 23 to demonstrate the extracted data for the MCA.

This procedure was applied to a sample containing only a single amplicon (HA) with melting temperature of 76 °C (see Fig. 3A,B). We have then added to the sample a second amplicon (NA) with a melting temperature of 68 °C. A second peak corresponding to this amplicon can be observed in the respective MCA (Fig. 3C,D). Increasing the amount of NA added compared to HA lead to an even faster increase of the magnitude of peak at 68 °C (Fig. 3E,F). Extracting the fluorescence amplitude from the derived curves for each cycle at 68 °C and 76 °C respectively, results in two PCR amplification curves. Figure 4A shows the two amplification curves extracted for the experiments with a higher concentration of NA than HA (experiments A1 to A5 in Table 2).

The sample spiked with the cDNA of the HA gene yielded only a single amplification curve with melting temperature of 76 °C, which was expected. For all other experiments we were able to extract two amplification curves, one at a temperature of 68 °C and the second one at temperature of 76 °C. Threshold cycles (C_T) were defined in the usual way. It was found that the difference in C_T (ΔC_T) of the two curves corresponded to the expected difference according to the ratio of concentrations of HA and NA. An overview of all conducted experiments is presented in Table 1. The results indicate that ΔC_T corresponds to the expected values. We can then conclude that the method can be used for multiplexed

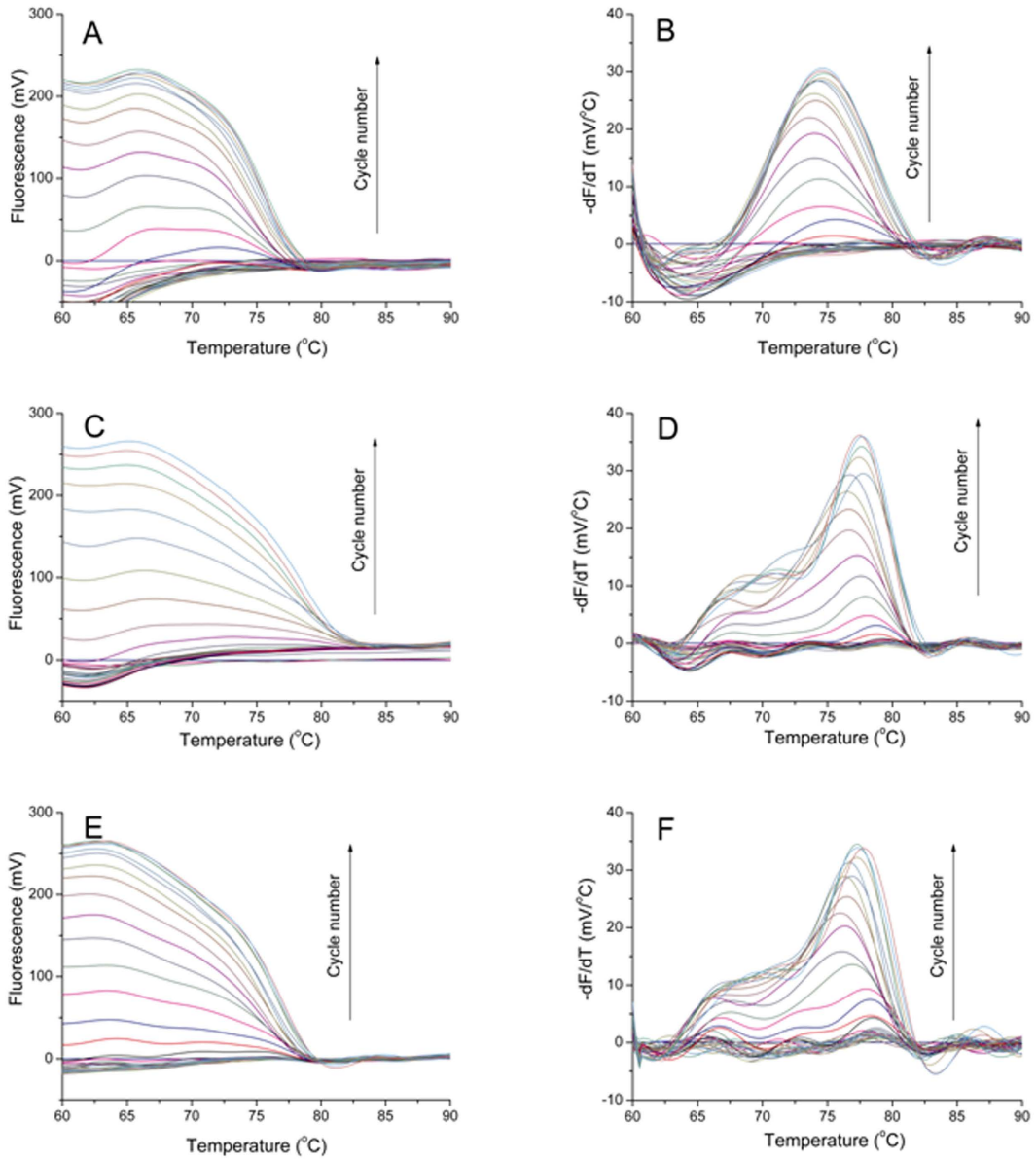

Figure 3. Melting curves (**A**, **C**, **E**) and corresponding to their first negative derivative (**B**, **D**, **F**) for all 40 cycles with cycle number as parameter. **A** and **B** are data from sample containing only HA. C and D are data from sample containing HA and twice more of NA. **E** and **F** are data from sample containing HA and ten times more NA.

quantitative PCR. As an example, (see Table 1) sample A5 has the concentration of NA 19 times higher than the concentration of HA. With 100% PCR efficiency one would expect a ΔC_T of 4.25 ($\log_2 19$). We have found the ΔC_T value to be 4.0 ± 0.4 which is efficiency of 84%, reasonably close to the ideal value.

We have observed MCA peak broadening in our experiment due to applied conditions. It is necessary to run several replicates of the same experiment to suppress random errors and improve the result precision. The MCAs are recorded at a scanning rate of over 20 °C/s while the commercial systems for high resolution melting curve analysis (HRMCA)[17] are usually operating with low temperature scan rates between 0.1 °C/s and 0.5 °C/s. Differentiation of amplicons with melting point differences ΔT_m as small as 1.2 °C have been demonstrated in HRMCA. However the method presented in this contribution requires greater ΔT_m due to peak broadening caused by the high heating rate.

We assume that a difference in amplicons melting temperatures' of at least 5 °C would be sufficient to differentiate them from each other. This could be achieved by primer design since the melting temperature is a function of amplicon length and ratio of CG/AT content. Therefore an extension temperature of 60 °C and a denaturation temperature of 95 °C would allow for 6 different amplicons to be detected in the same droplet, assuming a ΔT_m of 5 °C.

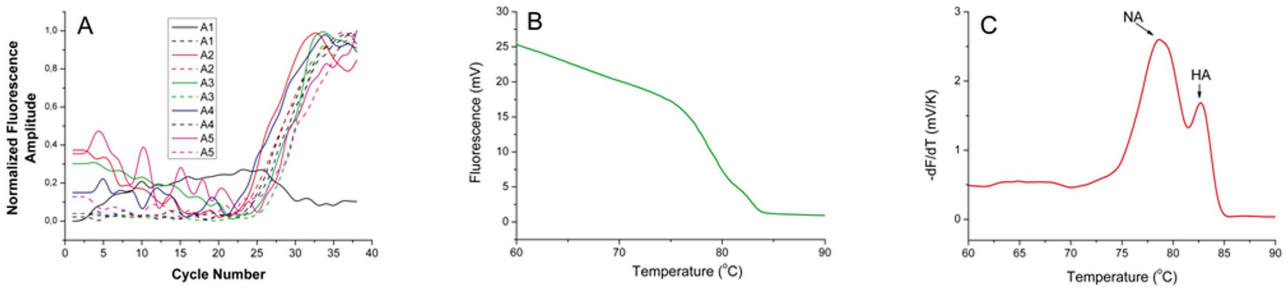

Figure 4. Amplification curves extracted for samples A1–A5 (referring to experiment codes in Table 2) at 68 °C (solid lines) and 76 °C (dashed lines). Sample A1 shows no amplification at 68 °C (black line) as expected (**A**), end point high resolution melting curve analysis of sample A2 after 40 cycles on the LightCycler (**B**–C)

Experiment Code	Concentration of HA (ng/μL)	Concentration of NA (ng/μL)	CT at 68 °C (NA)	CT at 76 °C (HA)	Difference between CT at 68 °C and 76 °C
A1	$1.0*10^{-07}$	0	—	22.5	—
A2	$5.0*10^{-07}$	$5.0*10^{-07}$	22.8	22.4	0.4 ± 0.3
A3	$3.2*10^{-07}$	$6.4*10^{-07}$	25.8	24.7	1.0 ± 0.5
A4	$9.0*10^{-08}$	$9.1*10^{-07}$	23.7	20.9	2.8 ± 0.3
A5	$5.0*10^{-08}$	$9.5*10^{-07}$	25.7	29.5	4.0 ± 0.4
B1	0	$1.0*10^{-07}$	27.5	—	—
B2	$5.0*10^{-07}$	$5.0*10^{-07}$	23.1	22.9	−0.1 ± 0.8
B3	$6.4*10^{-07}$	$3.2*10^{-07}$	23.4	24.6	−1.2 ± 0.1
B4	$9.1*10^{-07}$	$9.0*10^{-08}$	26.7	30.0	−3.3 ± 0.3
B5	**$9.5*10^{-07}$**	**$5.0*10^{-08}$**	**23.4**	**27.0**	**−3.5 ± 0.1**

Table 2. Overview of conducted experiments, found threshold cycles (CT) for both melting temperatures as well as the difference between both threshold cycles.

Furthermore, the temperature measured by the sensor in HRMCA corresponds practically to the sample temperature due to the slow scanning rate. In our approach the sample temperature lags behind the temperature measured by the sensor underneath the sample[18]. This can be seen from the comparative end point HRMCA done with the LightCycler, Fig. 4B shows the fluorescence amplitude plotted as function of temperature with a temperature gradient of 0.1 °C/s. In Fig. 4C the first negative derivative of this curve with respect to temperature is shown, displaying two distinct peaks. Both melting temperatures found on the LightCycler are 8 °C higher than the temperatures we measured in our system. Nevertheless this T_m offset has no influence on quality of the results especially when this lag is known and the resulting temperature offset is calibrated.

Ideally the test should be performed with a clinical sample containing H7N9 virus starting with sample preparation followed with reverse transcription. VRC-based RT-PCR demonstrating almost all those steps was shown earlier, detecting both RNA from H5N1 avian influenza virus[19] as well as from virus of severe acute respiratory syndrome (SARS)[20]. Processing clinical sample containing virus of avian influenza or SARS would also require laboratory classified as biosafety hazard level 3 which we do not have available. In previous work we developed the system based on spiking blood sample with RNA, here in this work we spiked PCR master mix with two types of cDNA.

Conclusions

We have developed a method for quantitative, multi target PCR using only a single intercalating dye and thus only one fluorescence channel. Our approach allows researchers to perform affordable multiplex PCR using simple tools as well as reagents. Another advantage compared to conventional methods is small consumption of reagents due to small sample volume. Fluorescent amplitude sampling at rate above 100 samples per second is, however, required for constructing MCA during transition from annealing/extension to denaturation. This method might be particularly interesting for determination of serotype of virus such as dengue fever or an avian influenza. Other potential applications include measurement of viral loads in a sample, differentiation between H7N9 and H7N5, and quantitative detection of co-infections. We have experimentally verified the method using a homemade PCR system primarily

for convenience as we have 100% control of the tool. In principle any commercial real-time PCR device would be capable of performing the same protocol as long as it has available fluorescent amplitude sampling rate of 1kHz or higher and can process samples with small volume of a 1 μL or below.

References

1. Saiki, R. K. *et al.* Enzymatic amplification of beta-globin genomic sequences and restriction site analysis for diagnosis of sickle cell anemia. *Science* **230,** 1350–1354 (1985).
2. Saiki, R. K. *et al.* Primer-directed enzymatic amplification of DNA with a thermostable DNA polymerase. *Science* **239,** 487–491 (1988).
3. Higuchi, R., Fockler, C., Dollinger, G. & Watson, R. Kinetic PCR analysis: real-time monitoring of DNA amplification reactions. *Biotechnology (N Y)* **11,** 1026–1030 (1993).
4. Lee, L. G., Connell, C. R. & Bloch, W. Allelic discrimination by nick-translation PCR with fluorogenic probes. *Nucleic acids research* **21,** 3761–3766 (1993).
5. Kubista, M. *et al.* The real-time polymerase chain reaction. *Molecular aspects of medicine* **27,** 95–125, doi: 10.1016/j.mam.2005.12.007 (2006).
6. Cheng, J., Shoffner, M. A., Mitchelson, K. R., Kricka, L. J. & Wilding, P. Analysis of ligase chain reaction products amplified in a silicon-glass chip using capillary electrophoresis. *Journal of chromatography. A* **732,** 151–158 (1996).
7. Huang, Q. *et al.* Multicolor combinatorial probe coding for real-time PCR. *PloS one* **6,** e16033, doi: 10.1371/journal.pone.0016033 (2011).
8. Fixman, M. & Freire, J. J. Theory of DNA melting curves. *Biopolymers* **16,** 2693–2704, doi: 10.1002/bip.1977.360161209 (1977).
9. Andersson, A. *et al.* Paired multiplex reverse-transcriptase polymerase chain reaction (PMRT-PCR) analysis as a rapid and accurate diagnostic tool for the detection of MLL fusion genes in hematologic malignancies. *Leukemia* **15,** 1293–1300 (2001).
10. Gubala, A. J. Multiplex real-time PCR detection of Vibrio cholerae. *Journal of microbiological methods* **65,** 278–293, doi: 10.1016/j.mimet.2005.07.017 (2006).
11. Wittwer, C. T., Herrmann, M. G., Moss, A. A. & Rasmussen, R. P. Continuous fluorescence monitoring of rapid cycle DNA amplification. *BioTechniques* **22,** 130–131, 134-138 (1997).
12. Ririe, K. M., Rasmussen, R. P. & Wittwer, C. T. Product differentiation by analysis of DNA melting curves during the polymerase chain reaction. *Analytical biochemistry* **245,** 154–160, doi: 10.1006/abio.1996.9916 (1997).
13. Neuzil, P., Pipper, J. & Hsieh, T. M. Disposable real-time microPCR device: lab-on-a-chip at a low cost. *Molecular bioSystems* **2,** 292–298, doi: 10.1039/b605957k (2006).
14. Neuzil, P., Karasek, K., Sun, W.-X. & Manz, A. Nanoliter-sized Overheated Reactor. *Applied Physics Letters* **106,** 024104, doi: 10.1063/1.4905851 (2015).
15. Corman, V. M. E. M., Landt, O., Bleicker, T., Brünink, S., Eschbach-Bludau, M., Matrosovich, M., Becker, S., Drosten, C. Specific detection by real-time reverse-transcription reaction assays of a novel avian influenza A(H7N9) strain associated with human spillover infections in China. *Euro Surveill.* **18** (2013).
16. Mao, F., Leung, W.-Y. & Xin, X. Characterization of EvaGreen and the implication of its physicochemical properties for qPCR applications. *BMC Biotechnology* **7,** 76 (2007).
17. Pasay, C. *et al.* High-resolution melt analysis for the detection of a mutation associated with permethrin resistance in a population of scabies mites. *Medical and Veterinary Entomology* **22,** 82–88, doi: 10.1111/j.1365-2915.2008.00716.x (2008).
18. Neuzil, P., Cheng, F., Soon, J. B., Qian, L. L. & Reboud, J. Non-contact fluorescent bleaching-independent method for temperature measurement in microfluidic systems based on DNA melting curves. *Lab on a chip* **10,** 2818–2821, doi: 10.1039/c005243d (2010).
19. Pipper, J. *et al.* Catching bird flu in a droplet. *Nat Med* **13,** 1259–1263, doi: 10.1038/Nm1634 (2007).
20. Pipper, J., Zhang, Y., Neuzil, P. & Hsieh, T. M. Clockwork PCR including sample preparation. *Angew Chem Int Ed Engl* **47,** 3900–3904, doi: 10.1002/anie.200705016 (2008).

Acknowledgement

P. Neužil acknowledges partial financial support by Central European Institute of Technology (CEITEC), grant number CZ.1.05/1.1.00/02.0068. Authors would also like to acknowledge the editorial help of Eric Castro.

Author Contributions

C.A. ran the lab experiment and prepared all necessary reagents as well as the data processing in Matlab environment, A.M. helped with the experiment preparation and P.N. came with the original idea of real-time multiplexing using intercalating dye. All authors reviewed the manuscript.

Additional Information

Competing financial interests: The authors declare no competing financial interests.

How to cite this article: Ahberg, C. D. *et al.* Single Fluorescence Channel-based Multiplex Detection of Avian Influenza Virus by Quantitative PCR with Intercalating Dye. *Sci. Rep.* **5**, 11479; doi: 10.1038/srep11479 (2015).